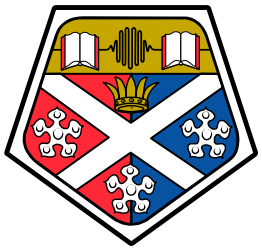

University of Strathclyde Glasgow

Strathclyde Institute of Pharmacy and Biomedical Sciences

A MODEL OF AGEING VITREOUS: IMPLICATIONS FOR DRUG DELIVERY

Lay Ean Tan

A thesis submitted to the University of Strathclyde in fulfillment of the requirements for the degree of Doctor of Philosophy

2010

DECLARATION OF AUTHENTICITY AND AUTHOR'S RIGHTS

This thesis is the result of the author's original research. It has been composed by the author and has not been previously submitted for examination which has led to the award of a degree.

Signed: Date:

This thesis is dedicated to the memory of my dearest grandmother,
Mrs. Ong Ah Eng, who passed away on the 30th August 2010.

ACKNOWLEDGEMENTS

In this thesis, Chapter 1, 2 and 3 were completed in the University of Strathclyde, Glasgow under the supervision of Professor Clive G. Wilson and Professor John M. Girkin. Chapter 4, 5 and 6 were completed in Allergan Inc. Irvine campus under the supervision of Dr. Patrick M. Hughes.

First of all, I would like to sincerely thank my principal supervisor Professor Clive G. Wilson for providing me the opportunity to pursue this PhD and for constantly ensuring that I obtained the highest quality of training throughout my studies. Thank you very much for your constant guidance and support, which has changed my attitude towards research allowing me to become a more confident and independent thinker. Many thanks to Mrs. Stephanie Wilson for her support in facilitating my research activities, particularly her help in driving me to the local abattoir at odd hours, which I appreciate greatly.

I would also like to thank my second supervisor, Professor John M. Girkin for his guidance and support as well as giving me the opportunity to work within the Institute of Photonics, which has allowed me to consolidate my knowledge of physics and its relation to pharmacy.

I am also very grateful to my industrial supervisor Dr. Patrick M. Hughes at Allergan Inc. for his advice and support during my stay in California. His guidance and supervision allowed me to explore life as an industrial scientist, which I found to be invaluable. To this point, many thanks to Professor Clive G. Wilson, Dr. Patrick M. Hughes and Professor Orest Olejnik for their enthusiasms in facilitating my learning experiences as well as Allergan Inc. for funding this research project.

I would not think that my research would ever go so far without the enthusiasm of all my collaborators across multi-disciplinary teams in the universities and Allergan Inc. Within the University of Strathclyde, I would like to thank Dr. Amanda Wright and Fiona Watt from the Institute of Photonics for their assistance and support during the experimental work on optical tweezers. Many thanks to Dr. Waleed al-Maliki for his

help in developing the perfused Miyake-Apple eye system and his teaching on ocular cannulation and relevant techniques. Many thanks to Dr. Dave Watson for his help in pharmaceutical analysis. I would also like to take this opportunity to thank Professor Stephen Marshall and Paul Murray from the Electronic and Electrical Engineering department for their help in composing the Matlab program for HRA wide-angle image analysis.

I am also thankful to Professor Raffaella Ocone from the Heriot-Watt University in Edinburgh for allowing me to use her rheometer in completing the first section of my study. I would also like to thank Professor Baljean Dhillon and Dr. Augustinus Laude at the Princess Alexander Eye Pavilion, Edinburgh, for their support on the clinical aspect of ophthalmic research. I am also grateful to Professor Godfrey Smith from the Glasgow University for providing the rabbit eye tissues, as well as Eileen and June who were always helpful in facilitating my experimental timetable and ensuring that my needs were taken care of during visits to their laboratory.

In Allergan Inc, I am deeply grateful to Dr. James Burke and Dr. Werhner Orilla from the biology department, for being enthusiastic and supportive during the development of the animal model. They provided me the opportunity to join their group in performing animal studies, learning about ophthalmological instruments and pre-clinical drug development studies, which were truly amazing experiences. I also wish to thank Dr. Wendy Blanda and Marianne Do; who have taught me so much on formulating implants and relevant skills. Their help and support have truly made a difference to my stay in Allergan. Many thanks also goes to Dr. Ruiwen Shi for his help in performing GPC and SEM studies. I would also like to thank Joshua Rowe, Hon Chan and Lisa Borbridge from the bioanalytical division for being extremely helpful and supportive in walking me through the final stages of pharmacokinetic studies. Many thanks to Gary, Hung, Kun, Donna from the formulation division as well as Ton, Susan Tsai, Larry from the biological department for their constant help during my visit.

Many thanks also to Ann (Secretary) in the department for helping with documents and administrative paper work. John, Tommy (SIPBS workshop) and Paul (IOP

workshop), thank you very much for your help in making tools and gadgets for my research project.

I would also like to take this opportunity to thank the inspectors working at the Paisley abattoir in Glasgow for their kindness in unlimited provision of ovine eye tissues, which have contributed a great deal to the whole project.

One of the key elements that was vital during my PhD study was peer encouragement and support. To this end, I wish to thank Anas, Andréa, Diana, Eileen, Jacklyn, Jamil, Jamal, Jasper, Jenifer, Jessica, Joe, John, Ju Yen, Maggie, Michaela, Mike, Mohammed, Patricia, Ruaridh and Sim from the University of Strathclyde, for all the years of fun, laughter and wonderful moments. Especially, Mameow, Khanittha, Nabila, Azra and Giacomo, thank you very much for your kind and thoughtful support through the ups and downs. Your encouragement and friendship over these years have truly meant a lot.

In Allergan, I was very lucky to have been able to work with good colleagues and friends who made my stay in California very enjoyable and memorable. Thank you to Chau, Cindy, Eric, Hui, Jenifer, Ke, Massoud, Mike, Mildred, Mouy, Nick, Pete, Shao Xing, Susan Lee and Walter for your great hospitality. Many thanks especially to Sukhon and Prem for your friendship and help during my stay, not to mention the great outings and food.

Last but not least, I am indebted to my dearest parents for their unlimited love, support and encouragement throughout my PhD study. Their careful nurture over the years has made me who I am today. I would also like to thank my sister Lay Nee; brothers Chiew Beng and Xu Chen. Although you are 10 thousand miles away, your constant courage and belief in me have meant a lot. Many thanks go to Uncle Chee Bin, Aunty Kit Yoke and Elaine for their constant care. A special thank you goes to Adrian for his endearing love, understanding, tolerance and support when it was most needed. Thank you so much for being always there to share the experiences and walking the journey together.

CONTENTS

ABSTRACT

This thesis concerns the development of ex-vivo and in vivo models of vitreous synchisis, a condition that develops in the elderly. The biophysical properties of the vitreous and the effects of liquefaction on the ocular disposition of intravitreally injected substances were investigated.

Conventional rheometry demonstrated that the vitreous is a non-uniform, lightly cross-linked viscoelastic solid gel, which, once destroyed, cannot be re-formed. Optical trapping was used to quantify the local viscosity with the objective of allowing repeat measurements in the same sample, a method validated using methylcellulose solutions. The technique was used to quantify viscosity changes induced by a freeze-thaw cycle, with the thawed samples having lower viscosity and more sample variables.

The vitreous microstructure was imaged using a blue LED and fluorescent microparticle suspension within the Miyake-Apple eye preparations. The microstructure was shown to be a barrier to particle movements, and its failure to re-anneal following injection, led to reflux along the needle track. In this model, intravitreal flow processes were found important in facilitating subsequent particle movement within the vitreous cavity.

By using hyaluronidase to destroy the vitreous hyaluronan, a model with ~50% vitreous liquefaction was developed in Dutch-belted rabbits. Following intravitreal injection, the distribution of sodium fluorescein and fluorescein isothiocyanate dextran was greater in the liquefied vitreous than in controls. Intravitreally injected fluorescent particles were found to sediment faster in the liquefied vitreous with a more dispersed and scattered distribution. Studies on the pharmacokinetics of the α_2-adrenergic agonist brimonidine administered either as a single bolus injection or a controlled-release implant, revealed that vitreous liquefaction affected the disposition of brimonidine to a greater effect following intravitreal injection than intravitreal implantation.

CHAPTER 1: INTRODUCTION

1.1 BLINDNESS AND THE ELDERLY

The increase in the occurrence of retinal pathologies with advancing age compromises sight and it is estimated that there are around 37 million blind and 124 million partially sighted people worldwide (Foster and Resnikoff, 2005). Based on the British (Evans *et al.,* 2002), Australian and American (The Eye Diseases Prevalence Research Group, 2004) demographic projections, blindness and visual impairment will be prevalent amongst the elderly population. This coincides with the rising proportion of the elderly in the population especially in developing countries (Figure 1.1) and therefore the impact of visual disabilities is expected to rise markedly in the years to come.

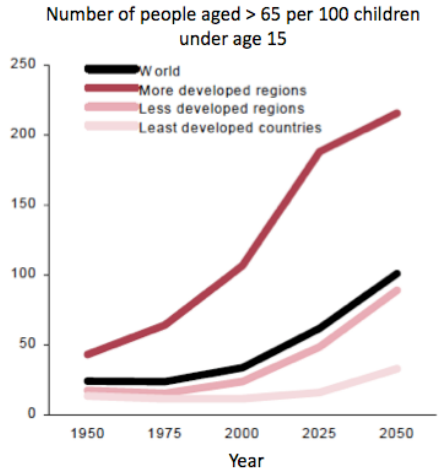

Figure 1.1 The ageing phenomenon of the world population. The change in social demographics is more prevalent in developed nations. (Adapted from Population division, United Nations)

Age-related macular degeneration (ARMD), glaucoma and cataract are the most common causes of blindness within the population. Early detection of disease progression through screening and referral with efficient therapy would almost certainly preserve more vision in the elderly age group (The Eye Diseases Prevalence Research Group, 2004). Whilst cataract is easily treated by surgical replacement of

the lens, ARMD and glaucoma affect the retina and are harder to treat; therapy based on systemic administration usually fails due to the limited accessibility through the blood-retinal barrier and dilution in the circulation. In addition, the high rates of blood flow nourishing the retina through the choroidal circulation, which lies between the tough white sclera and pigmented retinal epithelium, reduces the amount of drug available from external application. Research has suggested that melanin, the pigment that overlies the retina, may be an important reservoir for some drugs with high binding capacity. For example, memantine, which has been demonstrated to be neuro-protective in nerve crush models (WoldeMussie *et al.,* 2002) achieves significant retinal concentrations after topical administration (Hughes *et al*., 2005). If melanin could act as a depot, then the topical route might facilitate delivery of drugs to the posterior segment. For most drugs, rapid precorneal clearance and dilution by the lacrimal fluid and highly selective permeability of the cornea epithelial cells hampers the effectiveness of topical delivery. This has led to an increase interest in potential depots to reduce dosing frequency.

An obvious reservoir for drug treatment of the retina is the vitreous humour, a potential volume of around 4mL, which is enclosed, relatively featureless and non-perfused. Owing to its large volume and apparent simple structure, intravitreal injection is currently employed for the administration of therapeutic agents such as dexamethasone for macular edema secondary to retinal vein occlusion; however, the relatively rapid clearance requires regular injection to maintain therapeutic levels. Repeated injection increases the risk of endophthalmitis, retinal detachment and vitreous hemorrhage. Therefore, using the vitreous as a sustained delivery depot for controlled drug release system will be a better treatment option.

1.2 THE VITREOUS HUMOUR

1.2.1 PHYSICAL PROPERTIES AND BASIC FUNCTIONS

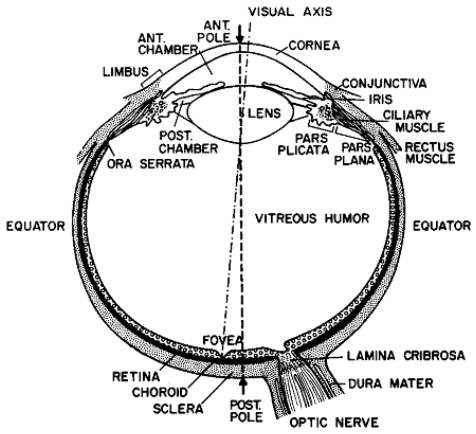

Figure 1.2 Vitreous humour and the surrounding ocular tissues (Adapted from Tripathi and Tripathi, 1984).

The vitreous humour fills the region between the lens and the retina (Figure 1.2), where it is attached anteriorly to the ora serrata, ciliary epithelium, zonular fibres and posteriorly to the optic nerve head, macula and the retina vessels, unless there is a posterior vitreous detachment (PVD). The vitreous occupies 80% of the globe and has a volume and wet weight of approximately 4 mL and 4 g respectively. The tissue density of approximately 1.0 g/mL (Soman and Banerjee, 2003), reflects a highly hydrated matrix of the vitreous as water constitutes the majority of its content (Sebag, 1989; Bishop, 2000).

Despite being in low concentrations, collagen and hyaluronan impart considerable elasticity and viscous properties to the vitreous humour (Bettelheim *et al.*, 2004). The viscoelastic behaviour enables the vitreous to serve as a shock absorber, cushioning the internal structure of the eye from injuries during sudden eye movements or strenuous physical activities involving rapid acceleration and deceleration of the head (Sebag, 1989; Soman and Barnerjee, 2003). Pressure within

the vitreous also mechanically protects the eye globe from collapsing when there is ocular trauma (Sebag, 1989).

In addition, the vitreous ensures visual clarity that enables approximately 85-95% of light (wavelengths 300-1400 nm) to be transmitted through and projected onto the retina with minimal scattering (Sebag, 1989). The transparency of the vitreous is vital for vision; and is partially maintained by the steric exclusion mechanism of hyaluronan, to ensure a minimum amount of cells and macromolecules present within the matrix (Sebag, 1989; Worst and Los, 1995). Additionally, the refractive index of 1.336 (Swindle *et al.*, 2007), slightly lower than that of the lens with an averaged measurement of 1.396 (Garner *et al.,* 1998), provides an index gradient of refraction required for optical focusing of the eye.

Ascorbic acid, secreted by the ciliary body is found in the vitreous at a concentration nine fold higher than the systemic circulation, serves as a scavenger for free radicals generated during photochemical reactions and tissue metabolism. Furthermore, the negatively charged vitreous hyaluronan protects the lens and retina from hydrated electrons by means of its surface anionic charges (Sebag, 1989). These protective roles of the vitreous are important for maintaining the physiological functions of the lens and retina. The vitreous also supplies these structures with nutrients such as glucose and amino acids. In addition, the vitreous serves as a barrier to oxygen diffusion and as such, an intraocular oxygen gradient between the lens and the retina is maintained. The lens is therefore, existing in a relatively hypoxic state of which condition is vital in preserving its clarity. Nevertheless, during vitrectomy, the removal of the vitreous increases oxygen diffusion towards the anterior direction, exposing the lens to an abnormally high oxygen tension. This is a likely cause of nuclear cataracts formation in patients undergo through a vitrectomy surgical procedure (Holekamp *et al.,* 2005).

A useful property of the vitreous humour is its tolerance to changes in pH. It has been demonstrated that the vitreous humour has a good buffering capacity and is able to resist pH changes (Conway *et al.,* 2008). The authors showed that the buffering

capacity of the vitreous against 0.1 N HCl and 0.1 N NaOH was 10 fold and 4 fold higher respectively as compared to 0.9% NaCl. After the addition of a 50 μL 40 mg/mL triamcinolone acetonide suspension (pH 5.8), the vitreous pH remained stable, leading the authors to conclude that the vitreous has the ability to buffer microliters of acidic or alkaline drug substances injected intravitreally.

1.2.2 VITREOUS COMPOSITION AND BIOCHEMISTRY

The vitreous humour consists of 99% water with the remaining 1% composed mainly of collagen and hyaluronan. Chondroitin sulfate, soluble proteins, glycoproteins, electrolytes and ascorbic acid form the minority of the vitreous content. Macromolecules show a regional variation in concentration as illustrated in Figure 1.3. Lower molecular weight molecules including electrolytes and amino acids have a higher concentration in the anterior region near to the ciliary body and lower at the posterior vitreous next to the retina. The topographical variation as such has been proposed to be associated with the active transport mechanism present at the ciliary epithelium that constantly secretes anions such as carbonate and phosphate into the posterior chamber, which then diffuse into the anterior vitreous. Nevertheless, the concentrations of pyruvic acid and lactic acid are higher at the posterior vitreous, which possibly related to the metabolic process occurring at the retina (Worst and Los, 1995).

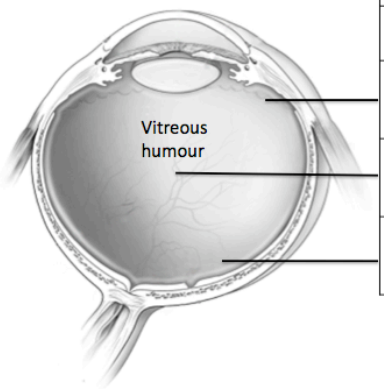

Solute concentrations (μg/mL)			
Collagen	Hyaluronan	Soluble proteins	Acidic glycoproteins
112	251	379	116
52	532	619	230
63	1190	960	325

Figure 1.3 Topographic variations in the distribution of collagen, hyaluronan, soluble proteins and acidic glycoproteins in the steer vitreous (Data was obtained from Balazs, 1960).

1.2.2.1 COLLAGEN

Collagen is the major structural protein of the vitreous humour and is essential for the rigidity of the vitreous gel. The removal would cause the collapse of the whole gel structure (Comper and Laurent, 1978). The fibrils are heterotypic, with a combination of type II, type V/XI and IX in a molar ratio of 75: 10: 15 respectively. The concentration of human vitreous collagen is approximately 300 μg/mL and the mean fibre diameter is estimated to be 10-25 nm (Sebag, 1989; Bishop, 2000). However, the fibrils are not uniformly arranged within the matrix: the highest concentration can be found at the vitreous base and peripheral cortical layer, followed by the posterior and central regions (Figure 1.3). The non-uniform distribution pattern has a direct impact on the local network density and consequently the rigidity of the gel structure (Balazs and Denlinger, 1984)

1.2.2.2 HYALURONAN (SODIUM SALT OF HYALURONIC ACID)

Hyaluronan, synthesized primarily by hyalocytes embedded within the posterior vitreous cortex, is the predominant glycosaminoglycan found in the vitreous. It is a long, linear polymer of a repeating disaccharide (D-glucuronic acid and N-acetylglucosamine) linked by alternating beta 1-3 and beta 1-4 bonds (Sebag, 1989). Depending on location, the concentration and molecular weight ranges found in the human vitreous are approximately 65-400 μg/mL and 2-4x10^3 kDa respectively (Sebag, 1989; Bishop, 2000). The lowest concentration was determined near to the lens, and gradually increases as sampling moves towards the retina. Although the anterior region contains the lowest concentration, the corresponding hyaluronans are of higher molecular weights as compared to the central and posterior regions. Since viscosity increases with the molecular weight of hyaluronan, areas near to the lens are more viscous than areas closer to the retina (Lee *et al.,* 1992; Bettelheim *et al.,* 2004).

1.2.2.3 MINOR VITREOUS CONSTITUENTS

Chondroitin sulphate forms a chain composed of a disaccharide repeat of D-glucuronic acid and N-acetyl-D-galactosamine, linked by alternating β(1→3) and β(1→4) linkages (Bishop, 2000). Two types of chondroitin sulphate chains are present in the vitreous, namely type IX collagen and versican, the later constituting the major component. Unlike type II and type V/XI collagen molecules, type IX collagen is not a fibrillar collagen. It has a characteristic of proteoglycan with chondroitin sulphate glycosaminoglycan α-chain attached to its non-collageneous domain. In the vitreous, the glycosaminoglycan chain is always identified on type IX collagen upon extraction process. Versican is a large aggregating proteoglycan that has a core protein substituted with several chondroitin sulphate side chains and possesses a N-terminal hyaluronan binding domain. Its interaction with hyaluronan is mediated through a link protein, identified by Reardon and colleagues (Reardon *et al.,* 1998).

Soluble proteins are non-fibrous proteins that can be recovered from the vitreous by high-speed centrifugation. The majority of soluble proteins in the vitreous are acid glycoproteins. Acid glycoproteins are fractions of albumin globulin and gamma globulin proteins, which are acidic in nature and contain large amount of carbohydrate components such as glucosamine, mannose and sialic acid (nine-carbon sugars) (Balazs, 1960). Their distributions are found to be the highest at areas near to the retina and the lowest near to the lens (Figure 1.3). Low-molecular weight proteins are predominant in the vitreous, as compared to higher molecular weight proteins due to the steric hindrance imposed by hyaluronan (Jaffe, 1969) as well as the blood-retina barrier that prevents the leakage of plasma proteins into the vitreous environment (Los and Worst, 1995).

Electrolytes, including sodium, potassium, chloride, calcium, phosphates and bicarbonate are present in small quantities in the vitreous humour. The presence of these ions in the vitreous is important for the arrangement of hyaluronan molecules, as the conformation relies on its ionic environment (Lee *et al.,* 1994b). For instance,

a decrease in the ionic strength can cause carboxylic groups on the polysaccharide backbone to become unshielded and repel each other, leading to the formation of an extended chain; whereas when the opposite occurs, the anionic charges are shielded, leaving the hyaluronan in its contracted state (Sebag, 1998). Hence, vitreous osmolarity plays a crucial role in balancing the physical state of the gel structures between the states of swelling and contraction.

As mentioned in section 1.2.1, the concentration of ascorbic acid in the vitreous is much higher than that in the plasma and ascorbic acid plays an important role in scavenging harmful metabolic and light-induced singlet oxygen. The high concentration of ascorbic acid is due to active transport by the cilliary epithelium. Patients subjected to increased oxidative stress, which occurs in the condition of proliferative vitreoretinopathy, show lower concentrations of ascorbic acid in their vitreous humour compared to normal individuals, suggesting the increased consumption of ascorbic acid engaged in anti-oxidative processes during adverse conditions (Takano *et al.,* 1997). Otherwise, it could imply outward diffusion from the vitreous cavity or reduced secretion.

1.2.2.4 MOLECULAR ORGANISATION OF THE VITREOUS GEL

The vitreous microstructure is formed by a spatially-constructed chemical relationship between collagen fibrils, hyaluronan and other glycosaminoglycans. There have been a few theories on how these components interact and associate; however, the complexity has not allowed the definition of a unified, agreed structure. Earlier studies have suggested that interaction between hyaluronan and collagen is important for stabilisation. For instance, the study by Comper and Laurent (1978) has demonstrated that when the collagen was removed from the vitreous matrix, a viscous solution of hyaluronan remained. On the other hand, when hyaluronan was depolymerized, the collagen gel shrank. In considering this, Smith and Serafini-Fracassini (1967) have proposed that the interaction between the two components must be weak since it could easily be disrupted by freezing and agitation. As

reviewed by Sebag (1998), the interactions could be mediated via chemical or electrostatic bonding or via an intermediate molecule.

Bishop and coworkers have investigated the structural roles of hyaluronan and chondroitin sulphate in the vitreous gel and have come to different conclusions (Bishop *et al.,* 1999). They reported that the enzymatic digestion of hyaluronan and chondroitin sulphate does not destroy the gel structure, which led the authors to suggest that collagen fibrillar network is sufficiently strong mechanically to support itself in solution. They proposed that if direct interaction between collagen and hyaluronan does occur, hyaluronan could be a short-range spacer (Bishop, 2000). This is similar to the concept developed by Tokita (1984) who suggested that hyaluronan acts as a cross-linker within the 'lightly' cross-linked collagen-hyaluronan network. In addition, the participation of other macromolecules such as opticin and chondroitin sulphate, which are present on the surface of the collagen fibrils has also been proposed and may indirectly join the collagen fibrils together forming a continuous network.

1.2.2.5 SPECIES VARIATIONS IN VITREOUS BIOCHEMISTRY AND PHYSICAL STATE

Generally all species, including humans, have similar vitreous components; however, the percentage composition varies and consequently the physical state between species differs. As shown in Figure 1.4, the vitreous of a squid consists mainly of a viscous fluid: the anatomy is much simpler without a defined anterior chamber as compared to other species. In chickens and tuna fish, the gel phase is divided from the liquid phase and restricted to areas posterior to the lens and areas next to the retina respectively. In owls, the vitreous body is a whole gel but the aqueous fluid has two regions of different viscosities; more viscous next to the corneal epithelium and more watery next to the lens. These physical states are certainly different from that seen in man, with a watery aqueous humour and a vitreous body that comprises of 80% gel phase and 20% liquid phase. Laboratory and domestic animals such as

rabbits, guinea pigs and cattle have been proposed to have a relatively similar vitreous physical state to man (Balazs, 1960).

In addition, variations in the percentage vitreous composition of collagen and hyaluronan (macromolecules) are evident among different species (Balazs and Denlinger, 1984; Lee *et al.,* 1994b). For instance, the concentration of vitreous collagen is higher in owl monkeys and rabbits as compared to man, whereas, hyaluronan is higher in humans as compared to rabbits, pigs and dogs (Balazs and Denlinger, 1984). Nevertheless, a correlation between the concentrations of macromolecules and rheological behaviour could not be established (Lee *et al.,* 1994b). For example, the viscosity of cow vitreous is significantly higher compared to human vitreous but does not reflect corresponding increases in collagen and hyaluronan concentrations. This led the authors to suggest that other factors including structural differences in the macromolecules might also influence the rheological properties of the vitreous humour.

Snowden and Swann (1980) have illustrated that the average fibril diameter of rabbits is ~7 nm as compared to ~10-13 nm in cows and dogs. In humans, the average diameter was found to be around 10-25 nm (Sebag, 1998). Additionally, the relative proportion of larger molecular weight hyaluronan (> 1.8 x 10^6 Da) in the vitreous gel is greater in sheep and goat as compared to human and pig vitreous (Noulas *et al.,* 2004). In comparison to cow (0.5-0.8 x 10^6), the molecular weight of human vitreous hyaluronan (2-4 x 10^6 Da) is larger; whereas, it is similar to that of the rabbit (2-3 x 10^6 Da) (Laurent *et al.,* 1983). These differences may also account for the variations seen in the viscosity of the vitreous among different species.

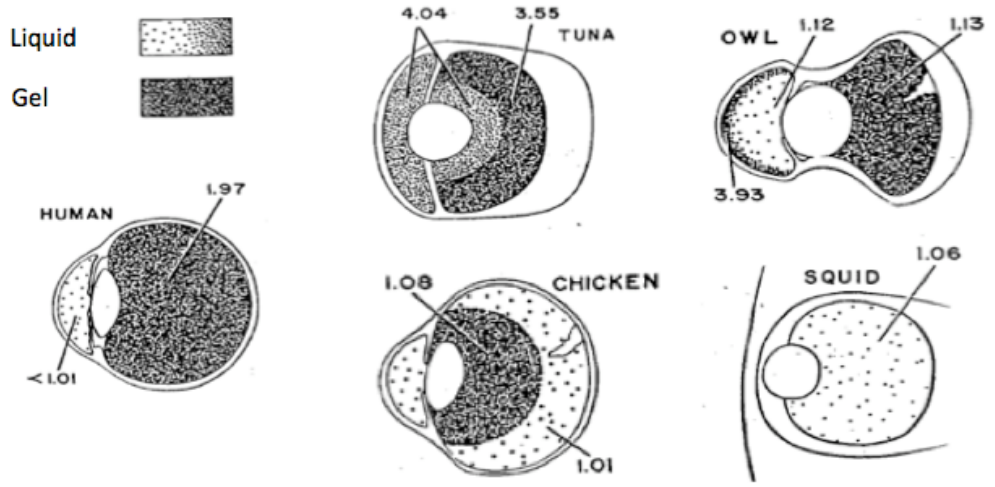

Figure 1.4 Physical states of the vitreous humour across animal species in comparison to human. Viscosity of the aqueous and vitreous fluids are indicated on the figure, which derived from experimental studies involving the measurements of liquid supernatant obtained from centrifugation of the vitreous body for 90-120 minutes at ~100,000xG (Adapted from Balazs, 1960).

The formation of vitreous during embryogenesis is not considered in detail, as the rheology of the mature vitreous is more important to the context of drug delivery. The subtle structural differences relate to changes during growth and senescence are considered later (section 1.6.5). Worst and Los have dealt with this matter in great detail in their book (Worst and Los 1995) and Figure 1.5 shows the figure from Busacca's work on the microscopic details of the eye referred to in their text. The remnant of Cloquet's canal is often noted and reflects structural components, which contribute to rheological differences in different parts of the vitreous. The cisternal structures will be considered in Chapter 2 and Chapter 3.

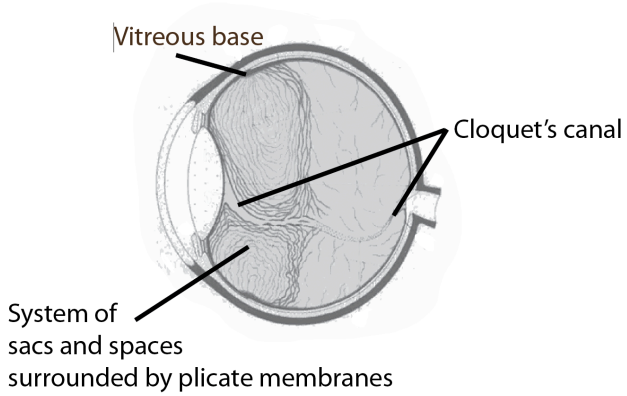

Figure 1.5 Adapted from Busacca (1967), illustrating Cloquet's canal and the vitreous sacs.

1.3 VITREOUS MEASUREMENTS

Viscosity is an important parameter since the measurement reflects the biophysical state of the vitreous humour. From a drug delivery standpoint, this parameter is important, determining the ocular disposition of drug formulations administered intravitreally. The primary intravitreal transport processes, diffusion and convective flow, are affected by viscosity (Stefánsson, 2009) and changes in vitreous rheology would almost certainly affect the drug movement and therefore the estimated pharmacokinetic parameters. In this thesis, conventional rheometry was used to quantify the rheological properties of the ovine vitreous and a novel application of the optical tweezers in the viscosity measurement of the liquid vitreous will be introduced.

1.3.1 RHEOLOGICAL MEASUREMENTS

Rheology is a science that describes the flow of fluid and deformation of solid materials. Rheological measurements are employed in various industries including food, paint and cosmetics to measure the consistency of products in order to ensure all essential criteria are met before being marketed. In pharmacy, the textural properties are paramount considerations in the formulation of creams, suppositories and tablet coatings in providing formulations that are aesthetically appealing to the

patient and at the same time maintaining physical and biological stability during the shelf-storage period (Sinko and Singh, 2006). In addition, rheology serves as a useful application for medicinal scientists and pharmacologists in measuring the consistency of biological fluids such as synovial fluid, mucus and vitreous humour in clinical and pathological research. For instance, the change in the rheological properties of the synovial fluid has been associated with old age and osteoarthritis (Borzacchiello *et al.,* 2004). Several rheological tests can be performed to characterize the physical properties of chemical and biological materials; however, two main measurements were utilized in this research (Chapter 2) namely, viscometry and oscillatory tests. These will be described in this section.

1.3.1.1 VISCOMETRY TEST

A principal requirement in viscometric analysis is that the sample is able to flow since the viscosity is measured as a function of shear rate, plotted as a flow curve that provides information on the behavior of materials under steady shear deformation.

The principle of Newton's law (Equation 1.1) can be explained by considering a block of fluid separated in layers by an infinite number of parallel plates sliding on top of each other with the bottom layer fixed as shown in Figure 1.6A. When a constant force is applied to the top surface of the fluid, the block will deform by a deflection, u, where the flow of each layer is proportional to its distance from the stationary layer (h). The deformation occurring is defined as shear strain ($\frac{u}{h}$), whereas the force per unit area that produces the deformation is known as the ***shear stress***. The velocity gradient between the two layers of liquid is called ***shear rate.***

Viscosity (η) = *Shear stress / Shear rate* **Equation 1.1**

For a Newtonian fluid, viscosity is linearly proportional to shear rate and shear stress. The flow curve as shown in Figure 1.6B, is a straight line that passes through

the origin and the viscosity can be obtained from the curve gradient as noted in Equation 1.1. Generally, biological fluids and most pharmaceutical formulations exhibit non-Newtonian behavior, and the flow pattern deviates from that described by Newton's law. Three main classes of non-Newtonian flow can be discovered from the flow curves, namely dilatant, pseudoplastic and plastic as shown in Figure 1.6B.

Dilatant flow is also known as shear-thickening, a condition where the viscosity increases with increasing shear rate. Shear thickening systems are commonly seen with suspensions with a high concentration (> 50%) of dispersed particles such as corn starch in water, which deflocculates upon shearing, leading to the expansion of the bulk system. ***Pseudoplastic flow***, on the other hand also known as shear thinning, occurs with increasing shear rate as a result of the shearing action on the sample, unfolding the tertiary structure; for this reason, pseudoplastic flows are often encountered in biopolymer solutions. Other examples include paint and emulsions ***Plastic flow*** is unique in the sense that flow does not occur until the shear stress applied exceeds the yield value. Once the material starts to flow, the behaviour follows a Newtonian model. Therefore, as indicated in the flow curve, the plot does not pass through the origin and the yield value can be obtained by extrapolating the linear part of the curve to the x-axis. An example of a material with a plastic flow system is tooth paste, which will not be extruded until a certain degree of pressure is applied to the tube.

Since shear rate is directly proportional to shear stress in a Newtonian fluid, a viscometer that measures at a single shear rate is sufficient to produce a flow curve. However, a single shear rate viscometer is meaningless for non-Newtonian fluid, as generally, no part of the flow curve is linear and hence, the viscosity cannot be represented by a single value. In these cases, a rotational viscometer that operates at multiple shear rates is required to produce a complete rheogram (flow curve) for non-Newtonian fluids. Examples of viscometers operating at single and multiple shear rates are the capillary viscometer and the cone-and-plate rotational viscometer respectively; the latter was employed in this research.

The viscometry test is relatively destructive as a measurement technique since analysis is performed using constant shear to grossly deform the structure of the sample. This does not provide information on the original structure as the material does not remain in its rheological ground state during measurement (Sinko and Singh, 2006). For such purposes, oscillatory tests will be more appropriate.

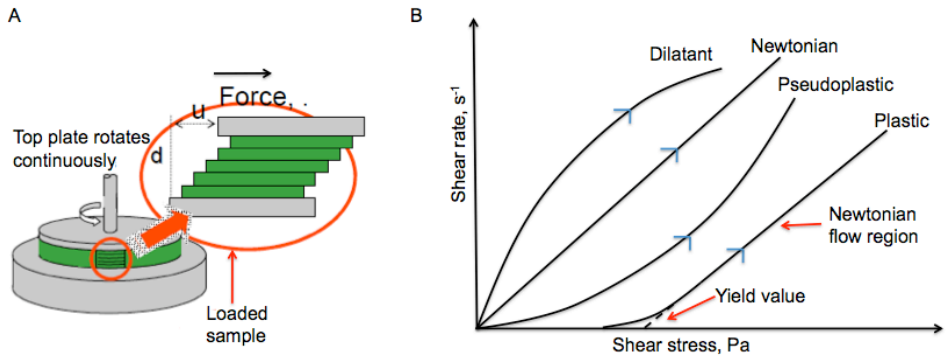

Figure 1.6 A) In the viscometry test, the top plate rotates continuously to apply a constant shear upon the sample to be analyzed. The flow behaviours under different shear conditions are recorded as a flow curve (Modified from Malvern Instrument training module 6), B) Flow curves of Newtonian and non-Newtonian fluids. All curves pass through the origin except a plastic system where material only starts to flow when the shear stress exceeds the yield-value.

1.3.1.2 OSCILLATORY TEST

A viscoelastic material has the viscous property of a liquid and the elastic property of a solid. Many of the pharmaceutical products and biological matrices are viscoelastic in nature and therefore, they demonstrate both solid and liquid behaviours. The elastic property is neither measurable by a viscometry test nor characterized by Newtonian flow; however, it can be described by Hooke's law as stated in Equation 1.2.

$$\sigma = G\gamma \qquad \textbf{Equation 1.2}$$

where σ is the stress; G is the elastic modulus; γ is the strain or deformation.

The strategy employed in the oscillation test is based on subjecting the sample to sinusoidal oscillatory shear stress that simulates a twisting motion, moving back and forth without destroying the sample (Figure 1.7). As such, a controlled sinusoidal stress at a fixed angular frequency (ω) is applied to the sample and the corresponding strain is measured as plotted in Figure 1.7.

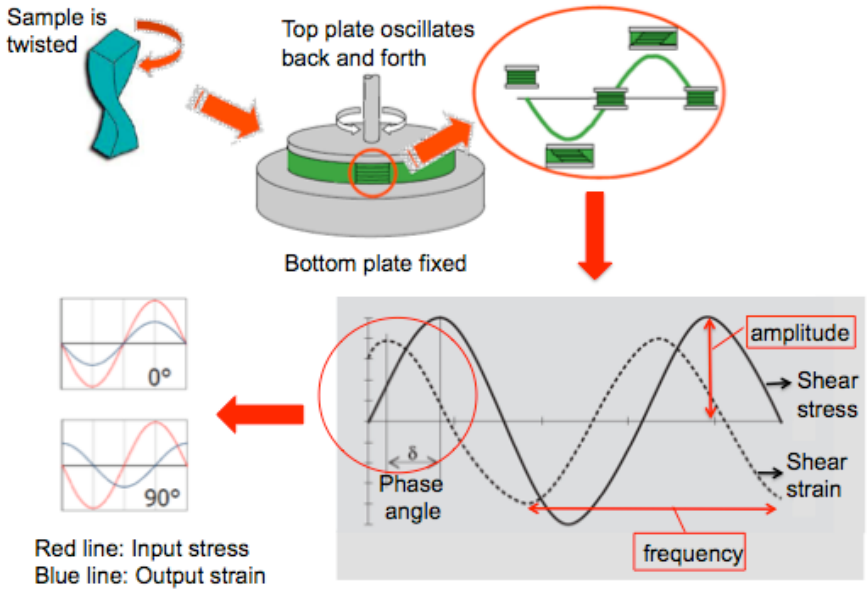

Figure 1.7 Top: In the oscillatory test, a sinusoidal oscillation shear stress is applied by oscillating the top plate back and forth against the sample. Bottom: The input stress and output strain are measured with the lag between two waves measured as phase angle. A phase angle equal to 0^0 means no lag between the stress and strain waves. However, a phase angle of 90^0 represents a lag of the strain wave behind the input stress wave. This condition frequently encountered in a liquid material that is viscous and will require time to flow (Modified from Malvern Instrument training module 6).

During the oscillatory test, it is common to perform an amplitude sweep test where a range of strain inputs are tested. The purpose of this test is to determine the linear viscoelastic region (LVR). The LVR corresponds to the reversible deformation range of the material, which indicates that the sample is measured at its state of rest.

As shown in Figure 1.8A, G' and G" are at constant values within the LVR, and graphically, the LVR limit can be identified when the G' (elastic modulus) starts to reduce. Once the linear viscoelastic region is established, frequency sweep tests can be performed to analyze the viscoelastic properties of the material on different time scales.

A frequency sweep plot (Figure 1.8B) reveals information on the elastic modulus (G'), viscous modulus (G"), phase angle (δ^0) and dynamic viscosity (η^*), which are useful parameters for understanding the viscoelastic properties of a material. G' is the ***storage modulus*** and it represents the elastic behaviour of a material or the deformation energy stored in the material during the shear process; whereas G" is the ***loss modulus*** and indicates the viscous behaviour of a material or the deformation energy, lost as heat from the material during analysis (Borzacchiello *et al.,* 2004; Mezger, 2006a). Additionally, the ***dynamic viscosity*** (η^*) is the ratio between the viscous shear modulus and angular frequency (G"/ω). A higher dynamic viscosity indicates a more viscous behaviour (Schachar *et al.,* 2007) and it is also a measure of energy loss from molecular stress relaxation processes such as shear-thinning (Patel, 2004). The ***phase angle*** (δ), is defined as a phase difference between the shear stress and the shear strain. As shown in Figure 1.7, when a solid recovers immediately following a stress input, there will be no lag in between the stress wave and the strain wave and the δ will be 0^0; in this case, the material exhibits elastic behaviour. If $0^0<\delta<90^0$, the analysed sample will be a semi-solid that exhibits both the viscous and elastic properties. It is worth noting that the amplitude of the strain wave is lower than the input stress wave. This is due to the nature of viscoelastic material where energy is lost with the shear process.

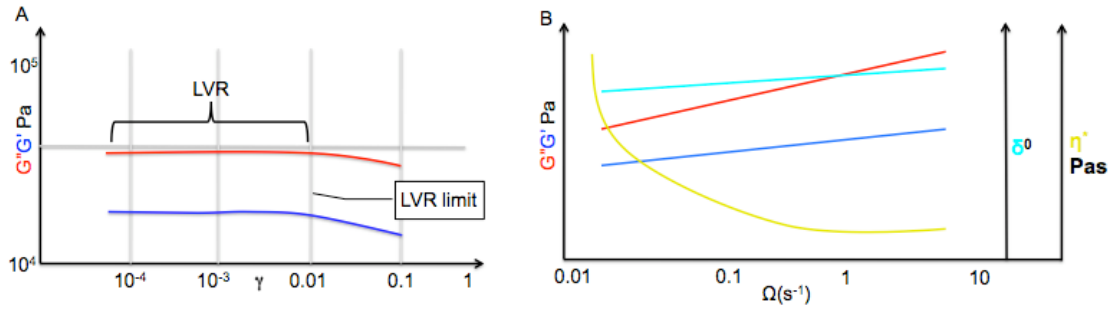

Figure 1.8 A) Amplitude sweep curve indicating the linear viscoelastic region (LVR) and LVR limit of ~0.01 strain. B) Frequency sweep curve with G' (elastic modulus, Pa), G" (viscous modulus, Pa), δ (phase angle ^{0}) and η^* (dynamic viscosity, Pas)

When the phase angle is known along with the stress/strain ratio, G' and G" can be determined based on Equations 1.3 and 1.4 respectively. Therefore, the ratio between the G" and G' can be represented as tanδ as shown in Equation 1.5. If G" > G' suggesting a more viscous liquid state, tanδ will be >1; whereas if G' > G", indicating a more elastic solid state, tanδ will be <1. At the sol-gel transition point, G'=G", tanδ will be equal to 1. Therefore, tanδ is used as an indicator during gel formation, hardening and curing processes. The characterization of a material using G', G", δ and tanδ can be summarized as listed in Table 1.1 (Mezger, 2006a).

$$G' = (\sigma/\gamma) \cos \delta \qquad \textbf{Equation 1.3}$$

$$G'' = (\sigma/\gamma) \sin \delta \qquad \textbf{Equation 1.4}$$

$$\tan\delta = G''/G' \qquad \textbf{Equation 1.5}$$

Parameters	Ideal pure viscous fluid behaviour	Viscoelastic liquid	50:50 viscous and elastic properties	Viscoelastic gel/solid	Ideal pure solid elastic behaviour
G' & G''	(G'→0)	G" > G'	G' = G"	G' > G"	(G"→0)
δ ^{0}	90	> 45 but < 90	45	> 0 but < 45	0
tanδ	(tanδ→∞)	>1	1	<1	(tanδ→0)

Table 1.1 Characterization of viscoelastic properties based on G', G", δ and tanδ (modified from Mezger 2006a).

1.3.2 OPTICAL TWEEZERS

1.3.2.1 STUDY BACKGROUND

Ashkin at Bell laboratories first developed the idea of optical tweezers in 1970. He discovered the forces of radiation pressure from a focused laser beam could be utilized to manipulate micron-sized transparent particles. In 1987, his team demonstrated for the first time that laser radiation pressure could successfully trap, manipulate and isolate viruses, bacteria, yeast, protozoa and human red blood cells. Moreover, Ashkin and co-workers have also shown that green argon-laser light induces optical damage to cells but infrared light achieves damage-free trapping (Ashkin, 2000).

The key attribute of laser tweezers in biological applications is a capability to measure forces in the order of 1 to 100 piconewtons. Forces of this magnitude work at the molecular scale; for example, it has been measured that forces of approximately 20 pN were required to break most protein-protein interactions and forces of around 50 pN are sufficient to convert DNA from a double helix to a ladder configuration (Molley and Padgett, 2002).

In addition, laser tweezers have also been extensively utilized in biochemical studies including rheological measurements of biopolymers and polymer solutions. Hough and Ou-Yang, (2006) have conducted a rheological study on telechelic poly(ethylene oxide) polymer solutions using optical trapping. In their experiment, the viscoelasticity of the polymer solution of concentrations ranging from 0.01 - 4.00% (w/w) was quantified. By interpreting the relaxation time obtained from the experiment, the formation and behavior of the micelles in the polymer solutions was better understood

Typically, particles of sizes 1-10 μm were trapped and such measurement scale allows quantification of the local mechanical properties of experimental medium to be performed. Velegol and Lanni utilized optical trapping to measure the local

mechanical properties in Type I collagen hydrogels. In the experiments, particles of sizes 2.1 μm were optically trapped and displaced by 10-100nm during measurements. The heterogeneity in the shear modulus (G) of the hydrogel was successfully identified and the variation in magnitude was found to be large from position to position. Additionally, the average shear modulus was found to compare well with that obtained using parallel plate rheometry (Velegol and Lanni, 2001). This demonstrated that optical trapping is a sufficiently accurate method and its capability to perform focal measurement *in situ* makes it more useful than conventional rheometry in characterizing non-homogeneous mediums, in which information on the local properties of the microenvironment is important to study.

1.3.2.2 BASIC PRINCIPLE AND MECHANISM

Radiation pressure is defined as a force per unit area exerted upon any surface (particle in this instance) as a result of a change in the momentum of the incident light (Williams, 2004). This occurs when a light beam passes through media of different refractive index (such as air to particle) where it is refracted, leading to a change in the direction of propagation and hence a change in momentum. According to Newton's second law, this in turn generates force, which is of equal magnitude but in an opposite direction to the momentum change of the light (Svoboda *et al.,* 1994; Williams, 2004). Based on this principle, transverse and axial trapping forces are required to trap a particle in 3-dimensions.

I. TRANSVERSE FORCE TRAPPING

When a Gaussian-profiled light beam (centre of the beam is more intense than the edges of the beam) passes through a transparent dielectric particle of higher refractive index than its surrounding medium, the rays are scattered and refracted (Figure 1.9A). When two rays (ray A and B) are considered (Figure 1.9A), with ray A closer to the beam axis than ray B, two forces ($\underline{F_a}$ and $\underline{F_b}$) are generated as a result of light refraction and momentum change of the light. In this case, $\underline{F_a}$, which is closer to the centre of the beam where there are more photons, is greater than $\underline{F_b}$.

The light intensity gradient produces a gradient force that acts towards the direction of the highest light intensity as shown in Figure 1.9. Therefore, the particle will be drawn towards the more intense region of the beam where it is trapped. In the case of a beam with a Gaussian intensity profile, the transverse gradient force is the predominant force that ensures the particle is trapped in the transverse direction (Svoboda *et al.,* 1994).

II. AXIAL TRAPPING FORCE

Although the transverse force could help to retain the particle within the highest intensity region of a Gaussian beam, it is not sufficient to prevent a particle from moving along with the light beam at the highest light intensity region. Therefore, an axial trapping force is required to stop this movement. Figure 1.9B illustrates the force components involved in axial force trapping. The basic principle is similar to that of transverse force trapping. When a focused laser beam (only ray 'a' and ray 'b' are considered here) impinges on a particle, the rays are refracted and the direction of propagation is changed. Considering $\underline{F_a}$ and $\underline{F_b}$ as shown in Figure 1.9B, the resultant force pulls the particle towards the beam focus in the axial direction.. To ensure the particle is pulled towards the focus of the beam (f) where it is trapped, the axial trapping force has to overcome the scattering force. The scattering force is defined as a force caused by light scattering and is intensity dependent. It acts in the same direction as light propagation and will draw the particle away from the trap if it is stronger than the trapping force.

The axial trapping force can be optimized by using a tightly focused beam generated from an objective lens with high numerical aperture, ideally ≥ 1.00. Figure 1.10 shows the numerical aperture of an objective lens that is denoted by $n\sin\Theta_{max}$ where n is the refractive index of the medium immediately below the objective lens and Θ_{max} is the angle of light that can be focused onto the particle. A high numerical aperture lens will have a higher focusing angle (Θ_{max}) than light at the direction parallel to the optical axis. This step is crucial in optimizing the light gradient

around the focal region to ensure a stable trap (Svoboda *et al.,* 1994; Williams, 2004; Molloy and Padgett, 2002).

Additionally, an oil-immersion objective lens, which is frequently utilized in many biological applications, can be beneficial in optimizing the trapping efficiency. It has a numerical aperture of around 1.3-1.4, and facilitates the matching of the refractive index with the cover slip. This avoids light bending and energy loss when light passes through two different mediums. Alternatively, a higher laser power can be used but care has to be taken to avoid cell damage. It is equally important for the diameter of the laser beam to fully or slightly overfill the back aperture of the objective lens (Svoboda *et al.,* 1994 and Molloy and Padgett, 2002). By doing this, the numerical aperture of the lens can be filled maximally and the smallest possible tightly focused spot can be obtained (Molloy and Padgett, 2006).

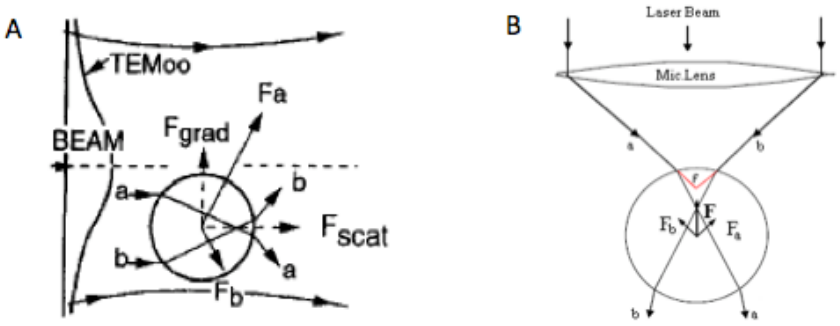

Figure 1.9 Schematic diagram illustrating the force components involve in the A) transverse force trapping (Adapted from Ashkin, 2000) and B) axial force trapping (Adapted from Williams, 2004).

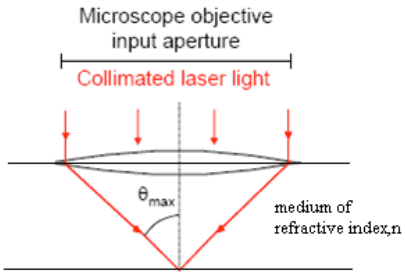

Figure 1.10 A schematic diagram showing the numerical aperture of the objective lens (Adapted from Williams, 2004).

1.4 VITREOUS IMAGING

1.4.1 SLIT-LAMP DARK BIOMICROSCOPY

The development of the slit-lamp biomicroscope by Gullstrand in 1912 allowed the clinical examinations of the vitreous structure. Sebag and Balazs utilized this technique to study the age and disease-related changes in vitreoretinal structures (Sebag and Balazs, 1985; Sebag and Balazs, 1989). By incorporating a dark-field slit illumination at an illumination-observation angle of 90° the light reflection and scattering were maximised, with higher density tissues highlighted more intensely (Worst and Los, 1995). This overcame the issue associated with vitreous transparency. In comparison with conventional microscopy, this technique has the advantage of visualizing the whole vitreous structure *in vitro* without dehydration and the use of tissue fixatives. The experimental setup is as illustrated in Figure 1.11 (Sebag *et al.,*1984) and Figure 1.16 (section 1.6.5) are examples from their pioneering work.

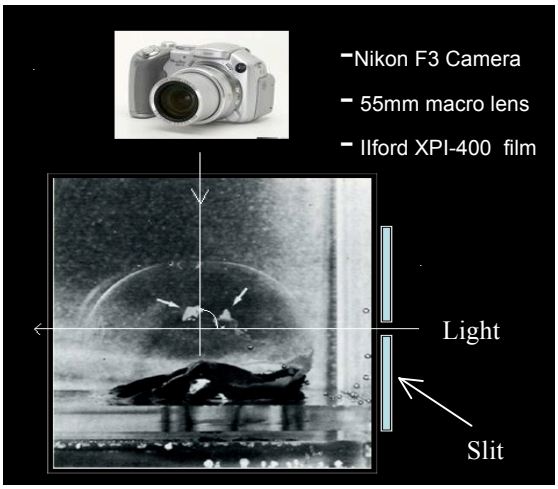

Figure 1.11 Human eye dissected of sclera, choroid and retina. Sutures through the limbus were used to mount the specimen on a Lucite frame. The entire specimen is placed in a lucite specimen containing isotonic saline and sucrose. A clear cohesive vitreous can be seen. Remnants of adherent retina (arrows) are occasionally present (Modified from Sebag and Balaz1984).

1.4.2 OCULAR FLUOROPHOTOMETRY

Ocular fluorophotometry permits the determination of fluorescence in the eye at certain defined and reproducible positions along the optical axis of the instrument before and after application of sodium fluorescein (Raines, 1988). A beam of continuous blue light is directed into the eye and the emitted fluorescence light collected by a photodetector. Fluorescein is a commonly used probe in ophthalmology and has an absorption maximum of 490 nm in the blue part of the spectrum and an emission maximum of 515 nm in the green part of the spectrum (Knudsen, 2002; Hassenstein and Meyer, 2009).

During measurement, both excited and emitted rays intersect within the eye to form a focal diamond at which point fluorescence intensity was measured (Figure 1.12). The focus is moved by a lens automated by a computer along the optical z-axis from the chorio-retinal surface to the front of the cornea. Each measurement is taken in steps of 0.25 mm and as many as 149 sequential readings can be obtained. Since the excitation and emission light will pass through the same optical lens system, they can be separated using specific filters before being detected (Van Best and Oosterhuis, 1983). The instrument is directly calibrated to measure fluorescein. The measurement is recorded and processed by a computer, and is subsequently presented as a plot of fluorescein concentration along the optical axis from the retina to cornea. Figure 1.12 illustrates a schematic diagram of a commercial fluorophotometer (Fluorotron Master, Coherent Radiation Inc.). Due to the autofluorescence feature of the ocular tissues, a background scan must be obtained prior to analysis. An example plot showing the autofluorescence of the ocular tissues is shown in Figure 1.12.

The use of fluorophotometric methods was quickly adopted especially for assessing the permeability of posterior barrier functions (blood-retinal barrier) in the diseased eye (Cunha-Vaz *et al.,* 1975; Ogura *et al.,* 1985; Moldow *et al.,* 1998; Moldow *et al.,* 1999; Moldow *et al.,* 2001; Sander *et al.,* 2001). Other applications include the diagnostic procedure to determine dry eye disease (Fahim *et al.,* 2006) and the

assessment of corneal epithelial barrier function (Gekka *et al.,* 2004) where the technique often termed anterior fluorophotometry.

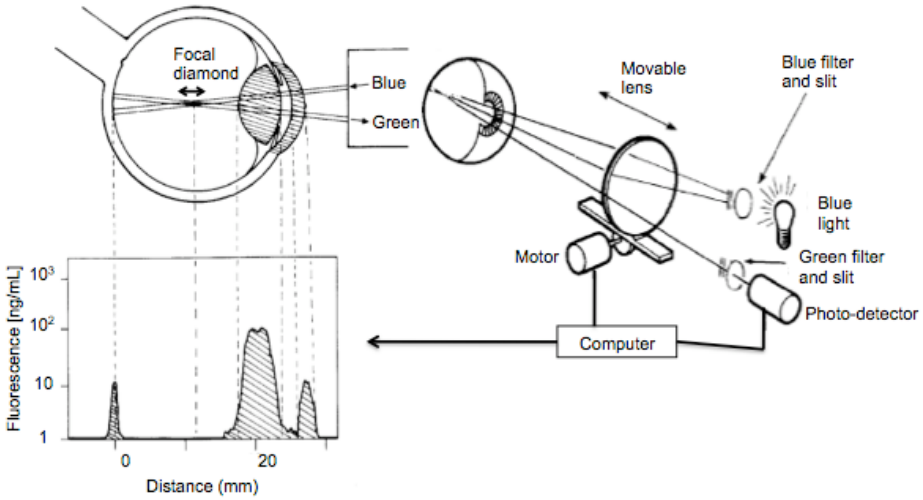

Figure 1.12 A schematic diagram showing the focal diamond (◄►) and depth of focus on the visual axis (right). A background scans measuring autofluorescence in the eye is as shown in the plot (left) (Modified from Van Best and Oosterhuis, 1983).

1.4.3 HEIDELBERG RETINAL ANGIOGRAPHY (HRA2) CONFOCAL LASER SCANNING SYSTEM

The Heidelberg Retinal Angiography (HRA2) is a confocal scanning laser ophthalmoscope (cSLO) designed for high contrast and high-resolution three-dimensional images of the choroid and retina. It is equipped with basic operating modes that allow the performance of fluorescein angiography (FA), Indocyanine green angiography (ICGA), autofluorescence imaging, blue (red-free) reflection and infrared reflection (IR) imaging. An optically pumped solid-state laser source is used to generate the blue light excitation (488 nm) for FA and red-free imaging, whereas diode-laser source of 790 nm and 820 nm are used for ICGA and IR imaging respectively (Jorzik *et al.,* 2005). Additionally, HRA 2 allows simultaneous use of two laser sources and barrier filters sweeping in alternation such as FA and ICG or red-free with IR enables a direct comparison of the pathological findings in the two

different angiographic modes, improving the diagnosis of vitreo-retinal diseases such as diabetic retinopathy and ARMD (Dithmer and Meyer, 2008).

The operating principle of HRA 2 is as described for the confocal scanning laser ophthalmoscope (cSLO) in Figure 1.13. A collimated low-power laser beam of ~ 1 mm diameter is focused on the pupil and projected by ocular optics to generate a 10 μm focal spot onto the retina. By sequentially changing the angle of the beam focusing on the pupil, a 2 dimensional scan of the fundus can be obtained. Light reflected from each scanned point will be returning back along the same path as the illuminating light and processed by the same optic components. Furthermore, confocality suppresses scattered light and light originating outside the focal plane, while allowing light conjugate to the focal plane to pass through a pinhole and be detected.

HRA 2 provides adjustable field of view that ranges from 10^0-30^0 and an optical resolution of 5-10 μm/pixel, which may vary according to the optical quality of the subject's eye. A wider field of view can be obtained by using a Staurenghi 230 SLO retina lens in conjunction with HRA. The lens system produces 50^0, 100^0 and 150^0 imaging fields when it is used with the HRA settings of 10^0, 20^0 and 30^0 respectively (Staurenghi *et al.,* 2005).

HRA 2 has various clinical diagnostic applications for posterior segment diseases. For example, red-free imaging is suitable for visualizing areas with very low red-light contrast such as microaneurysm, whereas ICGA is the most suitable operating mode for examining the choroidal circulation (Hassenstein and Meyer, 2009). In addition, HRA 2 provides an option to image the anterior segment and vitreous cavity (Mennel *et al.,* 2007). This can be done by adjusting the distance between the camera and the eye as well as tuning the focus until the area of interest comes into view (Dithmar and Holz, 2008). A sleeve can be placed in front of the camera as a reference point to standardize the focal plane if repetitive images are required from the same or different subjects during a long-term follow-up animal study.

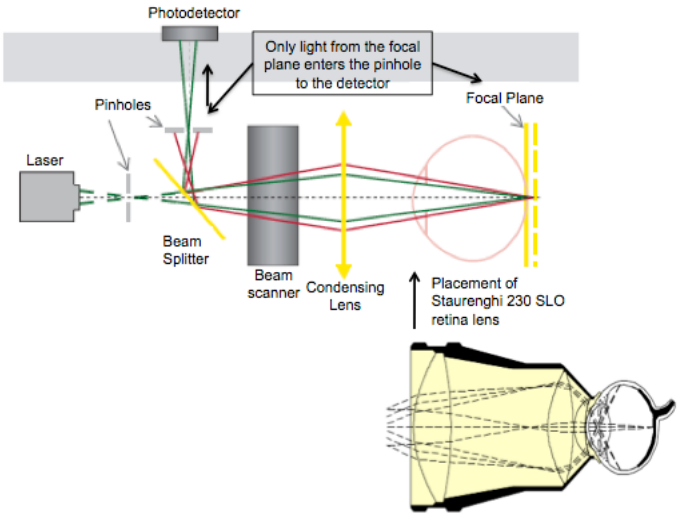

Figure 1.13 Staurenghi 230 scanning laser ophthalmoscope (SLO) retina lens can be coupled to a confocal scanning laser ophthalmoscope. Beam splitter in the instrument separates the illuminating and the reflecting light from the eye, whereas the beam scanner deflect the light in 2 dimensions for retina imaging in both x- and y-axis. (Modified from Girkin HRA engineering and Ocular Instruments Inc.).

1.5 INTRAVITREAL DRUG DELIVERY

1.5.1 MECHANISMS OF DRUG TRANSPORT

The flow processes within the vitreous can be described by passive diffusion and convective flow. The contributions to drug transport depends on molecular size and charges of injected materials (Pitkänen *et al.,* 2003), vitreous diffusivity (Friedrich *et al.,* 1997a) and pathophysiological conditions (Park *et al.*, 2005). The engineering description of this is embodied in the Peclet number, which allows the relative contribution of diffusion and convection to overall drug distribution to be attributed (Xu *et al.*, 2000; Stay *et al.*, 2003; Park *et al.*, 2005).

1.5.1.1 DIFFUSION

The diffusion process in the vitreous can be described using Fick's law of diffusion, which dictates solute flow is directly proportional to its concentration gradient as described by the following equation:
Flow (J)= - (diffusion coefficient (D)*concentration gradient (dC/dt) (Kim, 2004). Passive diffusion is the most fundamental transport mechanism for small molecules in liquid. It requires a differential gradient to provide motive force (such as pressure and concentration) towards creation of an equilibrium state at which point, no net diffusion occurs (Kim, 2004). Common laboratory techniques used to study the diffusion activity in the vitreous include diffusion cells (Gisladottir *et al.,* 2009) for *in vitro* study and vitreous fluorophotometry (Cunha-Vaz and Maurice, 1967; Araie and Maurice, 1991) as well as MRI (Kim *et al.,* 2005) for *in vivo* settings.

Understanding the diffusion process in the vitreous has always been a challenge to a formulator based on the fact that the vitreous is not a simple, uniform gel. Accordingly, the diffusion of materials through the vitreous would be expected to deviate sharply from that in water. This behaviour can be illustrated when the vitreous is destroyed by treatment with hyaluronidase, the movement of materials from mid-vitreous to choroid is significantly faster (exponential half-life 36 ± 13 minutes in controls compared to 20 ± 7 minutes in treated animals) suggesting that structural elements constituted by the vitreous components do contribute to a steric hindrance in the overall rate of material transport (Foulds *et al.*, 1985). Moreover, the diffusion of dexamethasone was found to be 4-5 times slower in the vitreous gel as compared to water (Gisladottir *et al.,* 2009).

Smaller drug molecules of low molecular weight (MW) < 10kDa, encounter lower steric resistance imposed by the vitreous structure, and hence, their migration in the vitreous is largely diffusive (Park *et al.*, 2005). The injection via the pars plana into the anterior segment of the vitreous allows free diffusion in all directions towards the anterior chamber and retina (Lund-Anderson and Sander, 2003). Nevertheless, the diffusion activity of larger molecules is limited by the fibrillar structure of the

vitreous meshwork and they preferentially move in between the polysaccharide compartment (Worst and Los, 1995). Therefore, convective flow may play a more important role in the transport of large molecules.

1.5.1.2 CONVECTIVE FLOW

Convection in the vitreous is possibly generated by a pressure drop from the hyaloid membrane across to the retinal surfaces as fluid permeates through the vitreous (Xu *et al.,* 2000). It undoubtedly contributes to intravitreal drug transport although current opinion is that it is less important for smaller molecules, except during injection when excess pressure is generated by expansion of the vitreous volume and temporary destruction of the vitreous integrity. It was estimated that approximately 30% of the intravitreal transport of small molecules such as acid orange 8 (MW 364 Da) was contributed by convective flow; whereas for larger molecules, convective flow is the main drive for movement (Xu *et al.*, 2000). Coincident with this, Kim and colleagues experimentally illustrated that convective movements have minimal effect on the concentration profiles of Gadolinium-diethylenetriamine penta-acetic acid (Gd-DTPA), which is a small molecule of molecular weight 938 Da. A similar finding was reported by Lee and colleagues, who have shown that intravitreal distribution of Gd-DTPA in post-mortem elderly eyes was not significantly affected by bulk flow induced by ocular movement (Lee *et al*., 2009).

Gisladottir and colleagues have related convective flow to Hagen Poisueille's law, which describes fluid flow due to a change in pressure along a capillary tube (Gisladottir *et al.,* 2009). The principle applies to the diffusion cell that was used by the authors in the experiments, because it can be approximated to be cylindrical in shape. In addition, the equation also suggests that the pressure gradient is along the longitudinal direction, and thus linear. However, the eye is spherical, and we have a pressure gradient from the aqueous humour (2000Pa) across the vitreous to the episcleral vein (1200Pa) (Stay *et al.,* 2003). So, this equation may be appropriate for describing a non-flow system such as the *ex vivo* and *in vitro* experiments, but less appropriate when measuring flow and convective current *in vivo*.

1.5.2 INTRAVITREAL CLEARANCE KINETICS

Drug substances administered intravitreally are cleared either anteriorly to the aqueous chamber or posteriorly to the retina (Maurice and Mishima 1984; Maurice, 2001). The elimination process reaches an initial equilibration phase, following first-order kinetics, which explains that the rate of material clearance is proportional to the concentration of drugs *in situ*. The intravitreal half-life of low molecular weight (MW) substances is usually a few hours but as the MW rises above 10,000 Daltons, clearance slows. For instance, the intravitreal half-life of dexamethasone (MW = 392 Da) is 5.5 hours in humans, as compared to 25 hours for vancomycin (MW = 1.5 kDa). Table 1.2 illustrates more examples of the difference in terminal half-life of compounds of different MW.

Compound	**MW**	**Terminal half-life**	**Study model**	**References**
Ganciclovir	255 Da	7.1 hours	Rabbit	(Lopez-Cortes *et al.*, 2001)
Dexamethasone	392 Da	5.5 hours	Human	(Gan *et al.*, 2005)
Gentamycin	464 Da	33 hours	Monkey	(Barza *et al.*, 1983)
Vancomycin	1.5 kDa	25 hours	Human	(Aguilar *et al.*, 1995)
Ranibizumab	48 kDa	3 days	Monkey	(Gaudreault *et al.*, 2005)
Bevacizumab	149 kDa	4 days	Rabbit	(Bakri *et al.*, 2007)

Table 1.2 Intravitreal half-life comparison of small and large molecular weight drug compounds.

From an ocular therapeutic point of view, the retina is the target for treating posterior segment diseases such as age-related macular degeneration and diabetic retinopathy. In terms of exposure, this means that if a drug were to be cleared from the vitreous compartment, the posterior route will be more favourable. Yet, the fate of a drug molecule being eliminated via forward or retinal clearance depends very much on its physicochemical properties (such as lipophilicity, hydrophilicity and molecular size) and its affinity for active transport mechanisms in the retina (Chastain, 2003).

1.5.2.1 FORWARD CLEARANCE (ANTERIOR ROUTE)

The rapid turnover of aqueous humour in the anterior chamber is the main drive for forward clearance. Araie and Maurice have shown that clearance of fluorescein glucuronide (508Da) and fluorescein dextran (66kDa) from the vitreous cavity into the posterior chamber encountered a minor barrier at the anterior hyaloid membrane (Araie and Maurice, 1991). In mathematical modeling, hyaloid membrane is always assumed to offer negligible resistance to flow due to its porous and thin structure (Balachanran *et al.,* 2008, Stay *et al.,* 2003). Despite the case, the lens at the anterior central position remains as the main barrier to forward movement of injected substances from the vitreous (Worst and Los, 1995). Thompson and Glaser confirmed the characteristics of this barrier system by showing that the rates of movement of 20 kDa and 70 kDa dextran from the vitreous into the anterior chamber increased significantly after extracapsular lensectomy with posterior capsulotomy (Thompson and Glaser, 1984). In addition, according to the study performed by Stepanova and colleagues, the transport mechanism present at the lens epithelium generates uni-directional flow that moves fluids towards the retina rather than the anterior chamber (Stepanova *et al.,* 2005). The lens epithelium has also been reported to impose a considerable barrier to fluorescein entry, but permeability through the lens capsule was regarded as minimum and therefore, it is an area, where the exchange of substances between the lens and the surrounding fluid may occur (Kaiser and Maurice, 1964). Substances that successfully enter the anterior chamber are subsequently removed along with aqueous humour by the trabecular and uveoscleral outflow (Cunha-Vaz, 1997; Urtti, 2006).

The constant aqueous drainage from the anterior chamber generates a sustained ‘sink condition’ for intravitreally administered substances, resulting in the formation of a concentration gradient that spreads across the vitreous cavity originating from the injection pocket. Maurice illustrated this diffusional behaviour using a concentration contour map that shows the clearance process is parallel to the posterior capsule of the lens with the lowest concentration located at the hyaloid membrane that gradually increases towards the retina (Araie and Maurice, 1991).

Typically, hydrophilic molecules that are unable to exit through the lipophilic layer of the retina are removed via the anterior route. For example, Atluri and Mitra investigated the vitreal disposition of short-chain aliphatic alcohols with varying degrees of lipophilicity in rabbits using ocular microdialysis techniques. Their findings reveal that hydrophilic methanol achieved the highest concentration at the anterior chamber whereas the concentration of lipophilic 1-heptanol was undetectable (Atluri and Mitra, 2003). In agreement, Araie and Maurice have shown that hydrophilic molecules such as fluorescein glucuronide and fluorescein isothiocyanate dextran have poor retinal permeability and are eliminated mainly through the anterior route (Araie and Maurice, 1991).

Large molecules that cannot transverse through the retinal barrier of the inner eye will also be removed by the aqueous system (Urtti, 2006). For instance, bevacizumab, an anti-human vascular endothelial growth factor (VEGF) with a molecular weight of 149 kDa, was cleared through the anterior pathway with an estimated intravitreal half-life of 4.3 days (Bakri *et al.,* 2007).

In addition, active transport processes present at the blood aqueous barrier has been reported to play a role in the outward transport of fluorescein from the aqueous humour following intravitreal injection in the normal eye (Cunha-Vaz and Maurice, 1967). Blood aqueous barrier is composed of the endothelium of the iris blood vessels and the non-pigmented layer of the ciliary epithelium. These cell layers exclude substances such as blood proteins from the aqueous humour and vitreous humour that would impair transparency as well as osmotic and chemical equilibrium of the intraocular fluids (Cunha-Vaz, 1997). Other examples of substances that are actively transported across the ciliary body epithelium are organic anions such as antivirals, antibiotics and anticancer drugs. The clearance rate of these substances was reduced by probenecid, indicating the role of organic anionic transporter in drug efflux (Pelis and Delamere, 2009).

1.5.2.2 RETINAL CLEARANCE (POSTERIOR ROUTE)

The posterior elimination pathway has been proposed to be the primary elimination route for small and lipophilic molecules. Once removed from the retina, materials will be subsequently transported away by the choroidal blood flow and this circulation system maintains a constant concentration gradient between the vitreous and retina. If melanin binding is significant, accumulation in the melanocytes of the uveal tract will occur.

The main barriers to the elimination of molecules using the retinal route are the lipophilic retinal layer and the highly regulated blood retinal barrier. Blood retinal barrier affects outward movement from the retina into the blood (Cunha-Vaz, 1997). The anatomy of this barrier is separated into an inner and outer blood barrier. The endothelium of the retinal vessels composes the inner part of the barrier, whereas the retinal pigment epithelium (RPE) represents the outer blood-retinal barrier (Hughes *et al.,* 2005). Large molecules or probes cannot permeate the retina easily due to the tight intercellular junction at the RPE. Therefore, molecular size is an important determining factor involved in this transport process. Sakurai and colleagues showed that particles of sizes 200 nm and below can transverse the retina but not 2 μm which were found to mainly clear through the trabecular meshwork (Sakurai *et al.,* 2001). Pitkänen and coworkers have also reported that the permeability of carboxyfluorescein (376 Da) was 35 times higher as compared to FITC-dextran 80kDa (Pitkänen *et al.,* 2005).

In addition, molecular movement across RPE can occur through passive diffusion or active transport processes (Pitkänen *et al.,* 2005). Passive diffusion of materials occur either through the paracellular or transcellular routes; The former takes place at the tight junction of the retina endothelium and less lipophilic molecules are more likely to use this route. Highly lipophilic molecules such as metoprolol can permeate through phospholipid cell membranes. An *in vitro* study has shown that retinal permeability is 8-20 times higher for lipophilic than hydrophilic molecules, suggesting a higher efficiency level of the transcellular pathway (Pitkänen *et al.,*

2005). The gradient of diffusion across the vitreous is parallel to the retinal surface with the highest concentration at the injection site and the lowest when closer to the retina surface where the drug is cleared (Araie and Maurice, 1991).

Reddy and colleagues demonstrated the presence of retinal active transport mechanisms in the late 1970s for the removal of amino acids from the vitreous humour into the systemic circulation against solute concentration gradient (Reddy *et al.,* 1977). Active transport processes play an important role in posterior clearance of drugs such as β-lactam antibiotics. However, inflammation of the RPE which is a common problem encountered in patients with endophthalmitis, damages the retinal pump function thereby decreasing the intravitreal half-life of molecules eliminated by this system (Ficker *et al.,* 1990). The presence of active transport mechanisms and the large retinal surface for absorption, suggests that molecules eliminated via this route will have a shorter intravitreal half-life, typically 2-5 hours as compared to forward clearance of 20-30 hours (Dias and Mitra, 2000). A comparison between the forward and retinal clearance has been summarized as illustrated in Table 1.3.

	Forward clearance	**Retinal clearance**
Site of activity	Aqueous chamber	Retina
Barrier system	Blood-aqueous barrier, lens	Blood-retina barrier
'Sink' condition	Aqueous humour turnover	Choroidal blood flow
Diffusional contour	Parallel to the posterior capsule of the lens	Parallel to the retina surface
Active transport	Ciliary epithelium and iris	RPE and retinal capillaries
Drug molecule	Hydrophilic	Lipophilic
Examples	Aminoglycoside (Cobo *et al.,*1981; Barza *et al.,* 1983) Fluorescein glucuronide (Araie and Maurice, 1991) Fluorescein dextran (Araie and Maurice, 1991) Methanol (Atluri and Mitra,2003)	β-lactam antibiotics (Barza *et al.,* 1983) Fluorescein (Araie and Maurice, 1991) 1-heptanol (Atluri and Mitra, 2003) Cu^{++} ions (Bito *et al.,* 1987)

Table 1.3 Comparison between the forward and retinal routes of clearance.

1.5.3 VITREAL PHARMACOKINETIC ANALYSIS

1.5.3.1 BASIC PRINCIPLES

Pharmacokinetic studies are usually performed to understand the absorption, distribution, metabolism and excretion in various ocular compartments, which are the four key physiological processes that describe the drug-tissue interactions (Short, 2008). These studies provides information such as the drug residence time, elimination rate, absorption rate, and distribution volume, parameters that could relate to the pharmacological effect of a drug substance. During the pre-clinical drug development, pharmacokinetic analysis is an important element in establishing the safety and efficacy of a drug substance or a delivery method; whereas in clinical setting, it is useful in optimizing drug dosage regimen and assisting more rational therapeutic decision to be made for the patients (Riverre, 2003).

Intravitreal pharmacokinetics has been a major interest in the treatments of bacterial endophthalmitis, age-related macular degeneration and cytomegalovirus retinitis. Treatments could be in the form of simple solution or drug depot. Simple solutions are commonly applied for acute conditions where a high initial dose is required for short period of time such as infections and inflammation. A drug delivery depot would probably be required when longer-term treatment is necessary such as in the treatment of retinitis due to cytomegalovirus infection. Due to the difference in rate of drug release, concentration-time profiles will therefore vary with different dosage forms.

I. SIMPLE SOLUTION

Drug molecules within simple solutions such as antibiotics diffuse quickly throughout the vitreous chamber once intravitreally injected. The initial concentration is a result of initial dose and extended distribution (Meredith, 2006). After an initial period of equilibration, drugs start to clear by first-order kinetics, and

the average concentration present in the vitreous at time, *t*, after injection can be determined using Equation 1.6 (Maurice, 2001).

$$C_v = C_d e^{-kvt} \qquad \textbf{Equation 1.6}$$

where $C_d = m_r/v_v$ **Equation 1.7**

m_r is the initial dose, v_v is the vitreous volume and k_v is the elimination rate constant, which can be calculated as $k_v = 0.693/t_{1/2}$ (drug half-life).

II. DRUG DEPOT OR IMPLANT

The release mechanism of a controlled released drug depot may follow a zero-order, first-order release or mixed kinetics. Zero-order release kinetics represents a constant rate of drug release that is independent of concentration. The release profile appears as a straight line when plotted as a concentration against time and the rate of drug release, k = slope of the line. A first-order release profile shows that the rate of drug release depends on concentration and concentration decreases over time with an exponential constant.

For sustained delivery depots with zero-order release profiles, the average intravitreal concentration of free drugs can be calculated using Equation 1.8.

$$C_v = C_d /(t_r * k_v) \qquad \textbf{Equation 1.8}$$

where t_r is the time over which the drug is released.

In the equation, C_v is proportional to m_r/t_r, therefore, a careful tuning of drug loading and release rate will ensure effective drug level attained throughout the delivery period (Maurice, 2001).

Equation 1.9 can be used to determine C_v if a drug is released from a device that assumes first-order release kinetics with a time constant, k_r.

$$C_v = C_d (k_r/k_v) e^{-krt} \qquad \textbf{Equation 1.9}$$

The exponential term in Equation 1.9 shows that m_r is proportional to k_r, this explains that by assuming a constant release rate, increasing the drug loading can extend the lifetime of the device (Maurice, 2001).

1.5.3.2 PHARMACOKINETIC MODELS OF INTRAVITREAL DRUG DELIVERY

Pharmacokinetic models can be used to understand drug disposition and obtain pharmacokinetic parameters such as area under the curve (AUC) and drug clearance (CL). A non-compartmental model was used in this thesis and therefore, will be discussed in this section.

The non-compartmental model is relatively simple, versatile and can be applied to almost all pharmacokinetic data. It measures the response of a drug within a physiological structure and allows pharmacokinetic parameters that are not structure specific to be estimated from the concentration-time profile. The functional of non-compartmental modeling is based on three fundamental assumptions: 1) distribution and elimination processes are linear, 2) elimination is from a single structure such as the vitreous and 3) pharmacokinetics of the system do not change over the sample collection period (Gupta and Henthorn, 2009). However, the advantages are that non-compartmental modeling does not require any assumptions on the shape of the curve such as mono or multiexponential decline (Gaudreault *et al.,* 2005).

The determinations of area under the curve (AUC) and terminal rate constant (k) are the two main calculation processes involved in the engineering of a non-compartmental model. $AUC_{0\text{-}tlast}$ (from time 0 to the last time point) can be calculated based on the linear trapezoidal rule. Terminal elimination rate constant (k_{el}) can be determined from the log-linear portion of the terminal elimination phase with a minimum of three data points as shown in Figure 1.14. Using both parameters, other parameters including $AUC_{0\text{-}\infty}$ (from time 0 to infinity), mean residence time (MRT), drug clearance (CL), apparent volume of distribution at steady state (V_{ss}) can be subsequently derived. AUC and MRT are measures of drug

exposure and rate of elimination respectively. Therefore, both parameters are useful in estimating therapeutic efficacy. Clearance is a parameter that quantitates drug elimination from an organ or body system in which the drug was distributed, per unit time. V_{ss} is the volume in which the mass of administered drug is diluted at steady state. C_{max} (maximum concentration) and T_{max} (time to C_{max}) can be obtained directly from the drug concentration-time curves.

The application of a non-compartmental model in intravitreal drug delivery is common. For example, López-Cortés and coworkers have performed a non-compartmental pharmacokinetic analysis to evaluate the concentration of ganciclovir and foscarnet achieved at the retina following intravitreal injection. The pharmacokinetic analyses showed that ganciclovir achieved higher and more sustained retinal drug level than foscarnet, which led the author to suggest that ganciclovir will have a better pharmacokinetic profile suitable for the treatment of retinitis due to infection with cytomegalovirus (López-Cortés *et al.,* 2001).

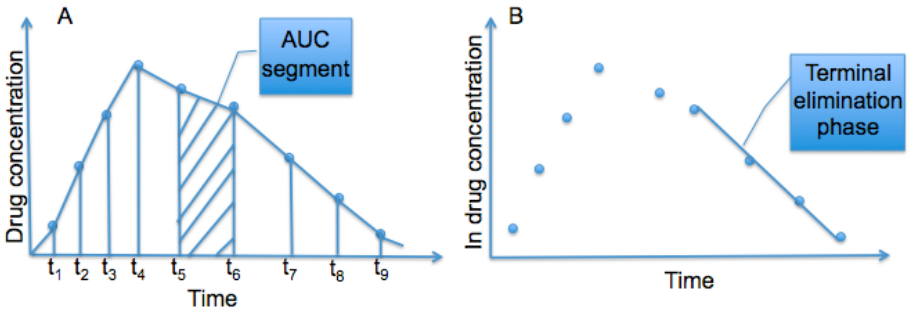

Figure 1.14 Determinations of A) area under the curve ($AUC_{t0\text{-}tlast}$) using the linear trapezoidal rule, which is an expression that sums up individual segments under the curve B) Elimination rate constant, k, from the log-linear terminal elimination phase.

1.5.4 ANIMAL MODELS AND THEIR SHORT-COMINGS

Laboratory animals including mice and rabbits are frequently used as models in pharmacokinetic studies. Nevertheless, inter-species anatomical differences, especially vitreous volume and vitreous diffusional path length, may make the direct

allometric translations of data to the human model unreliable. The vitreous volume in the rabbit is around 1.5 ml, about one third the vitreous volume in man. As a direct comparison, the amount in terms of initial concentration, achieved in human eyes would only be about 35% of that in the rabbit. The increased vitreous volume could account for the differences in the estimated pharmacokinetic parameters since a larger vitreous volume would imply a longer duration required for equivalent distribution.

In addition, a difference in vitreous diffusional path length affects drug distribution. Hughes and colleagues collated the results from histological examinations, which were in part previously reported by Short in 2008 as shown in Figure 1.15 (Hughes, 2008; Short, 2008). From these cross-sections, the authors calculated the theoretical diffusional distances across the eye and the data illustrate the dramatic differences. For example, the vitreous diffusional path length in the rat and rabbit is estimated to be 4.4 mm and 9 mm respectively compared to the distance in the human of 22 mm. Since the diffusional drive decreases according to the square root of time, the resulting concentrations at a distant target risk being too small to be effective from a depot placed in the anterior globe. In terms of clearance, the shorter vitreous diffusional path length in the rabbit reduces the half-life by 1.7 times for posterior clearance and is twice as fast for anterior clearance as compared to man (Maurice and Mishima, 1984). In a recent study by Zhu and colleagues (Maurice, 2001; Zhu *et al.*, 2008), the terminal half-life of bevacizumab in humans was shown to be 6.7 days compared to 4.3 days measured in the rabbit (Bakri *et al.,* 2007). Overall, the divergence of drug clearance rates from human suggests that experimental data obtained from animal studies cannot be directly translated for human application.

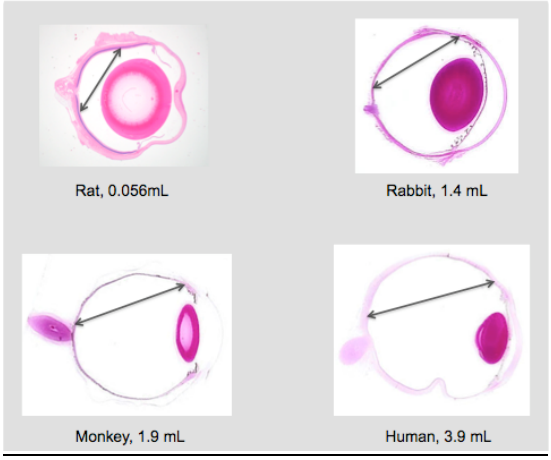

Figure 1.15 Examinations of the histological cross-sections of animal ocular tissues (Hughes, 2008).

1.6 DISEASES OF THE POSTERIOR SEGMENT OF THE EYE

1.6.1 AGE-RELATED MACULAR DEGENERATION (ARMD)

ARMD is a common cause of irreversible blindness among the elderly in the developing countries. Worldwide, 20-25 million people are affected and this figure will rise by three fold in 30-40 years time due to the expanding elderly population (Chopdar *et al.,* 2003).

ARMD can be described as a disorder of the macula area, which is important for central vision (Matthew *et al.,* 2003). Two forms of ARMD identified clinically, which are the 'dry' and the 'wet forms. Both forms of ARMD are the consequence of an inherent deficiency of retinal pigment epithelium cells in the metabolism of abnormal substrates such as damaged photoreceptor molecules and melanin granules. With age, the content of the residual bodies builds up in the retinal pigment epithelium (particularly at the macula region of the retina), leading to the formation of lipofuscin, basal laminar deposits and drusen. This blocks the nutrient exchange between the choroicapillaries and the retina leading to progressive degeneration of retinal pigment epithelium cells. This form of ARMD is described as the 'dry' type

ARMD, and blindness will only take place after a few years (Chopdar *et al.,* 2003, Young 1987)

Whilst, the 'wet' form of ARMD develops when the choroidal vessels grow into the Bruch's membrane lies beneath the basal laminar layer of the retinal pigment epithelium. These new vessels are fragile, they bleed into the retinal pigment epithelium and subretinal space through the gaps where attachment has been weakened during the calcification of the drusen. As a result, retinal detachment and degeneration of retinal pigment epithelium and photoreceptors at the macula occur. This subsequently leads to rapid vision loss. Clinically, wet ARMD is more sight-threatening and accounts for 80%-90% of the visual loss (Chopdar *et al.,* 2003; Mathews *et al.,* 2003).

Currently, pegaptanib (Macugen®) and ranibizumab (Lucentis®) are approved treatments for wet ARMD (Abraham-Marin *et al.,* 2007). They are anti-VEGF (vascular endothelial growth factor) agents injected intravitreally every six and four weeks respectively. Lately, bevacizumab (Avastin®), a drug treatment for colon cancers has been employed as an angiogenesis inhibitor to prevent the formation of new blood vessels in wet ARMD. Despite being effective and well tolerated, the off-label application has yet to be officially approved.

1.6.2 GLAUCOMA

Glaucoma (Glaucomatous optic neuropathy) is defined as a progressive optic neuropathy, characterized by optic nerve damage and retinal ganglion cell loss, related partly to abnormal intraocular pressure (IOP) (EID and Spaeth, 1999; Kroese *et al.,* 2002). It is the second leading cause of blindness worldwide after cataracts (Kroese *et al.,* 2002; Quigley *et al.,* 2006; Fung *et al.,* 2007). Estimates that 60 million people around the world will be affected by 2010 with open-angle glaucoma and angle-closure glaucoma were published some time ago (Quigley *et al.,* 2006; Fung *et al.,* 2007).

The treatment of glaucoma involves the use of intraocular lowering agents that either reduce the formation of aqueous humour (such as beta-blockers, carbonic anhydrase inhibitors and sympathomimetics) or increase the aqueous outflow (such as prostalglandin analogue, parasympathomimetics and sympathomimetics). Nonetheless, optimal control of intraocular pressure in glaucomatous patients does not seem to stop retinal ganglion cell death and subsequent vision loss. This suggests that a neuroprotective agent should be used in conjunction with current therapeutic treatment. Neuroprotection can be achieved by blocking the glutamate action through inactivating the *N*-methyl *D*-aspartate (NMDA) receptor. One such example is memantine, which is an uncompetitive NMDA receptor antagonist, has been shown to be neuroprotective in several animal models (WoldeMussie *et al.,* 2002). Memantine operates by a single mode of mechanism of action and therefore, will have no effects against other physiological chemicals such as TGF-β and TNF-α that are released concomitantly during the apoptosis process. Additionally, this would also suggest that the activity of memantine would only be limited to ganglion cells with a decent density of NMDA receptors. For these reasons, the inadequate clinical efficacy of oral memantine seen in glaucomatous patients during phase 3 clinical trial could be partially explained. Having to make this point, however, the idea of neuroprotection should not be abandoned and it remains crucial in the treatment of glaucoma. Substances with multiple mode of action such as epigallicatechin gallate (ECGC) might have more potential in this context or even a combination of memantine and ECGC has been proposed to be useful (Osborne, 2009).

1.6.3 UVEITIS

Generally, uveitis refers to the inflammation of the uveal tract, which comprises of the iris, ciliary body and choroid. It occurs in 38 to 714 people out of 100,000 in the population and is more prevalent in the younger age group of between 29 to 59 years old. Uveitis accounts for approximately 10% of visual impairment in the Western communities (Wakefield *et al.,* 2005). Uveitis can be caused by the microorganisms present within the host, microorganisms that invade from the environment or external injury to the uvea (Kanski, 1987).

Uveitis is a medical condition that usually requires prolonged treatment (Mruthyunjaya *et al.,* 2006) and recurrence remains an issue to its managements. Intravitreal injection of triamcinolone acetonide has been attempted and it is useful for short-term delivery that lasts for approximately 3 months. Therapeutic maintenance is better achieved with the use of fluocinolone acetonide implant, which can sustain delivery for approximately 3 years (Jaffe *et al.,* 2005; Mruthyunjaya *et al.,* 2006). The main concerns with regards to the use of intraocular corticosteroids are the development of cataracts and increase in intraocular pressure. Therefore, the majority of patients receiving treatment for uveitis may need to take antiglaucomatous agents or undergo trabeculectomy or cataract surgery. This will limit its applications in patients of a younger age. Biodegradable tacrolimus scleral plugs and a cyclosporine A intravitreal implant have been developed. The implant was shown to be non-toxic and effective in suppressing the inflammation of experimentally induced chronic uveitis (Dong *et al.,* 2006). Newer treatments such as infliximab (a monoclonal anti-TNFα antibody) and interferon alpha have been evaluated in patients with refractory posterior uveitis. However, their efficacy and safety profiles have yet to be confirmed in more controlled studies (Bodaghi *et al.,* 2007). In addition, bevacizumab has been proposed for patients with severe uveitis to prevent the development of proliferative vitreoretinopathy (Sugita, 2007).

1.6.4 CYTOMEGALOVIRUS (CMV) RETINITIS

Cytomegalovirus retinitis is an opportunistic herpes viral inflammation of the retina affecting 6-38% of patients with adenovirus immuno-deficiency syndrome (AIDS). Typically, initial symptoms include blurred and reduced vision as well as loss of peripheral or central vision, although in some patients, CMV retinitis may be asymptomatic (Friedbergh, 1997). Retinal detachment was a common complication before the initiation of highly active antiretroviral therapy (HAART) but the onset varies with the condition of the vitreo-retinal attachment; slower in younger patients with well-formed attached vitreous (Williamson, 2008). CMV retinitis will eventually lead to blindness if untreated.

The treatment of CMV retinitis involves the use of high dose antiviral agents to reduce the viral load and disease progression. Official treatments for cytomegalovirus retinitis include ganciclovir, foscarnet and cidofovir, which can be administered locally via the intravitreal route (Friedbergh, 1997). Intravitreal delivery is justified for patients who have failed to respond to systemic therapy or are unable to tolerate the associated side effects. However, relapse could occur when inadequate doses or frequency of injections were given. Therefore, while intravitreal injection is effective for temporary control of CMV retinitis, chronic maintenance is more efficient with controlled release ocular devices. Ganciclovir sustained release ocular implant (Vitrasert) has been proven to be effective in suppressing the progression of retinitis for up to 8 months with a lower relapse rate as compared to intravenous route of administration. Additionally, Vitrasert has been shown to improve patient's quality of life, with a significantly reduced occurrence of systemic related side effects (Muccioli and Belfort, 2000).

1.6.5 AGEING VITREOUS

With age, the vitreous humour undergoes progressive structural and biochemical changes. These processes are usually described as vitreous syneresis (contraction) and synchisis (liquefaction). The mechanism by which vitreous degeneration occurs remains uncertain, but a few mechanisms has been proposed. Visible light excites riboflavin to generate harmful radicals and oxygen species such as superoxide anion, hydrogen peroxide, hydroxyl radical and singlet anion (Ueno *et al,* 1987; Akiba *et al.,* 1994). These components were known to account for the degradation of hyaluronan and cross-linking of calf collagen *in vitro* (Akiba *et al.,* 1994, Kakeshi *et al.,* 1994) and *in vivo* (Ueno *et al.,* 1987). Based on the fact that riboflavin is a photosensitizer that exists naturally in the vitreous environment, the authors proposed that light exposure could be the mechanism underlying the occurrence of age-related vitreous degeneration. In addition, Akiba (1995) showed that whole serum as well as a combination of serum protein (transglutaminase) and fibronectin promotes collagen cross-linking leading to vitreous gel contraction. The leakage of

plasma proteins from the intravascular space into the vitreous body is possible as a result of vascular incompetence associated with aging retinal and cilliary body vasculature (Sebag, 1989). This clinical scenario is reflected by the increased concentration of soluble proteins in the vitreous, from approximately 0.5-0.6 mg/ml at ages 13 to 50, to 0.7-0.9 mg/ml at ages 50-80 and 1.0 mg/ml above 80 years. Furthermore, age-related increase in proteolytic activities within the vitreous may also contribute to vitreous liquefaction (Thomas, 2000). The concentration of plasmin, a proteolytic enzyme in the vitreous was found to increase with age, which may be caused by the degeneration of surrounding tissues. In the vitreous, plasmin may combine with membrane type matrix metalloproteinase-1 (MMP-1) to activate progelatinase-A (proMMP-2), which has been documented to have the capability to cleave off hybrid type of V/XI collagen and liquefying the vitreous gel *in vitro* (Brown *et al.,* 1996).

Balazs and Denlinger first established human vitreous liquefaction in a post-mortem biopsy test performed on 610 human eyes of age around 5-90 years (Balazs, 1982). They measured the volume of vitreous gel and liquid separately and plotted them against the age of the donor. According to the volume-age chart, young human adults of around 20 years of age have an approximately 80% gel phase whereas this figure decreases to about 50% in the elderly population above 60 years. This shows that the decrease in gel volume was accompanied by a parallel increase in liquid volume.

Later, Sebag and Balazs illustrated these changes seen in the elderly eyes using dark-field slit-biomicroscopy (Sebag and Balazs, 1985; Sebag, 1987). Human vitreous from donors aged 53-88 years were dissected from the sclera, choroid and retina with the anterior segment remained attached. Without any tissue fixations, the vitreous was mounted in a transparent chamber containing isotonic saline and sucrose (3.5 g/L). Bundles of parallel and thick fibers coursing along the anterior-posterior direction as well as areas of liquid pockets can be seen in the vitreous of a middle age man by trans-illumination as illustrated in Figure 1.5. These structures became more prominent in the vitreous of an older person (80-90 years) where fibers were no longer parallel and linear in shape but rather tortuous and broken in structures as

described by the authors. Additionally, enlarged liquid pockets in areas devoid of collagen fibers can also be seen at the central and peripheral areas of the vitreous. Therefore, disruption of the fibrous structure and advanced liquefaction leads to eventual collapse of the whole vitreous; observations which can be explained by changes to the organization of the vitreous components. Chondroitin sulfate, hyaluronan and opticin, which previously filled the space in between fibrils, are dissociated from the collagen fibrils leading to lateral aggregation of collagen fibrils into bundles of fibers (Bishop, 2000). As a result, areas devoid of collagen fibrils are filled with liquid vitreous containing depolymerized hyaluronan and other soluble substances (Bishop, 2000). As opposed to a juvenile vitreous (Figure 1.5), the elderly vitreous is more fibrous in appearance and shrunken in size. Nevertheless, these subtleties, which appear as a result of the aging process are not evident on simple dissection of the eye and are often neglected. Drug delivery stratagems have therefore tended to ignore the ageing changes in considering the pathophysiology of the elderly patients. This property may have a significant impact on drug disposition and clearance, and is therefore the subject of this thesis.

Figure 1.16 Vitreous structural changes with age. A. Vitreous humour of a 6 year-old child (x 4); B. Vitreous humour of a 59 years old adult (x 8.3); C. Vitreous humour of a 88 years old adult (x 2.7) (Adapted from Sebag, 1987). The lower part of the image indicates the position of the lens.

1.7 RESEARCH OBJECTIVES

The primary objective of this thesis was to investigate the effects of aging vitreous on the ocular disposition of brimonidine, either administered as a single intravitreal injection or within an intravitreal drug delivery system. In order to achieve this goal, a basic understanding of vitreous structure was needed and an animal model with a similar degree of vitreous liquefaction to that observed in the elderly population had to be developed. With this in mind, the following studies have been performed to achieve the above objectives.

1) Characterization of the rheological properties of the ovine vitreous using a rheometer and optical tweezers in Chapter 2 with the aim to understand the regional variation in the viscoelastic properties within the vitreous humour.

2) Development of an *ex vivo* vitreous imaging technique to visually study the vitreous microstructure and intravitreal events in Chapter 3.

3) Development of a partially liquefied vitreous model in Dutch-belted rabbits using hyaluronidase in Chapter 4. The effects of vitreous liquefaction on intravitreal distribution were investigated on three molecular probes of different molecular weights, namely sodium fluorescein, fluorescein isothiocyanate-dextran 150 kDa and a 1µm fluorescent particle suspension using the ocular fluorophotometer and HRA 2.

4) Development of a biodegradable and injectable posterior segment ocular drug delivery system (DDS) that releases brimonidine in a controlled manner for a period of one month in Chapter 5. The DDS was produced using Poly D, L-lactide (PLA) and Poly D, L-lactide-co-glycolide (PLGA). DDS with the optimum release characteristic was used in the preclinical drug development studies in Chapter 6. Brimonidine was selected in this study due to the fact that it is currently undergoing clinical trials for treating patients with geographic atrophy associated with age-related macular degeneration and

retinitis pigmentosa. Therefore, the data generated will be relevant as it specifically targets the elderly population.

5) Finally, pharmacokinetic studies investigating the effects of partial vitreous liquefaction on the ocular disposition of brimonidine administered as a single intravitreal injection or as a single intravitreal DDS are described in Chapter 6. The studies were conducted in the same model as that developed in Chapter 4. Tissue concentration of brimonidine was quantitatively measured using liquid chromatography-mass spectrometry (LCMS-MS) analytical technique and the data was analyzed using a non-compartmental model.

CHAPTER 2: CONVENTIONAL AND NOVEL CHARACTERISATIONS OF THE VITREOUS RHEOLOGY

2.1 INTRODUCTION AND OBJECTIVES

In juvenile vitreous, pseudoplastic hyaluronan that is trapped within the elastic collageneous network contributes to the stiffness of the vitreous gel by imposing an internal tension against the collagen fibrils as it swells to achieve an equilibrium hydration state (Nickerson *et al.,* 2005). However, owing to the unequal distribution of the collagen and hyaluronan (Balazs, 1960; Lee *et al.,* 1994b; Matsuura *et al.,* 2004), the gel phase is in essence non-homogeneous in its viscoelastic properties and density (Zimmerman, 1980; Lee *et al.,* 1992; Lee *et al.,* 1994a). Normally these changes are not visible to the naked eye. However, when there is a change to the chemical structures of the macromolecules, for instance, during vitreous syneresis and synchisis in the elderly, the non-homogeneous matrix becomes apparent and appears as coarse fibers and liquid pockets under trans-illumination (Sebag and Balazs, 1985). In this case, rheological measurement of samples taken from various points in the vitreous is useful to show the change in vitreous structure from a biochemical perspective (Bettelheim and Zigler, 2004).

Fowlks (1963) has suggested the presence of a meridonial flow at the periphery of the vitreous, flowing from the corona ciliaris to all points of the retina. Diffusion processes within the pararetinal zone of the vitreous were postulated to be relatively fast, since small molecules injected via the pars plana could reach the posterior pole (4-5 mm from the optic nerve head) in as short a time as 15 minutes (Fowlks, 1963). This rate of solute movement reflected a region of lower resistance to flow compared to that in vitreous core. It is expected that drug movement through this region of low viscosity will influence exposure of the tissues.

Rheological studies of the vitreous humour have been performed previously by several investigators whose research focused on potential vitreous substitutes (Mensitieri *et al.,* 1994; Suri and Banerjee, 2006; Swindle *et al.,* 2008) and the

understanding of the physiological structures and functions of the vitreous humour (Bettelheim and Wang, 1976; Zimmerman, 1980; Tokita *et al.,* 1984; Lee *et al.,* 1992, Lee *et al.,* 1994a; Nickerson *et al.,* 2005). From these studies, it was appreciated that the composition and structure of the vitreous macromolecules varies among animals of different species (Lee *et al.,* 1994a; Lee *et al.,* 1994b; Noulas *et al.,* 2004) and hence species-variation in rheological properties is not unexpected. While bovine and porcine vitreous humour were most commonly studied. Ovine (sheep) vitreous has received limited study. Sheep eyes are easy to obtain at the local abattoir from freshly slaughtered animals and have little use in the food industry. We have not successfully identified a study with a detailed description of the rheological properties of the ovine vitreous, except that by Mensitieri *et al.,* (1994) in which details of the measurement protocol were only briefly mentioned.

The gap in this area of research together with its relevance to our goal is the primary focus of this chapter, which was to investigate the viscoelastic properties of the ovine vitreous humour. In tackling the objective, a rheological protocol based on standard viscometry and oscillatory tests was developed, to investigate different areas of the ovine vitreous humour. This was appropriate since the vitreous is a heterogeneous matrix and regional samplings would provide more meaningful data to aid interpretation. The secondary objective of this chapter was to establish the application of optical tweezers in quantifying the viscosity of the liquid vitreous. In this experiment, a rabbit model was used rather than sheep since the volume of the liquid phase is generally larger in rabbit than in sheep, which makes the measurement easier at this stage of method development. The use of optical tweezers was aimed at overcoming some of the drawbacks (which will be discussed later) related to conventional rheological analysis, and allow measurements to be performed in an intact eye preparation.

2.2 MATERIALS AND METHODS

2.2.1 RHEOLOGICAL MEASUREMENT USING A ROTATIONAL RHEOMETER

2.2.1.1 MATERIALS

Sodium chloride, minimum purity 99.5% Ultra (batch # 039K0175) was purchased from Sigma-Aldrich, Germany. Deionized water was obtained from the Purite deionized water dispenser system purchased from the Purite Ltd (Oxon, UK).

2.2.1.2 INSTRUMENTATION

Sodium chloride was weighed using a laboratory balance (Ohause, via VWR, UK). A computer-automated rotational rheometer (Bohlin Gemini HR Nano, Malvern Instrument Ltd, Worcestershire, UK) was used to perform the viscometry and oscillatory tests. Customized Malvern software was used for data acquisition and graph plotting during the rheological studies.

2.2.1.3 PREPARATION OF 0.9% SODIUM CHLORIDE SOLUTION

0.9 g sodium chloride crystal powder was dissolved in deionized water (100 mL) to produce a 0.9% w/v sodium chloride solution. The solution was vortexed for approximately 2 minutes to ensure complete dissolution.

2.2.1.4 VITREOUS SAMPLE PREPARATION

Fresh sheep eyes (age: 6 months-2 year) were obtained from a local abattoir and collected in an ice box, kept moistened with 0.9% sodium chloride solution at all times before analysis. Aqueous humour was first aspirated using a syringe with an

attached 27-gauge needle. The cornea, iris and lens were carefully removed using a pair of scissors and forceps, leaving the vitreous humour retained within the posterior vitreous cavity. The regional separation technique employed by Lee and colleagues (1992) was modified slightly and adopted in this experiment as illustrated in Figure 2.1. A circumferential excision of approximately 2 mm of the sclera from the top edge of the vitreous opening was made, thereby exposing the vitreous base and the posterior half of the *pars plana ciliaris*. This region was excised across the eye horizontally using a scalpel and identified as the anterior region of the vitreous in this study. The centre region was obtained by scooping the middle zone of the vitreous 5 mm away from the retina from all angles using a round-edge plastic spatula. Since the sheep vitreous is sufficiently gel-like, the central vitreous was scooped out without the collapse and mixing of the gel. The remaining vitreous was regarded as the peripheral-posterior region, which was carefully removed using a pair of blunt forceps to avoid the retina peeling off. Then, a sufficient aliquot of sample representing each region was used for rheological measurements. For simplicity, the term peripheral-posterior region was replaced by posterior region for the rest of the chapter.

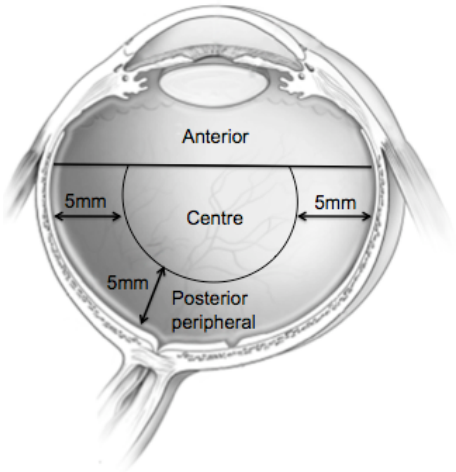

Figure 2.1 Regional sampling of the vitreous humour samples.

2.2.1.5 VISCOMETRY TEST

A viscometry test was performed using a rotational rheometer with a cone and plate (CP) 4^0 angle and 40 mm diameter in geometry to characterize the non-linear flow properties of the vitreous samples collected from different regions of the vitreous cavity. The measurement was started with a delay time of 3 minutes for the sample to equilibrate, followed by application of a low shear rate of 0.1/s, which was gradually increased to 100/s over a period of 60 minutes. Six repeated measurements were performed for each region to establish the reproducibility of the method parameters and instrument settings. The parameters and settings chosen in this study were optimized based on the flow dynamics observed through several experiments using different delay time, geometry and gap size. All measurements were performed at 37 ^{0}C to simulate body temperature, although the shear modulus of the vitreous has been demonstrated to be independent of the temperature at 10 ^{0}C to 40 ^{0}C (Tokita *et al.,* 1984). In order to avoid water evaporation and samples drying out over time, a moisture-controlled unit padded with wetted tissue papers was used to cover the samples in a way that a closed, humid atmosphere was generated. The viscosity measured under different shear conditions was plotted on a logarithmic scale from which, a regional variation in the flow properties of the vitreous could be compared and understood. Furthermore, the degree of damage caused by the steady shear force was investigated by repeating the analysis on the same sample for two separate occasions with a time interval of 5 minutes. A longer period was deemed not to be necessary, since the deformed samples would undergo further collapse under their own weight and subsequently dry out.

2.2.1.6 AMPLITUDE SWEEP

A parallel plate (PP) of 60 mm diameter in geometry was used with the rotational rheometer to determine the oscillatory strain amplitude confined within the linear viscoelastic region (LVR) of the vitreous samples. In this case, the cone and plate geometry was considered not appropriate as the high compression force imposed upon the centre of the sample will generate a non-uniform normal force profile and

destroy the vitreous network (Nickerson *et al.,* 2008). The samples were subjected to a range of oscillatory strain amplitude of 0.005-0.5, at a fixed frequency (1 Hz). The strain amplitude approximately 2/3 along the linear viscoelastic region was recorded and was applied in the following frequency sweep test.

2.2.1.7 FREQUENCY SWEEP

A parallel plate (PP) of 60 mm in geometry was used and the samples were subjected to a range of frequency (0.01-10 Hz), fixed strain (0.03) and initial stress (0.004) over a period of 45 minutes. Longer time length was not attempted as the sample edge started to dry out over time, which would lead to artificial data. The oscillatory strain amplitude was obtained through the amplitude sweep test. Similar to the viscometry tests, all oscillation tests were performed at 37 ^{0}C and evaporation was minimized using the same moisture-controlled unit aforementioned. The dynamic modulus of the samples including the elastic modulus (G'), viscous modulus (G"), dynamic viscosity (η'), complex viscosity (η*) and phase angle (δ) were calculated by the instrument software that tracked the magnitude and the phase lag of the torque at a given oscillatory frequency of the plate (Suri and Banerjee, 2006). The data was then plotted as a function of frequency (Hz). The dynamic viscosity-frequency (f) profiles were then fitted to a power law equation ($\eta' = Kf^{n-1}$) using Microsoft® Excel 2008, where consistency index (K) and power law index (n) for each region could be derived and compared.

2.2.2 VISCOSITY MEASUREMENT USING OPTICAL TRAPPING

2.2.2.1 MATERIALS AND INSTRUMENTATION

Phosphate buffered saline tablets (Batch #119K8219) were purchased from Sigma-Aldrich, Germany. Methylcellulose powder, USP (Metolose) 3.96 cP (Grade SM-4; Batch # 6065526) was kindly provided by Shin-Etsu Chemical Co. Ltd (Herts, UK). 3 μm polystyrene beads in dry powder and solution forms were purchased from

Polysciences Inc (Eppelheim, Germany). Sodium chloride was weighed using a laboratory balance (Ohaus, via VWR, UK). A propeller type overhead stirrer (Silverson SL2T, Chesham Bucks, UK) was used during the preparation of the methylcellulose solution.

2.2.2.2 PREPARATION OF PHOSPHATE BUFFERED SALINE (PBS)

A PBS tablet was dissolved in deionised water (200 mL) to produce 0.01 M phosphate buffer saline, pH 7.4 at 25 °C.

2.2.2.3 PREPARATION OF 2% (W/W) METHYLCELLULOSE SOLUTION

A methylcellulose viscosity standard was prepared by dissolving 2.0 g of powder in 100 g of deionised water and heated to 90 ^{o}C. The resulting mixture was stirred with a propeller-type stirrer until complete hydration and solution was achieved. The temperature of the solution was adjusted to 21 ^{o}C for use in the optical trapping experiments.

2.2.2.4 PREPARATION OF THE RABBIT LIQUID VITREOUS HUMOUR FOR ANALYSIS

Vitreous samples were obtained from six New Zealand white rabbits, age range 33-64 weeks, weighing 2.3-4.0 kg respectively. The rabbits were killed 5 minutes after being euthanized using an overdose of pentobarbital and were used secondary to another research project to minimize animal usage. The ophthalmic globe was dissected from the rabbit within 5 minutes of death. The globe was then washed with phosphate buffered saline to remove traces of blood. Subsequently a 25-gauge needle fitted to a 1 mL syringe was used to aspirate the aqueous humour to prevent contamination. An incision was made approximately 5 mm posterior to the limbus

using a scalpel. A pair of surgical scissors was used to cut along the sclera, taking care to separate the anterior from the posterior segment of the eye. On removal of the anterior segment, the adhesion between the lens and the anterior cortical vitreous gel was trimmed off with a scalpel. Subsequently, the liquid phase of the vitreous was separated from the gel phase and was poured into a cuvette for further analysis. To analyze the effects of freezing and thawing on the vitreous humour, the vitreous sample was frozen and maintained at -80 ^{o}C until required. On thawing, the liquid phase was isolated from the gel phase and loaded onto a sample cell followed by an addition of the 3 μm dry polystyrene beads. The sample cell was prepared by attaching a microscope cover slip (No $1^{1}/_{2}$) onto a metal plate with a hole in the middle as illustrated in Figure 2.2.

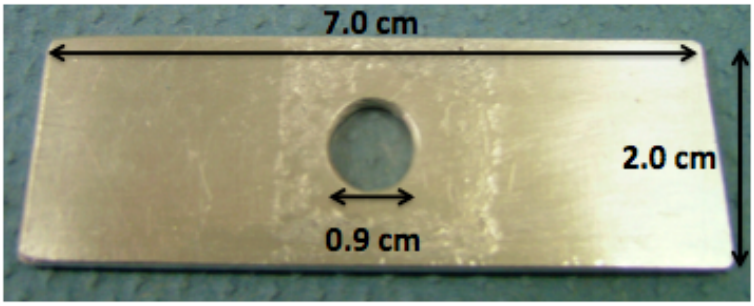

Figure 2.2 Sample cell of dimension 7.0 cm (width) x 2.0 cm (height) was made using a metal plate with a hole of diameter 0.9 cm drilled in the middle for sample loading.

2.2.2.5 OPTICAL TRAPPING

To characterize the optical trapping force and measure the local viscosity, we used an established technique known as the viscous drag force method (Malagnino *et al,* 2002). An optically-trapped particle was exposed to a viscous drag force by moving the fluid surrounding the particle. The viscous drag force, $F_{v.d}$, exerted on a particle trapped in a Newtonian fluid with a Reynolds number less than 1 can be expressed using Stoke's Law, such that,

$$\underline{F}_{v.d} = -6\pi r\mu \underline{V} \qquad \textbf{Equation 2.1}$$

where r is the radius of the particle, μ the viscosity of the surrounding fluid and V the relative velocity between the fluid and the trapped particle.

Figure 2.3 illustrates the optical configuration used for the measurements. A 532 nm continuous wave laser beam with a maximum power of 500mW was provided by a frequency doubled Nd:YAG source (LASER 2000, Northants, UK). The beam was elevated to the required height and expanded (x10) to fill the back aperture of the microscope objective (Nikon x100, 1.25NA Oil). The sample was illuminated by white light focused by an air objective (Nikon x10, 0.25NA) mounted opposite the trapping lens. This light was then collected by the trapping lens before being imaged onto a CCD camera (Pulnix, Progressive Scan) via a beam splitter. An orange filter was used to prevent the laser beam saturating the CCD array.

The sample was mounted on a piezo-electric stage (Hera P-625.ICD, Physic Instrument), which was moved at a known frequency using a signal generator (IOS-Tech IGC2231) in order to exert the viscous drag force. The signal and the subsequent stage motion were displayed on an oscilloscope to interrogate the system ensuring smooth sinusoidal movement. For all of the trapping studies, 3 μm diameter polystyrene beads (Polysciences Inc.) were trapped at a constant trap depth to remove the variability due to spherical aberration and surface effects (Vermeulen *et al.*, 2006). The amplitude of stage movement was kept constant at 46 μm and frequency increased until the stationary trapped bead escaped from the trap (Wright *et al.,* 2003).

The intra- and inter-day accuracy and precision were assessed by comparing the measured viscosity of the 2% (w/w) methylcellulose solution and with the data provided by the manufacturer (Certificate of Analysis, Shin-Etsu). System accuracy and precision were expressed as % accuracy and % RSD (relative standard deviation) respectively using the following equations.

Accuracy, % = [mean observed concentration/nominal concentration) x 100]

Precision, %RSD = [Standard deviation/mean x 100]

In order to calibrate the system and to determine its repeatability and day-to-day fluctuations, initial experiments were undertaken in water samples at the start of each day. A suspension of 3 µm polystyrene beads was used for both calibration and viscosity measurements.

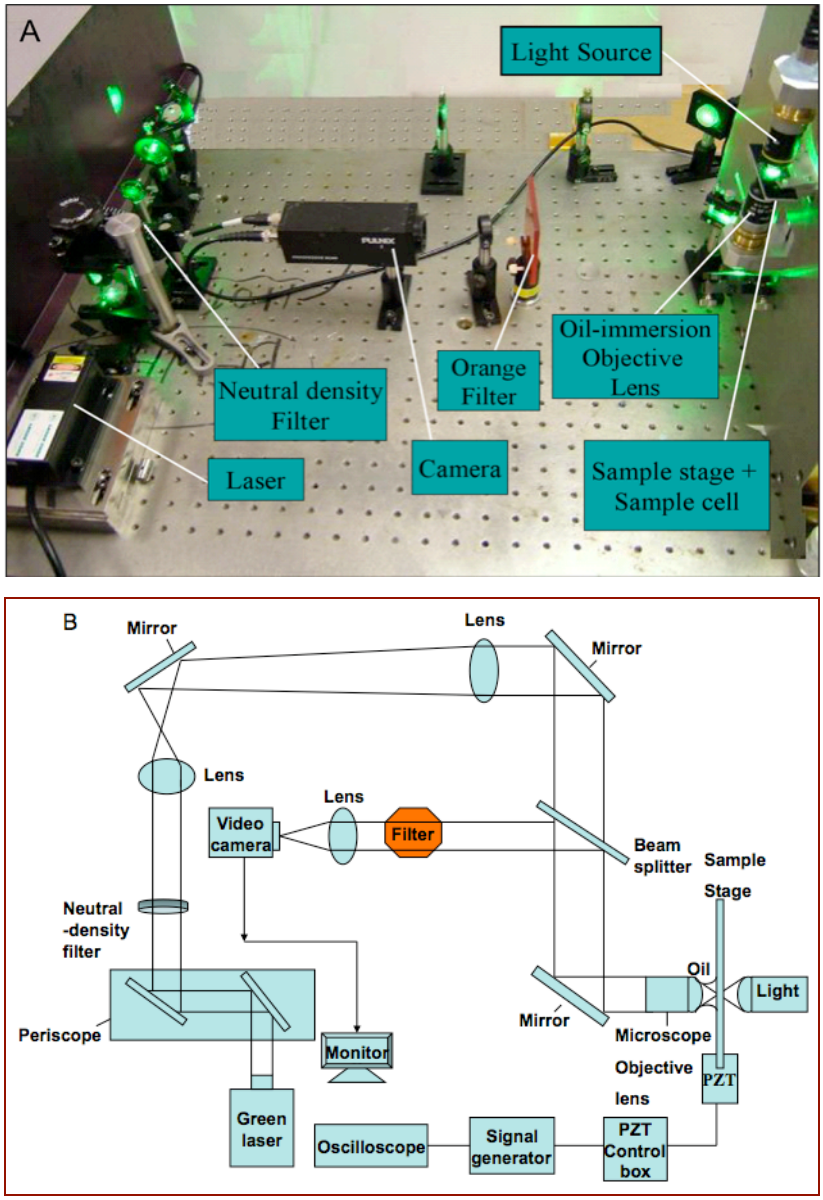

Figure 2.3 (A) Overview illustration and (B) Schematic diagram of the optical trapping system. **(**Courtesy of Mrs. Fiona Watt, IOP)

2.2.2.6 VISCOSITY MEASUREMENT

The viscosity was determined from plots of stage velocity at the point of particle release versus laser beam power. This relationship was compared for 3 μm beads trapped in both water and the test samples.

Assuming the optical trapping force, $f_{o.t.,}$ to be proportional to the laser beam power (P) and the refractive index (n) of the fluid surrounding the particle, $f_{o.t.}$ can be expressed as,

$$f_{o.t} = \frac{QnP}{c} \qquad \textbf{Equation 2.2}$$

where c is the speed of light and Q the quality factor describing the efficiency of the trap (Malagnino *et al.,* 2002). From equations 2.1 and 2.2, the gradient of velocity versus power plots can be expressed as,

$$\frac{dV}{dP} = \frac{Qn}{c6\pi r\mu} \qquad \textbf{Equation 2.3}$$

The trap efficiency and size of the trapped bead were assumed to be the same in water as in the samples of interest. The refractive indices for water (1.33), the vitreous humour (1.336) (Swindle *et al.,* 2007) and methylcellulose (1.3442) (Brau *et al.*, 2007) have been previously reported in the literature. Therefore, the viscosity of the samples of interest can be determined by comparison of the gradients of the velocity-power plots with respect to water.

Since the liquid phase studied is predominantly water and collagen fibres are not present, the low concentration of the solutes is unlikely to cause deviation from Newtonian behaviour (Repetto *et al.,* 2006). This was supported from measurements of the stress-strain relationship using conventional viscometry test.

2.3 RESULTS

2.3.1 RHEOLOGICAL MEASUREMENT USING A ROTATIONAL RHEOMETER

2.3.1.1 VISCOMETRY TEST

Figure 2.4 illustrates the shear thinning behaviour of the anterior, centre and posterior regions of the vitreous humour in a log-log scale. Viscosity decreases with increasing shear rate from 0.1 s^{-1} to 100 s^{-1}. The small standard deviations suggest good reproducibility of the rheological method for all studied regions. Signal noise was detected starting from the shear rates of 30/s, 20/s and 40/s for the anterior, centre and posterior regions respectively. Prior to these areas of noisy signal, a stretch of Newtonian flow period between 15-25/s, 10-20/s and 25-30/s were correspondingly observed in the viscosity-shear rate profiles (Figure 2.5). This suggests a period of time where pseudoplastic materials were absent from the measurement plates and fluid with Newtonian flow behaviour such as water was predominantly detected. Therefore, the noise signal that subsequently appeared could be due to the vitreous fluid drying out; whereas the absent of solutes such as that giving the non-Newtonian behaviour did not suggest disappearance, rather it appeared that materials were gradually stuck to the edge of the geometry as the plate rotating continuously over time.

Figure 2.6 shows that the viscosity of the vitreous obtained from the second measurement was lower than that established in the first measurement. This suggests that the steady shearing action imposed by the geometry irreversibly damaged the vitreous structure. The vitreous microstructure once broken down was unable to re-establish and the sample from the centre vitreous was damaged to a greater degree as compared to the anterior and posterior vitreous.

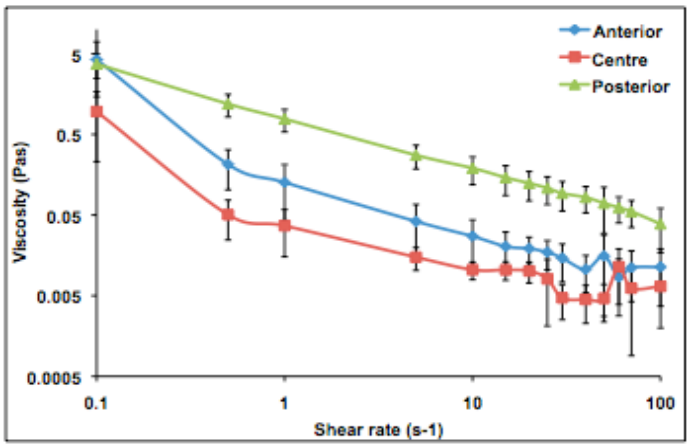

Figure 2.4 Viscosity (mean ± s.d) reduced with increasing shear rate at all regions of the vitreous humour (log-log scale). Signal noise was detected at 30/s, 20/s and 40/s for the anterior, centre and posterior regions of the vitreous humour respectively. A total of six samples (n=6) were examined for each study region.

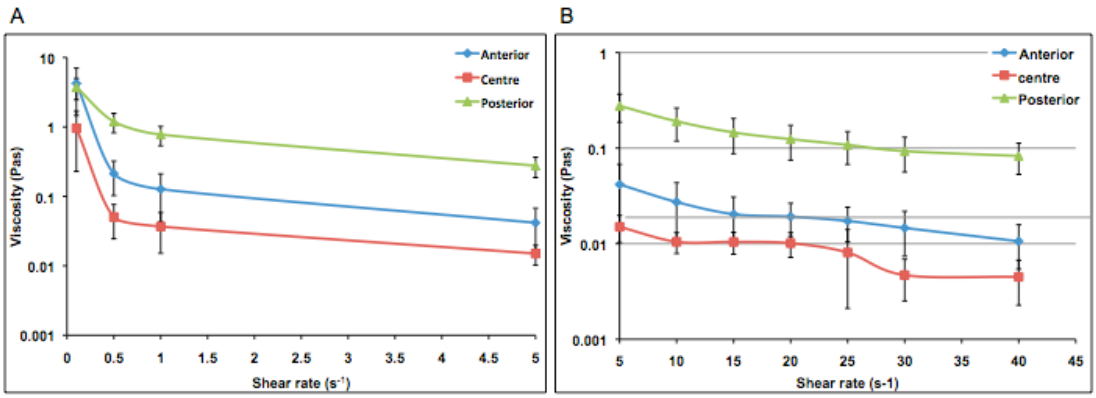

Figure 2.5 Vitreous samples exhibited Newtonian flow behaviour at high shear rate. X-axis is not in logarithmic scale in order to illustrate the actual shear rates imposed.

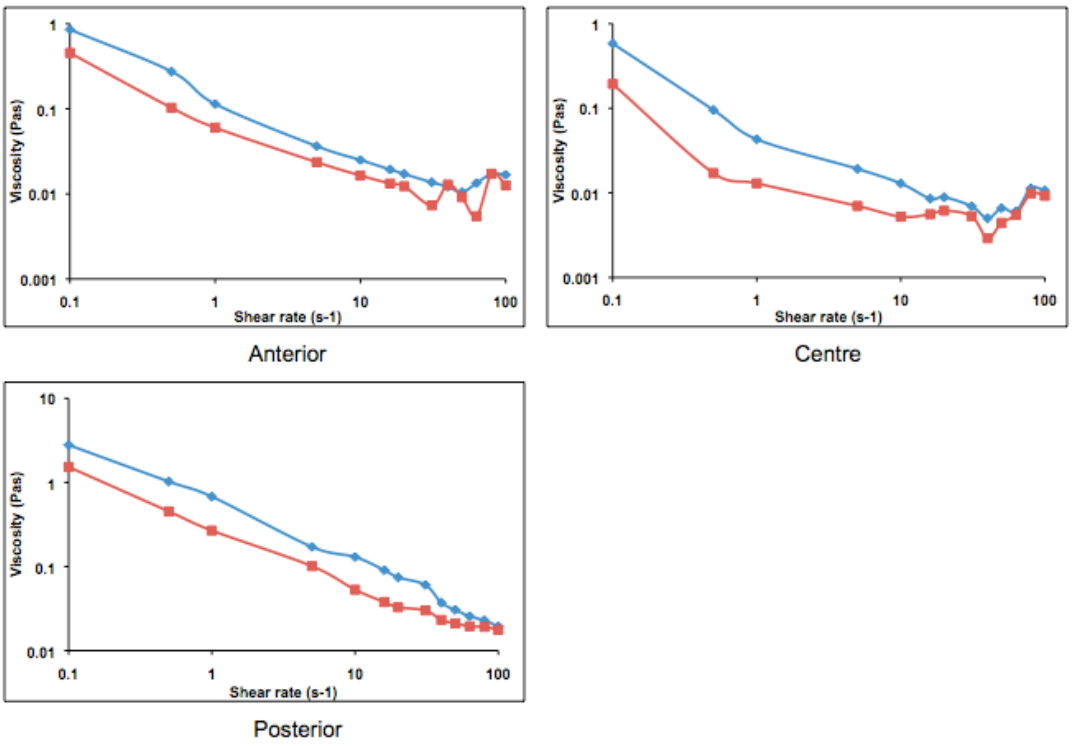

Figure 2.6 Viscosity curves of the anterior, centre and posterior vitreous when subjected to repeated analysis (log-log scale). The lower viscosity of the second measurement as compared to the first measurement suggests that the vitreous structures once broken down would not rebuild.

2.3.1.2 OSCILLATORY TEST

Logarithmic plots of the elastic modulus (G'), viscous modulus (G''), phase angle (δ^0) and complex viscosity (η') over a range of angular frequency (Hz) are as shown in Figure 2.7. The viscous moduli at the anterior, centre and posterior regions were 0.18 ± 0.02 Pa, 0.02 ± 0.01 Pa and 0.10 ± 0.02 Pa respectively; whereas the elastic moduli were 0.80 ± 0.07 Pa, 0.06 ± 0.01 Pa and 0.29 ± 0.03 Pa respectively. Good reproducibility was demonstrated by minimum degrees of standard deviation observed for all samples. The viscous and elastic moduli of the vitreous samples were almost a parallel function to the angular frequency and are significantly higher at the anterior region as compared to the posterior and central regions. The mean phase angle at the anterior, centre and posterior regions were 12.8 ± 0.5^0, 18.4 ± 3.0^0,

and 15.7 ± 1.2^0 respectively, below the gel-sol transition point of 45^0. Complex viscosity (η^*), which consists of both the viscous (dynamic viscosity,η') and elastic (η'') components decreased monotonically with angular frequency and the decreasing function was relatively linear. This suggests shear thinning, of which magnitude could be regionally compared for the three vitreous areas by fitting the dynamic viscosity to the power law equation.

Figure 2.8 shows the mean dynamic viscosity-frequency profiles of the vitreous fitted to the power law equation. An estimate of the goodness of fit was indicated by the correlation coefficient values of greater than 0.99 (Table 2.2). Table 2.2 also shows the consistency index (K) and power law index (n) calculated based on power law equation. The consistency index describes the viscosities of the fluid across the frequency range that was modeled. It was the highest at the anterior region and the lowest at the centre region. However, the power law index (n) calculated from the slope of the linear least-squares regression was an indicator for the rate of viscosity decrease with frequency. The lower power law index at the anterior region, suggested that the anterior vitreous was more prone to shear thinning than the centre and posterior.

Figure 2.9 compares the complex viscosity obtained from the oscillatory test to the shear viscosity measured using the viscometry test. It was found that shear viscosities were lower than complex viscosities for the anterior and centre but not for the posterior region. In other words, the shear viscosity of the ovine vitreous could be ranked in the order of posterior > anterior > centre; whereas the ranking for the complex viscosity was anterior > posterior > centre.

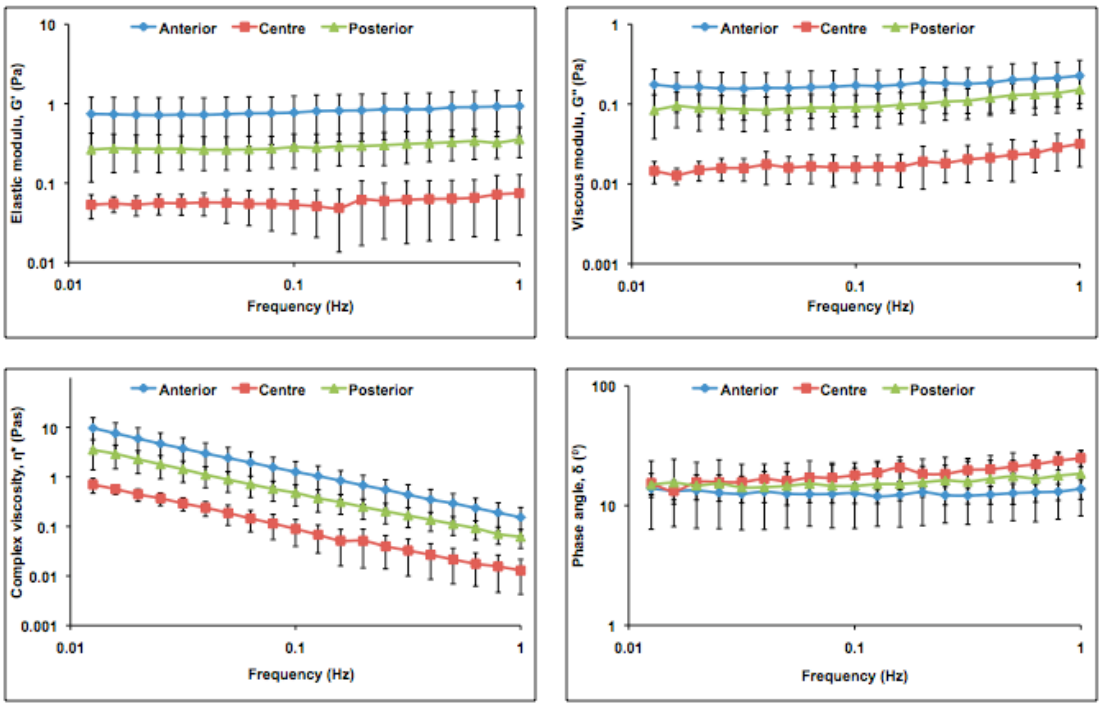

Figure 2.7 The mean ± standard deviation of the viscous modulus (G'), elastic modulus (G") (right panel), phase angle (δ^0) and complex viscosity of the anterior (n=5), centre (n=4) and posterior (n=5) regions of the vitreous humour when plotted against frequency in a log-log scale.

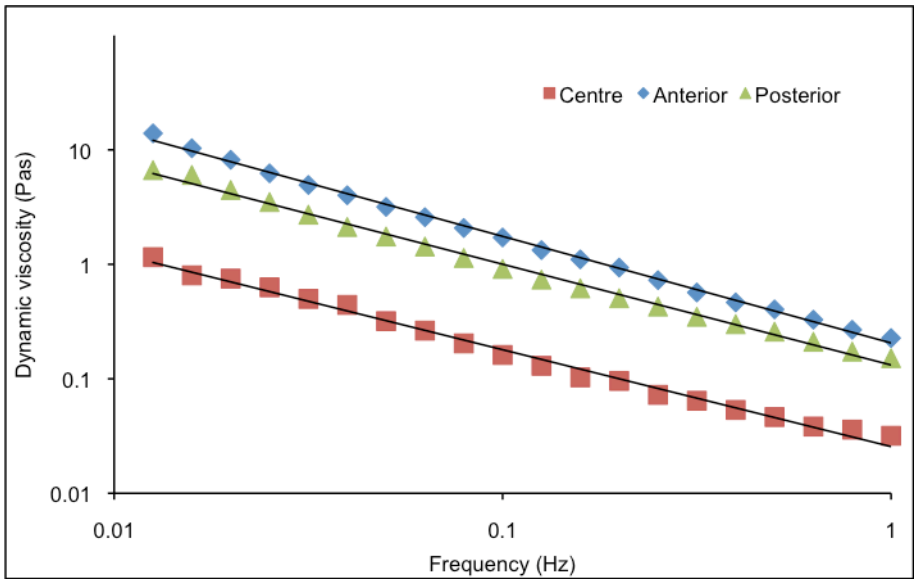

Figure 2.8 The mean dynamic viscosity-frequency profiles fitted to the power law equation.

Vitreous samples	Consistency (K), Pas	Power law index (n)	R-squared
Anterior	0.2055	0.068	0.998
Centre	0.0256	0.153	0.992
Posterior	0.1320	0.120	0.996

Table 2.2 Comparison of the consistency index (K) and power law index (n) of the vitreous at different regions within the vitreous cavity. The r-squared values of > 0.99 suggests good fitting of the vitreous dynamic viscosity-frequency profiles to the power law equation for shear thinning fluid.

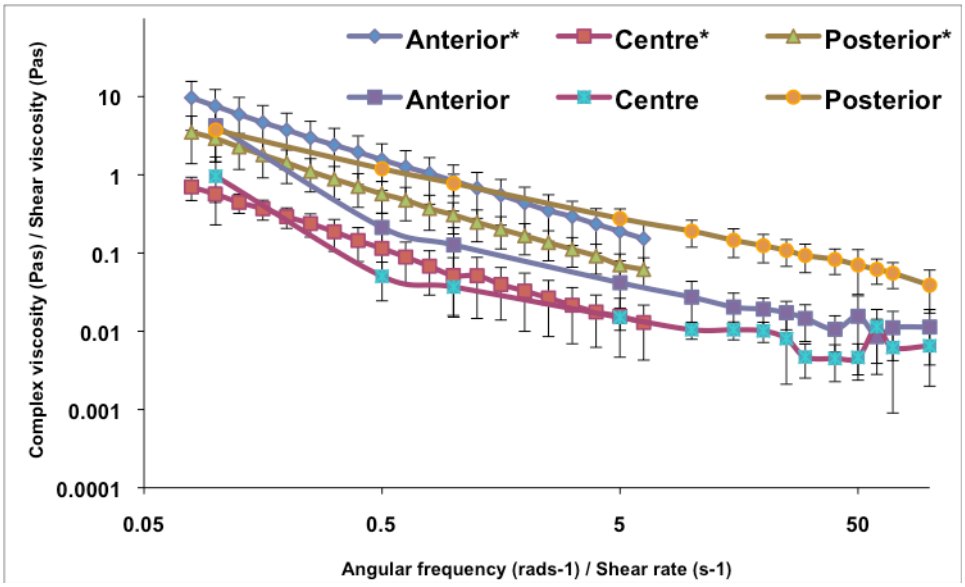

Figure 2.9 Comparison between the viscosity curves of complex viscosity (η*) against angular frequency ($rads^{-1}$) and shear viscosity against shear rate (s^{-1}). * symbol on the graph represents complex viscosity.

2.3.2 VISCOSITY MEASUREMENT USING OPTICAL TRAPPING

2.3.2.1 SYSTEM VALIDATION USING WATER AND 2% (W/W) METHYLCELLULOSE SOLUTION

Figure 2.10 shows a representative velocity-power plot comparing beads trapped in water to those trapped in methylcellulose solution. The experiment was repeated nine times over a 3 days period for validation purposes. All the results showed good linear correlation (R^2 = 0.99) between the fluid velocity and the laser beam power, demonstrating good system repeatability. Each point on Figure 2.10 represents an average of ten measurements used to determine the error.

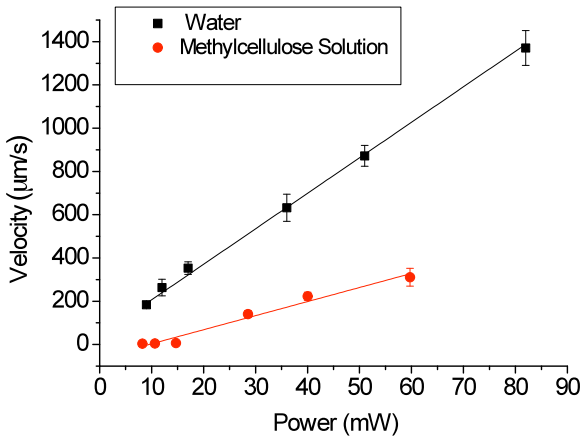

Figure 2.10 Stage velocity at the point of particle release against laser beam power for water and 2%(w/w) methylcellulose solution (n=3).

The measured viscosity of the methylcellulose was calculated to be 3.78 ± 0.12 cP which was in close agreement with expected values (3.96 cP). The intra- and inter-day system accuracy were found to be 98.39% and 95.56% respectively; whereas the intra- and inter-day system precision were 3.43% and 3.25% respectively.

2.3.2.2 VISCOSITY MEASUREMENT OF THE FRESH AND FROZEN LIQUID VITREOUS

Good linear correlation (R^2 = 0.98-0.99) between stage velocity at which the particle was released from the trap and laser beam powers was demonstrated in both fresh and thawed liquid vitreous (Figure 2.11). Each point on Figure 2.11 represents an average of eight measurements used to determine the error. The data suggests that at these forces the liquid vitreous behaves as a Newtonian fluid, confirming that equation 1 was applicable.

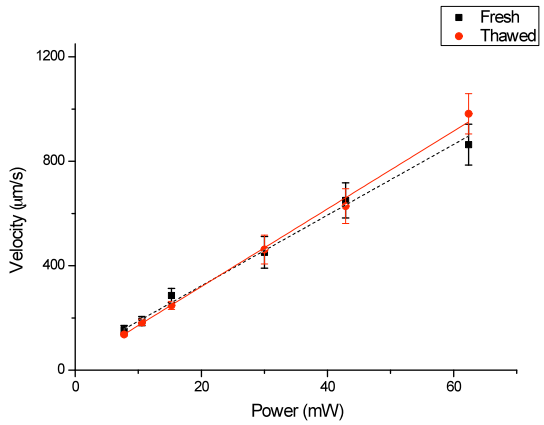

Figure 2.11 Plot of stage velocity at which the particle released from the trap at different powers for fresh and thawed liquid vitreous (n=6)

The viscosities of the fresh and thawed liquid phase vitreous, measured using the optical trapping technique are presented in Figure 2.12. Thawed samples were found to have lower mean viscosity (mean ± s.d., 1.46 ± 0.12 cP) with a larger standard deviation as compared to the fresh samples (mean ± s.d.,1.53 ± 0.07 cP).

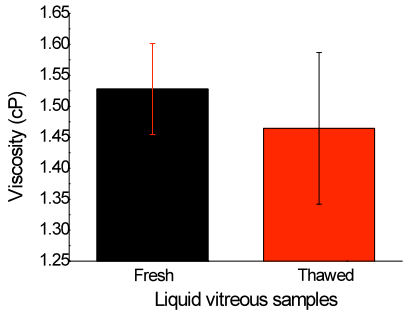

Figure 2.12 Effect of thawing on the viscosity of the liquid vitreous samples (n=6)

2.4 DISCUSSION

2.4.1 VISCOSITY MEASUREMENT OF THE OVINE VITREOUS HUMOUR

In this study, it was demonstrated that both the viscometry and oscillatory tests were able to measure the flow resistance of the vitreous humour. However, it will be important to also understand that the operating principles behind these two methodologies differed and therefore, results obtained may not be in agreement (Li *et al.,* 1997). The viscosity determined under continuous shear conditions by a rotational viscometry test is known as shear viscosity. Since shear viscosity changes with shear rates and temperatures, it is normally reported as a single value together with the conditions under which it was measured. On the other hand, the viscous behaviour measured by an oscillatory test is known as dynamic viscosity (η'), which is also referred to as the real part of the complex viscosity (η*) (Chan and Titze, 1999). Complex viscosity is a vector sum of both the viscous (η'=G"/ω) and elastic (η"=G'/ω) portions, which therefore provides a complete description on the viscoelastic behaviour of a non-Newtonian fluid. Since measurements were performed using very low amplitude stress, the periodic shear deformation was minimum and approximate to the resting state of the structure (Mensitieri *et al.,* 1994; Mezger, 2006a).

In the vitreous, the viscosity is predominantly contributed by the hyaluronan (Swindle and Ravi, 2007), and flow resistance will therefore be strongly dependent on the concentration and molecular weight of the solute (Falcone *et al.,* 2006). The η* obtained from the oscillatory data suggests that the anterior vitreous was more viscous than the posterior and centre regions. Although posterior regions contain a higher concentration of hyaluronan as reported by Balazs (Balazs, 1960) and Lee *et al.* (1992, 1994b) in cow, pig and human, there was a larger abundance of higher molecular weight hyaluronan in the anterior region (Bettelheim and Zigler, 2004). Therefore, as suggested by Bettelheim and Zigler, this may overcome the deficit in concentration and provided a more viscous environment to anterior vitreous. In

contrast to the η*, the shear viscosity obtained from the viscometry data was higher at the posterior region as compared to the anterior region. Such discrepancy suggests that there were different molecular interactions generating different forms of microstructures inside the vitreous system, which basically behave differently under the different types of deformation. The weak interactions between macromolecules with a high, complex viscosity in the anterior vitreous could be broken down under conditions giving rise to a measured lower shear viscosity; however, this could be compensated for in the posterior vitreous by other molecular interactions that were absent in the anterior vitreous including steric hindrance of the polymeric chain systems resisting de-entanglement or alignment, which would show an increase in the shear viscosity. Baxter *et al.,* (1971) and Fraser *et al.,* (1972) have shown that chemical bonding including electrostatic interactions between proteins and hyaluronan increased the strength of the collagen gel. Therefore, it was anticipated that the higher abundance of soluble proteins at the posterior vitreous as compared to the anterior and centre vitreous might facilitate the formation of a stronger fibrillar gel network. As a result, this explains the increased resistance to deformation of the posterior vitreous during the viscometry test.

Furthermore, the disagreement between the viscosity curves of shear viscosity and η* observed in this study has also been noted previously by Mensitieri and colleagues in the ovine vitreous (Mensitieri *et al.,* 1994). The authors attributed the discrepancy to the fact that the simple viscosity test would not correctly measure the flow dissipation energy of the vitreous humour. Shear viscosity relates to deformation of the entanglement network alone, the measurement of which is not sufficient to characterize the viscoelastic properties of a material. This may explain the measured lower shear viscosity than η* for the anterior and centre vitreous.

Additionally, the significant drop in the shear viscosity of the anterior and centre vitreous between 0.1/s and 0.5/s suggested that the vitreous was significantly deformed within the observed time interval; whereas a similar degree of viscosity (η*) decrement occurred over a wider range of frequency in the oscillatory test. This indicates that steady rate of shear was more destructive than sinusoidal oscillatory

shear to the vitreous structure as expected; and rotational shear rate as low as 0.5/s could destroy the vitreous network. Upon repeating analysis, the viscosities obtained from the second measurement were lower as compared to the first measurement, pointing towards irreversible network destruction. In this case, the interaction between polymer chains and fibrils would be degraded, leading to an irreversible damage (Mezger, 2006b) and the vitreous structure could not be reformed once broken. This observation is in line with the understanding of the ageing process where the vitreous structure does not redevelop following the onset of syneresis and synchisis. Therefore, based on the analyses presented, it will be appreciated that vitreous samples subjected to shear stress cannot be reused for further analysis. Moreover, the absences of a constant shear viscosity value in the low shear range of the viscosity curves suggests that the vitreous may consist of a lightly cross-linked network that was delicate and sensitive to deformation even when subjected to oscillatory shear at low frequency (Mezger, 2006b).

2.4.2 OVINE VITREOUS SHEAR THINNING

Although the viscometry test is destructive, the measurement provided a good illustration of the shear thinning and non-Newtonian behaviours of the ovine vitreous humour. Similar findings were also demonstrated in the oscillatory shear deformation test where dynamic viscosity decreased with frequency and further supported the viscometry result on vitreous shear thinning. Shear thinning, also known as pseudoplastic flow, is a characteristic property of chain-like linear macromolecules (Megzar, 2006b) and biological matrixes such as synovial fluids (Borzacchiello *et al.,* 2004) and blood (Anand and Rajagopal, 2004). The flow behaviour could be explained using the dynamics of entanglement (Borzacchiello, 2004). At rest, vitreous macromolecules such as hyaluronan adapt a random coil configuration. At the same time, these molecules can entangle together to form macromolecular aggregates above a concentration of 300-500μg/mL (Balazs and Denlinger, 1984). During the shear process, the molecules became disentangled and stretched along the streamline of flow (Mezger 2006b) alongside the collagen fibrils. In doing so, the polymer chains were able to slip through one another leading to a

decrease in the flow resistance. When the degree of disentanglement became greater at higher shear force, the molecules were deformed and the polymer chains and fibrils were torn into smaller fragments, which subsequently led to a decrease in flow resistance. In effect, the medium became thinner and the viscoelastic properties dissipated (Borzacchiello *et al.,* 2004). Both collagen (Lai *et al.,* 2008) and hyaluronan (Falcone *et al.,* 2006) are susceptible to shear thinning, which implies that the overall pseudoplastic flow of the vitreous resulted from contributions from the degradation of both macromolecules. In practice, the shear thinning behaviour of the vitreous suggests that it would be completely destroyed if it were to pass through a needle bore or vitrector during vitrectomy surgical procedure.

As modelled by the power law equation, the magnitude of flow resistance and shear thinning varied with vitreous location. Anterior vitreous was more viscous than posterior and centre vitreous over the measured range of frequency. The explanation for the regional variation in measured viscosity is as described previously (section 2.4.1). The more shear thinning behaviour of the anterior region on the other hand may imply that there is a higher content of higher molecular weight hyaluronan and larger abundance of collagen fibrils *in situ*. Falcone and colleagues have shown that higher molecular weight hyaluronic acid demonstrates shear thinning due to its longer polymer chains, which start to disentangled at low frequency of oscillations (Falcone *et al.,* 2006). Similarly, concentrated collagen solutions showed more shear thinning than lower concentrations (Lai *et al.,* 2008), although an explanation for this observation was not provided. The central region, which showed the least shear thinning and viscosity, reflecting an area with a lower concentration of viscoelastic solutes. This may be the reason for the higher tendency of vitreous liquefaction that appeared during development and aging processes to localize at the centre zone according to Denlinger and Balazs (1984).

2.4.3 RHEOLOGICAL PROPERTIES OF THE OVINE VITREOUS HUMOUR

The general trend of the mechanical spectra established in this study agrees with that reported by Mensitieri *et al.,* (1994) for ovine vitreous humour. However, our measured dynamic shear moduli were lower than that reported by Mensitieri's group. This could be attributed to a variation in sample handling method and the age difference between the animals used. Their measurements were performed on the whole gel and an average viscosity of the bulk sample was presented; whereas in our case, we performed a regional analysis. According to Nickerson and colleagues (2005), fluid rich in hyaluronan seeps out from the vitreous when it is removed from the eye. The gel mass decay following dissection was unavoidable and it was anticipated that gel mass loss would be even greater from our sample isolation technique. This may explain the lower moduli that we obtained as compared to those by Mensitieri *et al.,* (1994). With this proviso, the technique reported in this chapter has the advantage of exploring the regional variation in the rheological properties of the ovine vitreous. Additionally, the eyes employed in the other author's experiments were obtained from younger age group sheep of 1-2 months as compared to 6 months to 2 years old as used in our experiments. Physically, eyeballs of a few months old were generally smaller than that of 1-2 years old sheep, an observation that we made throughout the experimental study. Additionally, matrix differentiation has been microscopically illustrated by Los (2008) in the rabbit vitreous at different phase of maturation. Vitreous lamellae were found to grow broader at the age of 5-8 months as compared to 2 weeks old. Although similar growing process has yet to be established in the sheep eye, the difference in the size of the eyeball implies an underlying matrix development phase. Therefore, the older animals (larger eye globe size) that we used may partially explain the different results that we observed.

In addition, our data showed a consistently higher G' as compared to G" at all frequencies for the three studied regions, suggesting that the ovine vitreous overall is more elastic than viscous. The phase angle of smaller than 45^0 is typical of a solid-like gel behaviour. Based on these findings, therefore, we can deduce that the ovine

vitreous behaves as a viscoelastic solid-like gel that is more rubbery than viscous. Such rheological description matches exactly with that proposed by Mensitieri *et al.,* (1994) for their ovine samples. In fact, similar findings have also been reported for the bovine (Tokita *et al.,* 1984; Mensitieri *et al.,* 1994; Nickerson *et al.,* 2008), caprine (Mensitieri *et al.* 1994; Suri and Banerjee 2006), porcine (Mensitieri *et al.,* 1994; Nickerson *et al.,* 2008; Swindle *et al.,* 2008) and leporine (Mensitieri *et al.,* 1994) vitreous. This indicates that the vitreous humour of most laboratory animals is generally a viscoelastic solid-like gel, even though the absolute value varies among species. In addition, it was also noted that the elastic and viscous modulus were almost parallel across the whole range of frequencies, showing the vitreous is stable to the compression stress from strenuous physical activities and ocular trauma (Suri and Banerjee, 2006).

As demonstrated previously by Balazs, Lee and colleagues for human, bovine and porcine vitreous, the viscous and elastic behaviours vary with vitreous locations (Lee *et al.,* 1992; Lee *et al.,* 1994a). A similar finding was also observed in our study with ovine vitreous. G' was found to be the highest at the anterior region, followed by the posterior and the lowest at the centre region. These observations match the topographical variations in the abundance of vitreous macromolecules established in cattle. In cattle, Balazs (1960) has shown that the collagen fibrillar network was denser around the cortical gel next to the ciliary epithelium and retina at the ora serrata, which are areas within the anterior region defined in this study, and less dense at the rest of the areas adjacent to the retina, which corresponds to the peripheral posterior region of this study. The central region was the least structured zone where collagen fibrillar network was found to be the least dense at this location, explaining its lowest G' value as compared to others. As mentioned earlier, even though higher concentration of hyaluronan was found at the posterior region, viscous behaviour (G") was more notable at the anterior region, which was associated with the presence of higher molecular weight species that sufficiently overcome the deficit in hyaluronan concentration (Bettelheim and Zigler, 2004). This provides an explanation for the higher G" seen at the anterior region as compared to the posterior

regions. Coinciding with the viscometry data, the centre region was the least viscous among others.

Since we have correlated our data with that reported for other species, it is worth discussing a few comments presented previously by other authors on this aspect. It has been noted previously that regional variations in the mechanical properties and the concentration of macromolecules of the vitreous could be very sensitive to sampling location (Lee *et al.,* 1994b). For instance, Lee and colleagues have found a higher concentration of collagen and thus, greater elastic modulus (G') at the bovine posterior vitreous than anterior vitreous, contradicting to the earlier study presented by Balazs (1960). The authors attributed the discrepancy observed between the two studies to the fact that the anterior zone from their studies were obtained from the frontal area of the lens and pars plana; where in the case of Balazs, it was isolated from the small area behind the ciliary epithelium. Clearly, a deviation in sampling protocol made data comparison between studies more tricky in the sense that a small but influencing area in the vitreous would produce a great difference seen in the data produced. However, our data based on samples obtained from areas covering both the ciliary epithelium and frontal areas of the lens seems to fit better to that presented by Balazs than those by Lee and colleagues, indicating the contribution from the ciliary epithelium to overall result outcome was greater than that of the frontal area of the lens.

2.4.4 EFFECTS OF FREEZING AND THAWING ON THE RABBIT VITREOUS HUMOUR

Once the vitreous humour was removed from the globe, it collapsed with a loss of free water and dissolved solutes. Although a statistical difference between fresh and thawed samples was not evident, the increase in variability suggests processing changes have occurred. The solutes must contain some larger molecules contributing to viscosity, which did not reconstitute after a freeze-thaw cycle. Swann and Constable examined the changes in a mixture of sodium hyaluronate and bovine serum albumin following snap freezing in liquid nitrogen and also freezer storage at

-20 ˚C (Swann and Constable 1972). In both treatments, there was a loss of solid content, reflected in the reduction of hyaluronate in the thawed sample. This suggests that the liquid phase may be too dilute to reform as a hydrogel on thawing. Thus, freezing may interfere with the structure of the vitreous and therefore the evaluation of vitreous humour viscosity and measurements should always be made in eyes that are as fresh as possible.

2.4.5 THE APPLICATION OF OPTICAL TRAPPING IN VISCOSITY MEASUREMENT OF THE VITREOUS HUMOUR

We have demonstrated that optical trapping is a method suitable for measuring the viscosity of the vitreous humour. This was confirmed from results based on methylcellulose solution, which showed close agreement to expected values; however, further improvements are possible. The published values for the refractive index of the vitreous relate to the vitreous as a whole rather than the liquid phase although we believe this error to be small. Recent improved trap characterization methods, for example monitoring the Brownian motion of the trapped particle using a fast camera or quadrant photodiode (Keen *et al.,* 2007) have become available. Such techniques might improve the accuracy and repeatability of the measurement by removing the need to move the trapped particle relative to the fluid and hence minimize any potential sample damage. A key unavoidable error in our viscosity measurement is the variation in size of the particle, quoted by the manufacturer to be ± 0.16 μm.

In addition, this method has a few advantages over conventional rheological methods. The major advantage is that it only requires a small sample volume of 0.15 mL, which can be even smaller if a smaller sample cell were employed. This feature is particularly favorable in measuring the vitreous liquid phase, which otherwise would require pooling of samples from different animal eyes. Secondly, it is a less destructive method and measurements were performed at a micron length scale. This will then allow local viscosity rather than average viscosity of the bulk sample to be

quantified. Using this technique, regional dissection as has been done in this study could be avoided since multiple particles could be examined simultaneously in a single piece of gel. This will improve the accuracy and precision of the results. Therefore, the advantages provided by optical tweezers are clearly promising for samples with heterogeneous biopolymer distribution such as the vitreous humour. Further modifications to the current system will be undertaken to optimize the optical power and depth of field in order to extend its application to the whole vitreous humour. This will allow its future application in an intact eye based on the design of a Miyake-Apple eye preparation, which will be described in the next chapter.

2.5 Conclusion

A protocol for measuring the rheological properties of the ovine vitreous humour using a rheometer was successfully developed. Unlike previous studies, regional examinations of the ovine mechanical properties have been performed. Our measurements show that the ovine vitreous is a non-uniform matrix, with anterior region being more viscoelastic than the centre and posterior regions. However, the peripheral-posterior zone next to the retina was found to consist of a stronger fibrillar network that was capable of resisting a greater degree of deformation as compared to the rest of the vitreous. The unique design of the vitreous could protect the retina under strenuous condition and stress. Despite the regional variations observed, a unified conclusion could be drawn for all areas; the vitreous, is a lightly cross-linked viscoelastic solid gel, that is more rubbery than viscous. It exhibits pseudoplastic flow upon shearing and the structure, once deformed, is unable to regenerate. Therefore, samples cannot be reused after analysis.

In addition, optical tweezers were successfully employed to measure the local viscosity of the liquid vitreous phase. The method was used to quantify the viscosity changes induced by the freezing and thawing processes; with thawed samples generally having lower viscosity and a larger mean standard deviation. This observation may be a result of the water expansion effects that destroy the vitreous structure. Thus, freezing at -80 ˚C may not be an ideal storage condition for high water content tissues such as the vitreous humour.

CHAPTER 3: *EX VIVO* VITREOUS EXAMINATION AND IMAGING IN A MIYAKE-APPLE EYE PREPARATION

3.1 INTRODUCTION AND OBJECTIVES

The vitreous humour has a transparent structure with an extremely low light reflectivity and is inherently challenging to image. The tissue is enclosed in darkness within the posterior chamber by the sclera, choroid and retina alongside the lens at the anterior segment further limiting the visual examination. Isolation of the vitreous from the globe may allow complete imaging of the vitreous structure as has been performed by Sebag and Balazs using dark field slit-microscopy technique (see Chapter 1). However, vitreous mass decay following dissection procedure is unavoidable and more importantly, the effects of vitreous boundary on intravitreal kinetics could not be fully assessed. This in turn suggests that examination of an intact vitreous is strictly restricted to and from within the only ocular window, that is through the cornea.

Yamamoto and colleagues (2007) have utilized aqueous colloidal quantum dots as a method of detecting vitreous lesions in facilitating the imaging of the Weiss Ring that forms during the final step of posterior vitreous detachment (PVD). Using this method, the vitreous cortex was stained distinctly, thereby allowing a more confident vitrectomy surgical procedure to be performed in an intact eye preparation. Although the technique was deemed useful surgically, depth and field of view through the cornea remains an issue if the kinetics of the injected materials are to be followed. The inadequate vitreous imaging through the cornea leads to consideration of more advance imaging tools such as Magnetic Resonance Imaging (MRI). MRI allows the kinetics of molecular probe or drug delivery system to be evaluated effectively in a non-invasive fashion. Unfortunately, the application is limited by the number of useful agents of which gadolinium-diethylenetriaminopentaacetic acid (Gd-DTPA) is the most widely used as a contrast agent. This molecule has a molecular weight of

938 Daltons and is considered relatively small for assessing the diffusional barrier imposed by the vitreous structure, since the mesh structure as described by Worst and Los (1995) is coarse.

The lack of an adequate imaging technique to examine the vitreous structure *in situ* led us to develop a more versatile way of *ex vivo* imaging technique for vitreous examination. The design of the imaging technique was based on the Miyake-Apple eye preparation first introduced by Drs. Miyake and Apple for posterior photography of the intraocular lens. This technique is currently used by ophthalmologists in experimental surgery of the anterior segment of the eye (Chew & Werner 2006, Pereira *et al.* 2009); in this study, we used it to image the vitreous humour. As part of the study objective, we also assessed the feasibility of integrating the Miyake-Apple eye preparation to an arterially perfused enucleated eye model. The perfused eye model has several historical applications in pharmacology (Kodama *et al.* 1983, de Coo *et al.,* 1993, Shiels *et al.,* 1999) and pharmacokinetic research conducted by previous postgraduates in our laboratories (Zhu *et al.,* 1996, Koeberle *et al.,* 2006). The system offers several advantages over an *in vivo* experiment based on the fact that the isolation of the eye from the systemic circulation allows for complete control over the circulatory supply, and the results obtained were uncomplicated by the effects from other organ systems. Additionally, the perfusion experiment further benefits from the feasibility to generate a Miyake-Apple window on the sclera, a surgical procedure which would otherwise not be practical on a live animal. Eyes cannulated via one of the long posterior ciliary arteries and perfused with essential nutrients and supplied with metabolic needs, have been proven to remain viable for between 9 hours (Koeberle *et al.,* 2006) to 9 days (de Coo *et al.,* 1993). This preparation clearly complements the Miyake-Apple imaging technique as vitreous examination is conducted within an eye preparation that is physiologically viable. A cautionary observation is that the generation of a Miyake-Apple window on a perfused eye preparation may damage part of the circulatory supply that lies beneath the sclera, rendering the perfusion process unsuccessful. For these reasons, the validity of the Miyake-Apple perfused eye model was evaluated by monitoring the

viability parameters including the intraocular pressure (IOP), arterial perfusion pressure (APP), glucose consumption and lactate dehydrogenase enzyme levels.

3.2 MATERIALS AND METHODS

3.2.1. CHEMICALS AND REAGENTS

Minimum essential medium (M4655, LOT 107K2348), ethylenediaminetetraacetic acid (EDTA) (E9884, LOT 094K0195), penicillin G sodium salt (PENNA, LOT 086K1286), streptomycin sulphate salt powder (S6501, LOT 086K1263), gentamycin sulphate salt (G3632, LOT016K1120), insulin (I6634, LOT 126K1082), holo-transferrin (T1283, LOT 076K0421), atropine sulphate (11330, LOT 1278263), sodium selenite (S5261, LOT 106K1923), in vitro toxicology assay kit, LDH based (TOX-7, LOT 067K8406) and type-II S collagenase from clostridium histolyticum (C1764, LOT- 077K8615) were purchased from Sigma-Aldrich (Germany). Optium blood glucose test strips were purchased from Boots pharmacy (Glasgow, UK). A medical grade carbogen (95% oxygen and 5% carbon dioxide) gas mixture was bought from BOC gas (Surrey, UK).

3.2.2 ISOLATION OF OVINE VITREOUS

The ovine eyes were obtained fresh from the local abattoir in an ice box, 1-2 hours after the animals were killed. The aqueous humour was first aspirated using a 27G x ½ inch needle (Beckton Dickinson, Oxfordshire, UK) attached to a 1 mL syringe. A circumferential incision was then made approximately 5 mm posterior to the limbus using a scalpel, carefully separating the anterior from the posterior segment of the eye. Upon removal of the anterior segment, the adhesion between the lens and the anterior cortical vitreous gel was trimmed off using a scalpel. Subsequently, the vitreous was poured over onto a petri dish and due to the relatively large sample volume, approximately half of the gel phase was excised vertically along the optical axis and transferred into a cuvette for imaging purpose.

3.2.3 *EX VIVO* MIYAKE-APPLE EYE PREPARATION

The eyes were first inspected for corneal clarity and tissue quality to ensure no cataracts, perforation or infection had occurred to the eye. An 8 mm Siefel disposable biopsy punch (Schuco Int. Ltd, London, UK) was carefully used to create a circular window on the sclera. A pair of surgical scissors was used to trim off part of the sclera that was not completely removed; and tissue residues, if any, were gently removed using a pair of forceps. A thin layer of Loctite cynoacrylate super glue (gel type) was then applied to the sclera that formed the round edge of the window. Then, a 13 mm circular glass cover slip, no $1^1/_2$ (Agar Scientific, Essex, UK) was centered over the window and sealed upon carefully to avoid the formation of air bubbles. Gentle pressure was applied at the sealing points to ensure complete adhesion and the preparation was allowed to set for approximately 5 minutes. An illustration of the Miyake-Apple ovine eye preparation is as shown in Figure 3.1. The cornea of the eye preparation was irrigated with saline solution throughout the experimental studies to maintain corneal clarity and hydration.

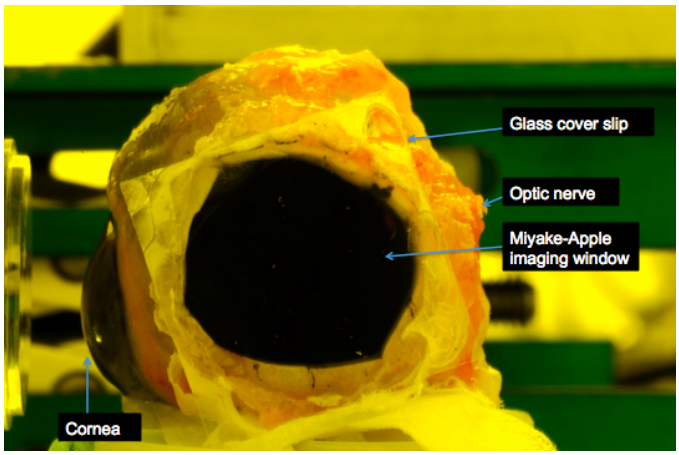

Figure 3.1 Ovine eye preparation with a 12 mm Miyake-Apple imaging window.

3.2.4 PREPARATION OF COLLAGENASE-MICROPARTICLES SUSPENSION

Ten microlitres of diluted 10 μm Fluoresbrite® yellow-green polystyrene latex particle suspension was pipetted into a 50 μL 10 mg/mL type II collagenase and the suspension was vortexed to ensure complete mixing. The preparation was prepared fresh on the day of use.

3.2.5 *IN VITRO* AND *EX VIVO* FLUORESCENT MICROPARTICLES IMAGING SYSTEM

The Miyake-Apple ovine eye was first securely placed on a custom-made perspex eye holder and 50 μL 10 μm Fluoresbrite® yellow-green polystyrene latex particle suspension (excitation max = 441 nm, emission max = 486 nm; Park Scientific, Northampton, UK) was injected into the vitreous humour using a 27G x ½ inch needle (Beckton Dickinson, Oxfordshire, UK). The microparticles were illuminated through the cornea with a high intensity blue LED (emission λ=460nm, Roithner Laser Technik, Vienna, Austria), at a right angle to the inspection port, consisting of a Nikon D300 digital camera equipped with a Nikon 60 mm f2.8 G AF-S macro lens and an orange filter (Figure 3.2). The images were taken using the Aperture mode and the settings were ISO 200, F45 and exposure compensation of -2. For the *in vitro* cuvette studies, the same experimental setting was employed, but the eye sample and eye holder were replaced by the cuvette. Additionally, for the collagenase experiment in the cuvette, injection was replaced by the collagenase-particle suspension as prepared under section 3.2.4.

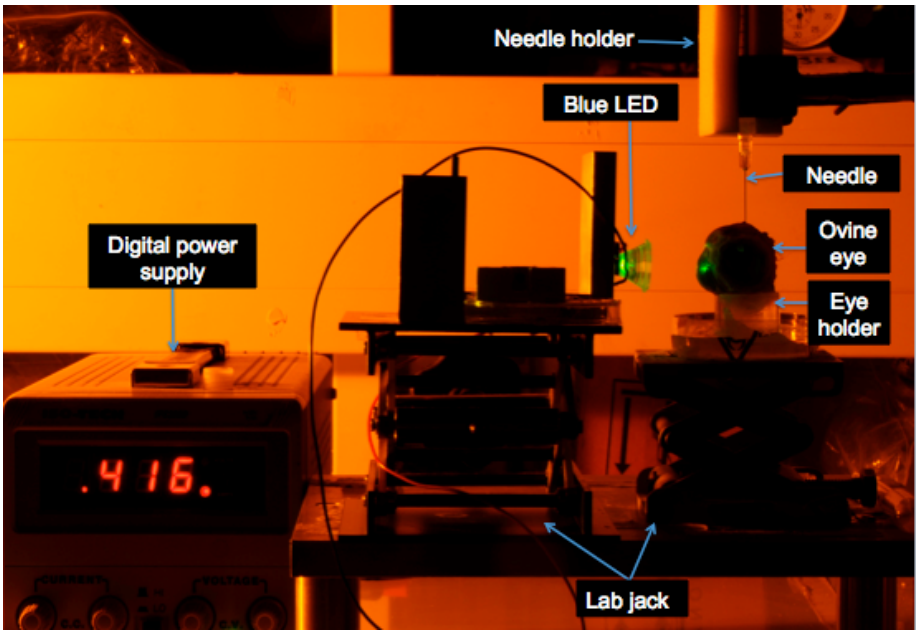

Figure 3.2 Experimental setup for illuminating the microparticles using a high intensity blue LED. The setting was imaged using a Nikon D300 digital camera equipped with an orange filter and a Nikon 60 mm f2.8 G AF-S macro lens. The blue LED appeared green in the diagram was an effect from the orange filter.

3.2.6 PREPARATION OF PERFUSION MEDIUM

The formula used in the preparation of the perfusion medium was based on the study by Koeberle *et al.,* (2006). In this study, the eyes were maintained at 37 ^{0}C and arterially perfused with oxygenated serum-free minimal essential medium supplemented with antibiotics, insulin, transferrin, and sodium selenite to cope with the metabolic need of the eye tissues. The compositions of the perfusate used are as shown in Table 3.1. The pH of the perfusion medium was adjusted to 7.4 using 1 M sodium hydroxide.

Compositions	Concentration
Serum-free minimum essential medium	1L
EDTA ~99-100% powder	0.2922g
Penicillin G sodium salt	0.061g (100kU/L)
Streptomycin sulphate salt powder	0.1g (73kU/L)
Gentamycin sulphate salt	0.08g
Insulin from bovine pancreas powder	1.852mg (50U/L)
Holo-transferrin	2.5mg
Atropine sulphate salt monohydrate	0.5mg
Sodium selenite powder ~98%	$2.5x10^{-6}$ g

Table 3.1 Composition of the perfusion medium.

3.2.7 EXPERIMENTAL PERFUSION SYSTEM

The assembly of the perfusion system is as illustrated in Figure 3.3. The perfusion medium was first saturated with 95% oxygen and 5% carbon dioxide for at least 45 minutes prior to the start of the experiments. To ensure complete mixing, the perfusate medium was stirred using a magnetic stirrer throughout the experiments. Then, it was pumped through a 25 mm (diameter), 0.2 μm (pore size) Acrodisc® syringe filter (VWR, Leicestershire, UK) using a peristaltic pump (101UU/R Watson-Marlow, Islfeld, Germany) to a glass condenser (VWR, Leicester, UK) at a rate of 1.0 mL/min. The inlet of the glass condenser was connected to a water bath of which temperature was set at 37 ^{0}C; whereas the outlet was connected to a bubble trap and a pressure transducer (Transtar Medex, Smith medical, Kent, UK), which was monitored by a computerized data-logger system (Picotech, Cambridgeshire, UK), recording the real-time arterial perfusion pressure (APP) and intraocular pressure (IOP).

A wire mesh was bent to fit the surface of the glass chamber (VWR, Islfeld, Germany) in order to form a platform for placing the eye globe. A 65 mm top diameter polyethylene funnel (Fisher scientific UK) was placed within the perfusion chamber with the funnel stem inserted through the bottom opening for venous

perfusate drainage. The system was linked together by the two outlets of the glass chamber using Tygon tubing (I.D 1.6mm, O.D 3.2 mm; VWR, Leicestershire, UK); top outlet was connected to the glass condenser and the bottom outlet was connected to the same water bath as the glass condenser aforementioned. The same assembly was connected together in triplicate so that perfusion could be performed on three separate eyes at one occasion. A schematic diagram of the perfusion system is as illustrated by Koeberle *et al.,* (2006).

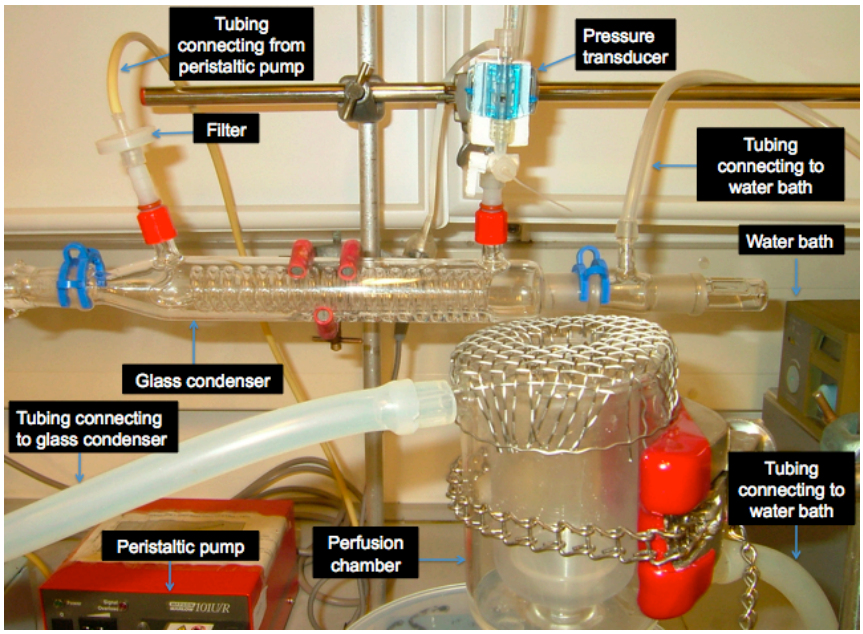

Figure 3.3 Single assembly of the perfusion system.

3.2.8 CANNULATION OF OVINE CILIARY ARTERY

The ovine eyes were obtained fresh from the local abattoir within 1-2 hours of animal death. The eyes were inspected for corneal clarity and tissue qualities including the lens status, clarity and turbidity of the aqueous chamber, general turgidity of the eyeball and ocular injuries and infections. Unhealthy eyes (from injury or infection) were excluded from the studies. Prior to cannulation, each healthy eye was placed on a petri dish lined with saline wetted gauze, where excess adnexal tissues were removed using a pair of surgical scissors and forceps. Approximately 5 mL of the perfusion medium was used to cleanse off any foreign

materials or blood traces appeared on the surface of the eye globe. The long posterior ciliary artery was then identified and only one artery was cannulated because circulation of the lateral and medial long posterior ciliary arteries merged within the eye and the cannulation of either one or both of them together produced insignificant changes to flow and IOP (Shiels *et al.,* 1999). The cannulation process was first initiated by securing one of the ciliary arteries using a braided silk wax surgical suture (Pearsalls Sutures, Somerset, UK). The suture was then stretched slightly and positioned using a sticky bluetack at a distance approximately 3 cm away from the eye to aid in cannulation. Then, a tapered polyethylene cannula 3 mm O.D, 1.65 mm I.D connected to a male luer connector (Sigma-Aldrich, Germany) was filled with perfusion medium using a syringe-needle before it was catheterized into the artery. Sutures were then gently tied over the site of catheterization and the process was repeated twice to ensure the cannula was securely fastened (Figure 3.4).

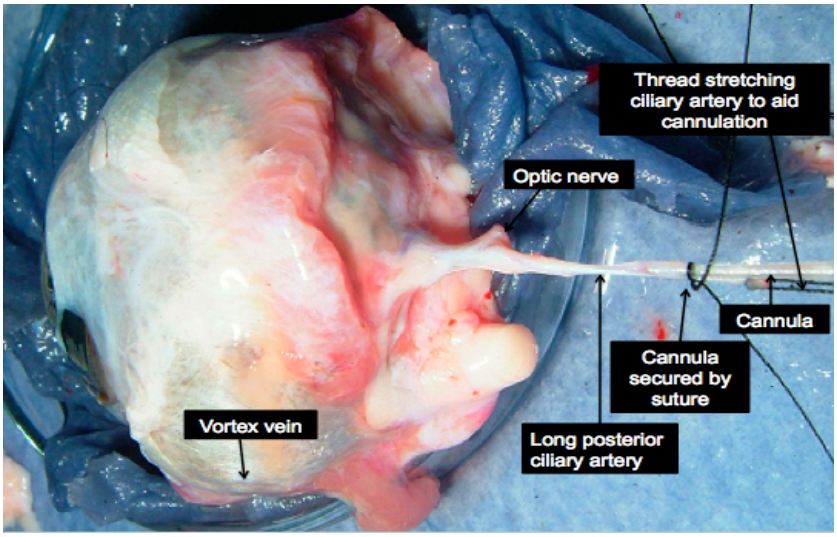

Figure 3.4 An illustration of the cannulated ovine eye.

3.2.9 PERFUSION PROCESS

Once the cannulation procedure was completed, the eye globe was immediately placed onto the wire mesh ready for perfusion. Approximately 20 mL of the perfusion medium was irrigated over the eye to further cleanse off any blood traces and contaminants from the ocular surface. The eye globe was then covered with a

piece of polyethylene film (cling film) to protect it from dehydration. The perfusion process was first started at a flow rate of around 0.2 mL/min, which gradually increased to 1.0 mL/min over a period of 30-45 minutes. Immediately following the commencement of perfusion, the vortex vein was inspected for flow. Occasionally, blood clot could form within the vortex vein that blocked the outflow of the venous blood. In this case, a cut at the edge of the vortex vein was made to initiate the flow. IOP measurement was started at approximately 15-20 minutes into the perfusion process. A 27-gauge needle connected to a 8 cm silicone tubing (0.76mm I.D, 1.65mm O.D; Scientific Laboratory Supplies, Lanarkshire, UK) was first filled with phosphate buffer saline and subsequently directed into the aqueous chamber at an angle perpendicular to the cornea surface approximately 3 mm away from the limbus. This procedure was performed with caution in order to avoid any damage caused to the ciliary body and the lens.

3.2.10 ARTERIALLY PERFUSED MIYAKE-APPLE EYE PREPARATION

Once a stable IOP and APP were achieved, a 4 mm or 8 mm disposable biopsy punch (Schuco Int. Ltd, London, UK) was used to carefully generate a window on the sclera at area devoid of long posterior ciliary arteries and vortex veins. A 10 mm or 13 mm circular glass cover slip, no $1^1/_2$ (Agar, Essex, UK) was then immediately sealed over the window using the Loctite cynoacrylate super glue (gel type). An illustration of an arterially perfused Miyake-Apple ovine eye preparation is as shown in Figure 3.5. Since the 8 mm Miyake-Apple eye preparation provided a wider field of view through the window, the preparation was subsequently used to assess microparticle movement within the vitreous chamber. A similar injection volume of microparticles as described under section 3.2.4 was used for perfusion study. The impact of the perfusion process on particle movements was investigated by comparing the images captured from perfused and non-perfused Miyake-Apple eye preparations.

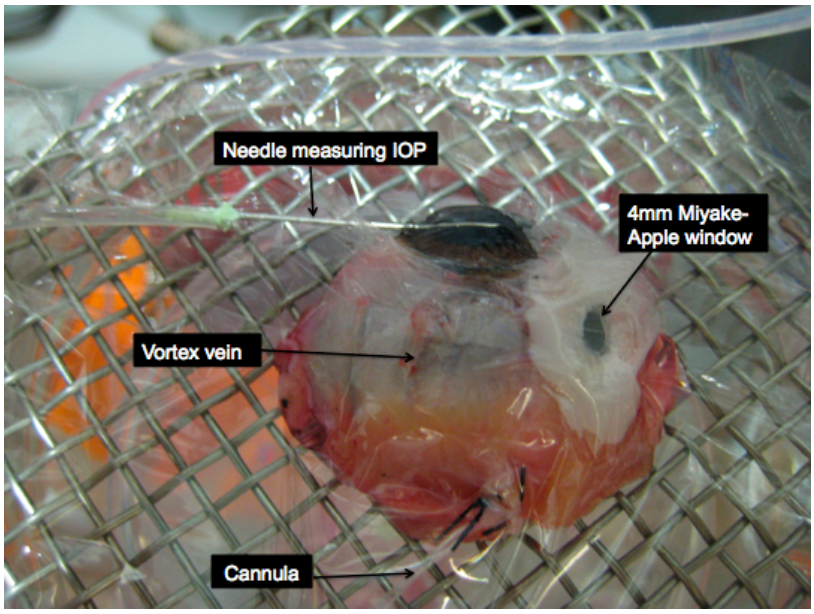

Figure 3.5 An arterially perfused 4 mm Miyake-Apple ovine eye preparation covered with polyethylene film (cling film) to protect the ocular tissues from dehydration.

3.2.11 VALIDATION OF VIABILITY PARAMETERS

The viabilities of the perfused eyes with or without a Miyake-Apple window were validated against several parameters, including the intraocular pressure (IOP), arterial perfusion pressure (APP), glucose consumption and lactate dehydrogenase (LDH) level. Only eyes that met the inclusion criteria were accepted for subsequent studies. Intraocular pressure (IOP) monitoring provided a measurement of the aqueous humour production by the ciliary process and its drainage by the trabecular meshwork and uvea-scleral outflow. Therefore, any damage to one of these mechanisms would be reflected in the IOP readings. On the other hand, APP was a measure of the resistance of the eye to perfusion, which would therefore, be an indicator for the integrity of the blood-aqueous and blood-retinal barriers (Koeberle, 2003). Any changes to the APP readings could suggest deterioration of these barrier functions of the eye. Based on the facts presented, three basic criteria were designed to assess the viability of the perfused eyes after an equilibration period of 30-60 minutes.

The criteria include:

1. The eye should maintain a stable IOP, with fluctuations of less than 3 mmHg over a 15 minutes period. An acceptable IOP should not exceed 12 mmHg since the IOP of a normal sheep eye lies in the range of 9-12 mmHg (Candia *et al.,* 2010, Gerometta *et al.,* 2009).
2. The eye should maintain a stable APP range of less than 60 mmHg, with no drift of more than 3 mmHg/h.
3. The eye should have free flow of perfusate from at least 2 vortex veins.

Furthermore, perfused eyes that had sudden rise in IOP of more than 20 mmHg, which failed to return to its previous value within 5 minutes or APP increased above 100 mmHg at any point of experiment would be excluded from the study. Eye samples that were damaged during the cannulation process and presented with a leakage of perfusate from the long posterior ciliary artery during the perfusion process were also excluded from the study.

In addition, the lactate dehydrogenase (LDH) levels were also measured as part of the validation process. LDH is a cytoplasmic enzyme that catalyzes the conversion of pyruvate to lactate during cellular metabolism process during periods of low oxygen supply. As an intracellular enzyme, LDH remained within the cellular environment unless the protection layer of plasma membrane is breached. Therefore, its level was frequently measured in the extracellular environment to inspect for cellular damage during pharmacological studies (Adamson and Harman 1988, de Coo *et al.,* 1993). In this study, LDH level was measured to monitor for tissue damage that occurred during the cannulation, Miyake-Apple and perfusion processes. Its detection in the venous perfusate that released from the extraocular tissues would indicate tissue deterioration. Therefore, if two consecutive LDH level of the venous perfusate were higher than the earlier level, this may suggest that the integrity of the tissues was compromised.

Furthermore, glucose consumption by the ocular tissues was measured to accomplish the validation process. The measurement could assess the viability of the tissues

since the process of cellular glucose uptake across the cell membrane for energy production requires a functioning cell. Nevertheless, Koeberle (2003) proposed that glucose measurement was not a sensitive indicator for tissue damage, unless the degree of damage was severe. For this reason, the author utilized glucose consumption as an indicator for appropriate perfusion rather than tissue viability. Therefore, similar protocol was adapted in this study, where glucose concentration in the venous perfusate was measured, with the expectation that the measured level should be lower than the concentration present in the perfusion medium to assure appropriate perfusion.

3.2.12 LACTATE DEHYDROGENASE (LDH) MEASUREMENTS

The level of LDH in the venous perfusate was determined using a LDH *in vitro* toxicology kit purchased from Sigma-Aldrich (Germany). The assay method was based on the reduction of NAD to NADH by LDH. The produced NADH was then reacted with the tetrazolium dye to produce a reduced coloured product, which could be detected spectrophotometrically at 490 nm. Since the reaction is a stoichiometric conversion, the amount of coloured product is proportional to the amount of NADH (Technical bulletin, Sigma-Aldrich).

The sample preparation procedures for LDH measurement were performed according to the manufacturer's recommendation. Twenty-five μL of calibration solution or venous perfusate was added to 50 μL reagent mixture composed of LDH assay substrate, cofactor and dye solutions. Then, the 75 μL of sample-reagent solution was further diluted with minimum essential medium to make up the final volume of 750 μL. The sample-reagent mixture was then incubated for 20 minutes prior to analysis. During the incubation period, the sample was covered with aluminium foil to protect it from light exposure. The coloured product from the chemical reaction between LDH and reagent mixture was then quantified using a Cary 50 UV-visible spectrophotometer (Varian, Oxford, UK). Using this method, a series of standards (n=3) with varying LDH activities (0.03-3U/mL) was prepared to produce a

calibration curve, from which LDH level in the venous perfusate was calculated. Samples with concentrations higher than the calibration standards were diluted by 5-10 fold using perfusion medium.

3.2.13 GLUCOSE MEASUREMENTS

The concentration of glucose in the venous perfusate was measured using a blood glucose self-monitoring device purchased from the local pharmacy (Boots, Glasgow, UK). This type of measurement technique has been employed previously to monitor glucose consumption in cell culture studies (Nayak and Herman 1997, Kurkela *et al.,* 1993). It provides a rapid and inexpensive method, which further benefits from the unnecessary need to gain access for a spectrophotometer or clinical auto-analyzer (Nayak & Herman 1997). According to the manufacturer instruction, an approximately 10 μL of sample solution was dropped onto the test strip for each measurement. A series of standard solutions (0.6-2g/L) was first performed to obtain a calibration curve, from which the concentration of glucose in the venous perfusate was determined.

3.2.14 IMAGE PROCESSING AND QUANTIFICATION

All images presented in this chapter were captured using the Nikon camera aforementioned (section 3.2.5). The images were subsequently analyzed using Image-J software. All images were first converted from RGB into a 32 bit grey scale. Then, image of an early time point was subtracted from that of the later time point using the image calculator function of the software. This would allow two images of subsequent time points overlaid on a single image where they could be compared quantitatively.

The quantification process was first initiated by calibrating the scale of the image against a known reference point, which was a copper strip behind the cuvette and 10 μm particle for *in vitro* and *ex vivo* eye preparations respectively. Then, the distance travelled by the particles was determined by first drawing a straight line across the

two target points with the first point being the particle position at an earlier time point and the second being the particle position at a later time point. The length of the straight line was subsequently measured by the software based on the scale preset. Similar measurement method was used to calculate the movement of the injection pocket in the cuvette study.

3.3 RESULTS

3.3.1 *IN VITRO* IMAGING OF THE FLUORESCENT MICROPARTICLES

Figure 3.6 shows the imaging of 10 μm fluorescent particle suspension injected into the dissected ovine vitreous contained within a cuvette. Immediately following injection, particles were observed to track back along the needle path. This demonstrated a pathway of low resistance established by the penetration of the needle. As can be seen, the injected particles immediately defined an optically transparent structure within the vitreous sample. After 30 minutes post-injection, settling of particles within the injection pocket was observed, accompanied by the deformation of a cisternal structure. The subsequent pattern of distribution remained unchanged for at least 5 hours, without particles settling to the bottom of the cuvette. In contrast, a more gradual dispersion occurred when the particles were injected along with the collagenase (Figure 3.7) although the initial spreading kinetics of the particles was similar to that in Figure 3.6. Thereafter the enzyme started to digest the surrounding collageneous fibres as noted at approximately 1 hour following injection and cause further dispersion of the particles. The dimension of the vesicles continued to expand alongside the digestion process, which lasted for at least 5 hours. Additionally, the viscosity within the digested vesicles was clearly reduced and convective movement driven by the small thermal effect of the illuminating diode was observed.

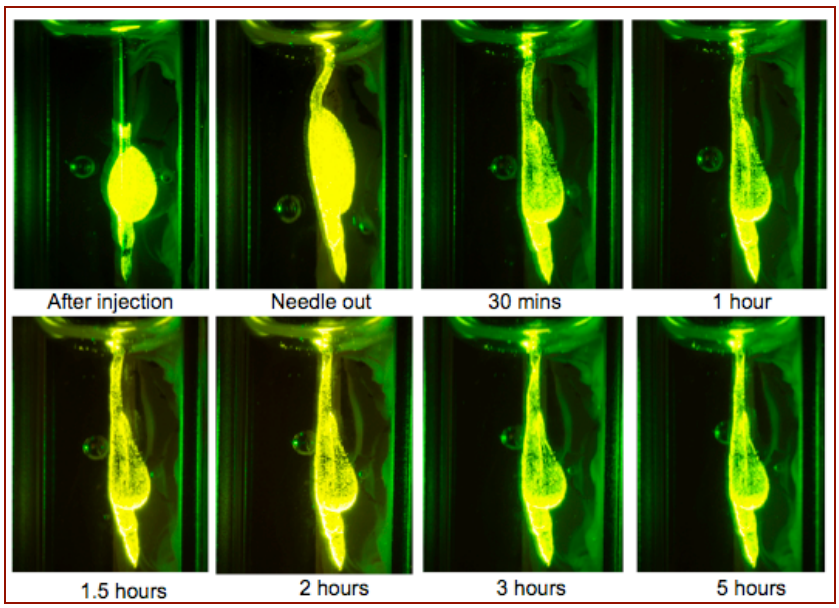

Figure 3.6 Imaging of 10 µm particle suspension injected into a cuvette contained dissected ovine vitreous. This pattern stayed stable for at least 5 hours.

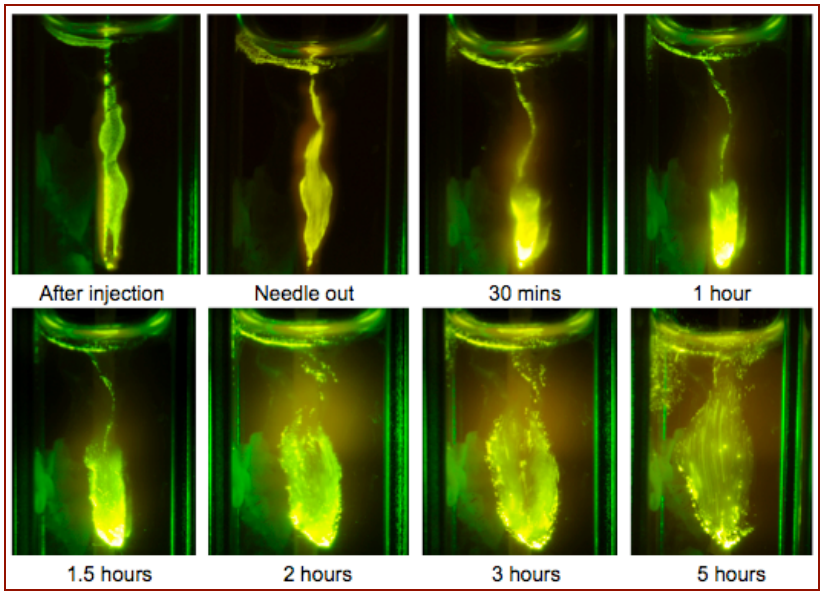

Figure 3.7 Imaging of 10 µm fluorescent particles-collagenase suspension injected into the ovine vitreous contained within a cuvette. Owing to the collagenase effect on vitreous collagen, injection pocket as outlined by the microparticles grew larger with time. Faster particle movement promoted by stronger thermal convective current was observed.

In Chapter 2, it was illustrated that the rheology of the ovine vitreous was more elastic than viscous. An elastic response could be observed *in vitro* as illustrated in Figure 3.8. Figure 3.8a was produced as an overlap image of Figure 3.6 after injection and needle out. After 30 minutes, further displacement is noted (Figure 3.8b) but no changes beyond this time (Figure 3.8c, 60 minutes). From Figure 3.8a, the retraction of the pocket was calculated to be large with a shift of 0.65 mm vertically and 6.7 ^{0} diagonally. The injection of water causes a change in the tertiary structures, which come to an equilibrium after approximately 30 minutes post-injection).

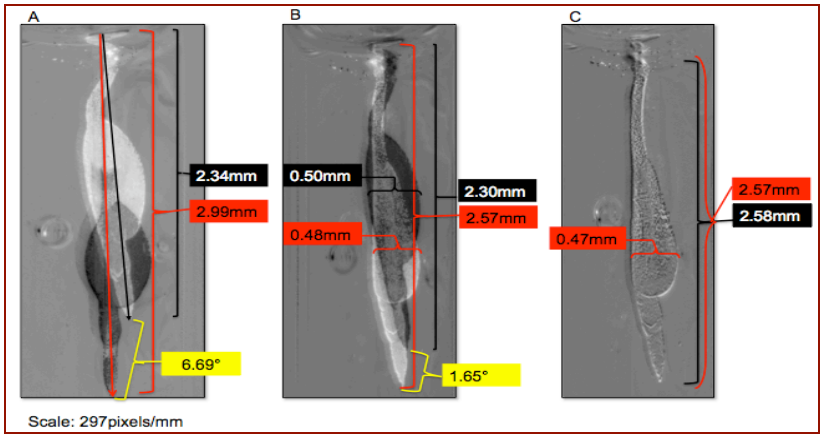

Figure 3.8 The images were originally similar to Figure 3.6, which were processed to demonstrate the elastic behaviour of the vitreous. A: (overlap images of after injection and needle out); B: (overlap images of needle out and after 30 minutes; C: (overlap images of after 30 minutes and after 60 minutes)

3.3.2 *EX VIVO* IMAGING OF MICROPARTICLES IN A MIYAKE-APPLE OVINE EYE PREPARATION

Figure 3.9 illustrates an *ex vivo* Miyake-Apple ovine eye preparation with injected microparticles. The needle track appeared more tortuous than in Figures 3.6 and 3.7 suggesting a regional variation in the structural and rheological properties of the vitreous humour.

Figure 3.10 illustrates another *ex vivo* non-perfused Miyake-Apple eye preparation injected with diluted 10 μm particle suspension. The shape of the injection pocket remained relatively static throughout the two hours study period, however, particles within the injection pocket were found to move freely on further analysis from sequential images (Figure 3.11). Initial particle movement was estimated to be the fastest at the upper left quadrant but particles at the lower tail quadrant were estimated to move faster at later time points. When the image captured at 3 minutes was compared to that at 120 minutes (Figure 3.11), it was found that the injection pocket had rebounded back in an upward-diagonal direction, which coincides with that observed previously in Figure 3.8, showing the elastic response of the vitreous.

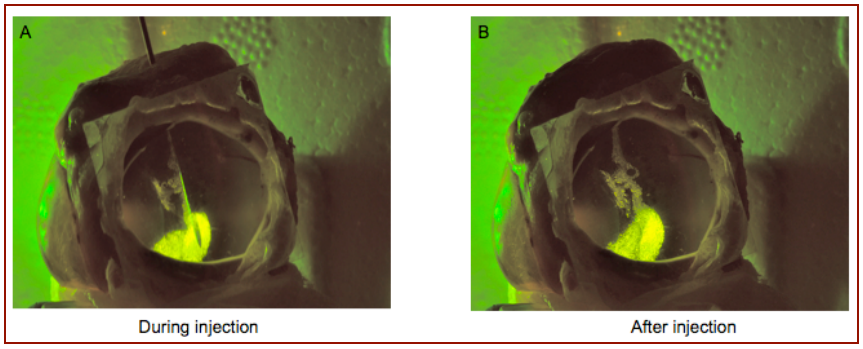

Figure 3.9 Imaging of intravitreally injected 10μm particle suspension through the Miyake-Apple window. A- during injection; B- after injection.

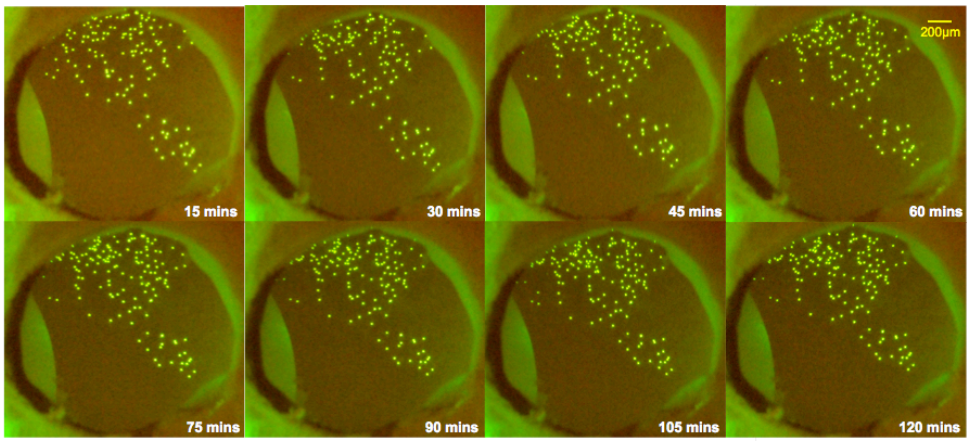

Figure: 3.10 Imaging of 10μm particles injected into a Miyake-Apple ovine eye preparation. No significant changes to the general appearance of the injection pocket and microparticles were noted throughout the two hour study period.

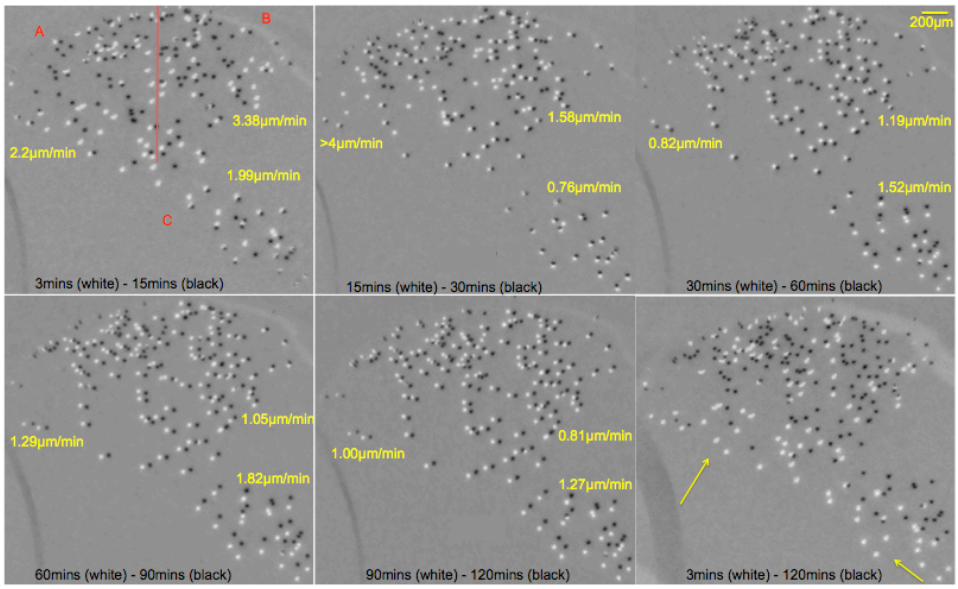

Figure 3.11 Estimation of the average velocities of 10 µm particle movement for three separate locations (upper left (A), upper right (B) and lower tail (C)), based on images shown in Figure 3.10. Each image was produced by subtracting an image of an early time point from that of the later time point (refer to method section). The contained microparticles were found to move with the relaxation of collagen fibers in an upward-diagonal direction. Fastest particle movement was found within the first 30 minutes after injection of which kinetic energy could possibly derive from the osmotic and ionic forces.

3.3.3 ARTERIALLY PERFUSED MIYAKE-APPLE OVINE OCULAR MODEL

3.3.3.1 VIABILITY PARAMETERS

3.3.3.1.1 PERFUSED OVINE EYE

The viability parameters of the perfused ovine eyes (n=6) without a Miyake-Apple procedure were investigated. The intraocular pressure (IOP) and arterial perfusion pressure (APP) of all samples were found in the range of 4-10 mmHg and 20-40 mmHg respectively, suggesting that the aqueous humour production and drainage as

well as the barrier function of the eye were normal during the perfusion experiment. A representative recording of the ocular pressures is as shown in Figure 3.12 (top). The bottom section of the same figure illustrates the glucose and LDH levels in the venous perfusate of the same eye. It was noted that the LDH level fluctuated throughout the perfusion study, which were however, not reflected in the ocular pressures. Moreover, no significant change in the glucose level was detected throughout the study.

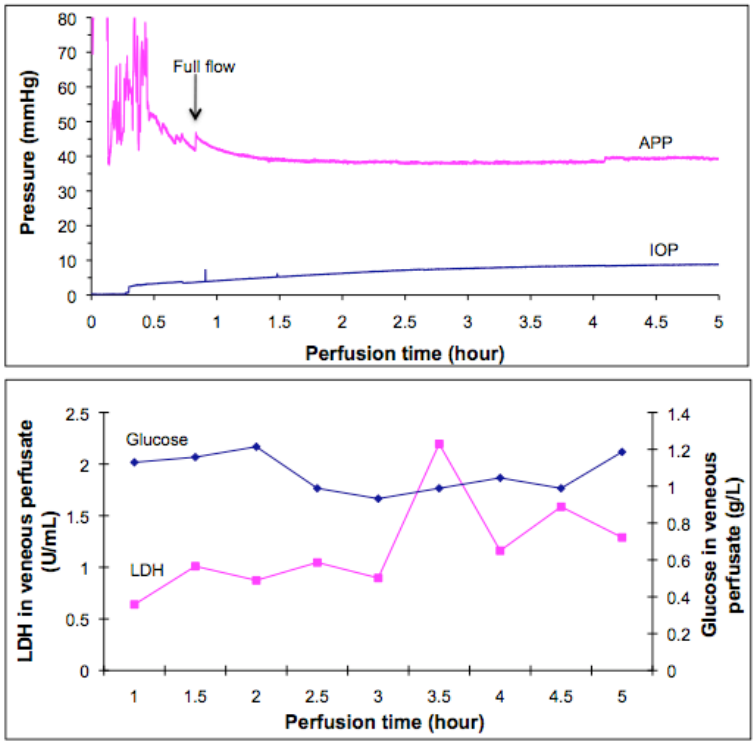

Figure 3.12 Top: A representative recording of the arterial perfusion pressure (APP) and intraocular pressure (IOP) measured from a perfused ovine eye without Miyake-Apple eye preparation over a period of 5 hours. APP fluctuation at the beginning of perfusion was allowed since misalignment of the cannula with the artery could block the flow of the perfusate (Koeberle *et. al.* 2006). Stable ocular pressures were achieved after the full flow period.

Bottom: A representative measurement of the glucose and lactate dehydrogenase (LDH) levels. The LDH level fluctuated throughout the experimental study. Similar changes in the ocular pressures and glucose venous level were not detected.

3.3.3.1.2 4 MM MIYAKE-APPLE PERFUSED OVINE EYE

When a 4 mm Miyake-Apple window was generated on the perfused ovine eye, the viability of the ocular tissues was also investigated in the same manner as was performed for eyes without a Miyake-Apple preparation. The viability parameters were examined for four eyes. The IOP and APP were in the range of 4-12 mmHg and 21-44 mmHg respectively, which were relatively comparable to eyes without a Miyake-Apple preparation. This suggests that a stable ocular pressure was achieved and maintained in a 4 mm Miyake-Apple perfused eye model. A representative recording of the ocular pressures obtained from a 4 mm Miyake-Apple perfused eye is as shown in Figure 3.13 (top) below.

Figure 3.13 (bottom) also shows that the LDH concentration in the perfusate following the 4 mm eye preparation was higher than that found in the eye without a Miyake-Apple preparation, suggesting the Miyake-Apple surgical procedure induced tissue damage and the LDH detected could possibly originate from the site of operation. However, the measured glucose consumptions were similar.

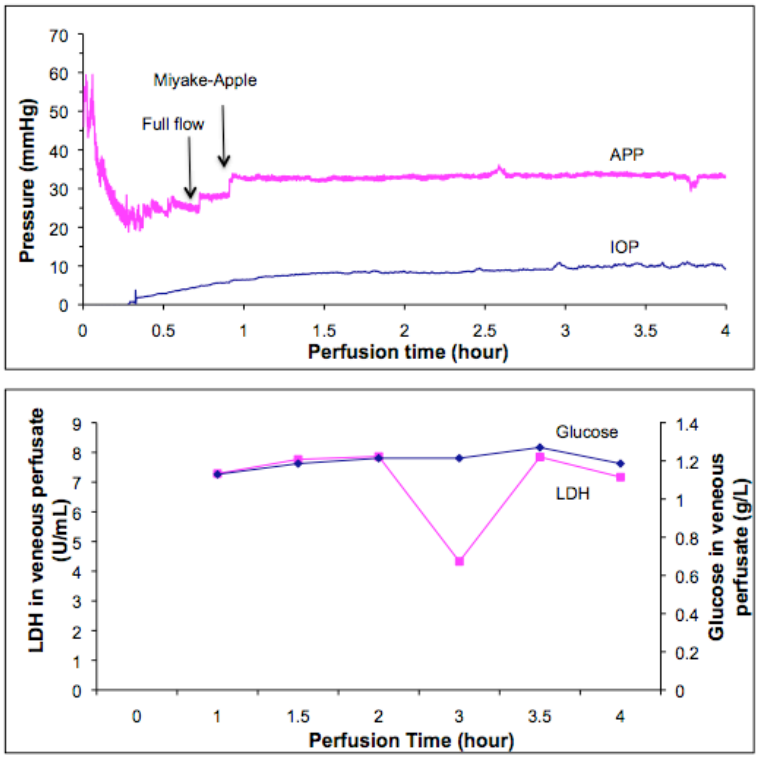

Figure 3.13 Top: A representative plot of the arterial perfusion pressure (APP) and intraocular pressure (IOP) recorded from a 4mm Miyake-Apple perfused ovine eye preparation over a period of 4 hours.
Bottom: A representative measurement of the glucose and LDH levels in the venous perfusate of the same eye. Higher level of LDH was noted in this preparation as compared to that of without a Miyake-Apple eye preparation.

3.3.3.1.3 8 MM MIYAKE-APPLE PERFUSED OVINE EYE

In the case for 8 mm Miyake-Apple preparation, the IOP and APP were within the range of 4-7 mmHg and 27-55 mmHg respectively based on 4 eye samples. Although the IOP was lower as compared to eyes with a 4 mm Miyake-Apple preparation and eyes without a Miyake-Apple preparation, stable ocular pressures were maintained. Figure 3.14 is a representative recording of the IOP and APP as well as the LDH and glucose levels in the venous perfusate. Similar to the case for 4 mm preparation, the level of LDH was higher than the eye without Miyake-Apple eye preparation. No conclusions could be drawn from the glucose measurements.

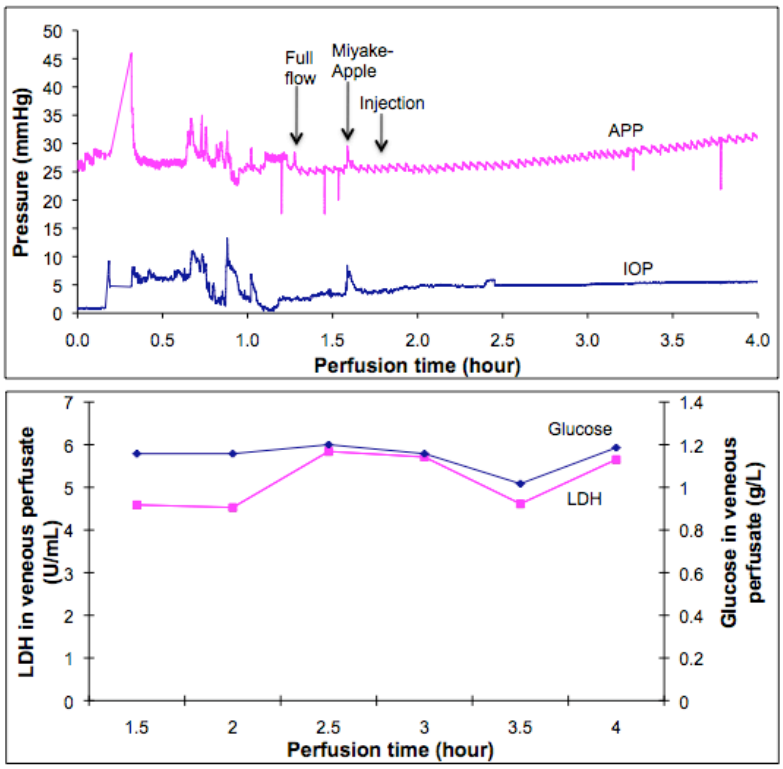

Figure 3.14 Top: A representative recording of the arterial perfusion pressure (APP) and intraocular pressure (IOP) obtained from a 8 mm Miyake-Apple perfused ovine eye over a perfusion period of 4 hours.
Bottom: A representative plot of the glucose and lactate dehydrogenase (LDH) levels in venous perfusate of eye preparation with 8 mm Miyake-Apple eye preparation.

3.3.3.2 *EX VIVO* IMAGING OF MICROPARTICLES IN AN ARTERIALLY PERFUSED MIYAKE-APPLE OVINE EYE PREPARATION

Figure 3.15 shows the imaging of 10 μm particles within the vitreous cavity of a 8 mm Miyake-Apple perfused eye preparation. Initially, the particles moved along the needle track and the movements were largely confined within the injection pocket for up to approximately 60 minutes. They then moved deeper into the tissue, away from the focal plane and the injection pocket. The image of the microparticles captured at 120 minutes was therefore less distinct than at 15 minutes following

injection. The images from Figure 3.15 were further analyzed and the results were as presented in Figure 3.16. The analysis shows that microparticles tend to move in an upward direction towards the injection site in the first 60 minutes after injection, presumably due to the increase in volume followed by absorption of the aqueous phase. At later time points, the forward movements were less obvious with particles moved deeper into the tissue. Since the images were tracked by focal plane and not captured in three-dimensions, the velocity readings provide only an approximate estimation. Figure 3.17 compares the particle movements between the perfused and non-perfused eye preparations. The illustrations suggest that the flow patterns were different. Particle movement within the vitreous of the non-perfused eye preparations was consistent with an elastic response to the injection. The same elastic response to injection was also observed in the vitreous of the perfused eye preparation but particles were found to move away from the injection pocket at later times deeper into the tissue. This suggests that intravitreal flow processes produced by perfusion and the pressure gradient generated the movements.

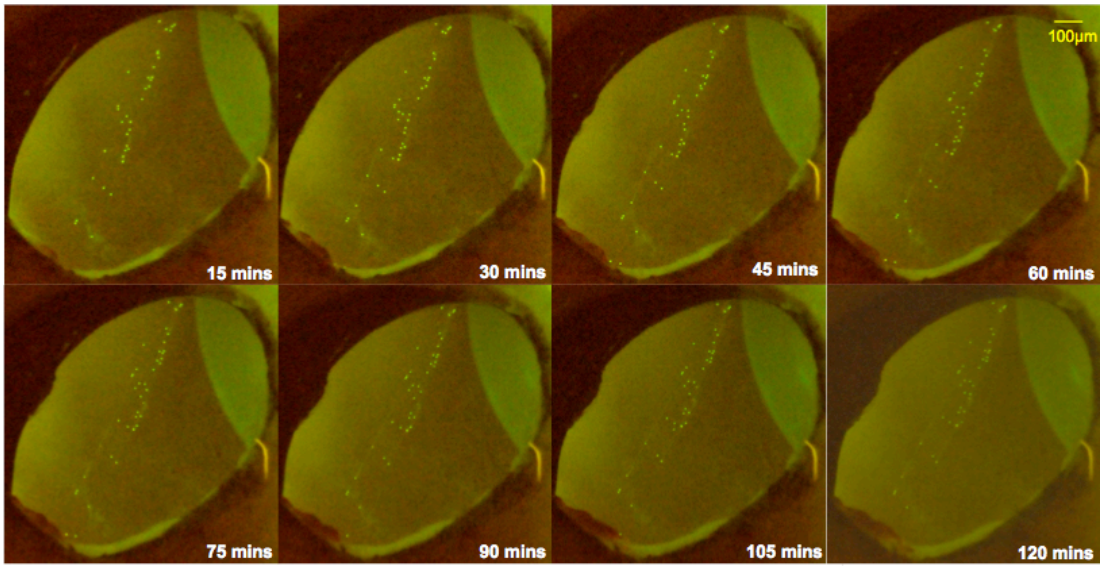

Figure 3.15 Imaging of 10 µm particles 2 hours post injection into the perfused 8 mm Miyake-Apple ovine eye preparation. The initial particle movements were found to confine within the needle track but with time, particles moved away from the focal plane (injection pocket) and became less distinct.

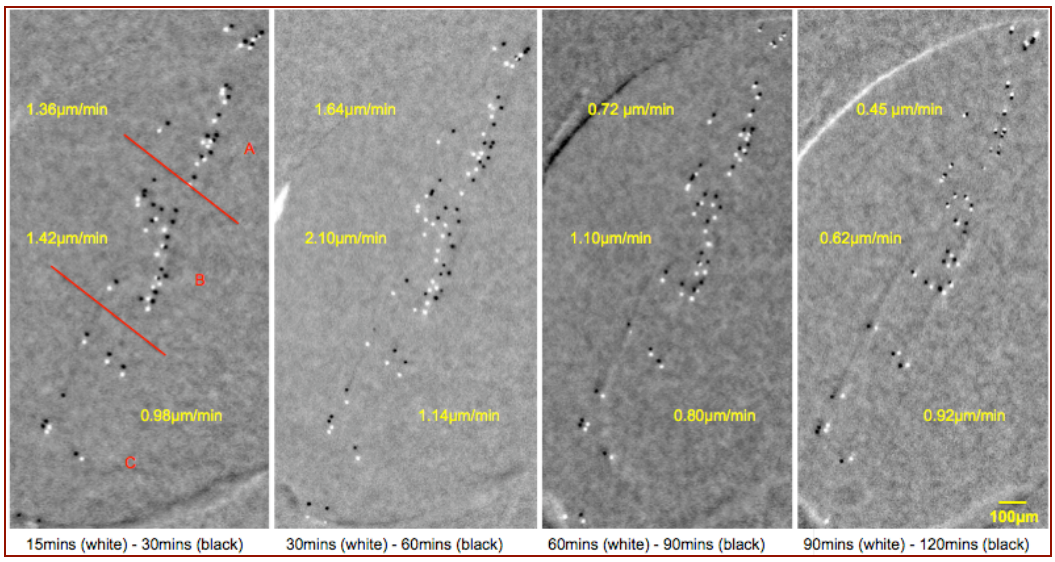

Figure 3.16 Estimation of the average velocities of 10 µm particles in three separate locations (upper (A), middle (B) and lower (C)) based on images shown in Figure 3.15. Each image was produced by subtracting an image of an early time point from that of the later time point (refer to method section). Microparticles were found to move in an upward direction within the first 60 minutes and faster movements were noted at the upper and middle zones. However, the upward movement was no longer apparent when images obtained at 60 minutes and 90 minutes were compared. Additionally, movements became slower within the upper zones at later time points compared to middle and lower zones.

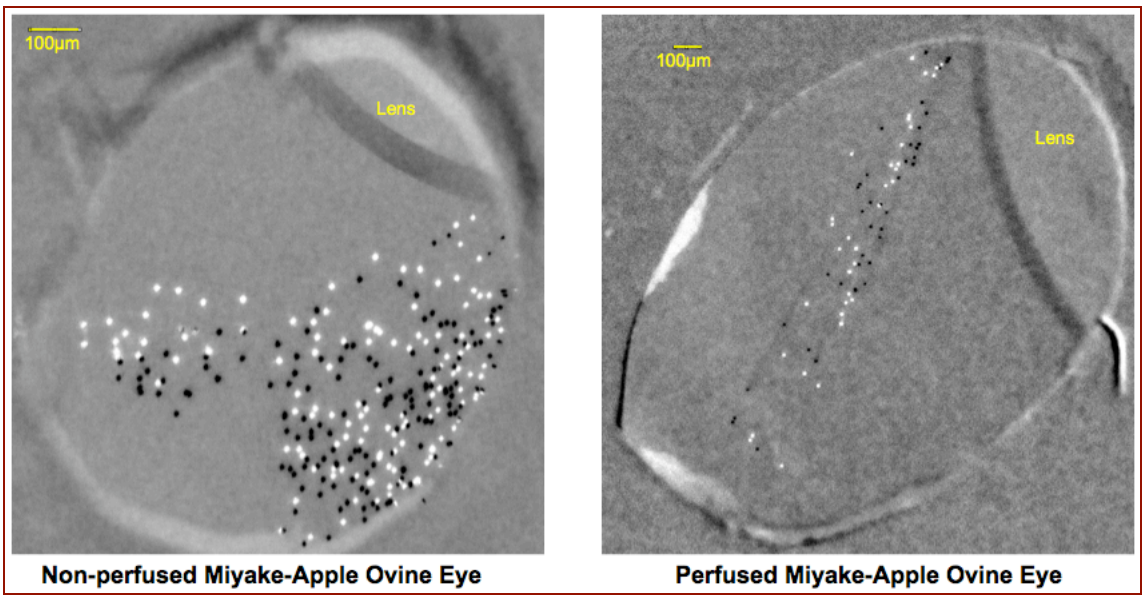

Figure 3.17 Comparison of microparticle movement in between perfused and non-perfused eye preparations, of which representing static and dynamic intravitreal systems respectively. White dots were microparticles captured at 15 minutes after injection; whereas black dots were microparticles captured at 2 hours after injection.

3.4 DISCUSSION

3.4.1 VITREOUS AS A BARRIER TO DIFFUSION

The cisternal structure of the human vitreous provides a barrier function to molecular transport. The barrier is mainly passive with no cellular interference. As described by Worst and Los, (1995), it is primarily constituted by collagen and hyaluronan. Collagen fibres (10-25 nm) and thinner fibrils (3-5 nm) interconnected together, forming a network filter of varying mesh sizes. On the other hand, hyaluronan, which is a polyanionic molecule, can occupy a large volume of the vitreous space by binding a considerable amount of water. The dispersion in between the collageneous meshwork further reduces the pore diameter of the vitreous network. However, it is well known that the vitreous is not an effective barrier to diffusion of small molecules. For instance, the intravitreal half-life of ganciclovir (255Da) is 7.1 hours in rabbit (Lopez-Cortes *et al.,* 2001) whereas polymer microspheres of 7-10µm in

diameter were found to be trapped in the vitreous space for at least seven to ten days with forces of gravity and convection serving as important factors (Algvere and Bill, 1979). Therefore, microparticles would be appropriate for assessing restricted diffusion and for this reason, a suspension of 10 μm particles was selected as the physiological probe in this study.

Our data shows that the cisternal structure of the vitreous remained preserved even when the vitreous was decanted into the cuvette. The localization of the injection pocket at the injection site clearly illustrated the collagenous structures of the vitreous limiting particle movement. The observation appeared to be consistent with the literature since the dimension of the meshwork found at the most dilute central zone of the vitreous was reported to be at least 3 μm (Worst and Los, 1995). Additionally, Fatt (1977) reported an intravitreal pore diameter of about 400 nm calculated based on transvitreal water flow rate. Peeters and colleagues (2005) found that particles of sizes between 220 nm and 575 nm were able to diffuse through the vitreous. These findings provided estimations on the intravitreal mesh size, which were clearly smaller than the size of our injected particles.

In addition, it was also noted that the microparticles outlined the injection pocket. This observation suggests particle interaction with collagen fibres since the polystyrene latex particles have a slight negative charge of approximately -60mV at neutral pH (Foged *et al.,* 2005) due to the presence of residual sulfate groups left over from the synthesis with anionic surfactants (information from manufacturer). The anionic surface characteristics will promote binding to the collagen fibres through hydrophobic interaction. This interaction was previously shown by Peeters and colleagues (2005) who demonstrated that when the hydrophilicity of the polystyrene particles increased, particles moved more freely in the vitreous. This suggests collagen fibres partly contribute to the restricted movement of larger objects. The barrier imposed by the collagen fibres was susceptible to destruction by collagenase. Collagenase was shown to break down the fibrillar structure, leading to the formation of liquid vesicles. The mechanism by which it occurred was most likely mediated through the unraveling of the protein triple helix structure, rather

than degradation into smaller segments (Sebag 2005). Within the liquefied vesicles, microparticles were observed to move under the influence of thermal convection, suggesting that the contents have low viscosity.

3.4.2 IMPACT OF MICROPARTICLE INJECTION ON DISTRIBUTION KINETICS

Following the needle injection, the liquid does not freely mix with the vitreous and refluxes along the needle wall, allowing particles to funnel along the needle path back to the injection site from a mid-needle bleb. When the needle was withdrawn from the vitreous following injection into the central zone, the exiting path became tortuous and coiled like a snake, suggested that the cisternal wall constricts the column. Based on this observation, we can deduce that needle penetration and injection imposed a hydrostatic force that stretched the rubbery fibrillar network, which relaxed when the stress was partially alleviated upon withdrawal of the needle. This behaviour is more complex than that described in models which simplify for example in finite element modeling, to approximate that of spherical or cylindrical shape. This may be true of the partially liquefied vitreous humour, devoid of cisternal wall, which represents the situation in the elderly subject.

This raises the question of what happens on repeat injections as it might be expected that frequent intravitreal injection would alter the vitreous structure over time. More importantly, the appearance of the needle track may explain the vitreous reflux event that commonly encountered clinically. Boon *et al.,* (2008) have noted that most of the patients who had a previous reflux history were likely to show similar amount of reflux with subsequent injections. The images obtained in this study appear to suggest that the inter-subject variation in the state of the vitreous could be a contributing factor.

Injections of particulates produced very different initial distribution compared to solutions in the vitreous. For example, injection of particles outlined a pocket as shown in the Miyake-Apple preparation and resembles the picture seen when the

suspension was injected into vitreous humour in a cuvette. This would confine the particulate in a finite fluid volume, from which the drug diffuses. A particulate, which behaves in a manner similar to that shown in this chapter, will result in a boundary layer phenomenon between solid and liquid, generating an exponential concentration around the limits of the injection pocket. Thus, flow patterns around a depot formulation will influence the maximal concentration at a target site.

3.4.3 PERFUSED AND NON-PERFUSED MIYAKE-APPLE OVINE EYE MODELS

The ciliary artery is one of the major arterial blood supplies to the eye. Two branches of the ciliary artery, namely the medial and lateral long posterior ciliary arteries were identified, one on each side of the optic nerve (Keough *et al.,* 1981) as shown in Figure 3.18. They run anteriorly and are visible through the sclera until just before the limbus, where they penetrate fully into the sclera. It was also noted that the lateral long posterior ciliary artery branches off to two or three retinal vessels and short posterior ciliary arteries at intervals as it coarses along the sclera (Prince *et al.,* 1960). Eventually, when both long posterior ciliary arteries arrive at the anterior segment, they anastomose with each other alongside the anterior ciliary artery (from the muscular and lachrymal branches of the ophthalmic artery) forming the major arterial circulation of the iris that supplies blood flow to the cilary body (Simoens and Ghoshal, 1981). Therefore, the cannulation of one of the long posterior ciliary arteries would be sufficient to maintain the production of the aqueous humour by the ciliary body.

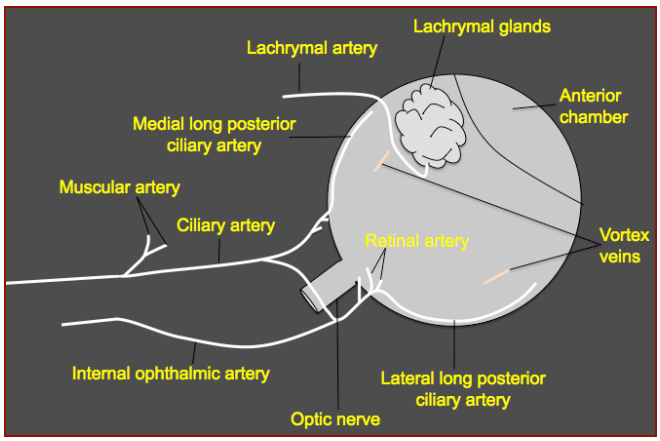

Figure 3.18 Schematic diagram illustrating the orbital arterial system of the ovine eye (modified from Prince *et al.,* 1960).

Aqueous humour production is mediated by both the passive and active processes (Miller, 2008). The passive processes include diffusion and ultrafiltration of the plasma fluid, whereas the active processes include energy-dependent transport mechanisms such as Na^+, K^+-activated ATPase and Cl^- channels. The aqueous fluid that formed in the ciliary capillaries is secreted into the stroma of the ciliary processes through the ciliary epithelium, and subsequently passed into the posterior chamber (Civan and Macknight, 2004). The aqueous humour flows through the pupil into the anterior chamber. Aqeuous drainage occurrs via the trabecular meshwork and the uveoscleral route with the latter contributed about 3-15% of the overall aqueous outflow. The equilibrium between the aqueous production and drainage maintained a relatively constant intraocular pressure within the eye (Miller, 2008). In the presence of this pressure, the shape and firmness of the eye ball can be maintained (Reece, 2005). The intraocular pressure of the perfused ovine eye was approximately 4-12 mmHg in sheep and this pressure gradually decreases across the vitreous chamber with the lowest pressure found across the sclera. The pressure difference between the anterior and posterior segment of the eye provides a driving force that promotes a steady flow down the pressure gradient into the vitreous humour (Stay *et al.,* 2003). Within the vitreous humour, some of the fluid would be absorbed across the retina into the choroidal circulation. Therefore, the intravitreal flow processes apparently played a role in the movement of microparticles as shown in the isolated perfused eyes. The lack of the flow processes within the non-perfused

eye preparation suggests that convective current is required for the intravitreal movement of microparticles and passive diffusion alone is not effective within the experimental time period.

3.4.4 PERFUSED OVINE EYE MODEL WITH AND WITHOUT MIYAKE-APPLE EYE PREPARATION

The LDH level in the venous perfusate of the perfused eyes without a Miyake-Apple preparation fluctuated throughout the study and this occurred in the majority of the eyes perfused during the experimental study. Such variation in the LDH level may reflect tissue deterioration, however, the ocular pressures were not affected. In fact, the majority of the IOP readings achieved were very close to the range observed for the live sheep.

This study also shows that a stable IOP and APP could be achieved and maintained in a 4 mm or 8 mm perfused Miyake-Apple eye preparation for at least 4 hours. However, the IOP achieved with the 8 mm eye preparation was lower than that in the 4 mm preparation. This could be attributed to the greater pressure loss through the formation of larger size window and the drop in pressure could not be fully compensated for by the subsequent perfusion process. The pressure range of 4-7 mm Hg was considered acceptable since similar range of IOP has been reported for in the bovine model and ocular disposition study performed under this pressure condition has been reported (Koeberle *et al.,* 2006). Nevertheless, it was apparent that the LDH levels measured in the venous perfusate was higher in the Miyake-Apple preparations as compared to that without a Miyake-Apple, suggesting the surgical process induced further tissue injury as expected.

The wider window of the 8 mm preparation offered a wider field of view that better served the study objective. Imaging through the 4 mm window has been attempted, however, the method was much less robust and very often the imaging of the particles was hindered due to the limited field of view. However, if future application

were not limited by the field of view, 4 mm eye preparation would be more advantageous as the IOP could be further optimized.

3.5 CONCLUSION

Our study has shown that vitreous imaging using 10 μm fluorescent particles and blue LED was a useful tool in assessing the diffusional barrier of the vitreous humour. Collageneous fibers were demonstrated to impede particle distribution and its association with polystyrene latex particle could be mediated through hydrophobic interaction. Additionally, the observation of a needle track was deemed useful in further understanding the vitreous reflux event seen clinically. Based on this finding, it should also be appreciated that the injection volume that was frequently assumed to be as a spherical or cylindrical shape should be best described as a wavy needle path leading to and beyond the injection pocket. The confinement of microparticles within the injection pocket suggests that the initial drug distribution from a microparticle delivery system would differ from that of a solution. Additionally, stable ocular pressures were feasibly achieved with both 4 mm and 8 mm Miyake-Apple eye preparations and imaging of the intravitreal particle movement within the system was successfully performed. Intravitreal flow processes played a role in the movement of microparticles and diffusion processes alone were ineffective in this instance.

CHAPTER 4: DEVELOPMENT AND ASSESSMENT OF A PARTIALLY LIQUEFIED VITREOUS MODEL

4.1 INTRODUCTION AND OBJECTIVES

With aging, the vitreous degenerates progressively and collagen fibrils, which are kept apart by glycosaminoglycans and proteoglycans in the juvenile eye aggregate into coarse fibers (Sebag and Balazs, 1985; Sebag, 1987; Sebag and Balazs, 1989). The detached collagenous fragments, together with cells and pigment, are clinically perceived as 'floaters' by affected patients. In addition, the hyaluronan component segregates into a pool of liquid, presumably as a result of depolymerization of its linear chain (Sebag, 1998). The vitreous of an elderly patient (> 60 years old) will therefore have a higher content of free water with a gel-liquid ratio of approximately 1 (Balazs and Denlinger, 1982). Most of the populations treated for many posterior segment diseases such as age-related macular degeneration are by definition elderly. Previous literature contributed by vitreo-retinal surgeons has described the role of vitreous structure as a diffusional barrier (Pitkänen *et al.,* 2003; Peeters *et al.,* 2005) and have considered the implications of loss of vitreous gel structure to movements of material around the eye (Foulds *et al.,* 1985; Ficker *et al.,* 1990; Chin *et al.,* 2005; Sebag *et al.*, 2007; Lee *et al.,* 2010).

The design of treatment regimens for most ocular problems is largely based on data obtained from young animal models, rabbits and rats, which have a fully formed vitreous with a high gel content (~80%). For this reason, the impact of vitreous liquefaction on the distribution of drugs and carriers has largely been unexplored. This led to one of the aims of the current study, which was to quantitatively and reproducibly generate a partially (~50%) liquefied vitreous model in laboratory rabbits that mimics the aged condition to better assess drug disposition in the aged eye.

4.2 MATERIALS AND METHODS

4.2.1 PREPARATION OF HYALURONIDASE, SODIUM FLUORESCEIN, FLUORESCEIN ISOTHIOCYANATE-DEXTRAN (FD) 150 kDa SOLUTIONS AND 1μm FLUORESCENT PARTICLE SUSPENSION

Lyophilized ovine testicular hyaluronidase with enzyme activity of ≥ 1000 IU/mg (MP biomedical, OH, USA) was reconstituted with 0.9% normal saline and serial dilution was performed to produce hyaluronidase injection solutions of concentration 0.005I.U./20μL. Fluorescein isothiocyanate-dextran, average molecular weight 150 kDa (Sigma, St. Louis, MO), was dissolved in 0.9% normal saline to produce a 0.01% (w/v) solution. A 10% w/v sodium fluorescein solution (Akorn, Inc., Buffalo Grove, IL) was diluted in 0.9% normal saline to 0.01% w/v prior to use. A fluorescent polystyrene latex microsphere water suspension (Fluoresbrite®, 1μm) was purchased from Polysciences Inc. (PA) and was used without further dilution.

4.2.2 *IN VIVO* MODEL OF VITREOUS LIQUEFACTION

All animal handling procedures involved in this study were approved by the Allergan Animal Care and Use Committee and complied with the ARVO statement for the use of animals in ophthalmic and vision research. Fourteen Dutch-belted rabbits weighing 2-3 kgs of ages ranging from 3 months to 2 years old were involved in the development phase of the model. Before the start of all experiments, the eyes of all animals were examined externally to exclude abnormalities. Prior to intravitreal injection, the rabbits were locally anaesthetized using topical 0.5% Tetracaine HCl ophthalmic solution USP (Bausch and Lomb, Tampa, FL) and the pupils were dilated using topical 10% Phenylephrine HCl (Akorn, Inc., Buffalo Grove, IL) and 1% Tropicamide USP (Alcon Laboratories, Fort Worth, TX). Twenty μL of hyaluronidase solutions of 0.005 I.U. (n=11) was injected intravitreally to induce vitreous liquefaction; while another 4 animals received bilateral injections of 20 μL

normal saline to act as control. The animals were euthanized 24 (n=5) or 48 hours (n=6) later with intravenous injection of pentobarbital (Eutha-6, Western Medical Supply Co., Arcadia, CA), and the eyes were enucleated and dissected to obtain the vitreous humor. The vitreous samples were then collected onto a petri dish and the gel-liquid ratio was determined by first weighing the entire vitreous then weighing the liquid phase after removing the gel phase with a pair of forceps. The percentage vitreous gel content was calculated as [(mass of gel phase/total mass of vitreous)*100%]. The significance of differences in the percentage gel phase between normal and enzyme-treated eyes was evaluated using the student t-test with the significant level defined at p-value < 0.05. During the study, evidence for ocular toxicity was monitored using a fundus camera.

4.2.3 *IN VIVO* MEASUREMENTS OF FLUOROPHORES DISTRIBUTION USING HEIDELBERG RETINAL ANGIOGRAPHY (HRA) CONFOCAL LASER SCANNING SYSTEM AND OCULAR FLUOROPHOTOMETER

After developing the model, nine animals were used to study the effects of vitreous liquefaction on material distribution. Twenty μL of 0.005 IU hyaluronidase solution was injected unilaterally in the animals leaving the contralateral eyes untreated (normal vitreous) to act as control. Forty eight hours later, animals received bilateral intravitreal injections of 10 μL 0.01% sodium fluorescein (n=3), 1% fluorescein isothiocyanate-dextran (FD) (MW= 150 kDa) (n=3) or a suspension of 1 μm fluorescent particles (n=3). The distribution of the injected fluorescent molecules was monitored for a month using the HRA 2 (Heidelberg Engineering, Vista, CA) with a wide-angle ocular Staurenghi 230 Scanning Laser Ophthalmoscope (SLO) retinal lens, and an ocular fluorophotometer (Ocumetrics. Inc., San Francisco, CA). HRA allows the imaging of fluorescent probes in both x- and y- axis while ocular fluorophotometry detects the fluorescent intensity along the optical (z) axis. Ocular fluorophotometry data of the study groups were compared using the student t-test with a confidence level of $p < 0.05$ considered as statistically significance.

4.2.4 IMAGE ANALYSIS

The experimental images obtained using HRA were analysed using an image processing feature in Matlab (The Mathworks Inc, Natick, MA) to quantitatively compare the retention of fluorescent mass of sodium fluorescein and FD 150 kDa in the enzyme-treated and contralateral normal vitreous. Using this method, the degree of distribution and clearance of injected molecules was correlated to its fluorescent intensity (in pixels) detected within the vitreous chamber with lower intensities indicating faster rate of transport. By calculating the fluorescent intensity ratio of normal to liquefied vitreous, the relative distribution and clearance of both models can be compared.

4.3 RESULTS

4.3.1 DEVELOPMENT OF A MODEL OF VITREOUS LIQUEFACTION

Figure 4.1 shows the degree of vitreous liquefaction induced by 0.005 I.U. of hyaluronidase with either 24 hours or 48 hours post-dosing period. The 24 hours post-injection period produced a lower degree of liquefaction (77.9 ± 6.1%; $p>0.05$) than that at 48 hours post-injection period.

In addition, 0.005 I.U. dose with post-injection period of 48 hours generated the target degree of vitreous liquefaction in rabbits in a reproducible fashion. In comparison to control, there was a slight haziness in the vitreous chamber of hyaluronidase-treated eyes but no gross ocular tissue changes were identified (Figure 4.2). This model was then used to assess the effects of vitreous liquefaction on the disposition of three model compounds injected intravitreally.

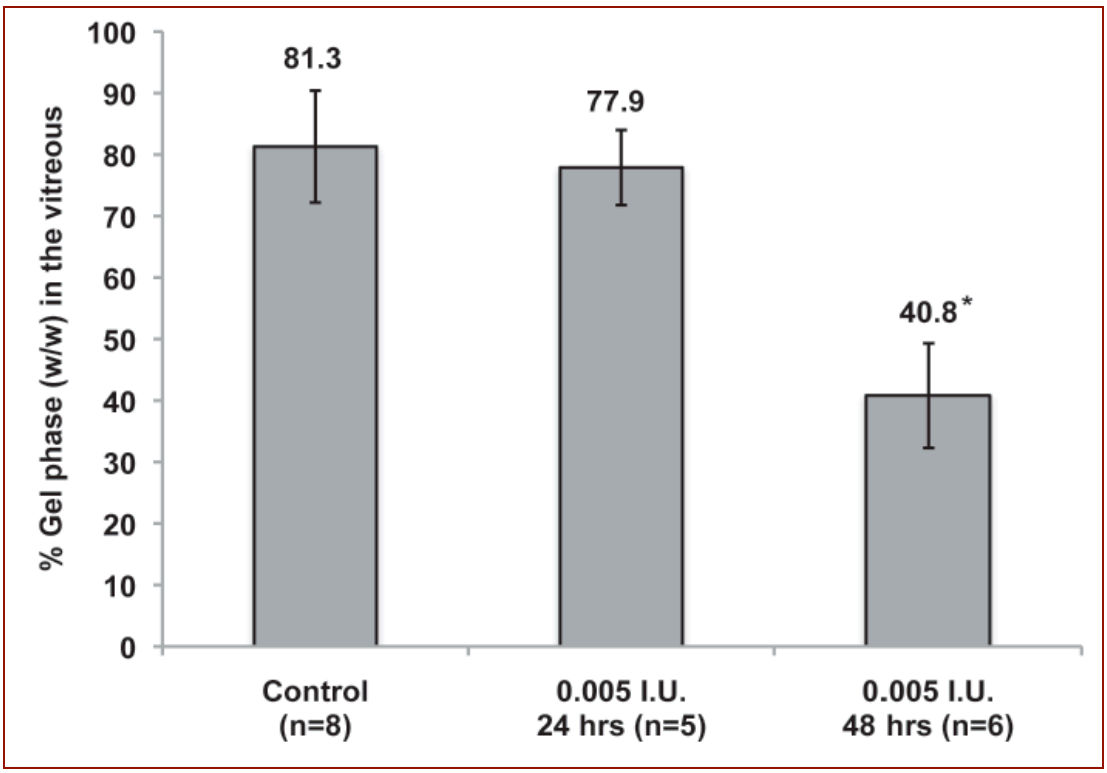

Figure 4.1 Percentage vitreous gel phase of control and hyaluronidase-treated groups. The difference in percentage gel phase between control and 0.005 I.U. (48 hours post-injection) hyaluronidase-treated group was statistically significant * ($p < 0.05$).

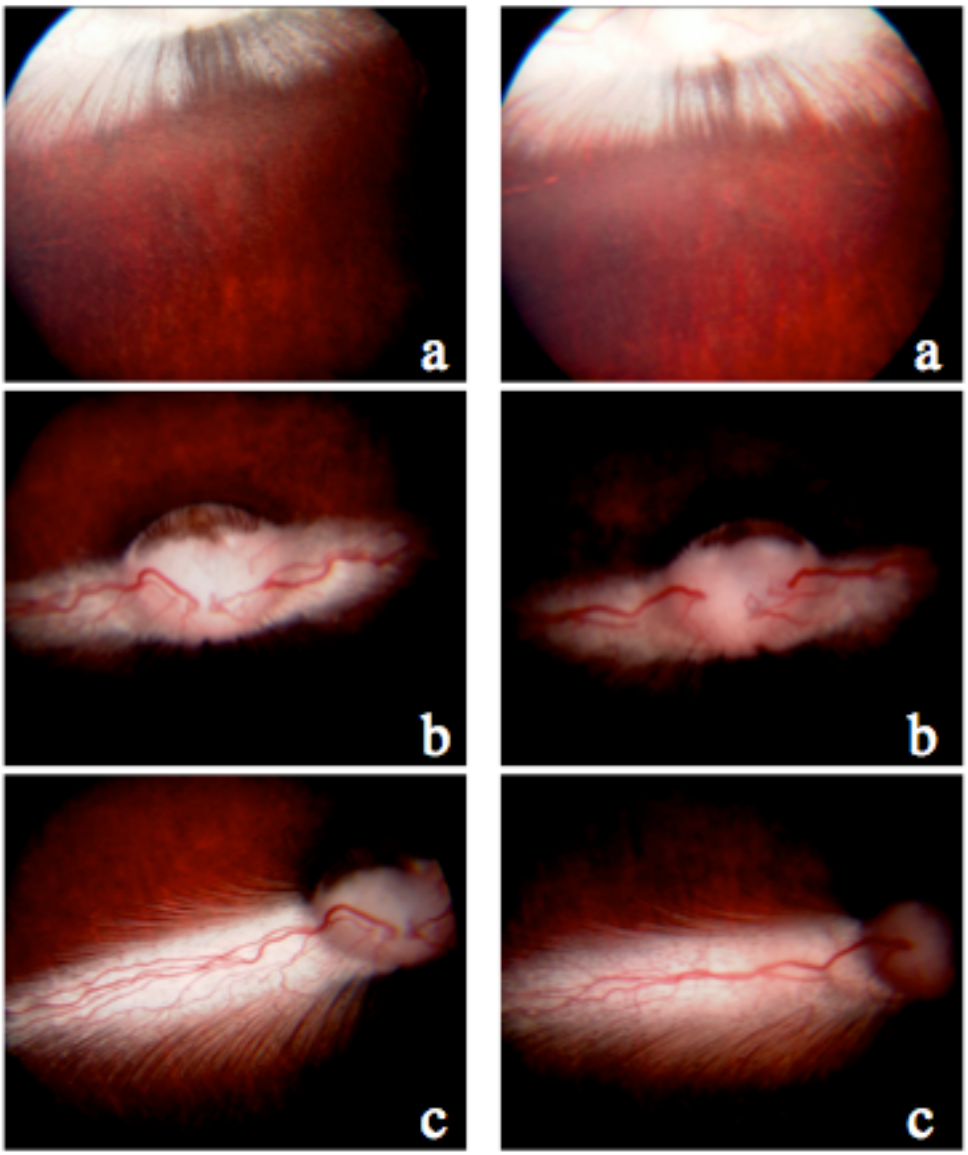

Figure 4.2 Fundus assessments of the medullary rays and optic nerve head in control (left panel) and hyaluronidase-treated (right panel) eyes. a: Medullary rays; b: Optic nerve head; c: Right medullary rays and optic nerve head.

4.3.2 EFFECTS OF VITREOUS LIQUEFACTION ON THE DISPERSION OF MODEL COMPOUNDS

4.3.2.1 SODIUM FLUORESCEIN

Figure 4.3 shows a set of representative HRA images comparing the intravitreal distribution of sodium fluorescein in both normal (control) and liquefied (hyaluronidase-treated) vitreous at 2 and 5 hours after injection. The fluorescent depot in the liquefied vitreous spread out faster from the injection pocket and perhaps from the vitreous cavity. An analysis constructed using the Matlab programme used in our laboratories indicated that sodium fluorescein clearance as measured by fluorescence intensity was 1.4 and 1.5 times faster in the liquefied vitreous at 2 hours and 5 hours respectively as compared to that measured in control. Figure 4.4 shows the distribution profiles along the z-axis of the eye at 2 hours and 5 hours for both models. At the same injected dose, sodium fluorescein concentration was found to be lower in the liquefied vitreous at all times ($p<0.05$). However, the fluorescent mass distributed with a similar concentration gradient in both models. The plateau in the control eye data at 2 hours between 17 and 21 mm from the origin probably indicates penetration into the lens. The probe does not continue a forward diffusion since the vectoral fluid flow in the lens opposes diffusion, unloading absorbed fluorescein back into the vitreous humour at 5 hours post administration (Stepanova *et al.,* 2005). The behaviour is less obvious in the liquefied vitreous, presumably because the concentration gradient cannot be sustained. Table 4.1 is a summary of the HRA and ocular fluorophotometry results for the study models.

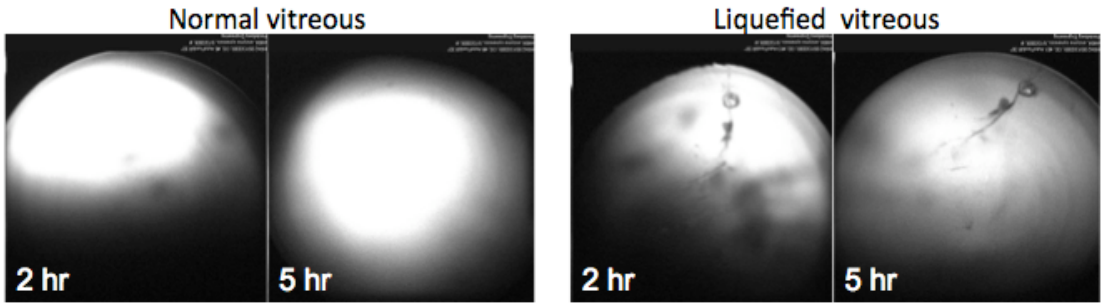

Figure 4.3 Representative HRA images obtained from one animal 2 hours and 5 hours after receiving 10 µL intravitreal injection of sodium fluorescein solution. The fluorescent mass was well retained in the intact vitreous after 5 hours but is more diffuse in liquefied vitreous.

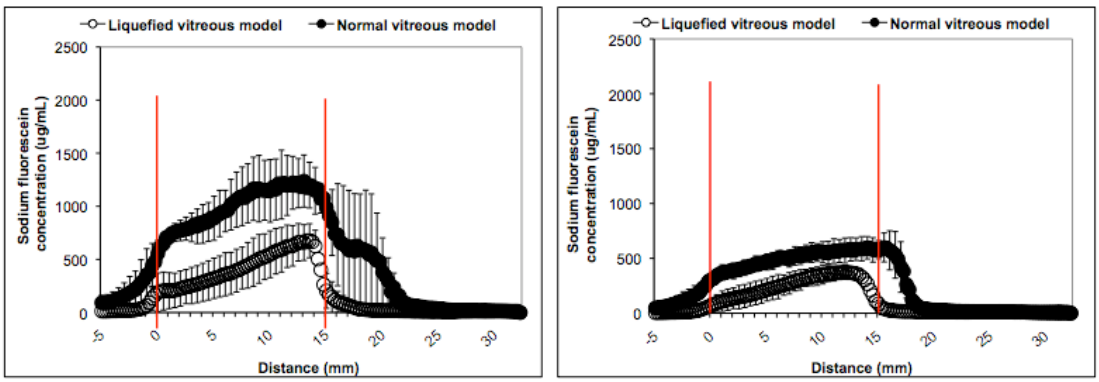

Figure 4.4 Ocular fluorophotometry of intravitreally injected sodium fluorescein depot at 2 hours (left) and 5 hours (right) after injection (n=3). On these graphs, zero mm represents the vitreo-retinal interface while 15 mm represents the back of the lens.

4.3.2.2 FLUORESCEIN ISOTHIOCYANTE-DEXTRAN (FD) 150 kDa

Figure 4.5 is a set of representative HRA wide-angle images obtained from one animal comparing the distribution of FD 150 kDa in the vitreous cavity over a period of one month. The figure also shows that the FD 150 kDa solution formed a defined depot that lasted for at least 5 hours after injection and gradually spread across the vitreous cavity thereafter as indicated by the increasing diameter of the fluorescent

mass. There was no significant difference in the distribution of FD 150 kDa between the models until day 3. However, from day 6 onwards, the amount of FD 150 kDa, which remained in the vitreous was lower in the liquefied model as compared to control. There was no residual FD 150 kDa detected optically in the liquefied vitreous model on day 30 but a low degree of fluorescent intensity remained visible in the normal vitreous, suggesting FD150 kDa had a shorter intravitreal half-life in the liquefied vitreous. Figure 4.6 shows the graph generated using Matlab to calculate the fluorescent intensity of FD 150 kDa remaining in the vitreous humor over time. The y-axis on the plot represents fluorescent intensity (in pixels) remaining within the vitreous cavity and the scale is in arbitrary units. FD 150 kDa was cleared faster in the liquefied vitreous as compared to the normal vitreous model. Figure 4.7 shows the plots obtained from the ocular fluorophotometry study. At one hour after injection, most of the injected FD 150 kDa remained at the site of injection in both models. However, the 2 and 5 hours data suggest that FD 150 kDa moved towards the anterior chamber in the liquefied vitreous, while remaining in place in the normal vitreous. On day 2, FD 150 kDa started to spread across the optical axis as shown by the more even fluorescence distribution. Additionally, the fluorescence gradient was steeper in the liquefied vitreous than the normal vitreous on days 2 and 3. On day 6 the gradient decreased, indicating that the initial phase of diffusive equilibration was completed. This data was in agreement with the HRA wide-angle image, where the fluorescent intensity was evenly distributed across the chamber for the liquefied vitreous. In the normal vitreous, the general fluorescence gradient did not change considerably over similar time periods. As the FD 150 kDa was cleared from the vitreous cavity of the study models, the fluorescent intensity reduced in both x- and y-axis as detected by HRA and ocular fluorophotometry. Statistical analyses showed that the fluorescent intensity of FD 150 kDa was significantly higher ($p<0.05$) in normal vitreous on day 21 and day 30, which agreed with HRA observations.

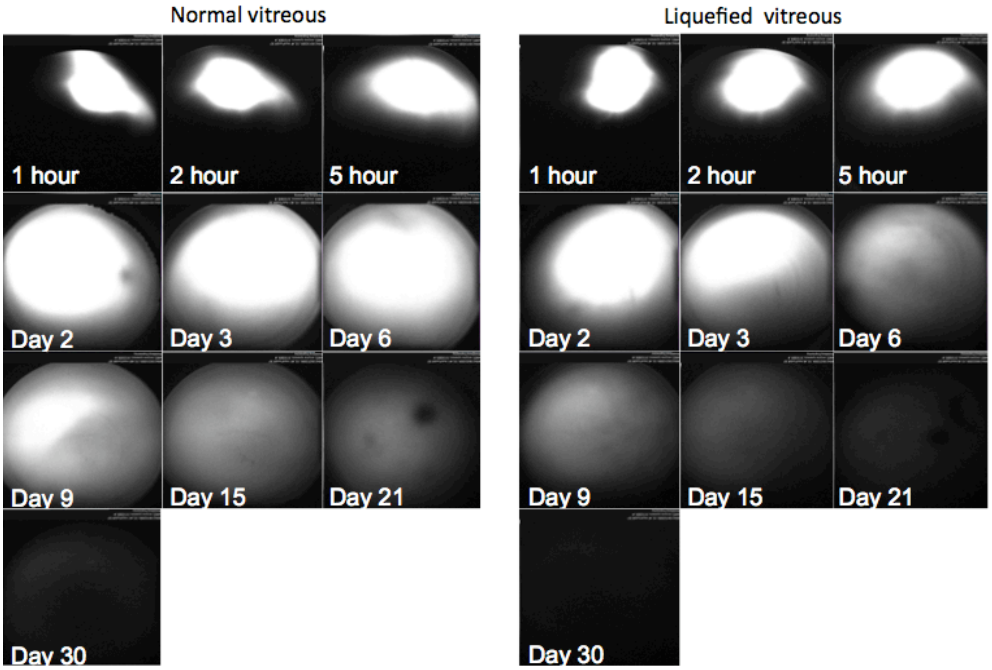

Figure 4.5 HRA wide-angle images of intravitreally injected fluorescein dextran 150 kDa in the normal and liquefied vitreous models from 1 hour to day 30 after injection.

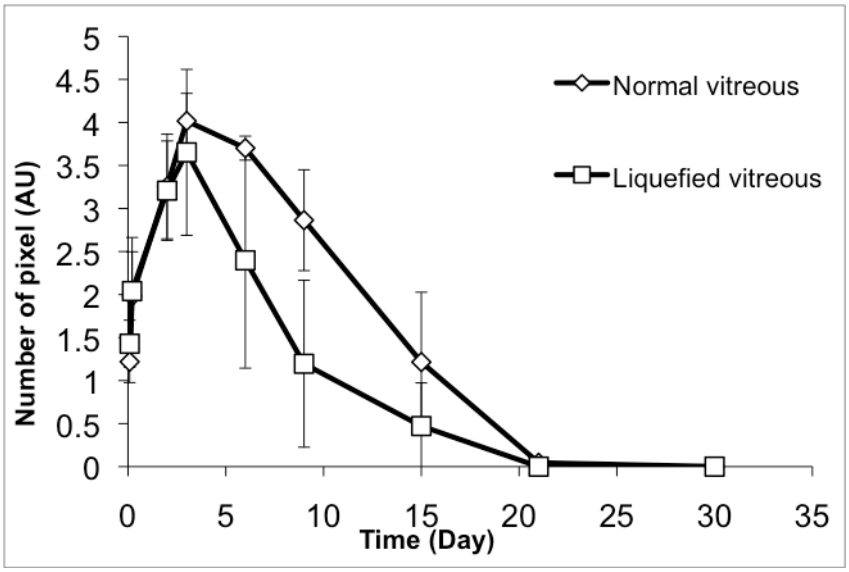

Figure 4.6 Plot generated using Matlab (based on HRA images) comparing the fluorescent intensity of FD 150 kDa from 2 hours to 30 days after injection in both liquefied and normal vitreous models. Means (n=3) ± standard deviations are shown. The curves were consistent with the HRA findings.

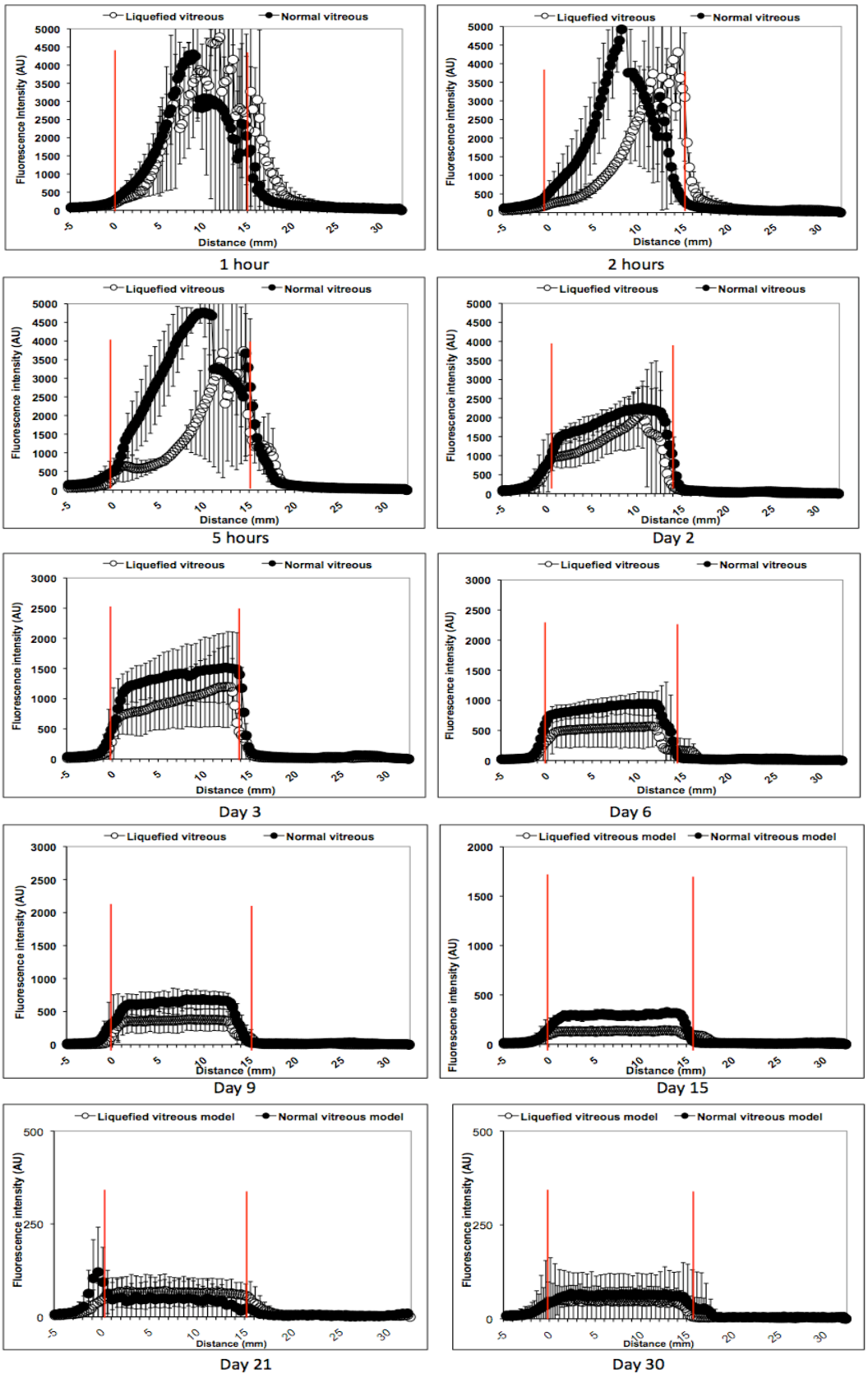

Figure 4.7 Ocular fluorophotometry data obtained from the study animals (n=3) showing the fluorescent intensity along the optical axis from the back of the lens (15 mm) through to the surface of the retina (0 mm).

	Sodium Fluorescein			Fluorescein Dextran (FD) 150 kDa									
Time points	1 hr	2 hr	5 hr	1 hr	2 hr	5 hr	D2	D3	D6	D9	D15	D21	D30
HRA Intensity ratio	1.1	1.4	1.5	0.87	0.84	0.97	1.04	1.15	2.6	3.8	>10	>10	2.17
OF Student t-test	p<0.05 *			p>0.05	p<0.05 *								

Table 4.1 The summary data for sodium fluorescein and FD 150 kDa in the study models. HRA results were presented as the fluorescent intensity ratio of normal to liquefied vitreous. While the average sodium fluorescein concentration and average fluorescent intensity of FD150 kDa obtained from ocular fluorophotometry (OF) analysis were compared using student t-test. Hr: hour; D: day.

*: Average concentration of sodium fluorescein and fluorescent intensity of FD 150 kDa were significantly lower in partially liquefied vitreous at all time points except at 1 hour after injection of FD 150 kDa.

4.3.2.3 1 μm PARTICLE SUSPENSION

The intravitreal distribution of 1μm fluorescent particles was assessed using HRA. The images obtained are shown in Figure 4.8. Gravitational forces resulted in sedimentation of microparticles in the liquefied vitreous model on day 9 whilst microparticles in the normal vitreous settled later. In the normal vitreous, microparticles sedimented without much lateral diffusion as opposed to the liquefied vitreous where the particles appeared more dispersed and scattered.

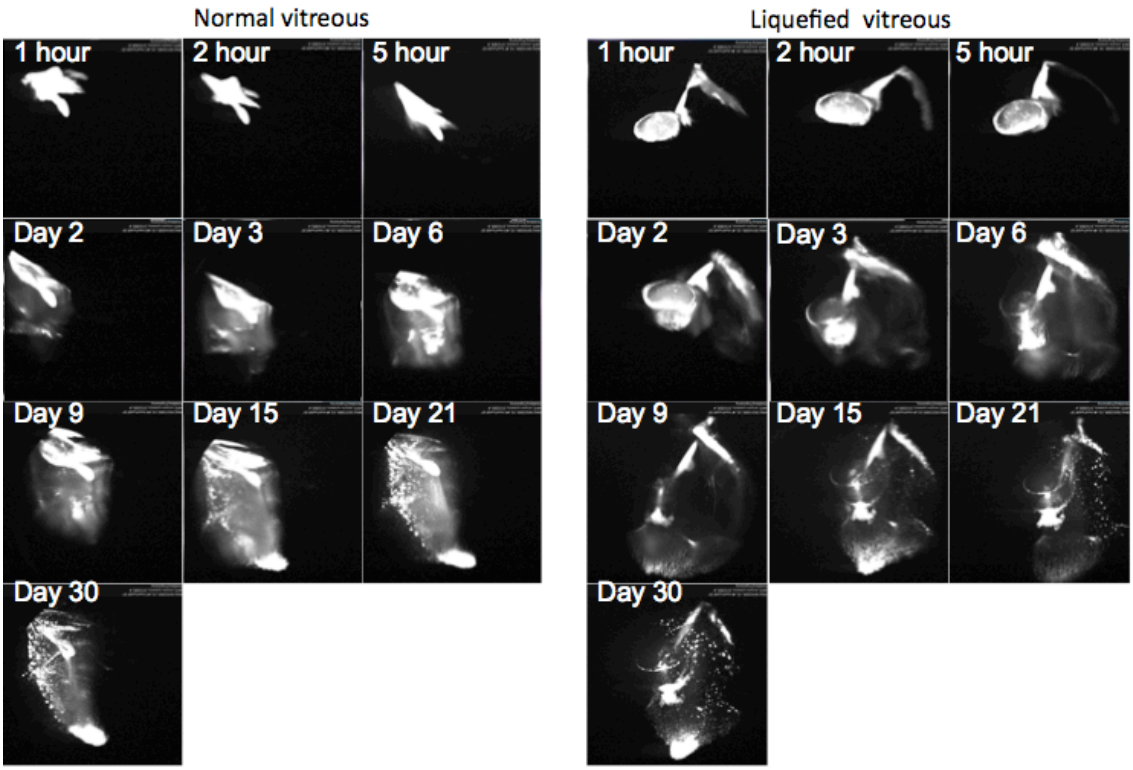

Figure 4.8 A representative set of HRA images obtained from one of the three animals involved in this study. The images were taken from 1 hour until day 30 after injection. The upper part of the image represents the superior area of the rabbit vitreous. Microparticles remained relatively in place at the injection site (superior-temporal) in both models for at least 5 hours post-injection.

4.4 DISCUSSION

In this study, a partially liquefied vitreous model was successfully developed in Dutch-belted rabbits for ocular drug delivery research. To the best of our knowledge, no study to date has quantitatively established a partially liquefied vitreous model using hyaluronidase. Several studies have described intervention for vitreo-retinal problems employing hyaluronidase to induce posterior vitreous detachment (PVD) with varying success (Harooni *et al.,* 1998; Hikichi *et al.,* 2000, Wang *et al.,* 2005). Tanaka and Hui, (2000), Gottlieb *et al.,* (1990) and others (Pirie, 1949; Winkler and Cohn, 1985) have demonstrated that vitreous liquefaction was feasible following hyaluronidase injection without quantifying the degree of liquefaction.

In addition, our data shows that in an unmodified rabbit vitreous only ~20% of its content was composed of a liquid phase, which was similar to that of young human adults (Balazs and Denlinger, 1982). Hyaluronidase liquefied the vitreous by cleaving the glycosidic bonds of the vitreous hyaluronan and changed its structural conformation (Narayanan and Kuppermann, 2009). The resultant depolymerization altered its hydration property leading to the release of bound water as indicated by the increase in vitreous liquid volume and decrease in the gel wet weight observed in this study. We concluded that 0.005I.U./20uL with 48 hours exposure time period achieved the target degree of liquefaction representative of the elderly vitreous. Bracketing this concentration with single point administrations at higher and lower amounts of enzyme suggested that this concentration and exposure time is optimal. In further studies with this model in-house, we have seen no further changes in the sol-gel ratio between 3 and 30 days post-injection of the enzyme, administered to similar animals at the same doses. This observation was further supported by the literature, which has reported that hyaluronidase-induced disaggregation of vitreous hyaluronic acid remained for at least a month before being replaced by the newly formed hyaluronic acid (Pirie, 1949). Based on the old observations by Pirie, it was possible that partial vitreous liquefaction persisted for the entire duration of experiment. Nevertheless, we were unable to confirm in this study if the liquefaction generated was in the form of bulk fluid or several liquid pockets embedded in the gel phase. This process will have to be further investigated.

The inter-animal variability (~9%) was similar in both normal and hyaluronidase-treated groups, emphasizing the robustness of the liquefied model. In addition, it has been reported that hyaluronidase was non-toxic to rabbit retina at a dose of 1U (Gottlieb *et al.,* 1990). The safety of this enzyme was not a prime objective investigated in this study but no gross ocular tissue changes were observed with fundus examination.

Three model compounds were selected to assess the impact of partial vitreous liquefaction on the intravitreal movements of molecules with different molecular weights. The molecular size of sodium fluorescein can be a representative compound

to many intravitreal antimicrobial agents and steroids used in the treatments of ocular infection and inflammation. FD 150 kDa is a large molecule and thus the molecular size might model for antibodies such as bevacizumab. While 1μm fluorescent particles can be representative of the sizes used in microparticulate delivery systems, they are also ideal for examining intravitreal convective flow since diffusive movement is limited for this object size. Drug movements within the vitreous chamber and their intravitreal life-time depend largely on molecular size. Our data shows that FD 150 kDa spread slower and had a longer intravitreal half-life of approximately 30 days as compared to sodium fluorescein, which was cleared within 48 hours. Microparticles, which were the largest among others, remained in the vitreous for longer than a month. These common findings with respect to larger molecules being retained better in the vitreous as compared to smaller molecules have been documented (Park *et al.,* 2005). The likely explanation for this phenomenon is that the diffusion process of larger molecules is limited by the barrier functions of collagen-hyaluronan network (Worst and Los, 1995). Unlike small molecules, which can diffuse in all directions, macromolecules have to move in between the porous gel meshwork and thus, the transport process is largely depending on convective flow (Xu *et al.,* 2000; Stay *et al.,* 2003; Park *et al.,* 2005).

Ocular fluorophotometry shows the presence of concentration gradient across the vitreous chamber with the highest concentration near the anterior chamber and the lowest at the vitreo-retinal surface, suggesting diffusion towards the retina. The clearance pathways of sodium fluorescein and FD 150 kDa were not investigated in this study. However, Araie, Maurice and Cunha-Vaz (Cunha-Vaz and Maurice, 1967; Araie and Maurice, 1991) based on their work in examining the vitreous sections of the frozen eye following intravitreal injection of fluorescent molecules have related this type of distribution pattern to retinal clearance. Fluorescein is a small hydrophile and its clearance from the vitreous appears to be aided by a small nucleotide transporter, termed P2Y2 (Takahashi *et al.,* 2004). However, FD 150 kDa is a relatively large molecule, hydrophilic in nature, which is not transported by this route, and permeation through the retinal layer remained in question. Dias and Mitra (Dias and Mitra, 2000) attributed this observation to the possibility that FD 150 kDa

were cleared via the paracellular or endocytic mechanism present at the retina layer. In addition, the movements of microparticles were more restrictive and slower as compared to sodium fluorescein and FD 150 kDa. This could be due to its hydrophobic interactions with collagen fibers as discussed in Chapter 3.

Moldow and coworkers (Moldow *et al.,* 1998) showed that the diffusion profile of fluorescein in the elderly liquefied vitreous was more homogeneous as opposed to a healthy vitreous. In addition, Foulds and colleagues demonstrated that hyaluronidase increased the clearance of tritiated water (Foulds *et al.,* 1985). These studies demonstrated that small molecules were distributed and cleared faster in the liquefied vitreous system, an observation, which was also illustrated in our study on sodium fluorescein. Since diffusion is the main drive for the transport of small molecules, it is possible that diffusivity in liquefied vitreous may be enhanced. On the other hand, the movement of large molecule depends on convective flow processes (Park *et al.,* 2005). In partially liquefied vitreous, FD 150 kDa was cleared faster which may indicate greater convective movement in the liquefied vitreous circulation. A lower concentration of FD 150 kDa was detected in the liquefied vitreous, suggesting a faster rate of distribution and the capability of the vitreous in sustaining injected doses had significantly reduced. The plot derived from ocular fluorophotometry suggests that there was a temporary forward flux in partially liquefied vitreous model during the first few hours after injection. The same observation was not noted in a normal vitreous. This indicates that the flow processes in the liquefied vitreous generated this movement. Interestingly, forward flux was not evident in the case of sodium fluorescein. We may attribute this to the fact that sodium fluorescein diffused away faster than FD 150 kDa, and thus if present, it may take place at the first few minutes after injection which was not captured in this study. The temporary forward flux of FD 150 kDa in partially liquefied vitreous resulted in a steeper vitreous concentration gradient. However, the gradient pattern remained the same with the level of FD 150 kDa reducing from anterior to posterior at later time points. Hence, we deduced that partial vitreous liquefaction increased the rate of material clearance but materials still moved along the same concentration gradient. More importantly, this observation could explain the need for more frequent injections of bevacizumab

among the elderly population (mean age: 68.5 years; 3.75 injections) as compared to younger individuals (mean age: 39.5 years; 1.75 injections) seen clinically by Spielberg and Ley (Spielberg and Leys, 2009). Therefore, for larger molecules such as antibodies and antibody fragments dosed into the vitreous, the faster rate of clearance in partially liquefied vitreous has to be taken into consideration as part of current research investigating dosing schedule optimization in elderly patients.

In the case of 1 μm fluorescent particles, HRA was used to investigate the difference between the normal and liquefied vitreous models. The fluorescence signals from the microparticles measured with the ocular fluorophotometry had a high level of noise leading to unreliable data. HRA data shows that clusters of fluorescent microparticles were more scattered and sedimented faster under gravitational pull in the partially liquefied vitreous system versus the control eyes. Therefore, tissue exposure at the inferior quadrant of the eye may be greater in the more liquefied vitreous due to faster sedimentation of injected microparticles. In contrast, the local injection site will experience a higher concentration in a more gel-like vitreous, particularly if there is reflux back to the point of injection. Maurice proposed that particle sedimentation might increase the risk of dangerously high drug concentration achieved at the retina layer especially if the patient was sleeping in a supine position (Maurice, 2001). Localized multinuclear giant-cell reaction has also been reported around retina tissues that were in contact with the polymeric microspheres (Giordano *et al.,* 1993). This information will be beneficial to the design of microparticulate formulations, in optimizing the particle size, drug loading, duration and rate of drug release as well as targeting to the desired site of action for the elderly population.

4.5 CONCLUSION

In summary, we have quantitatively established a reproducible partially liquefied vitreous model in laboratory rabbits that represented the degree of vitreous liquefaction occur in the general population of ages around 60 years. Therefore, it can serve as a useful investigative tool in the future of ocular treatments for the elderly population. We have determined the percentage gel phase of unmodified rabbit vitreous and the result showed a close similarity to young human adults. Therefore, the use of juvenile animal models may underestimate the influence of convective forces present in the elderly patients, thereby overestimating drug efficacy. The joint operation of ocular fluorophotometry and HRA in current study provided a better understanding of intravitreal events. We managed to correlate data from both techniques in a quantitative manner. Unlike previous studies, we were able to relate the degree of vitreous liquefaction to material transport. Therefore, data provided in this study are more relevant to actual clinical situations. More studies are currently being undertaken in our laboratory to further understand the influence of vitreous liquefaction on drugs released from controlled release devices. However, the limitation of our current model is that it has neglected the influence of collagen fibers formed upon aging, which may be important for drug molecules prone to protein binding. Future studies should take this factor into consideration.

CHAPTER 5: FORMULATION OF BRIMONIDINE TARTRATE POSTERIOR SEGMENT OCULAR DRUG DELIVERY SYSTEM

5.1 INTRODUCTION

Brimonidine tartrate [5-bromo-6-(2-imidazolidinylideneamino) quinoxaline L-tartrate] is a highly selective α_2-adrenergic agonist. The empirical chemical formula is $C_{15}H_{16}N_5O_6Br$ and the chemical structure is as shown in Figure 5.1. It is a small molecule having a molecular weight of 442 Da; with a pKa of 7.78±0.05. Brimonidine tartrate is highly soluble in water at low pH and solvents such as DMSO (dimethylsulfoxide).

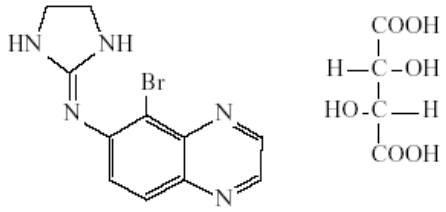

Figure 5.1 Chemical structure of brimonidine tartrate

Commercially, brimonidine is available in its tartrate salt form as 0.1% and 0.15% w/v sterile ophthalmic solution (Alphagan® P) and as a 0.2% w/v sterile ophthalmic solution (Alphagan®)). Brimonidine tartrate is also available in combination with timolol in the commercial product Combigan™ (Brimonidine Tartrate, Timolol Maleate Ophthalmic Solution 0.2%/0.5%). It is used to reduce the intraocular pressure in open-angle glaucoma and ocular hypertension. It is also administered prior to phacoemulsification cataract surgery and after argon laser trabeculoplasty to prevent post-operative increase of intraocular pressure. Studies have shown that the hypotensive effect of brimonidine is associated with an initial decrease in aqueous humour production, followed by an increase in uveoscleral outflow on long term treatment.

Pharmacologically, topically administered brimonidine achieves sufficient concentrations in the posterior segment (vitreous and retina) to activate α_2-adrenoceptors, in the nuclear layer of the retina cells and in the retinal ganglion cells (Kalapesi *et al.,* 2005). The activation of the receptors appears to be associated with protection against degeneration of the retinal ganglion cells and the optic nerve; a condition which if not properly controlled may lead to progressive vision loss. The neuroprotective effects have been validated in animal disease models, which include chronic ocular hypertension, optic nerve degeneration and ischemia/reperfusion injury with encouraging results (Yoles *et al.,* 1999, WoldeMussie *et al.,* 2001, Kent *et al.,* 2001, Lafuente *et al.,* 2001, Wheeler *et al.,* 2001). Clinically, glaucomatous patients have also gained better contrast sensitivity in their vision after topical instillation of brimonidine (Evans *et al.,* 2003).

Following a single intravitreal injection into female albino rabbit eyes, brimonidine tartrate has a short intravitreal half-life of approximately 1.4 hours, suggesting sustained drug delivery to the retina will be an issue (Allergan report PK-02-P023). Topical ocular administration of a 0.2% and 0.5% dose of brimonidine tartrate was associated with a short vitreal half-life (Acheampong *et al.*, 2002). Repeated dosing, perhaps q.d.s. may overcome the problems associated with a short intravitreal half-life but patient compliance would be an issue. This suggests a controlled release drug delivery system will provide a better control over disease progression. Colleagues at Allergan have developed a posterior segment ocular drug delivery system (Brimonidine Tartrate PS DDS), which sustained the release of brimonidine tartrate into the vitreous humor over a few months. Phase-II clinical trials of this system to investigate visual improvement in patients with previous rhegmatogenous retinal detachment as well as in patients with diabetic macular ischemia or geographic atrophy due to age-related macular degeneration and retinitis pigmentosa.

The effects of vitreous liquefaction on the release of brimonidine tartrate from a DDS has yet to be investigated and will be timely since the majority of patients treated for age-related macular degeneration are the elderly. This aspect of research

programme will be described in Chapter 6 and to support this activity; a brimonidine tartrate controlled drug delivery system was developed as described in this chapter.

5.2 STUDY OBJECTIVE

The objective of this study was to fabricate a biodegradable and injectable posterior segment ocular drug delivery system (DDS) that would be able to sustain the release of brimonidine tartrate for one month. It is intended that the DDS will then be used in preclinical drug development studies, which will be described in Chapter 6. In order to achieve the objective, the characteristics of the DDS were optimized using the Design of Experiment (DOE) approach to meet the following criteria:

1. 0.018-inch ± 10% in diameter in order to fit through a 25-gauge applicator system as illustrated in Figure 5.2, which will be used for intravitreal placement.

2. Near zero order drug release profile with the percentage drug release at each time point designed to be as shown in Table 5.1.

Sampling time point (Day)	% Cumulative brimonidine released
1	Minimal
3	<10
7	25
14	50
21	75
30	100

Table 5.1 Target percentage cumulative brimonidine released at each time point.

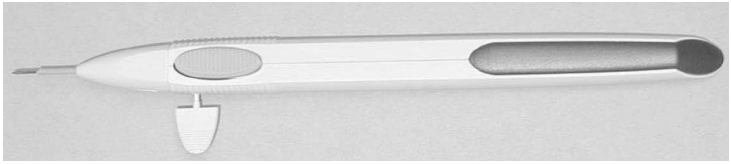

Figure 5.2 An illustration of a 25-gauge applicator system (Adapted from Haller *et al.,* 2009).

5.3 STUDY METHODOLOGIES

5.3.1 CHEMICALS AND REAGENTS

Brimonidine tartrate powder (Batch #: AL-II/M-01306) was kindly provided by Allergan Inc. Poly D, L-lactide, (R203s [I.V= 0.25-0.35dl/g, molecular weight range = 18000-28000 Da, end group= alkyl] batch #: 1034528) and Poly D, L-lactide-co-glycolide 50:50 (RG502 [I.V= 0.16-0.24dl/g, molecular weight range: 7000-17000 Da, encapped end group=alkyl ester] batch #: 0496) were purchased from Boehlinger Ingelheim (Ridgefield, CT, USA). The chemical structures of R203s and RG502 are as shown in Figure 5.3. Phosphate buffer solution (PBS) powder (batch #: 028K8214) was purchased from Sigma Aldrich (St. Louis, MO, USA). Deionized water was obtained from Mili-Q dispenser supplied by Milipore (Mili-Q POD, USA). Acetonitrile (batch #: CY 758) and methanol (batch #: CV 262) were obtained from Burdick & Jackson (via VWR, PA, USA). Formic acid 88% (batch #: E12635) and sodium hydroxide (10N) (batch #: G02506) were purchased from Mallinckrodt chemicals and JT Baker respectively.

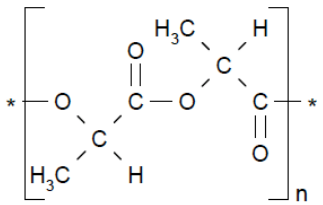

$-(C_6H_8O_4)_n-$

Poly (D,L-lactide)

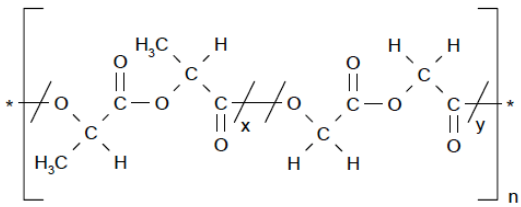

$-[(C_6H_8O_4)_x(C_4H_4O_4)_y]_n-$

Poly (D,L-lactide-co-glycolide)

Figure 5.3 Chemical structures of Poly (D,L-lactide), R203s and Poly (D,L-lactide-co-glycolide), RG502.

5.3.2 MATERIALS AND METHODS

Brimonidine tartrate and its polymer powders were weighed using a balance (Mettler Toledo MT6 Highstown, NJ). Powder blending was performed using a turbula

shaker (Glenn Mills Turbula T2F shaker, assigned ID #: Shaker-Turb0502-PDEV). The powder blend was compacted using a modified pneumatic drive powder compactor (Janesville Tool and Manufacturing Inc., model A-1024, assigned ID #: 4014) and DDS was extruded using a custom built piston extruder (APC engineering Inc, assigned ID #: EXT-0500-PDEV), which was coupled to a temperature controller and thermocouple (Watlow 93). DSC instrument and the Tzero pan and lid were purchased from TA instrument (New Castle, DE, USA). HPLC analyses were performed on a Waters 2690 HPLC system equipped with a Waters 996 PDA detector, mobile phase pump, sample injection system and column storage chamber. Data acquisition and integration were accomplished using Empower Pro software (version 2002). The dissolution studies were performed using a reciprocal shaking water bath (Thermo Scientific, Asheville, NC, USA). The individual DDS was inserted into a 25-gauge applicator system, which was kindly provided by Allergan Inc.

5.3.3 DESIGN OF EXPERIMENTS (DOE)

In an attempt to optimize critical parameters for the formulations, DDS with a linear combination of brimonidine tartrate and polymers (R203s and RG502) were initially manufactured to establish a correlation between drug loading and percentage composition of polymers. These first batches of DDS were assigned with identifiers 9623-16 to 9623-27 as listed in Table 5.2. DDS with batch numbers 9623-26 and 9623-27 were placebo implants. The drug release profiles of these DDS (962316 to 9623-27) as acquired from the *in vitro* release studies (Section 5.3.5) were then manually entered into the Statease® Expert version 6.0 software (Stat-Ease, Inc., MN, USA). A cubic model design as illustrated in Figure 5.4 was selected and the input factors were polymer R203s, polymer RG502 and brimonidine tartrate. Four constraints were applied to the percentage weight of the formulation components. 1) $10\% \leq$ Brimonidine $\leq 50\%$, 2) $0\% \leq$ R203s $\leq 90\%$ 3) $0\% \leq$ RG502 $\leq 90\%$ and 4) the percentage composition must add up to 1. The response outputs were extrusion temperature and percentage drug release on day 1, 3, 7, 14, 21 and 30. The calculated p-value based on the analysis of variance (ANOVA) was used to determine the

degree of significance of each input factor on the response output. The experimental sequence was subjected to randomization and repetition to improve the robustness of the model.

Formulation batch number	% BT	% R203s	% RG502
9623-16	10	-	90
9623-17	20	-	80
9623-18	30	-	70
9623-19	40	-	60
9623-20	50	-	50
9623-21	10	90	-
9623-22	20	80	-
9623-23	30	70	-
9623-24	40	60	-
9623-25	50	50	-
9623-26 (placebo)	-	100	-
9623-27 (placebo)	-	-	100

Table 5.2 Initial formulations consisting of a linear combination of brimonidine tartrate (BT) and R203s and RG502.

The design of experiment space can also be represented as a cubic model as shown in the diagram below. The red dots indicate the sampling points in the scheme of investigations, whereas the three vertices of the triangle each represent one input factor.

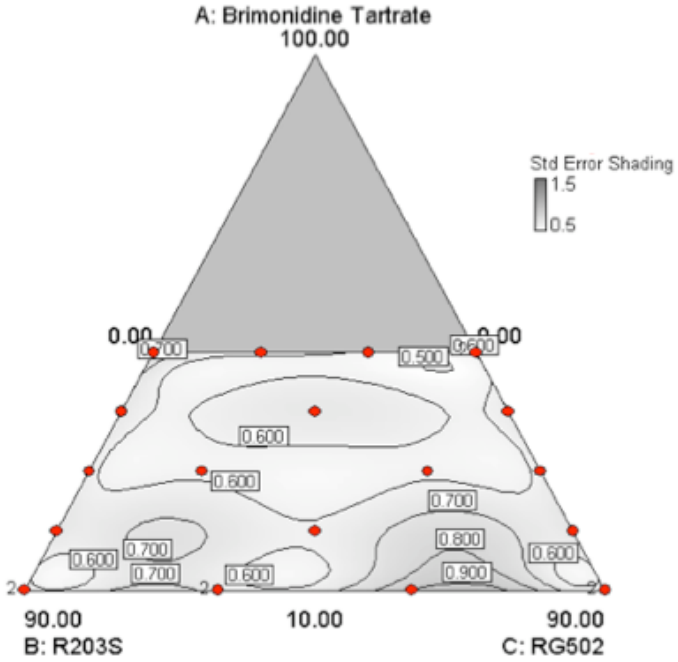

Figure 5.4 Cubic model design with standard error. Standard error was higher with 10% brimonidine tartrate RG502 DDS.

5.3.4 FABRICATION OF BRIMONIDINE TARTRATE POSTERIOR SEGMENT DDS

5.3.4.1 POWDER BLENDING AND COMPACTION

Brimonidine tartrate and polymer powders were weighed and mixed in a stainless steel container using a Turbula shaker and two small stainless steel balls for 15 minutes twice with manual mixing with spatula between shaking. When the powder mixture was ready, it was compacted using a powder compactor into a stainless steel barrel with a 420 µm nozzle attached. The powder-filled barrel was placed into the piston-extruder and left to equilibrate at the intended extrusion temperature for 30 minutes.

5.3.4.2 EXTRUSION OF BRIMONIDINE TARTRATE DDS

The extrusion temperature was determined based on the glass transition temperature of the polymers, which will be affected by the addition of active pharmaceutical ingredients (API), an effect known as plasticization. All DDSs were extruded using the speed setting number 0.0025. Once extruded, the diameters of the cooled rods were measured using vernier calipers. The DDSs were stored in a polypropylene tube, which was sealed in an aluminium pouch containing desiccants until further use.

5.3.5 *IN VITRO* DRUG RELEASE STUDIES

Phosphate buffered saline (PBS) was prepared from a preweighed mixture and dissolved in 1 L deionised water, yielding a 0.01 M phosphate buffered solution at pH 7.4. Three 1 mg DDS from each batch were cut and weighed and each was placed in a glass vial with 10 mL PBS. Samples were visually inspected to ensure that all DDS were immersed below the level of fluid in the vials and placed in a shaking water bath at a temperature 37 ^{0}C with a shaking speed of 50 rpm. Sampling of DDS media was performed on day 1, day 3 and weekly for a month. The dissolution media were replaced with fresh media at each sampling time point to ensure sink conditions were maintained.

5.3.6 EVALUATION OF BRIMONIDINE TARTRATE DISTRIBUTION IN DDS

5.3.6.1 CONTENT UNIFORMITY TEST

Ten DDS of 1 mg each were cut and weighed. Each DDS was then placed in a 10 ml glass vial. One mL of acetonitrile was added to each vial, in order to dissolve the DDS. The solution was briefly shaken, then sonicated for 3 minutes. Nine mL of deionised water was added to each vial and the solution was further sonicated for 2

minutes to achieve complete dissolution. One mL of the sample was subsequently transferred into a HPLC vial for further analysis.

5.3.6.2 DETERMINATION OF GLASS TRANSITION TEMPERATURE

The glass transition temperature (T_g) of DDS and powder blend was analyzed using modulated differential scanning calorimetry (MDSC). Approximately 3 mg of sample was weighed onto a Tzero low mass pan and sealed. The system was equilibrated at 20 ^{0}C for 3 minutes before the temperature was ramped up to 100 ^{0}C at 2 ^{0}C/minute. Subsequently, the temperature was reduced to 20 ^{0}C at 5 ^{0}C/minute. The sample was then maintained at 20 ^{0}C for 3 minutes before being heated to 100 ^{0}C at 2 ^{0}C/minute. T_g was calculated during the third cycle of the heating process.

5.3.7 GAMMA STERILISATION

Thirty 0.7 mg DDS from batch 9623-69 were cut and weighed. They were individually inserted into a 25-gauge applicator system and sealed in an aluminium pouch containing desiccants. The samples were then sent to an external contract lab (Sterigenics) for gamma sterilisation. The gamma dose used during sterilisation was around 25-40 kGy.

5.3.8 HPLC ANALYSIS

5.3.8.1 PREPARATION OF STOCK SOLUTIONS AND WORKING STANDARD SOLUTIONS

Three separate stock solutions of brimonidine tartrate were prepared by each weighing approximately 10 mg of brimonidine tartrate powder and dissolving in the appropriate volume of mobile phase to produce a 1 mg/mL solution. The stock solutions were stirred for 5 minutes with a magnetic stirrer and then sonicated for

another 5 minutes to ensure complete dissolution. Serial dilutions were performed on each stock solution to obtain a total of three calibration series and the preparation scheme of a calibration series is as shown in Table 5.3. Stock solutions and working standard solutions were prepared in amber borosilicate volumetric flasks and stored at 4 ^{0}C when they were not in use.

Brimonidine tartrate working solution ID	Concentration of solution used (µg/mL)	Volume of solution added (mL)	Volume of mobile phase added (mL)	Final volume (mL)	Final concentration (µg/mL)
WS1	1000	5	45	50	100
WS2	100	30	20	50	60
WS3	100	16	34	50	32
WS4	100	5	45	50	10
WS5	60	5	45	50	6
WS6	10	1	49	50	2
WS7	10	5	45	50	1
WS8	6	5	45	50	0.6
WS9	2	5	45	50	0.2
WS10	1	5	45	50	0.1

Table 5.3 Preparation scheme for working standard solutions.

5.3.8.2 HPLC ASSAY METHOD

An external standard assay method was employed in the analysis of brimonidine released from the DDSs. Using this method, a known concentration of brimonidine tartrate standard solution was used as a reference standard. The reference standard was run before and after every six samples and the concentration of the sample was calculated with reference to the standard solution using the following equation.

$$C_S = (P_S * C_R)/\text{Ave}\ (P_{R1}, P_{R2})$$

C_S = Sample concentration; C_R = Standard concentration; P_S = Peak area of sample; P_{R1} & P_{R2} = Peak areas of standards run before and after the sample

5.3.8.3 ANALYTICAL CONDITIONS

The HPLC system comprises of a pump, an autoinjector, a column storage chamber and a photodiode array detector (PDA). The analytical condition used is as described in Table 5.4. Prior to analysis, the HPLC system was conditioned (with column attached) for about 2 hours to stabilize the system pressure and column performance. Chromatography was performed under isocratic elution of the mobile phase. The detection of brimonidine was performed at wavelengths 240-270 nm. The spectral data collected at wavelength 246 nm was integrated and used for analyte quantitation.

Parameters	**Conditions**
Stationary phase (column)	Waters Symmetry C18, 3.5µm, 4.6x150mm
Column temperature	Room temperature
Mobile phase	0.1M sodium formate buffer pH3.0: methanol (85:15)
Flow rate	1mL/min
Detection wavelength	246nm
Injection volume	20µL
Sample diluent	Mobile phase
Run time	15 mins
Needle wash	Methanol: water (30:70)

Table 5.4 Brimonidine tartrate HPLC condition.

5.3.8.4 VALIDATION OF HPLC ANALYTICAL METHOD

5.3.8.4.1 SYSTEM SUITABILITY

A system suitability test was routinely performed prior to sample analysis in order to check for system stability. Two separate preparations of brimonidine standard solutions, namely working standard 1 (WS1) and working standard 2 (WS2), were run in a replicate of six and three respectively. The percentage recovery was

calculated as follows and any value between 98-102% was considered as acceptable in practice.

% Recovery = (Mean PA WS2/WS2 concentration)* (WS1 concentration/Mean PA WS1)*100

5.3.8.4.2 SELECTIVITY

The selectivity of the assay method was assessed against interference caused by polymers. The test was performed using placebo DDS. A placebo DDS was first dissolved in 10% acetonitrile and sonicated for 5 minutes until complete dissolution. An aliquot of the sample was analysed using HPLC. The assay method was considered selective if there was no interference peak observed at the same retention time as brimonidine.

5.3.8.4.3 LINEARITY

A linear regression curve of mean peak area against analyte concentration was generated using Microsoft Excel® software. Each curve contained at least six calibration standards over a concentration range of 0.2-60 µg/mL. The correlation coefficient (r^2) of the linear regression curve was used to determine the linearity of the assay method and detector response, with any values greater than 0.97 was considered as desirable in practice.

5.3.8.4.4 ACCURACY AND PRECISION

Inter- and intra-day accuracy and precision of the assay method were evaluated by comparing six measurements of three standards of concentration 0.2, 2 and 10 µg/mL on the same day (intra) and on two different days (inter). Accuracy and precision of the assay method were expressed as % accuracy and % RSD (relative standard deviation) respectively using the following equations.

Accuracy, % = [mean observed concentration /nominal concentration x 100]

Precision, %RSD = [Standard deviation/mean x 100]

The acceptance criteria for accuracy determined from both intra- an inter-day analysis will be within 85-115% of the nominal concentrations; while for precision, the calculated % RSD will be ≤ 15%.

5.3.8.4.5 LOWER LIMIT OF QUANTITATION (LLOQ)

The lower limit of quantitation of the assay method was determined as the lowest concentration that could be reliably quantified by the detector. The conditions for acceptance are as follows: (a) the analyte response peak of this concentration must be at least ten times greater than the baseline noise and (b) the triplicate measurement of this concentration must also meet the acceptance criteria set out for accuracy and precision as defined above.

5.4 RESULTS

5.4.1 DDS WITH LINEAR COMBINATION OF BRIMONIDINE TARTRATE AND POLYMERS

DDSs with a linear combination of brimonidine tartrate and poly D, L-lactide-co-glycolide (RG502) were extruded at 75-80 ^{0}C, whereas the extrusion temperatures were 80-85 ^{0}C with poly D, L-lactide (R203s) as shown in Table 5.5.

Formulation batch number	% BT	% R203s	% RG502	Extrusion temperature, ^{0}C	DDS diameter (inch)
9623-16	10	-	90	80	0.015-0.017
9623-17	20	-	80	75	0.016-0.018
9623-18	30	-	70	75	0.016-0.018
9623-19	40	-	60	80	0.016-0.018
9623-20	50	-	50	80	0.017-0.019
9623-21	10	90	-	85	0.015-0.017
9623-22	20	80	-	85	0.015-0.017
9623-23	30	70	-	85	0.016-0.017
9623-24	40	60	-	85	0.016-0.017
9623-25	50	50	-	85	0.016-0.017
9623-26 (R203s PLA placebo)	-	100	-	80	0.015-0.017
9623-27 (RG502 PLGA placebo)	-	-	100	80	0.014-0.017

Table 5.5 Extrusion temperatures of DDS with linear combination of brimonidine tartrate and polymers (R203s or RG502).

Figure 5.5 illustrates the classical triphasic release pattern of RG502 DDS, which was characterized by a lag phase that lasted for approximately 7 days, followed by a diffusional phase between day 7 and day 14, and then a burst release phase after day 14. The time required to 100% drug release varied with drug loading. At 10% drug loading DDS complete release achieved by day 21 and on day 30 for 20% and 30% drug loading DDSs. DDSs with 40% and 50% drug loading had a longer duration of drug release (>30 days), however, the release profile of 50% drug loading did not follow the general pattern seen at lower loadings.

Implants with 50% drug loading showed an initial burst release of 26% of the total drug on day 1 as compared to less than 10% in the case of DDSs at 10-30% drug loading. Both DDSs with 40% and 50% drug loading had higher percentage of drug release on day 1, 3 and 7 but lower percentage of drug release after day 14 as compared to lower drug loading DDSs.

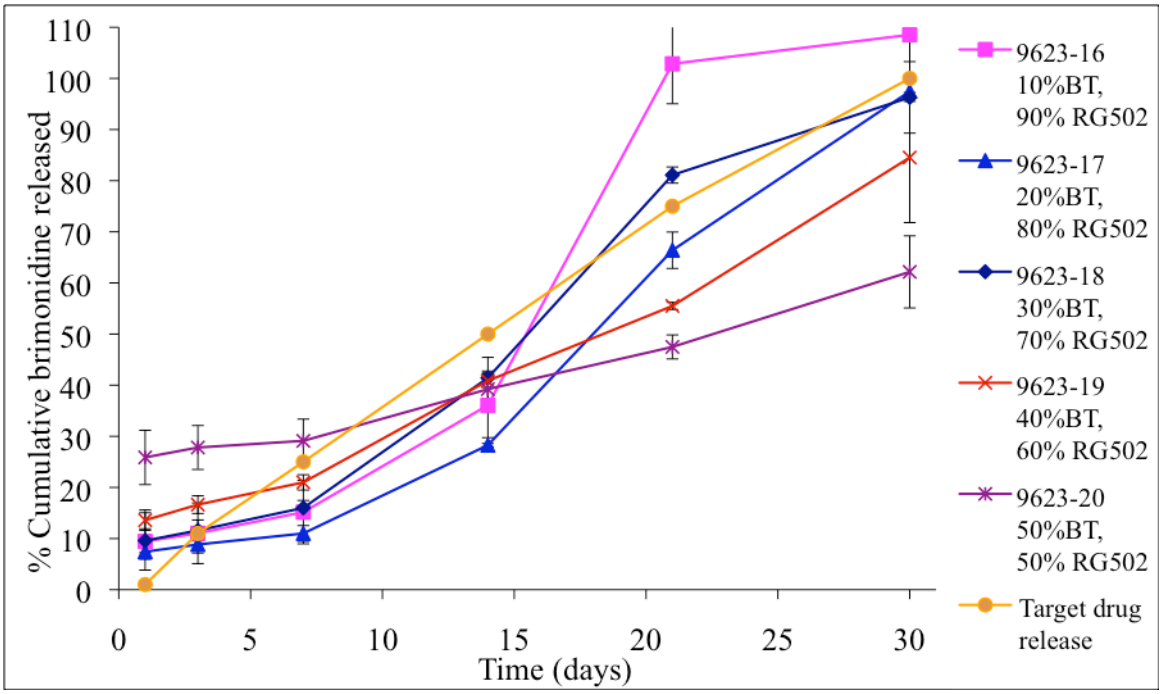

Figure 5.5 Cumulative drug release profile of RG502 implants with drug loading ranging from 10-50%. (n = 3 per measurement).

Figure 5.6 illustrates the release profiles of DDSs with a linear combination of brimonidine tartrate and poly D, L-lactide (R203s). As noted with RG502, the DDS

with 50% drug loading had a burst release on day 1. Generally, all R203s DDSs exhibited similar trend of release profiles characterized by a short lag time of little or no release, followed by an almost zero release phase that lasted over 7-8 weeks. In comparison to PLGA (refer to Figure 5.5), DDS produced using PLA had a slower rate of drug release.

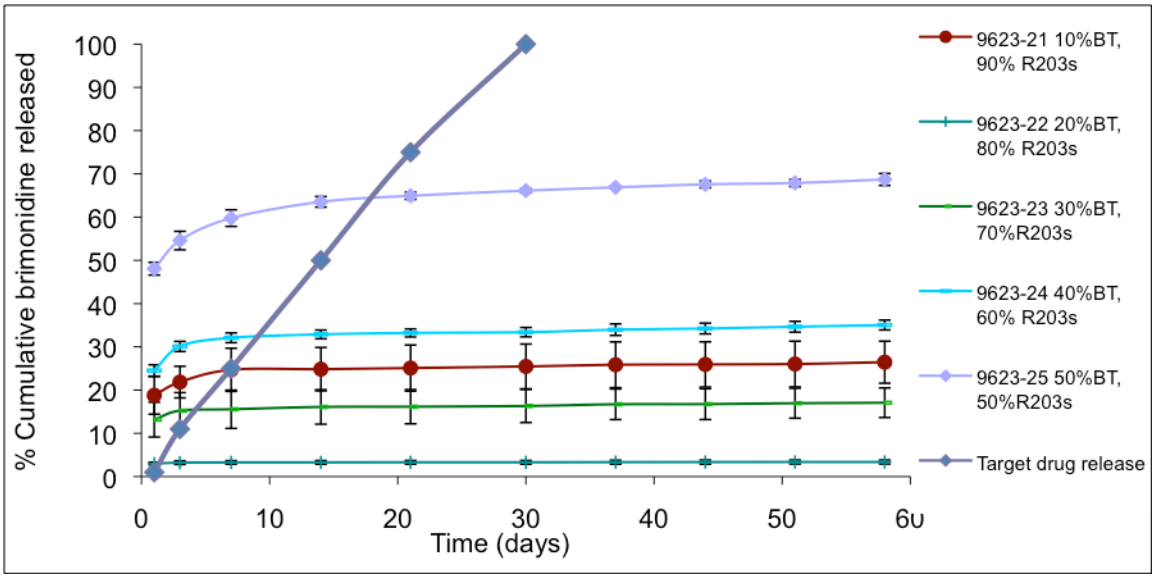

Figure 5.6 Cumulative drug release profile of R203s implants with drug loading ranges from 10-50%. (n=3)

Nevertheless, none of the DDSs produced based on a linear combination of either RG502 or R203s conformed to the target requirement. Hence, the formulations were further optimized using the Design of Experiments (DOE) approach.

5.4.2 DDS OPTIMISATION USING DOE MODEL

FIRST STAGE OF THE OPTIMISATION PROCESS

Based on the data obtained from the DDS with a linear combination of brimonidine tartrate and polymers (Figure 5.5 and Figure 5.6), DOE software recommended new formulations (Table 5.6) that have a mixture combination of drug loading and percentage composition of polymers. These DDSs were assigned with batch numbers 9623-64 to 9623-75.

Formulations	Input factors		
	% Drug loading	% R203s	% RG502
9623-64	10	60	30
9623-65	50	0	50
9623-66	50	16.67	33.33
9623-67	50	33.33	16.67
9623-68	10	60	30
9623-69	30	17.5	52.5
9623-70	10	30	60
9623-71	30	52.5	17.5
9623-72	20	40	40
9623-73	10	0	90
9623-74	10	90	0
9623-75	40	30	30

Table 5.6 DDS formulations suggested by DOE.

The extrusion temperatures and release profiles for these DDSs are as shown below in Table 5.7 and Figure 5.7 respectively.

Formulation batch number	% BT	% R203s	% RG502	Extrusion temperature, ^{0}C	DDS diameter (inch)
9623-64	10	60	30	79	0.015-0.018
9623-65	50	0	50	80	0.015-0.017
9623-66	50	16.67	33.33	78	0.015-0.018
9623-67	50	33.33	16.67	75	0.015-0.017
9623-68	10	60	30	80	0.016-0.018
9623-69	30	17.5	52.5	75	0.015-0.018
9623-70	10	30	60	75	0.015-0.018
9623-71	30	52.5	17.5	75	0.015-0.017
9623-72	20	40	40	75	0.016-0.019
9623-73	10	0	90	75	0.016-0.019
9623-74	10	90	0	75	0.016-0.019
9623-75	40	30	30	78	0.015-0.017

Table 5.7 Extrusion temperatures and DDS diameters for different drug-polymer blends.

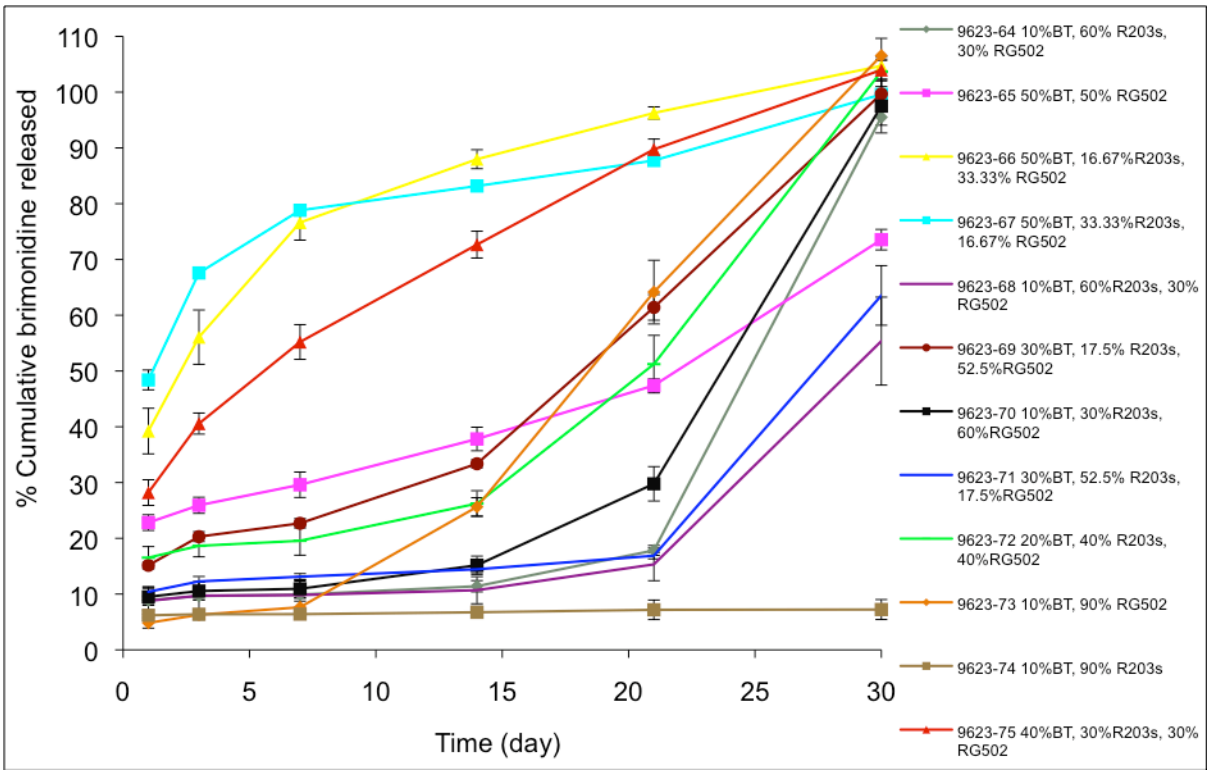

Figure 5.7 Cumulative drug release profile of implants with a mixture of drug loading and percentage composition of polymers.

Figure 5.7 shows that DDSs with higher drug loading (9623-65, 9623-66, 9623-67 and 9623-75) had burst release on day 1 and finished releasing by day 30 except 9623-65. In contrast, 10% drug loading DDSs (9623-64, 9623-68, 9623-70 and 9623-74) were associated with lower rate of drug release. DDS 9623-71 has a higher percentage of R203s, exhibited a more sustained drug release profile as compared to 9623-69 of similar drug loading. A variation in the release profiles was observed with DDSs of identical composition produced on two separate occasions, for example 9623-64 and 9623-68.

SECOND STAGE OF THE OPTIMISATION PROCESS

The drug-release data obtained from the first stage optimization process (9623-64 to 9623-75) went through a second stage optimization process using the DOE program. The software suggested that DDS (9623-112) with 31% drug loading, 15% R203s and 54% RG502 (Figure 5.8 right panel) would have a release profile of 84%

similarity to the target requirement. The predicted percentage release at each sampling time point is as listed in Figure 5.8 (right panel).

Nevertheless, Figure 5.9 below shows that the experimental release profile of 9623-112 deviated from that estimated in Figure 5.8, although the extrusion temperature of 77 ^{0}C remained as predicted. In fact, the release profile of 9623-69 was rather closer to that of predicted and target requirement. Therefore, 9623-69 was selected for use in preclinical drug development in this instance (Chapter 6).

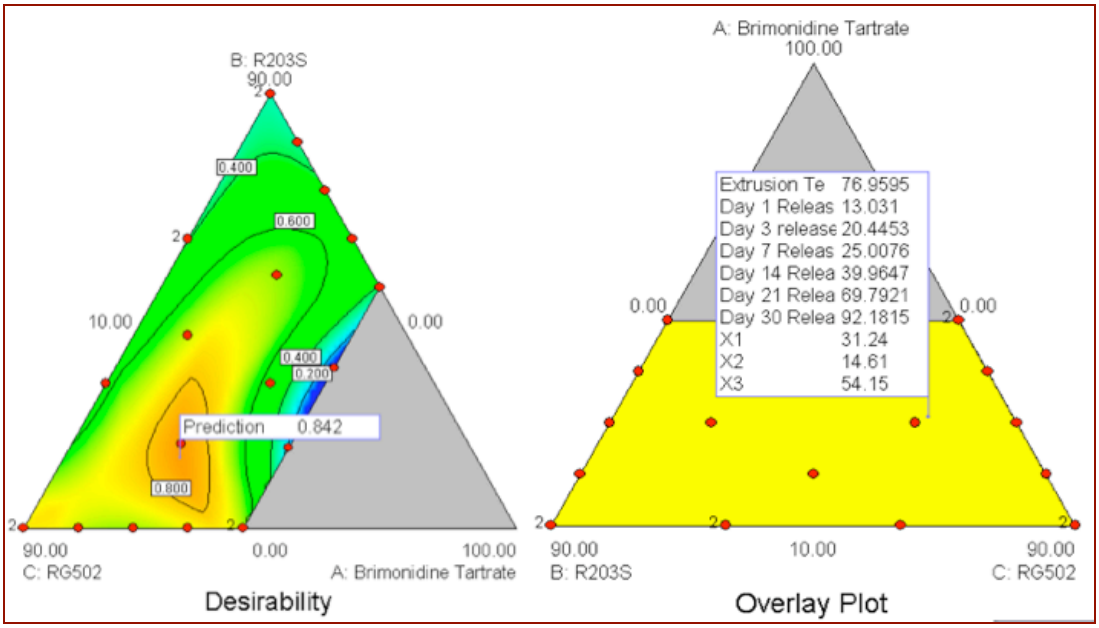

Figure 5.8 Best-predicted drug release profile with 84% similarity to the target lies on region covering 31% drug loading, 15% R203s and 54% RG502 (left). The corresponding predicted release profile is as listed on the right cubic model.

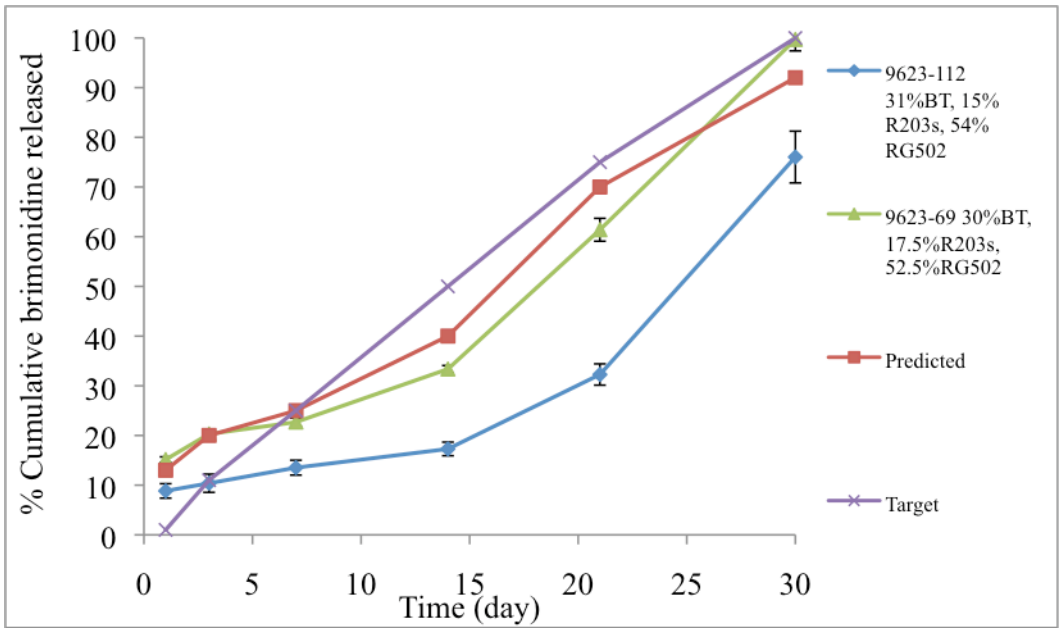

Figure 5.9 Comparison between the drug release profiles of 9623-112 (suggested) and 9623-69 to that of the target and DOE predicted (mean±s.d., n=3).

5.4.3 INTERACTIONS BETWEEN DRUG LOADING AND PERCENTAGE COMPOSITION OF POLYMERS

The effect of interaction between drug loading and percentage composition of polymers on drug release was assessed using ANOVA (part of Statease® software) with the significance level established at p-value < 0.05. Table 5.8 below shows that the effect of interaction between drug loading and polymers (AB and AC) was significant on day 1, 3 and 7; whereas, the effect of interaction between R203s and RG502 (BC) was significant on day 21 and day 30. This suggested that drug loading had a stronger influence during the initial diffusive phase; whereas composition and type of polymer were more important at later time point when the polymers were degraded. Day 14 marked the transition between the stages of drug diffusion and polymer degradation as the interaction was deemed significant only in the presence of all the factors involved (ABC).

Output response	Source	p-value	Significant Yes/No
Day 1 release	AB	0.0005	Yes
	AC	<0.0001	Yes
	BC	0.9919	No
	ABC	0.0328	Yes
Day 3 release	AB	0.0089	Yes
	AC	0.0025	Yes
	BC	0.7919	No
	ABC	0.0036	Yes
Day 7 release	AB	0.0093	Yes
	AC	0.0031	Yes
	BC	0.5044	No
	ABC	0.0018	Yes
Day 14 release	AB	0.0630	No
	AC	0.0246	No
	BC	0.1939	No
	ABC	0.0044	Yes
Day 21 release	AB	0.1896	No
	AC	0.0549	No
	BC	0.0471	Yes
	ABC	0.0013	Yes
Day 30 release	BC	0.0392	Yes

Table 5.8 The impact of interactions between drug loading and percentage composition of polymers on drug release, established using ANOVA statistical tests. A: Brimonidine; B: R203s; C: RG502

5.4.4 CONTENT UNIFORMITY TEST

The content uniformity of brimonidine was assessed using DDSs with 10% and 50% drug loading as described in Table 5.9. The result shows that content uniformity was poorer in 10% drug loading RG502 DDS as compared to R203s DDS of similar drug loading. Despite the case, the content uniformity of all DDSs tested was within the acceptable range of 10%.

Formulations			μg release (average)	μg release (St Dev)	% RSD
% BT	%R203s	%RG502			
10	0	90	110.00	12.06	10.96
50	0	50	522.18	36.68	7.02
10	90	0	109.91	7.47	6.80
50	50	0	513.20	44.51	8.67

Table 5.9 Percentage RSD of drug content calculated based on 10 separate DDSs.

5.4.5 GLASS TRANSITION TEMPERATURE

Table 5.10 shows that the glass transition temperatures (Tg) of unprocessed polymer powder were the same as the corresponding placebo polymer DDSs. A similar finding was also illustrated with 10%, 20% and 50% drug loading DDS, of which Tg was similar to their corresponding powder blends. However, when the powder blends of R203s and RG502 mixed together in equal ratio, the resulted Tg was an average Tg of both polymers, reflecting an effect of mixing both polymers together.

Samples	% Drug loading	% R203s	% RG502	Tg (^{0}C)
R203s powder blend	0	100	0	43.36
RG502 powder blend	0	0	100	38.20
50% R203s, 50% RG502 powder blend	0	50	50	40.95
R203s placebo DDS	0	100	0	43.44
RG502 placebo DDS	0	0	100	38.29
10% brimonidine, 90% R203s DDS	10	90	0	43.46
10% brimonidine, 90% RG502s DDS	10	0	90	37.71
50% brimonidine, 50% R203s DDS	50	50	0	43.56
50% brimonidine, 50% RG502 DDS	50	0	50	38.64
20% brimonidine, 40% R203s, 40% RG502 DDS	20	40	40	40.00

Table 5.10 Glass transition temperature of individual polymer powder blend, placebo implant, high and low drug loading implants.

5.4.6 EFFECTS OF GAMMA STERILISATION

Gamma sterilisation increased the rate of drug release as indicated by the steeper curve gradient illustrated in Figure 5.10. It was found that the rate of drug release from sterilised DDS had been increased by 21%, 38% and 37% on day 7, 14 and 21 respectively as compared to non-sterilised DDS. However, no difference was observed between both DDSs on day 1 and 3. Due to the faster rate of drug release from sterilised DDS at earlier time points, less than 5% brimonidine remained on day 21 as compared to ~40% in non-sterilised DDS. Therefore, sterilised DDS had a shorter duration of drug release.

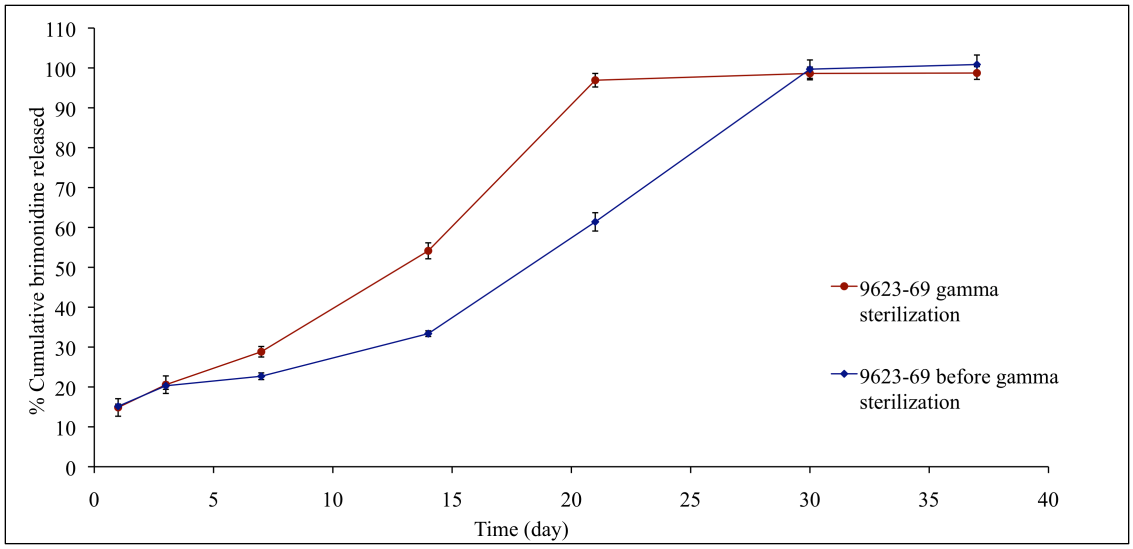

Figure 5.10 Cumulative drug release profile of sterilized and non-sterilized brimonidine DDS over a period of one month.

5.4.7 VALIDATION OF HPLC ASSAY METHOD

5.4.7.1 SYSTEM SUITABILITY

Percentage recovery was calculated on each occasion prior to sample analysis. Table 5.11 shows the mean percentage recovery calculated on two separate occasions of the validation process. WS1 and WS2 in context were 100 µg/mL brimonidine standard working solutions prepared from two separate stock solutions. The % recovery was > 99% for both occasions, which met the acceptance criteria for system suitability test.

Run 1	Peak Area WS1 (n=6)	RT WS2	Peak Area WS2 (n=3)	RT WS2
Mean	6609868	4.000	6605646	4.360
% RSD	0.31	0.14	0.08	0.07
% Recovery	99.90			
Run 2				
Mean	6607994	4.000	6593021	4.460
% RSD	0.11	0.09	0.08	0.18
% Recovery	99.80			

Table 5.11 Mean percentage recovery calculated from two separate occasions of the validation process.

5.4.7.2 SELECTIVITY

Representative HPLC chromatograms of PBS, mobile phase, placebo DDS sample solutions, and brimonidine DDS samples were as illustrated in Figure 5.11 below. The assay method was considered as selective since no interference peaks of polymers or reagents co-eluted with brimonidine.

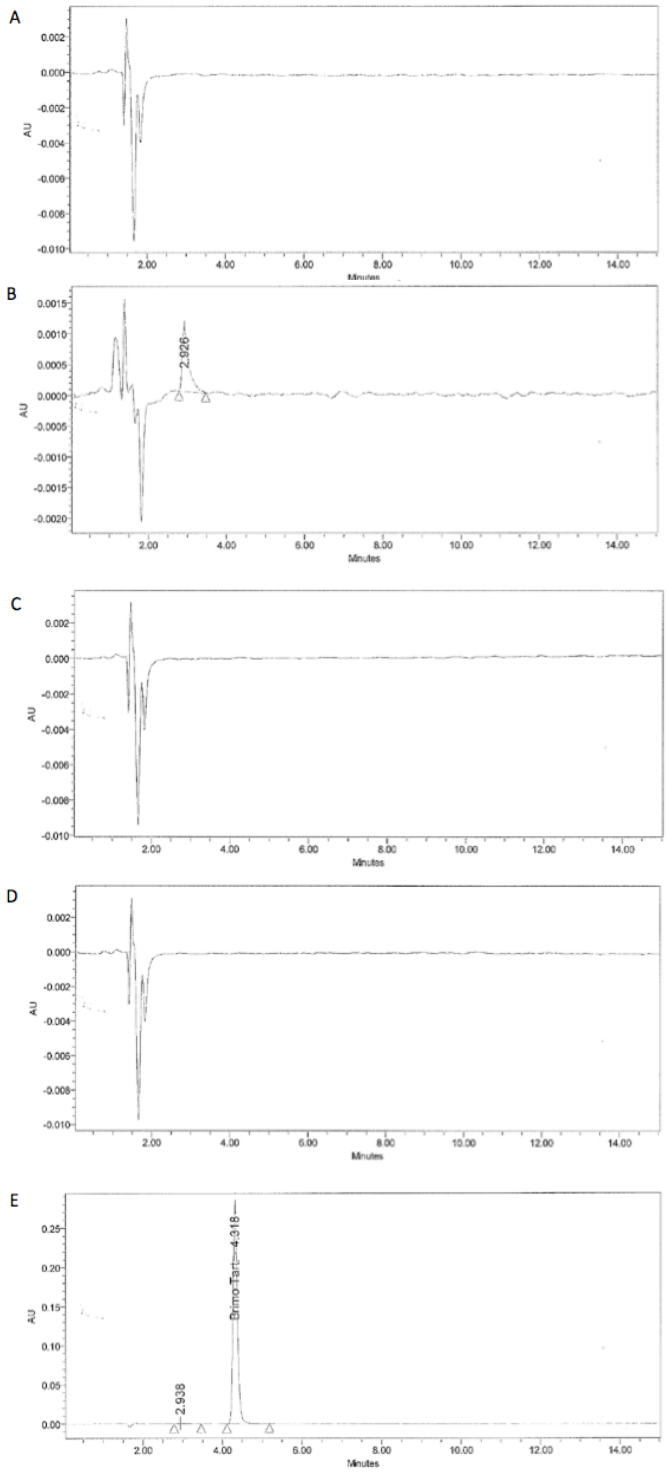

Figure 5.11 Representative HPLC chromatograms of A) PBS; B) mobile phase; C) Placebo (PLA) DDS sample solution; D) Placebo (PLGA) DDS sample solution; E) brimonidine DDS sample.

5.4.7.3 LINEARITY

Three separate linear regression curves of brimonidine peak area against concentration (60 μg/mL, 32 μg/mL, 10 μg/mL, 6 μg/mL, 2 μg/mL, 1 μg/mL, 0.6 μg/mL, 0.2 μg/mL) were plotted. The linearity parameters for these curves were as described in Table 5.12. The calculated correlation coefficients were 1 for the three calibration curves, suggesting good linear response from the detector.

	Linearity		
	Slope $(\mu g/mL)^{-1}$	Intercept	Correlation coefficient (r^2)
Run 1	66109	1110.7	1
Run 2	66048	1306.2	1
Run 3	65851	1764.4	1

Table 5.12 Linearity parameters for calibration curves.

5.4.7.4 ACCURACY AND PRECISION

The inter- and intra-day accuracy and precision were within 15% of the acceptance criteria as shown in Table 5.13.

	Nominal concentrations, μg/mL	Measured concentrations, μg/mL (mean ± S.D)	% RSD	% Accuracy
Intra-day assay (n=6)				
Run 1	10	9.96 ± 0.10	1.04	99.60
	2	1.97 ± 0.02	1.03	98.56
	0.2	0.19 ± 0.00	1.17	94.32
Run 2	10	10.02 ± 0.07	0.72	100.16
	2	1.96 ± 0.01	0.33	97.89
	0.2	0.18 ± 0.01	4.54	90.35
Inter-day assay (n=12)				
	10	9.99 ± 0.09	0.90	99.88
	2	1.96 ± 0.02	0.82	98.22
	0.2	0.19 ± 0.01	3.83	92.33

Table 5.13 Percentage accuracy and precision of brimonidine assay.

5.4.7.5 LOWER LIMIT OF QUANTITATION (LLOQ)

The limit of quantitation for brimonidine tartrate assay was found to be 0.2 µg/mL. The % accuracy and % RSD observed at this concentration were 92.67% and 2.97% respectively, which were within the acceptance criteria (Table 5.14).

Nominal concentrations, µg/mL	Measured concentrations, µg/mL	% RSD	% Accuracy
0.2	0.19 ± 0.01	2.97	92.67

Table 5.14 Percentage RSD and accuracy of brimonidine concentration assayed at the lower limit of quantitation (mean ± S.D) n =3.

5.5 DISCUSSION

5.5.1 POLYMER SELECTION AND ADMINISTRATION TECHNIQUE

PLA and PLGA are biocompatible in ocular tissues and have been approved by Food and Drug administration (FDA) for use in therapeutic devices. They were selected for controlled drug release purposes due to their biodegradability. When used as the matrix of the DDS, drug content will be completely emptied into the vitreous humour upon degradation of these polymers. The need for surgical removal is also eliminated upon the completion of treatment (Schmidt *et al.,* 1995). PLA and PLGA are degraded via a hydrolytic deesterification process. PLA is degraded into its monomers of lactic acid, whereas PLGA is degraded into lactic acid and glycolic acid. These monomers can be cleared from the eye.

The rationale of using a 25-gauge applicator system in administering the DDS was based on the fact that it is a safer and more effective option as compared to the conventional transpars plana incisional placement. The sutureless feature of the applicator system reduces ocular complications such as vitreous heamorrhage (Haller

et al., 2009), which may profoundly reduce vision (Williamson, 2007) and increase the risk of secondary open angle glaucoma (Spraul *et al.,* 1997).

5.5.2 MECHANISMS OF DRUG RELEASE FROM POLY (D,L LACTIDE) AND POLY (D,L LACTIDE-CO-GLYCOLIDE) DDS

Both poly (D,L lactide) and poly (D,L lactide-co-glycolide) are amorphous in structure. This facilitates water absorption and dissolution of drug particles (Schmidt *et al.,* 1995). The mechanism by which drugs were released from the DDS involves dissolution of drug particles, followed by diffusion through the swelling polymeric matrix and final release along with polymer degradation (Loo *et al.,* 2010, Desai *et al.,* 2008, Huang and Brazel, 2001, Göpferich, 1997, Zhang *et al.,* 1994).

Following the burst release on day 1, there was a lag time that represented a state of constant mass during the early time of mass loss (Göpferich, 1997). During this period, water began to penetrate the polymeric matrix initiating the process of polymer degradation (molecular weight loss). It was proposed that the duration of this lag period depended on the rate of degradation (Cui *et al.,* 2005), which was affected by the molecular weight (Göpferich, 1997). In this study, R203s had a larger molecular weight as compared to RG502 and this partly explains the longer lag period of the release profile of R203s DDS as compared to RG502. The lag phase was then followed by a moderate rate of diffusional release where brimonidine diffused out of the matrix via water channels and pores. When the matrix had become sufficiently soluble with critical degree of degradation, the DDS collapsed completely accompanied by a massive drug release (Sturesson *et al,* 1993).

The mechanism proposed agrees with that predicted by DOE analysis. The analysis showed that the interaction between brimonidine and individual polymers significantly affected drug release on day 1, 3 and 7. These earlier time points corresponded to both the lag and diffusional phases, during which brimonidine diffused from the polymeric matrix. However, the effects of drug loading became

less significant during later time points when drug release depended more critically on polymer degradation. Therefore, factors such as composition and type of polymers were more significant.

Since the duration of time that a DDS takes to achieve diffusional and final release phase was affected by polymer degradation, the absence of these two phases on the release profiles of R203s DDS, suggested a slower rate of R203s degradation as compared to RG502. The explanation for this observation will be further discussed within section 5.5.5.

5.5.3 EFFECTS OF DRUG LOADING AND TYPE OF POLYMERS ON INITIAL BURST RELEASE

The initial burst release observed in this study could be due to the porosity present in the matrix and liberation of surface-trapped drug (Lin *et al.,* 2003, Sturesson *et al.,* 1993) of which effects were greater in cases of higher drug loading (Brazel and Peppas, 1999, Pinon-Segundo *et al.,* 2004, Desai *et al.,* 2008) and lower polymeric concentration. DDSs with higher drug loading generated a greater diffusional gradient between DDS surface and dissolution medium. There would also be a higher probability that more drug particles were distributed on the DDS surface. Moreover, DDS with lower polymeric concentration had a less constructive polymeric structure, which allowed drug diffusion through the pores (Cui *et al.,* 2005).

Additionally, the initial burst was found to be greater in PLA formulations as compared to PLGA and this is in agreement with a previous study (Cui *et al.*, 2005). The authors attributed this observation to the more porous structure of PLA formulations, which led to the ease of drug diffusion through channels and pores. The characteristic burst release was commonly seen in the antibiotic-loaded implants where a high drug concentration presented at the site of action during the initial stage of therapy was important for accommodating infections (Gad *et al.,* 2008, Schmidt *et al.,* 1995, Yoo *et al.,* 2004). Nevertheless, a similar treatment strategy may not be

applicable for retinal therapeutics since high concentration of drug may potentially result in retinal toxicity and a vast burst release will reduce the effective lifetime of the DDS, rendering prolonged release unsuccessful (Huang and Brazel, 2001). Therefore, as suggested by some researchers, the initial burst effect could be overcome by first washing out the surface-coated drug, followed by drying the preparations (Schmidt *et al.,* 1995, Sturesson *et al.,* 1993). This method may be feasible for small scale laboratory production for proof-of concept purposes but may not be practical for larger scale manufacturing. As alternatives, the initial burst could be controlled through proper tuning of drug loading, percentage composition of polymers, type of polymers (Luan and Bodmeier, 2006) and fabrication techniques (Wang *et al.,* 2002, Huang and Brazel, 2001).

5.5.4 EFFECTS OF BASIC DRUG ON DRUG RELEASE PROFILE OF PLGA DDS

Hydrolytic degradation exposed the carboxylic end groups of PLGA (RG502), which were previously end-capped with the alkyl ester groups (Desai *et al.,* 2008). Additionally, the acidic degradation products acidified the core section of the DDS, in which environment brimonidine was highly protonated. The exposed carboxyl group has a tendency to interact with cationic residues of basic drug through ionic bonding (Miyajima *et al.,* 1998). Therefore, a large fraction of the polymer carboxyl residues were neutralized by ionic interaction with brimonidine (ionized form), minimizing the autocatalytic degradation, thereby leading to slower drug release. The drug-polymer interaction was more significant with higher drug loading DDS, which explains the inverse relationship between drug loading and percentage drug release observed for RG502 DDS. The release profiles of 50% drug loading DDS were no longer following the general sigmoidal pattern. The effects of basic drug content on release profile had been previously published (Miyajima *et al.,* 1998) Other examples include leuprolide acetate and timolol maleate where the interactions between the hydrolysed carboxyl groups of PLGA and the cationic species of the drug molecules slow drug release (Luan and Bodmeier, 2006, Sturesson *et al.,* 1993)

5.5.5 COMPARISON BETWEEN DRUG RELEASE PROFILES PLA AND PLGA DDS

The study on linear combination of drug loading with percentage composition of polymers produced two distinct drug release profiles, characteristic of PLA and PLGA. The release patterns are in good agreement to a microsphere study by Cui and coworkers (Cui *et al.,* 2005). PLA DDSs exhibited a slower release pattern as compared to PLGA, which agrees with previous study (Gad *et al.,* 2008). The authors attributed this observation to the more hydrophilic nature of poly-glycolic acid (PGA). The presence of PGA within the lactic acid chains enables the copolymer to absorb more water, leading to a faster rate of degradation and drug release compared to PLA polymer (Gad *et al.,* 2008, Loo *et al.,* 2010). Cui and colleagues also obtained a similar finding, showing that the time required for the degradation of PLGA preparation was significantly shorter as compared to the same formulation prepared using PLA (Cui *et al.,* 2005). In addition, other studies also showed that a higher glycolide unit in the copolymer led to a faster rate of DDS degradation, further underscoring the characteristic of PGA in promoting degradation (Spenlehauer *et al.,* 1989, Cui *et al.* 2005). This could explain our findings with regard to the faster rate of drug release from 9623-69 as compared to 9623-71, which had a lower percentage composition of PLGA in the preparation.

In addition, the methyl side group of the lactic acid (LA) provided steric hindrance against hydrolytic attack of its ester bonds. This reduced its water uptake leading to a slower rate of polymer degradation (Loo *et al.,* 2010). As a result, PLA maintained constant mass, characterized by the plateau phase of the cumulative drug release-time curve. Hence, the type of polymers used is an important factor in controlling brimonidine release from the DDS.

5.5.6 EFFECTS OF GAMMA-IRRADIATION ON DRUG RELEASE PROFILE

Spendelhauser and coworkers have shown that gamma-irradiation increased the degradation of PLGA polymer, leading to a 30-40% loss in polymeric molecular weight. In the study, a faster rate of drug release from gamma-sterilized DDS was also observed, which is in agreement with our finding on the faster rate of brimonidine release from gamma-sterilized DDS (Spenlehauer *et al.,* 1989). The effect of gamma irradiation on other polymers has been reported to be less marked, for instance, ocular inserts formulated using chitosan and PEG 400 did not experience a change in drug release with gamma sterilization (Gorle and Gattani, 2009).

5.5.7 EFFECTS OF MIXING AND EXTRUSION PROCESS ON THERMAL PROPERTIES OF PLA AND PLGA

Interaction between polymer and drug could occur with increased drug content, leading to the formation of a more rigid structure. According to Miyajima and colleagues, such interaction could be reflected in the Tg measurement (Miyajima *et al.,* 1998). In our study, the Tg of 10% drug loading PLA and PLGA DDS were similar to their corresponding 50% drug loading DDS, suggesting drug-polymer interaction did not occur or was minimal with increased drug loading. Additionally, the Tg of placebo DDS were found similar to their corresponding drug-loaded DDS indicating no plasticization occurred with brimonidine.

When PLA and PLGA powders were blended together, the resulting Tg reflected an effect of mixing both polymers. This indicates no interaction between these two polymers during the powder blending process. Additionally, Tg of the powder blend was found similar to that of the corresponding DDS, suggesting that the extrusion process did not alter the thermal properties of the polymers.

5.5.8 CONTENT UNIFORMITY

Content uniformity was seen to be poorer with DDS produced with PLGA as compared to PLA. This could be attributed to the more 'puffy' characteristic of PLGA powder blend that made the drug-polymer mixing less efficient especially when the drug amount was low. In addition, the piston extruder does not allow further mixing during the extrusion process. The poor mixing may explain the variation in the drug release profile seen for DDS with identical composition but produced on separate occasions.

6.0 CONCLUSION

In summary, it was evident that drug loading, percentage composition of polymers, type of polymers are important factors in controlling the rate of brimonidine release from the DDS. Using DOE, the effects of drug loading and percentage composition of polymers on drug release profile could be assessed. In addition, a correlation between the input and output factors could also be revealed, providing a better understanding towards polymer behaviors. Although DOE is a useful tool in formulation but DDS optimization was not successfully achieved in this study. This suggests that for a better prediction outcome in the future, more data on preliminary release study will be useful.

CHAPTER 6: PHARMACOKINETICS AND OCULAR DISPOSITION OF BRIMONIDINE IN PARTIALLY LIQUEFIED VITREOUS MODEL

6.1 INTRODUCTION AND OBJECTIVES

Diseases of the elderly such as age-related macular degeneration (ARMD) (Ferraz *et al.,* 2010; Fong *et al.,* 2010), diabetic retinopathy (Zonas 2007; González *et al.,* 2009) and glaucoma (Brouzas *et al.,* 2009; Yazdani *et al.,* 2009) remain as problems requiring advanced therapeutic solutions. These ocular problems are common causes of blindness worldwide (Foster and Resnikoff, 2005) and treatment modalities are aimed to prevent the occurrence of and to manage, disease progression as well as to improve visual acuity. The advantages offered by this route of administration include direct access to the retina, omitting the need to permeate through the selective blood-ocular barriers, thereby enabling therapeutic levels to be achieved with lower drug doses as compared to alternate techniques such as topical and systemic administration.

Many pre-clinical drug development studies reported in the literature have described the pharmacokinetics of drugs and fluorescent probes in live animals (Araie and Maurice, 1991; Liu *et al.,* 1998; Dias and Mitra, 2000). This data has then been utilized for computer modeling (Xu *et al.,* 2000; Missel, 2002; Stay *et al.,* 2003; Park *et al.,* 2005; Durairaj *et al.,* 2009) to examine physiological factors such as the influence of protein binding, flow processes and physicochemical properties of drug molecules on ocular disposition. However, such studies have not described the consequences of age-related vitreal structural changes on drug kinetics. In research described in this thesis (Chapter 4), a model in Dutch-belted rabbits was established with the degree of vitreous liquefaction mimicking that seen in elderly patients aged above 60 years. Intravitreally injected sodium fluorescein and fluorescein dextran 150kDa distributed and cleared faster in the more liquefied vitreous environment as assessed using a Heidelbergh Retinal Angiography (HRA 2) confocal laser scanning system and an ocular fluorophotometer. Lower vitreous gel content affected drug

disposition profiles and this feature clearly cannot be ignored considering that the treatment population for posterior segment diseases is primarily the elderly. A clinical study investigating the safety and efficacy of bevacizumab in the treatment of choroidal neovascularization has demonstrated that elderly patients required more frequent injections (mean age: 68.5 years; 3.75 injections) of bevacizumab as compared to a middle-aged population (mean age: 39.5 years; 1.75 injections) for a similar degree of clinical outcome (Spielberg and Ley, 2009). This would suggest an increased rate of drug clearance in the elderly eye. Furthermore, it has been reported that doses of antibiotics, which are usually non-toxic, were toxic when injected in vitrectrectomised rabbit eyes (Stainer *et al.,* 1977), indicating that the low vitreous gel content resulted in more immediate access to the retina. Based on these findings, it is clear that an investigation of the disposition of drug molecules in eyes with partial vitreous liquefaction would provide useful knowledge for optimizing the dosing schedule and reducing the occurrence of ocular toxicity in the elderly.

This has led to the primary objective of this chapter, which was to investigate the effects of partial vitreous liquefaction on the ocular disposition of brimonidine following a single intravitreal injection and a single placement of a posterior segment drug delivery system (DDS) that releases brimonidine over a period of one month. Subsequently, the disposition profiles of both single dose injection and DDS were compared and this aspect was evaluated as the secondary objective of this study.

6.2 MATERIALS AND METHODS

6.2.1 CHEMICALS AND REAGENTS

Brimonidine tartrate salt and brimonidine-d_4 (stable isotope labeled (deuterated) of brimonidine) were kindly provided by Allergan Inc. All reagents used were HPLC grades. Acetonitrile and methanol were purchased from Burdick & Jackson (via VWR, PA, USA), 98-100% formic acid was purchased from Riedel-de Haën (via VWR, PA, USA), and ammonium formate was bought from Sigma (St. Louis, MO,

USA). Deioned water was obtained from Mili-Q dispenser supplied by Milipore (Mili-Q POD, USA).

6.2.2 INSTRUMENTATION

All glassware and vials used for the preparation of brimonidine injection solution were sterile in an autoclave (Tuttnauer Brinkmann 2540E, serial no. 2301273, Canada) prior to use. Tissues samples collected from *in vivo* studies were mixed using a multi-tube vortexer (VWR, VX-2500, PA, USA) and a rotator (Glas-Col, LLC, IN, USA). A centrifuge (Beckman Spinchron, CA, USA) was used to sediment tissue residues. A sonicator (Branson model 5510, Branson Ultrasonic Corp. CT, USA) was used during the preparation of brimonidine stock solutions and mobile phase for LCMS analysis. The pH of the mobile phase was adjusted using a pH meter (Beckman model Phi 360, Beckman Coulter Inc. CA, USA) that was calibrated using pH standard buffer solutions of pH 4 and pH 7. A weighing balance (Mettler Toledo, max: 220g, d: 0.1mg) was used to quantify tissue weights. LCMS-MS analyses were performed on an Agilent 1100 HPLC system equipped with a PDA detector and connected to a PE Sciex LCMS/MS system (model API 2000, applied biosystems, CA, USA). Data acquisition and integration were accomplished using Analyst software (version 1.4.4 MDS Sciex, applied biosystems, CA, USA).

6.2.3 PREPARATION OF INTRAVITREAL HYALURONIDASE SOLUTIONS

Lyophilized ovine testicular hyaluronidase with enzyme activity of ≥ 1000 IU/mg (MP biomedical, OH, USA) was reconstituted with 0.9% normal saline to produce a 0.005 IU solution.

6.2.4 PREPARATION OF BRIMONIDINE TARTRATE INTRAVITREAL BOLUS INJECTION AND POSTERIOR SEGMENT DRUG DELIVERY SYSTEM (DDS)

A solution of 1.5 mg/mL brimonidine tartrate was prepared in 0.9% normal saline under sterilized conditions for intravitreal injection. Twelve 0.7 mg rod-shaped brimonidine tartrate posterior segment DDS with a diameter and length of approximately 0.46 mm and 3.12 mm respectively were weighed and cut. Each of these DDS was carefully inserted into a 25-gauge applicator system, which was then individually sealed in aluminum pouch for gamma sterilization prior to use. The manufacturing of the DDS is as described in Chapter 5 and the content details are as detailed in Table 6.1.

Brimonidine tartrate posterior segment DDS		
30% (w/w)	17.5% (w/w)	52.5% (w/w)
Brimonidine tartrate	Poly D, L-lactide (R203s)	Poly D, L-lactide-co-glycolide 50:50 (RG502)

Table 6.1 Composition of brimonidine DDS by weight.

6.2.5 STUDY DESIGN AND EXPERIMENTAL PROCEDURES

6.2.5.1 STUDY DESIGN

Twenty-four animals were used in this study. Twelve animals received a single dose brimonidine intravitreal injection to both eyes (Group1) and the other twelve animals received a single implantation of brimonidine DDS in the posterior segment of both eyes (Group 2). All animals received unilateral intravitreal injection of ovine testicular hyaluronidase 48 hours prior to their respective intravitreal dosing. At 1, 2, 4 and 8 hours postdose, ocular tissues were collected from animals in group 1; while at 1, 7, 14 and 28 days postdose, the same tissue collection process was performed for animals in group 2. The details of the study design are summarized in Table 6.2.

Test compound:	Brimonidine Tartrate
Animal species and strain	Dutch-belted rabbits
No. of animals	24 in total; 12 in each treatment group with 3 animals/time point
Treatment groups:	All 24 animals received single unilateral (right eye) intravitreal injection of ovine testicular hyaluronidase 0.005 IU, followed by the following treatments 48 hours later: Group 1: 30 µg brimonidine tartrate injection bilaterally Group 2: 210 µg brimonidine tartrate DDS bilaterally
Route of administration	Group 1: Intravitreal injection Group 2: Intravitreal implantation using 25-gauge applicator system
Treatment duration	1 month
Sample collected and analyzed	Aqueous humour, vitreous humour, iris-ciliary body, choroid/RPE (macula, superior, inferior, nasal and temporal), retina (macula, superior, inferior, nasal, temporal) and explanted implants
Sampling times	Group 1: 1, 2, 4 and 8 hours Group 2: Day 1, 7, 14 and 28
Analyte	Brimonidine analysed using LC-MS/MS
Quantitation range	Aqueous humour: 0.001-2.5 µg/mL Vitreous humour: 0.001-2.5 µg/mL Iris-ciliary body (ICB): 0.1-200 ng per ICB Choroid/RPE (Cho): 0.1-200 ng per Cho Retina (Ret): 0.1-200 ng per Ret Implant: 0.25-625 ng/mL

Table 6.2 Study design for assessment of intraocular pharmacokinetis of brimonidine following a single intravitreal injection or a single implantation of brimonidine tartrate DDS in Dutch belted rabbit eyes.

6.2.5.2 ANIMAL WELFARE STATEMENTS

This study was conducted in accordance to the Allergan Animal Care and Use Committee (AACUC) Protocol # 485.

6.2.5.3 ANIMAL SPECIES, SOURCE AND ACCLIMATIZATION

Twenty-four Dutch-belted rabbits (48 eyes) weighing approximately 3 kg each, and ranging from 3 months to 2 years old, were purchased from Covance Laboratories (Madison, WI). All animals were housed individually and identified by ear tags and identity cards displayed in front of the stainless steel cages.

The animals were acclimatized in the facility for a week before the studies commenced. During this time, animals were monitored daily to confirm adequate health for use in the studies.

6.2.5.4 INDUCTION OF PARTIAL VITREOUS LIQUEFACTION

All animals in this study received a unilateral (right eye) injection of 20 µL 0.005 IU ovine testicular hyaluronidase 48 hours before intravitreal dosing to achieve an approximately 50% vitreous liquefaction. Details on the development of the liquefied vitreous model are as described in Chapter 4.

6.2.5.5 ANIMAL PREPARATION AND DOSING

Conscious rabbits were prepared for intravitreal injection by placement in a custom-built stainless steel restrainer, which allowed easy access to the eyes. After topical placement of a drop of proparacaine HCl ophthalmic solution and a drop of topical povidone-iodine ophthalmic solution, the rabbit was placed on its side so that the

eye rotated ventrally which allowed good presentation of the supero-temporal aspect of the pars plana. A wire eyelid speculum was inserted to prevent eyelid closure and the globe was stabilized using forceps. A 0.3 mL BD® insulin syringe with a 29-gauge x ½ inch needle was used to deliver hyaluronidase or brimonidine solutions into the vitreous via the supero-temporal pars plana area. The needle was directed towards the centre of the vitreous and inserted at a depth of ¼ inch. The plunger of the syringe was slowly depressed to prevent turbulence that may damage the retina.

The DDSs were implanted in the supero-nasal region with the needle angled towards the inferior aspect of the eye using a 25-gauge applicator system and a biplane technique to minimize leakage. The tip of the needle was placed bevel up on the sclera 4 mm from the limbus and advanced tangentially through the scleral stroma parallel to the limbus 1-2 mm. The needle was then turned perpendicularly and advanced to enter the vitreous chamber until the rubber band on the needle came in contact with the sclera. The DDS was then deposited by pressing the actuator on the applicator system. Following deposition of the DDS, the needle was slowly withdrawn and the point of entry sealed with gentle pressure with the tip of a cotton swab. After the procedure, eyes were treated with a triple antibiotic ointment, which comprises of Bacitracin Zinc, Neomycin and Polymycin B (Polyfax treatment, Bausch and Lomb Pharmaceuticals).

Technical help with injection and implantation procedures was provided by Dr. Werhner Orilla at Allergan Inc.

6.2.5.6 TISSUE COLLECTION AND HANDLING

All collection tubes and containers were labeled and weighed prior to commencing the experiments. Animals in group 1 and group 2 were killed using an overdose of pentobarbital (Eutha 6®) and the time points are as described in Table 6.1. After the animals were euthanized, the eyes were enucleated and placed on clean, labeled petri dishes. A 1.0 mL syringe with a 27-gauge x ½ inch needle was inserted into the anterior chamber to aspirate the aqueous humour. The sample was subsequently

discharged into a 0.5 mL eppendorf tube. A circumferential incision was then made around the *pars plana*, separating the anterior segment from the posterior segment. The iris-ciliary body was first removed by separating it from the edge of the cornea using a blunt forceps. The sample was placed into a 16 x 125 mm silanised borosilicate screw cap glass vials. A small incision was made on the sclera of the peripheral area of the posterior chamber in order to reveal the position of the implant. Once identified, the location of the DDS in the vitreous was captured using a digital camera (Canon EOS 5D Mark II). Subsequently, it was removed using forceps and kept in a vial. The vitreous humour was aspirated carefully from the posterior chamber using a 1.0 mL syringe to prevent suction into the retina. The vitreous humour sample was transferred into a 2.0 mL eppendorf tube. By making a few incisions on the sclera, the posterior segment was cut open and laid flat on the petri dish. The sampling sites at the posterior segment of the eye are as described in Figure 6.1. A circular spot was made at each of these sampling regions using a 6 mm biopsy punch. Within each spot, retina and choroid layers were carefully scraped off from the sclera using a flat-bodied forceps. The samples were collected into their respective 16 x 125 mm silanised borosilicate screw cap glass vials. Since the RPE layer was attached to the choriocapillaries upon dissection, the choroid sample contains melanin-containing cell in the form of the RPE and the melanocytes of the choroid. The retina in this study is therefore the neuroretina. Drug concentration at the RPE and choroid was quantified as a single entity of choroid/RPE. For simplicity, the term choroid/RPE was replaced by choroid or cho for the rest of the chapter. The surgical tools used during the dissection process were rinsed clean with deionised water in between sample collections to prevent cross-contamination. The weights of the collected tissue samples were recorded and the samples were stored at -70 ^{0}C until further analysis.

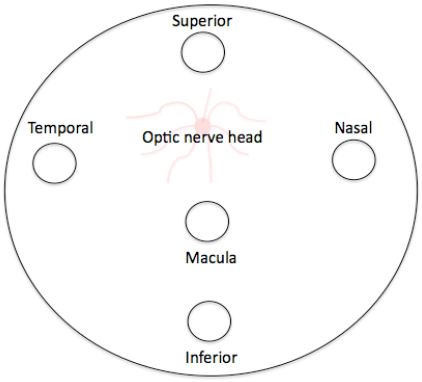

Figure 6.1 An illustration of the posterior segment of a right eye showing sampling sites for choroid and retina samples. Note that the macula region is not well defined in the rabbit; therefore a central zone in region of macula and optic disc was selected.

6.2.6 BIOANALYSIS

6.2.6.1 PREPARATION OF CALIBRATION STANDARDS, QUALITY CONTROL SAMPLES AND INTERNAL STANDARD SOLUTIONS

All stock and standard solutions were prepared in silanized borosilicate glass and stored at approximately -20 ^{0}C when they were not in use.

6.2.6.1.1 CALIBRATION STANDARDS AND QUALITY CONTROL SAMPLES (QC)

Approximately 100 mg brimonidine tartrate powder was weighed and dissolved in appropriate volume of mobile phase to yield a 1.00 mg/mL brimonidine tartrate stock solution and a 1.00 mg/mL brimonidine tartrate QC stock solution. The stock solutions were subsequently mixed well and sonicated for 5 minutes to ensure complete dissolution. On the day of sample analysis, stock solutions were serially diluted with mobile phase to obtain a series of brimonidine tartrate working

solutions and brimonidine tartrate QC solutions that range from 0.01-500 μg/mL as described in Table A6.1 and Table A6.2 respectively (Appendix).

6.2.6.1.2 INTERNAL STANDARD SOLUTION (IS)

100 μg/mL stock solution of brimonidine-d_4 in methanol was kindly provided by Allergan Inc., which was serially diluted to 0.1 μg/mL solution with mobile phase for sample analysis.

6.2.6.2 BIOANALYSIS OF OCULAR SAMPLES

Aqueous humour and vitreous humour were prepared for analysis using a liquid-liquid extraction method, which is a commonly used technique to separate compounds of a complex mixture based on their relative solubilities in two immiscible liquids, generally aqueous (hydrophilic) and organic solvent (hydrophobic). The extraction method is known to show a high variation in extraction recovery as a result of matrix effects and losses during sample handling. To compensate for these sources of error and other gross effects caused by variations in injection volume and detector response, a known amount of internal standard was added into each sample. This significantly improved the reproducibility of the assay method. Brimonidine-d_4 (isotopically labeled) was chosen as the internal standard as it is structurally identical to brimonidine and therefore has matching physicochemical properties. Brimonidine is a weak base (Figure 6.2) and normally exists in the unionized form at basic pH. To extract these molecules from the hydrophilic environments (aqueous and vitreous humour) using ethyl acetate, the samples were alkalinised with 1M NaOH to maximize the amount of analyte in the lipophilic, non-ionized form. The extraction process was performed three times to improve the extraction efficiency.

Those solid tissues initially processed by means of liquid-liquid extraction, were homogenized or cut into smaller pieces for better drug-solvent interactions. The grinding and cutting processes increase the risk of sample cross-contamination

arised from insufficient cleaning of blade or homogenizer used. In addition, tiny tissue residues generated during grinding process proved difficult to remove from the samples. 'Dirty' samples are known to generate a high level of baseline noise that could compromise system performance. Due to these shortcomings associated with liquid-liquid extraction, a soaking method was selected to process the solid tissues ICB, choroid and retina.

Using the soaking method, tissue samples were immersed in 95:5 methanol: water overnight. It was assumed that drug compounds would dissociate from tissue binding and partition completely into immersed solution. A period of 18-89.5 hours has been validated to be sufficient for the extraction process to take place (Allergan report number: BMS-05-057). The method offers a simpler and more accurate preparation procedure but the whole process consumed more analytical time (at least 2 days) than the liquid-liquid extraction.

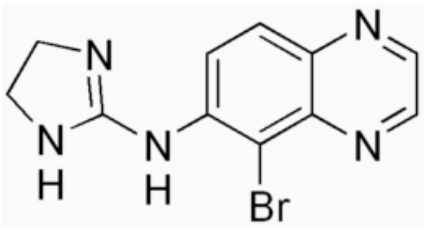

Brimonidine ($C_{11}H_{10}BrN_5$)
Molecular weight: 292.13

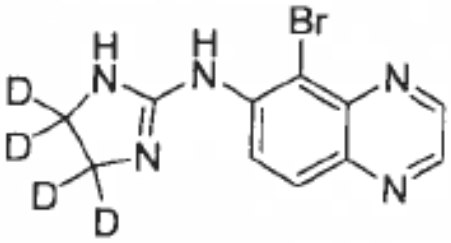

Brimonidine-d_4 ($C_{11}H_6D_4BrN_5$)
Molecular weight: 296.25

Figure 6.2 Chemical structures of brimonidine and brimonidine-d_4. Brimonidine-d_4 differs from brimonidine by having four of its hydrogen atoms replaced by deuteriums. Due to the structural similarity between these two compounds, brimonidine-d_4 was used as the internal standard for brimonidine.

6.2.6.2.1 AQUEOUS HUMOUR (AH)

50 µL aliquots of blank rabbit aqueous humour, calibration standards, quality control samples and actual experimental samples were transferred to 16 x 125 mm

silanized borosilicate glass screw top tubes. An internal standard (25 µL) was added to all tubes except the tissue control. This was followed by the addition of 1mL deionized water and the samples were vortexed for 1 minute. After mixing, 50 µL 1M NaOH was added and the samples were vortexed again for another minute. 4 mL of ethyl acetate was then added into all tubes and the samples were mechanically mixed for 20 mins using a rotator. The aqueous and organic layers were then separated by centrifugation at 3000 rpm for 5 minutes. The sample tubes were immersed in a dry ice-methanol bath for 2 minutes until the aqueous phase was frozen at the bottom of the tubes, separated from the organic layer. The organic phase was then poured into a clean 13 x 100 mm silanized borosilicate glass tube and evaporated to dryness under a gentle stream of nitrogen at approximately 40 ^{0}C. The same extraction process with ethyl acetate was repeated twice and each extract was dried under N_2 gas. The dried sample residues were reconstituted with 200 µL mobile phase and subsequently sonicated (~ 5 minutes) and vortexed (~ 5 minutes). The samples were then centrifuged at 3000 rpm for ~10 minutes to sediment tissue residues. 150 µL of the supernatant were transferred to a silanized HPLC vial for analysis. The preparation schemes of aqueous humour calibration standards and quality control samples were provided in Appendix (Table A6.3 and Table A6.4).

6.2.6.2.2 VITREOUS HUMOUR (VH)

The extraction procedure for the vitreous humour is as described for the aqueous humour (section 6.2.6.2.1), except that 100 µL aliquots of calibration standards and experimental samples were used. Early experimental samples which had a high predicted level of brimonidine were diluted with blank vitreous humour and 50 µL of IS was added to all tubes except the tissue control (double blank). The dried sample residues were reconstituted with 400 µL mobile phase with 200 µL of supernatant used for LC-MS/MS analysis. The preparation methods of vitreous humour calibration standards and quality control samples were provided in Appendix (Table A6.5 and Table A6.6).

6.2.6.2.3 IRIS-CILIARY BODY (ICB), CHOROID (Cho) and RETINA (Ret)

50 µL of 1M NaOH was added to blank ICB/Cho/Ret, spiked calibration standards, spiked quality control samples and actual experimental samples contained in 16 x 125 mm silanized borosilicate glass screw top tubes and the samples were briefly vortex mixed for 1 minute. Three mL of 95:5 methanol: water was added to each tube and gently shaken for approximately 10 minutes. All tissues were soaked below the liquid level before keeping them in a refrigerator at 4 ^{0}C overnight. After storing, the samples were removed from the refrigerator and vortexed for ~ 5 minutes before being centrifuged for 15 minutes at 3000 rpm. 1 mL of supernatant was transferred into a 13 x 100 mm silanized borosilicate glass tubes. At this stage, those experimental samples with predicted high brimonidine level were diluted with 95:5 methanol: water. The remaining supernatants were stored at -20 ^{0}C for potential re-analysis. Following this, 10 µL internal standard was added to all samples and the samples were vortexed for ~ 1 minute. The samples were evaporated to dryness under a stream of nitrogen gas at 40 ^{0}C. The dried residues were reconstituted with 400 µL mobile phase, which subsequently sonicated (~ 5 minutes) and vortexed (~ 5 minutes). All samples were centrifuged at 3000 rpm for 15 minutes to sediment tissue residues as debris may accumulate and block the analytical column. Two hundred µL of supernatant was transferred into a silanized HPLC vial for analysis. The preparation method of ICB, choroid and retina spiked calibration standards and spiked quality control samples were provided in Appendix Table A6.7 and Table A6.8.

6.2.6.2.4 EXPLANTED BRIMONIDINE TARTRATE DDS

Explanted brimonidine DDS was dissolved in 2 mL 50:50 acetonitrile:water mixture and subsequently sonicated (~ 10 minutes) and vortex mixed (~ 5 minutes) to ensure complete dissolution. Samples with predicted high levels of brimonidine were diluted with 50:50 methanol: water. An aliquot of 20 µL diluted solution was transferred to a 13 x 100 mm borosilicate glass tube containing 10 µL of internal

standard. The final volume of the solution was made up to 400 µL using 10% methanol. The sample was centrifuged at 3000 rpm for 15 minutes and 200 µL of supernatant was transferred to a silanized HPLC vial for further analysis. The preparation scheme of calibration standards and quality control samples for DDS analysis were provided in Appendix (Table A6.9 and Table A6.10).

6.2.6.3 DATA CALCULATION AND PHARMACOKINETIC ANALYSIS

Tissue concentrations were calculated using the Analyst® software by interpolating the experimental data on the linear regression curve performed on the day of sample analysis (refer to Section 6.2.6.5.2). The calculated concentrations were then normalized to ng/g of tissue weight for ICB, choroid and retina and µg/mL for vitreous humour and aqueous humour. The sum, mean and standard deviation of the tissue concentration at each sampling time point were calculated using Microsoft Excel Mac® 2008. Standard deviation was plotted on the graph as error bars with the same magnitude in both positive and negative limits. Tissue samples with drug levels below the lower limit of quantitation were denoted as BLQ. If more than half of the samples within a group were BLQ, the mean value was reported as 'not calculatable' (NC) and was substituted by zero in the calculation.

The time to peak concentration (T_{max}) and peak concentration (C_{max}) were determined from the concentration-time curve. Area under the curve from time 0 to the last time point ($AUC_{o\text{-}tlast}$) was used to represent the degree of cumulative drug exposure and was calculated based on the linear trapezoidal rule. Area under the curve from time 0 to infinity was calculated using the equation: $AUC_{o\text{-}\infty} = AUC_{o\text{-}tlast} + (Clast/kel)$ where kel was determined from the terminal phase of the log-linear regression curve as $kel = (\ln C_t - \ln C_0)/\Delta t$. Terminal half-life was calculated as $t_{1/2} = 0.693/kel$ and clearance was determined as $Dose/AUC_{o\text{-}\infty}$.

6.2.6.4 ANALYTAL CONDITIONS

The mass spectrophotometer was operating in multiple reaction monitoring (MRM) in triple quadrupole mode, which involves the Q1 and Q3 part of the detector to transmit the parent molecule and its fragment respectively. The mass spectras of brimonidine and its fragment (without a bromine atom) were revealed at m/z 292 and 212 respectively; whereas for brimonidine-d_4, the mass spectras of the parent molecule and its fragment were collected at m/z 296 and m/z 216 respectively. Only mass spectras of the parent molecules were used in quantitative analysis. The HPLC conditions used in conjunction with the mass spectrophotometer are as listed in Table 6.11.

<table>
<tr><th>Parameters</th><th>HPLC conditions</th></tr>
<tr><td>HPLC column</td><td>Waters C_{18}, 3.5 µm, 4.6x75 mm</td></tr>
<tr><td>Flow rate</td><td>0.5 mL/min</td></tr>
<tr><td>Mobile phase</td><td>A: 82% 10mM ammonium formate pH 3.0
B: 18% methanol</td></tr>
<tr><td>Injection volume *</td><td>50 µL</td></tr>
<tr><td>Column temperature</td><td>Room temperature</td></tr>
<tr><td>HPLC gradient</td><td>
<table>
<tr><td>Time (min)</td><td>% B</td></tr>
<tr><td>0.00</td><td>18</td></tr>
<tr><td>3.50</td><td>18</td></tr>
<tr><td>3.60</td><td>50</td></tr>
<tr><td>4.10</td><td>50</td></tr>
<tr><td>4.20</td><td>85</td></tr>
<tr><td>5.20</td><td>85</td></tr>
<tr><td>5.30</td><td>18</td></tr>
<tr><td>7.50</td><td>Stop</td></tr>
</table>
</td></tr>
</table>

Table 6.11 HPLC conditions

* The analyses of ICB and DDS samples were performed on a different machine where injection volumes of 40 µL and 20 µL respectively were applied. For all other tissues, a 50 µL injection volume was used.

6.2.6.5 VALIDATION OF LCMS/MS ANALYTICAL METHOD

Complete bioanalytical validations were performed for at least one tissue type for each extraction method and the parameters include selectivity, linearity, intra- and inter-day accuracy and precision as well as lower limit of quantitation (LLOQ) as shown in Table 6.12. The assay method that involved liquid-liquid extraction procedure was fully validated in vitreous humour and the extraction efficiency was also determined. The assay method of the aqueous humour was similar to that of vitreous humour and thus only went through partial validation where the extraction recovery, inter-day accuracy and precision tests were excluded. Inter-day system performance and extraction efficiency would not affect the accuracy and precision of aqueous humour concentrations since all experimental samples were analysed within a day. The assay methods for choroid, retina and ICB were validated for all parameters excluding extraction recovery, which has been reported (Allergan report number: BMS-05-057). The assay for explanted DDS was evaluated for all parameters except extraction recovery, which was not applicable.

Validation parameters	Ocular Tissues					
	Vitreous humour	Aqueous humour	Choroid	Retina	ICB	DDS
Selectivity	√	√	√	√	√	√
Linearity	√	√	√	√	√	√
Intra-day accuracy	√	√	√	√	√	√
Inter-day accuracy	√		√	√	√	√
Intra-day precision	√	√	√	√	√	√
Inter-day precision	√		√	√	√	√
LLOQ	√	√	√	√	√	√
Extraction recovery	√					

Table 6.12 Validation parameters involved in the tissue and DDS assay methods.

6.2.6.5.1 SELECTIVITY

Interferences caused by matrix components and other exogenous substances may potentially enhance or suppress the signal of analytes. Therefore, the selectivity of bioanalytical assay methods was established for brimonidine and brimonidine-d_4 using blank tissue matrix of aqueous humour (N=3), vitreous humour (N=3), ICB (N=3), choroid (N=3) and retina (N=3). In addition, blank tissue samples (N=3) spiked with internal standards were analyzed to assess the stability of brimonidine-d_4 in tissue matrix and during sample preparation. Assay methods were considered as selective if there were no interference components co-eluted at the same retention time as brimonidine and brimonidine-d_4.

6.2.6.5.2 LINEARITY

Weighted linear regression curves (weight = 1/ concentration^2) of concentration against peak area ratio were generated for all ocular tissues using Analyst® software. Each curve contained at least six concentrations over a range of 0.001-2.5 µg/mL for aqueous, vitreous humour and 0.1-200 ng/tissue for ICB, choroid and retina. The correlation coefficient (R^2) of the linear regression curve was used to determine the linearity of the assay method and detector response with any values greater than 0.97 considered as desirable in practice. In addition, the concentration of the calibration standards were back-calculated by Analyst® software based on the linear regression equation produced from the curve. By having at least 75% of the back-calculated concentration conform within ± 20% of the nominal concentration values, the system was considered valid for sample analysis. Brimonidine concentration in the tissues was determined by interpolating the experimental data on the linear regression curve.

6.2.6.5.3 ACCURACY AND PRECISION

Inter- and intra-day accuracy and precision of the assay method were evaluated by comparing at least triplicate measurements of three concentrations of quality control samples on the same day (intra) and on two separate days (inter). The quality control

samples were prepared as shown in the Appendix (Tables A6.4, A6.6, A6.8, and A6.10) for aqueous humour (0.002, 0.25, 1.25 µg/mL), vitreous humour (0.002, 0.05, 0.25 µg/mL), choroid (0.2, 50 and 100 ng), ICB (0.2, 50 and 100 ng), retina (0.2, 50 and 100 ng) and implant (0.5, 125, 500 ng/mL) respectively. Accuracy and precision of the assay methods were expressed as % accuracy and % RSD (relative standard deviation) respectively using the following equations.

Accuracy, % = [mean observed concentration/nominal concentration) x 100]

Precision, %RSD = [Standard deviation/mean x 100]

The acceptance criteria for accuracy determined from both intra- and inter-day analysis will be within 80-120% of the nominal concentrations; while for precision, the calculated % RSD will be less than or equal to 20%.

6.2.6.5.4 LOWER LIMIT OF QUANTITATION (LLOQ)

The lower limit of quantitation of an assay method was determined for all ocular tissue. This concentration was calculated as the lowest concentration of the calibration standards. The analyte response peak of this concentration must be at least three times greater than the baseline noise produced by the tissue matrix. The triplicate measurements of this concentration must also meet the acceptance criteria set out for accuracy and precision as defined above.

6.2.6.5.5 EXTRACTION RECOVERY

The efficiency of the liquid-liquid extraction method using ethyl acetate was evaluated for brimonidine and internal standard in vitreous humour by comparing the analyte response of six replicates of processed samples with three replicates of fortified samples. Processed samples were prepared as outlined for the vitreous humour samples under section 6.2.6.2.2, while the fortified samples were blank vitreous humour matrixes that were spiked with brimonidine solution of the same

concentrations as the processed samples after the extraction procedures. The extraction recovery of the assay method was determined using the following equation.

% Extraction recovery = [(Mean peak area of brimonidine or IS in processed samples/ mean peak area of brimonidine or IS in fortified samples) x 100]

6.2.6.6 CHARACTERISATION OF EXPLANTED DDS

6.2.6.6.1 SCANNING ELECTRON MICROSCOPY (SEM)

Prior to SEM imaging, explanted DDSs were freeze-dried overnight to eliminate the water content. The freeze-drying cycles were performed as described in Figure 6.3. SEM images of the DDSs were acquired using a Zeiss EVO 40 Electron Microscope. The samples for cross-section analysis were prepared by snapping the DDSs in liquid nitrogen. The sample surfaces were coated with a thin layer (12 nm) of gold using a K550X Sputter Coater (Emitech Ltd., Kent, UK).

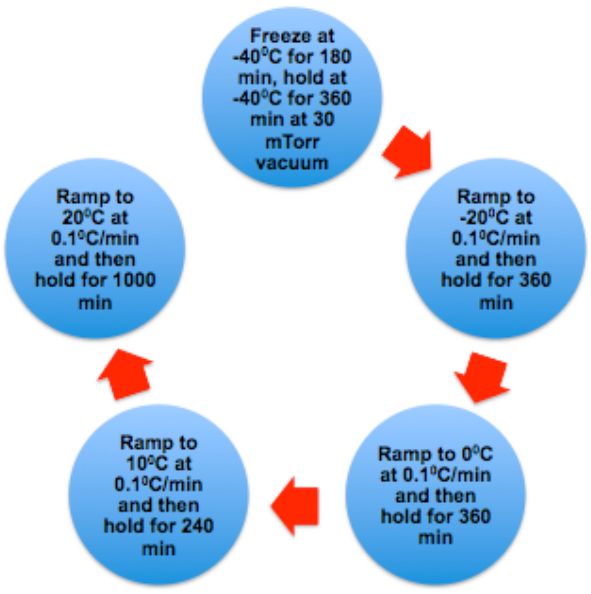

Figure 6.3 Freeze-drying cycles performed for explanted DDS prior to SEM imaging.

6.2.6.6.2 GEL PERMEATION CHROMATOGRAPHY

Following the SEM imaging, the DDSs were processed to determine the degradation of the polymers using a Gel Permeation Chromatography (GPC) system, equipped with a Waters 600 Controller, a Waters 717 plus Autosampler, and a Waters 2414 Refractive Index Detector. Three columns, Styragel® HR3, HR4E, and HR5 (7.8 x 300 mm), were used in tandem and were calibrated using polystyrene standards. Tetrahydrofuran (THF, J.T. Baker, HPLC grade, catalog #9441-03, lot #H05E00) was used as mobile phase and the flow rate was set at 1 mL/min. Temperatures of the columns and detector were set at 40 ^{o}C. The DDSs were dissolved in THF and centrifuged at 20,000 relative centrifugal force (rcf) for 20 minutes to sediment the gold particles carried over from the SEM imaging. The supernatants were then analyzed using the GPC system for detecting changes in molecular weight.

6.3 RESULTS

6.3.1 VALIDATION OF LCMS/MS ANALYTICAL METHOD

6.3.1.1 SELECTIVITY

Figure 6.4 to Figure 6.9 below are representative LCMS/MS chromatograms of the aqueous humour, vitreous humour, ICB, choroid, retina and DDS. In each figure, chromatograms of blank tissue, blank tissue spiked with internal standard and tissue spiked with brimonidine were illustrated to demonstrate the selectivity of the assay method. As can be seen, no interference peaks appeared at the retention time of brimonidine and brimonidine-d_4.

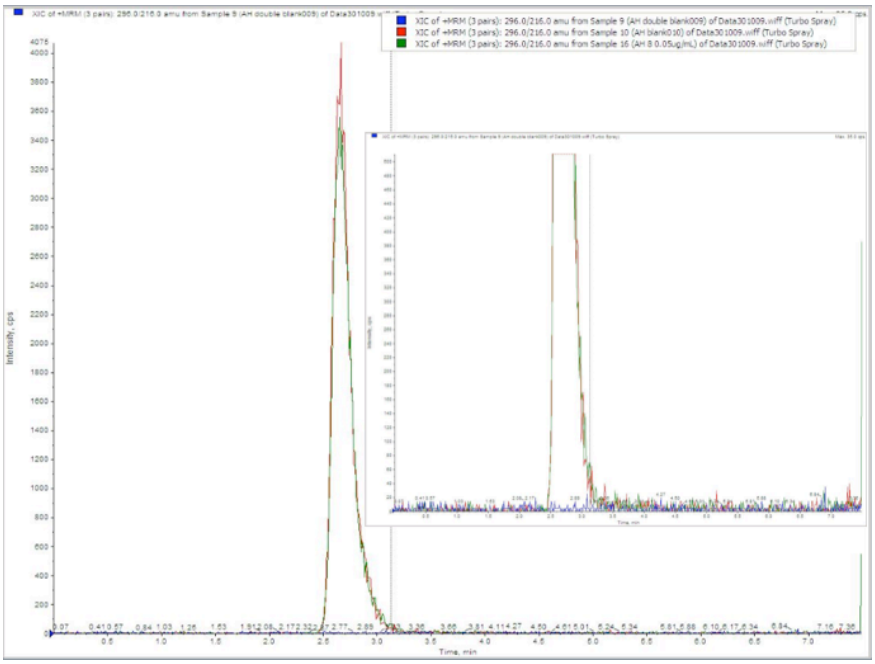

Figure 6.4 Representative LCMS/MS spectra of brimonidine and brimonidine-d_4 at concentration 0.05 µg/mL and 0.1 µg/mL respectively in the aqueous humour. Blue: Blank matrix; Red: IS; Green: Brimonidine sample**.**

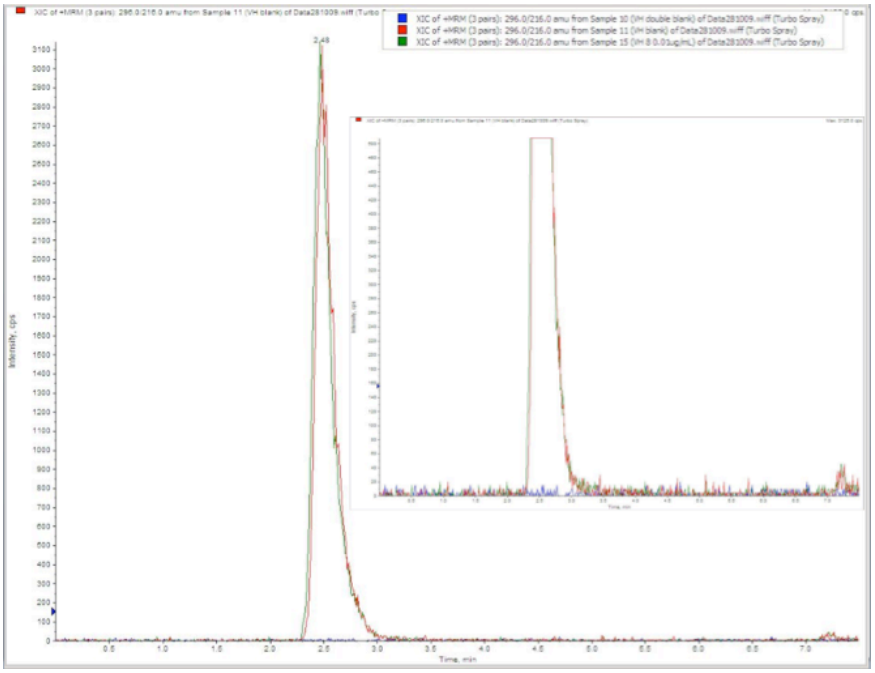

Figure 6.5 Representative LCMS/MS spectra of brimonidine and brimonidine-d_4 at concentration 0.01 µg/mL and 0.1 µg/mL respectively in the vitreous humour. Blue: Blank matrix; Red: IS; Green: Brimonidine sample.

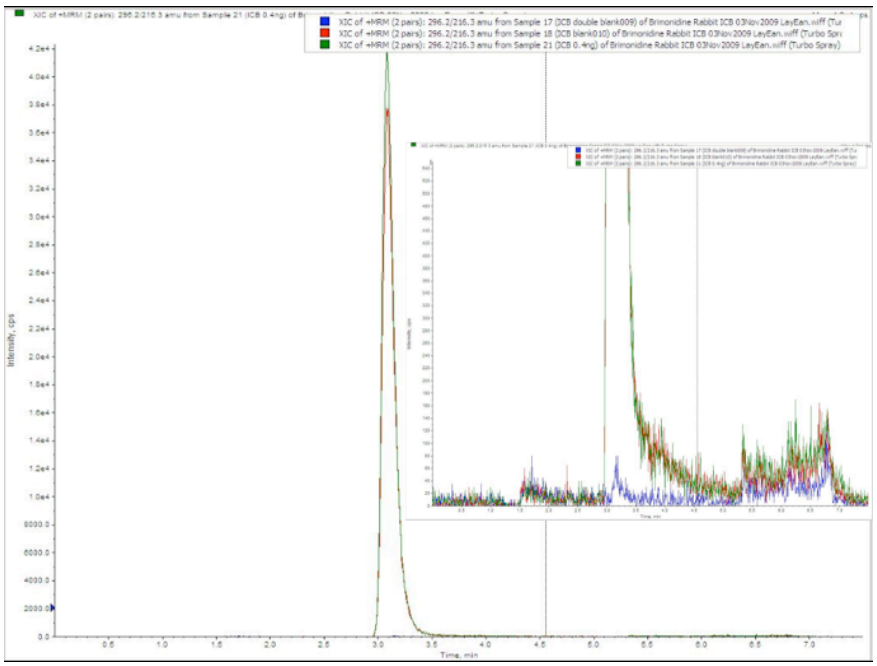

Figure 6.6 Representative LCMS/MS spectra of brimonidine and brimonidine-d_4 at concentration 0.4 ng/tissue and 0.1 µg/mL respectively in ICB. Blue: Blank matrix; Red: IS; Green: Brimonidine sample.

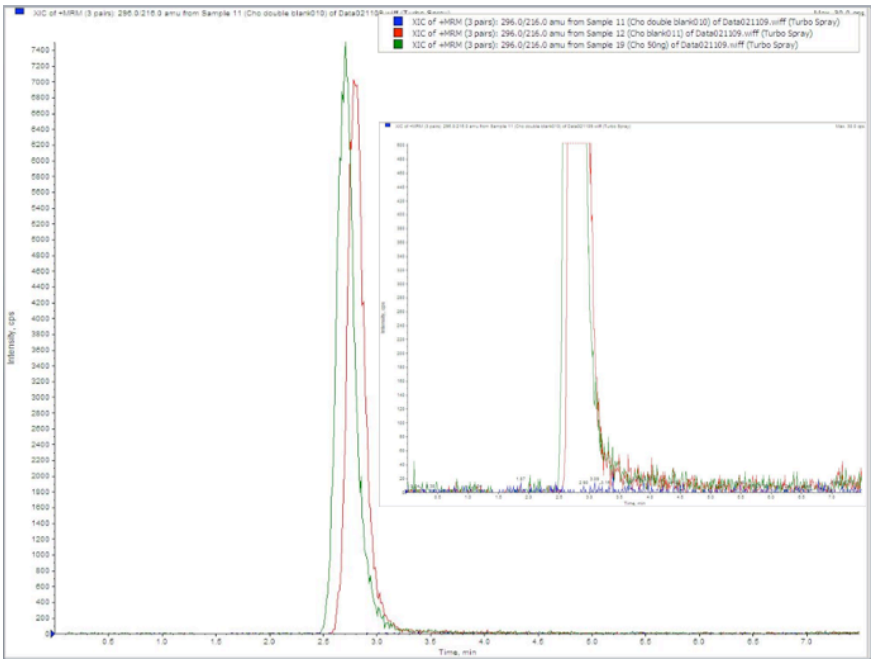

Figure 6.7 Representative LCMS/MS spectra of brimonidine and brimonidine-d_4 at concentration 50 ng/tissue and 0.1 µg/mL respectively in choroid. Blue: Blank matrix; Red: IS; Green: Brimonidine sample.

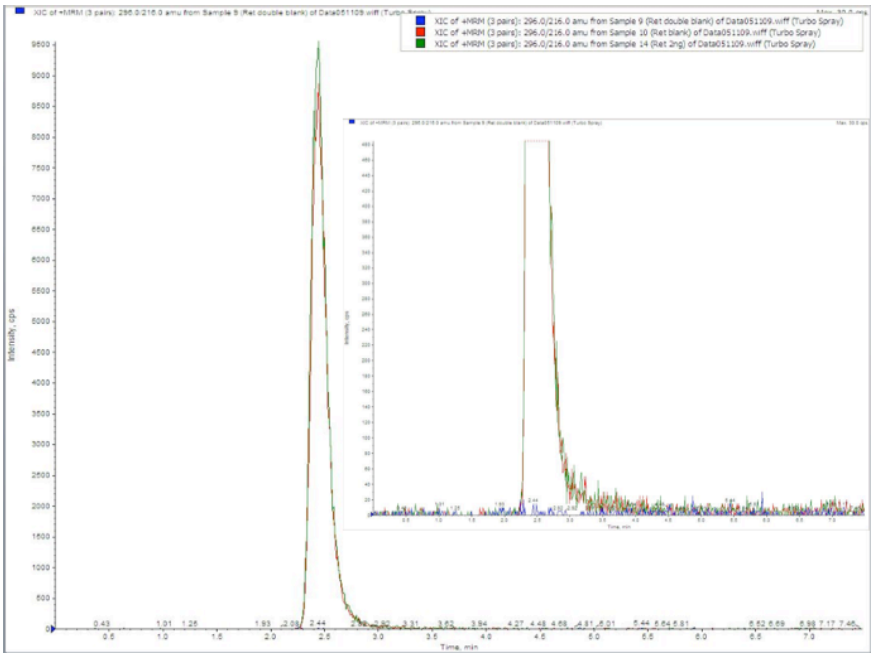

Figure 6.8 Representative LCMS/MS spectra of brimonidine and brimonidine-d_4 at concentration 2 ng/tissue and 0.1 µg/mL respectively in retina. Blue: Blank matrix; Red: IS; Green: Brimonidine sample.

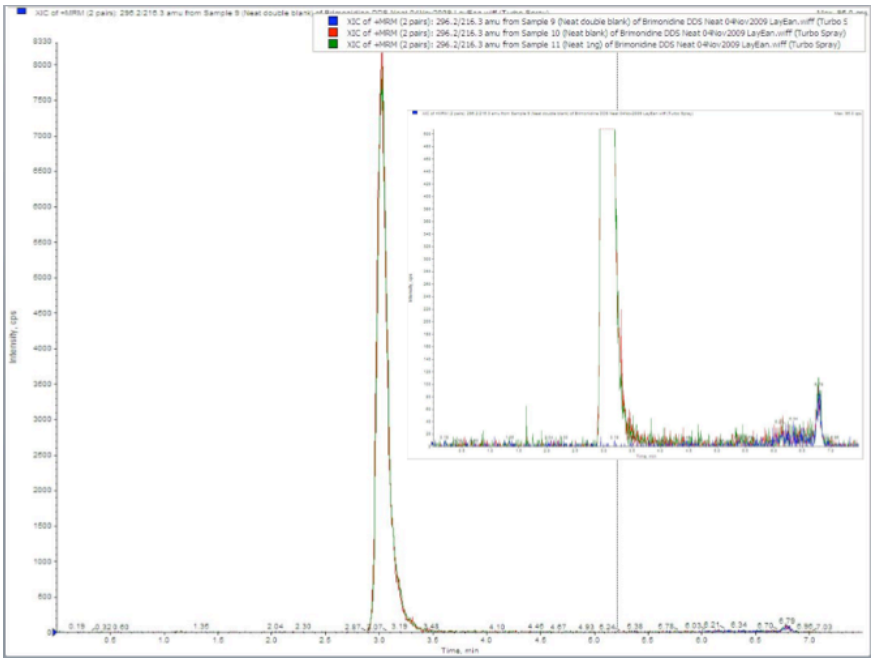

Figure 6.9 Representative LCMS/MS spectra of brimonidine and brimonidine-d_4 at concentration 1 ng and 0.1 µg/mL respectively in DDS. Blue: Blank diluent; Red: IS; Green: Brimonidine sample

6.3.1.2 LINEARITY

Table 6.13 is a list of linearity parameters for the ocular tissues. The correlation coefficients were greater than the acceptance criteria of 0.97, which suggested good linear response from the detector. Figure A6.1 to Figure A6.6 (Appendix) are the representative linear regression curves of the tissues tested. Concentration of the calibration standards was back-calculated using equations of the linear regression curves and the data are as tabulated in Appendix (Tables A6.11, A6.12, A6.13, A6.14, A6.15 and A6.16) for aqueous humour, vitreous humour, ICB, choroid, retina and DDS respectively. The calculated accuracy and precision of these back-calculated concentrations provided further evidence on the system linearity.

Tissue samples	N	Linearity		
		Mean Slope	Mean Intercept	Mean Correlation coefficient (r^2)
Aqueous humour	1	53.6 $(\mu g/mL)^{-1}$	0.0106	0.9986
Vitreous humour	4	86.067 $(\mu g/mL)^{-1}$	0.0347	0.9977
Choroid	5	0.086 $(ng)^{-1}$	0.0056	0.9980
ICB	2	0.066 $(ng)^{-1}$	0.0025	0.9990
Retina	3	0.0946 $(ng)^{-1}$	0.00295	0.9987
Implant	2	0.259 $(ng/mL)^{-1}$	0.003105	0.9993

Table 6.13 Linearity parameters obtained from the linear regression curves.

6.3.1.3 ACCURACY AND PRECISION

The intra- and inter-day accuracy and precision results for all tissue assays as determined using QC samples are as summarized in Table 6.14 and Table 6.15 below. The overall accuracy and precision of the assay were within the acceptance criteria of 20% of the nominal concentrations. Generally and as expected, variability was higher in the lower concentration as compared to higher concentration samples.

	Nominal concentrations, µg/mL	Measured concentrations, µg/mL (mean ± S.D)	% RSD	% Accuracy	N
Intra-day assay					
Aqueous humour (µg/mL)	0.002	0.002 ± 0.0001	7.55	92.00	3
	0.25	0.213 ± 0.032	15.23	85.07	3
	1.25	1.190 ± 0.000	0.00	95.20	3
Vitreous humour (µg/mL)	0.002	0.002 ± 0.000	12.03	88.50	6
	0.05	0.052 ± 0.001	1.60	103.40	6
	0.25	0.207 ± 0.005	2.35	82.80	6
Choroid (ng)	0.2	0.22 ± 0.02	8.67	110.00	6
	50	45.90± 3.96	8.62	91.83	6
	100	103.00 ± 2.24	2.18	102.62	6
ICB (ng)	0.2	0.20 ± 0.02	9.80	101.33	3
	50	53.00 ± 1.65	3.12	106.00	3
	100	108.00 ± 1.00	0.93	108.00	3
Retina (ng)	0.2	0.22 ± 0.02	7.33	110.20	5
	50	51.02 ± 0.77	1.51	102.04	5
	100	98.90 ± 3.39	3.43	98.90	5
Implant (ng/mL)	0.5	0.46 ± 0.03	7.05	92.27	3
	125	123.67 ± 2.31	1.87	98.93	3
	500	489.33 ± 5.77	1.18	97.87	3

Table 6.14 Intra-day accuracy and precision of QC samples.

	Nominal concentrations, µg/mL	Measured concentrations, µg/mL (mean ± S.D)	% RSD	% Accuracy	N
Inter-day assay					
Vitreous humour (µg/mL)	0.002	0.002 ± 0.000	15.49	100.50	12
	0.05	0.050 ± 0.002	3.27	100.60	12
	0.25	0.224 ± 0.019	8.39	89.60	12
Choroid (ng)	0.2	0.20 ± 0.06	16.08	99.04	12
	50	46.10 ± 4.13	8.96	92.15	12
	100	103.00 ± 2.27	2.20	103.31	12
ICB (ng)	0.2	0.21 ± 0.02	7.06	103.00	6
	50	52.60± 1.39	2.64	105.10	6
	100	107.50 ± 1.05	0.98	107.50	6
Retina (ng)	0.2	0.22 ± 0.02	10.30	107.65	10
	50	47.57 ± 4.88	10.26	95.14	10
	100	102.35 ± 4.45	4.34	102.35	10
Implant (ng/mL)	0.5	0.44 ± 0.05	11.40	88.37	6
	125	123.83 ± 1.83	1.48	99.07	6
	500	491.17 ± 5.74	1.17	98.23	6

Table 6.15 Inter-day accuracy and precision of QC samples.

6.3.1.4 LOWER LIMIT OF QUANTITATION (LLOQ)

The LLOQ, which was the lowest concentration of the calibration standards, was found to be 0.001 µg/mL for aqueous humour and vitreous humour, 0.1 ng for choroid, ICB and retina and 0.25 ng/mL for the DDS samples. The accuracy and precision results for all tissue assays at LLOQ were within the acceptance criteria of 20% of the nominal concentrations (Table A6.17). Tissues containing melanin such as choroid and ICB show higher variability as compared to other tissue types. This observation could be related to the matrix effects. However, such degree of variability was not observed in higher concentration samples (section accuracy and

precision, Table 6.14 and Table 6.15), suggesting that the influence of tissue components was relatively restricted to concentration at LLOQ.

6.3.1.5 EXTRACTION RECOVERY (LIQUID-LIQUID EXTRACTION)

The extraction recovery of brimonidine and brimonidine-d_4 were determined by assuming the peak area of the fortified samples representing 100% extraction recovery. Table 6.16 shows that the extraction recovery of brimonidine concentrations 0.005 µg/mL and 0.05 µg/mL in the processed samples were ~60% and ~70% respectively. Better extraction efficiency and lower variability were demonstrated for higher concentration brimonidine sample. In the same table, it was found that the extraction recovery of brimonidine-d_4 0.01 µg/mL was ~ 65%, which was similar to brimonidine, further underscored the relevance of this molecule as an internal standard for brimonidine.

	Brimonidine 0.005 µg/mL	Brimonidine 0.05 µg/mL	Brimonidine-d_4 0.01 µg/mL
Mean % extraction recovery	59.32	69.40	65.53
SD	8.46	4.74	5.86

Table 6.16 Extraction recovery of brimonidine and brimonidine-d_4 in the vitreous humour.

6.3.2 OCULAR TISSUE WEIGHTS AT NECROPSY

The weights of the ocular tissues collected from hyaluronidase-treated and control groups were compared as shown in Table 6.17. The average weights of ICB, choroid and retina isolated from hyaluronidase-treated eye were higher as compared to the same tissues isolated from the control group. This may be related to the higher water content present in the tissues of the liquefied eye. In addition, weight variability could be ranked in the sequence of AH<VH<ICB<choroid and retina. Tissues with

higher variability such as choroid and retina have lighter weight and more difficult to be isolated. Additionally, these tissue samples were in contact with intracellular water and have a blood supply with variably emptied capillaries made the standardization of the weighing method extremely difficult. Higher variability was also noted for vitreous humour of hyaluronidase-treated group as compared to control. This was because liquefied vitreous drained away easily as compared to gel vitreous, making the collection process trickier and less consistent. The weights of the ocular tissues were used in the quantitation of brimonidine, except aqueous and vitreous humour, of which the brimonidine content was calculated based on drug content per volume of reconstituted solution (μg/mL).

Tissues	Hyaluronidase-treated (g) n=12			Control (g) n=12		
	Mean	SD	RSD	Mean	SD	RSD
Aqueous humour	0.216	0.028	12.86	0.220	0.032	14.33
Vitreous humour	0.698	0.184	26.32	0.772	0.092	11.88
ICB	0.141	0.035	24.62	0.133	0.041	30.38
Choroid (macula)	0.007	0.004	54.48	0.004	0.003	57.81
Choroid(superior)*	0.006	0.002	40.84	0.003	0.002	62.04
Choroid (inferior)*	0.006	0.002	46.42	0.004	0.002	59.15
Choroid (nasal)	0.008	0.004	48.47	0.005	0.003	51.46
Choroid (temporal)	0.008	0.005	54.09	0.005	0.003	49.64
Retina (macula)	0.010	0.004	36.50	0.007	0.003	37.69
Retina (superior)	0.011	0.006	57.55	0.008	0.005	69.77
Retina (inferior)	0.010	0.006	61.23	0.007	0.003	38.12
Retina (nasal)	0.010	0.005	46.43	0.007	0.003	43.44
Retina (temporal)	0.011	0.006	48.44	0.007	0.003	45.75

Table 6.17 Weights of ocular tissues collected at necropsy.

* n=11 instead of 12 as one of samples was not available.

6.3.3 DDS LOCATION AT NECROPSY

The appearance and location of the implanted DDS were identified on day 28 at necropsy using a SLR digital camera (Canon EOS 5D Mark II). Three rabbits were euthanized on day 28 and the positions of the DDS in both eyes are as illustrated in Figure 6.10. The locations of some DDSs appeared to have shifted from the site of injection (supero-nasal) into the nasal and temporal quadrants of the vitreous cavity. Additionally, the appearances were found to be a mix of sizes and shapes (rod and round) and they varied by individual rabbits rather than study groups.

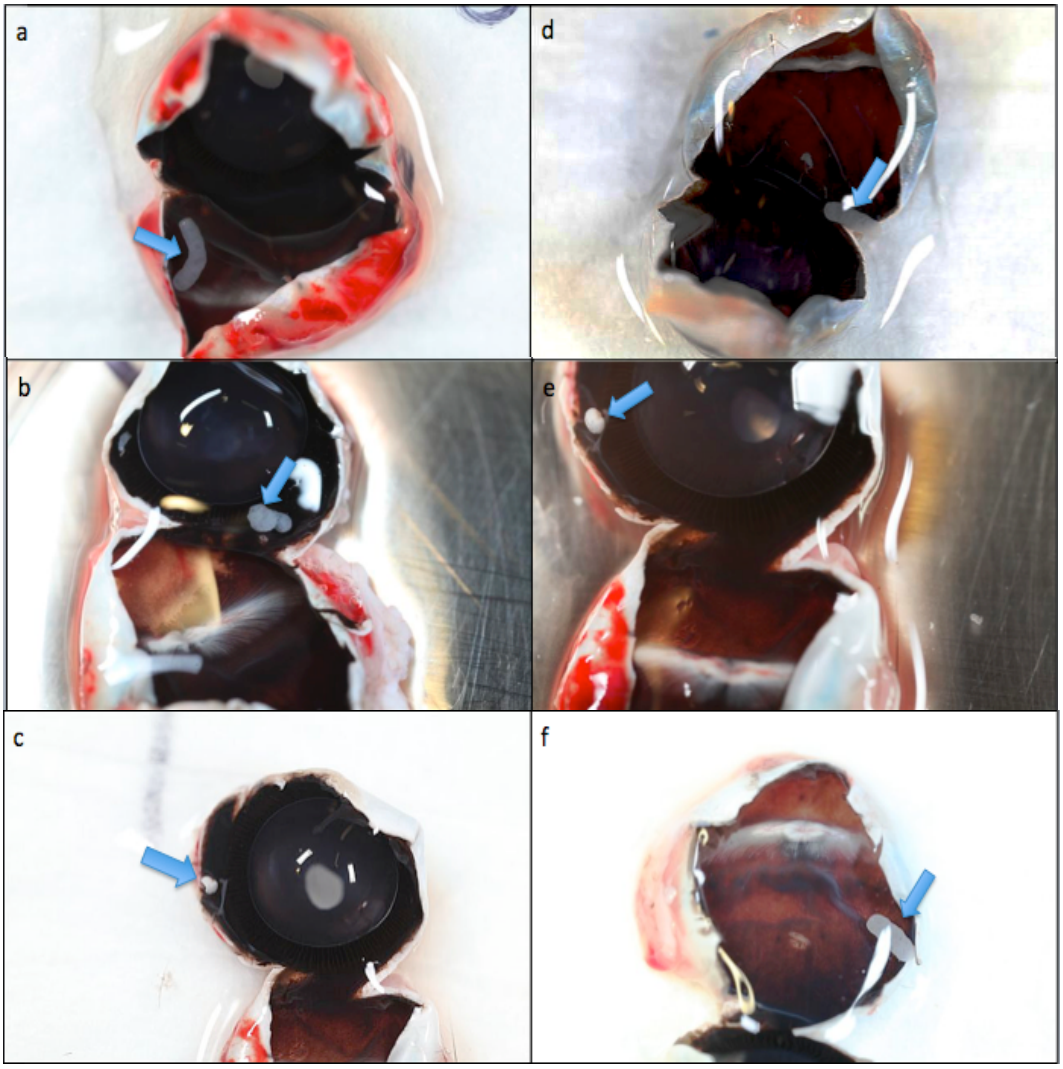

Figure 6.10 The appearance and location of DDSs in hyaluronidase-treated (a,b,c) and control (d,e,f) eyes on day 28 (n=3). Blue arrows indicate DDS position within the vitreous humour; a: Nasal, b: supero-nasal, c: temporal, d: temporal, e: nasal, f: temporal.

6.3.4 TISSUE CONCENTRATIONS FOLLOWING INTRAVITREAL INJECTION

Brimonidine concentrations were determined in aqueous humour, vitreous humour, ICB, choroid and retina of control (untreated) and hyaluronidase-treated eyes (treated) following a single intravitreal injection of 30µg/20µL brimonidine tartrate solution. The concentration-time profiles of brimonidine in aqueous humour (AH), vitreous humour (VH), ICB, choroid (cho) and retina (ret) of both eyes were compared as illustrated in Figure 6.11 and a summary table of the data can be found at appendix (Tables A6.18, A6.20, A6.22, A6.24 and A6.26). Figure 6.12 and Figure 6.13 below are semi-log plots that display tissue concentrations at 8 hours and peak concentration (C_{max}) of the ocular tissues respectively. The derived pharmacokinetic parameters of brimonidine in the ocular tissues are as listed in Tables 6.18, 6.19 and 6.20 below. Additionally, the distribution of brimonidine at different regions within the choroid and retina tissues was compared as shown in Figure 6.14 and Figure 6.15 respectively.

6.3.4.1 AQUEOUS HUMOUR (AH)

Figure 6.11 below shows that the mean concentration of brimonidine in the aqueous humour of control group was 7 ng/mL, 34 ng/mL, 19 ng/mL and 6 ng/mL at 1, 2, 4 and 8 hours post-injection respectively; whereas it was 14 ng/mL, 7 ng/mL, 8 ng/mL and 5 ng/mL at 1, 2, 4 and 8 hours respectively in hyaluronidase-treated group. The C_{max} was 2.4 fold higher in control than hyaluronidase-treated group with T_{max} achieved at 2 hour and 1 hour respectively (Table 6.18). The higher concentration in hyaluronidase-treated eyes at 1 hour suggested faster rate of initial distribution from the vitreous into the aqueous chamber and the maximum may have occurred earlier than the first sample point at one hour. The concentration declined gradually thereafter leading to lower cumulative tissue exposure ($AUC_{0-\infty}$) of 94 ng.h/mL as compared to the control group (152 ng.h/mL). Coinciding with this, slower clearance was observed in the case of control eyes. However, it was found that terminal half-life was shorter in control (2.47 hours) than hyaluronidase-treated group (4.23

hours), indicating a steeper terminal elimination phase in the control eye (Table 6.18). Brimonidine remained detected at 8 hours post-injection with similar drug level observed for both groups. When compared to other ocular tissues, aqueous humour had the lowest drug concentration during the entire study period (Figure 6.11).

6.3.4.2 VITREOUS HUMOUR (VH)

Since brimonidine was directly injected into the vitreous humour, a similar C_{max} was achieved at 1 hour in both eyes, (Figure 6.13, Table 6.18). As brimonidine distributed from the injection pocket, its concentration declined gradually from 10.8 ± 0.9 µg/mL at 1 hour to 0.4 ± 0.1 µg/mL at 8 hours in control eyes and from 9.9 ± 1.0 µg/mL at 1 hour to 0.3 ± 0.1 µg/mL at 8 hours in hyaluronidase-treated eyes (Figure 6.11). Consistent with the data from aqueous humour samples, a faster rate of initial distribution was observed in the vitreous humour of the hyaluronidase-treated group, where drug concentration reduced by almost 40% at 2 hour as compared to 10% in the control eye leading to a 1.6 fold lower drug concentration detected at the corresponding time point. This figure agreed with the 1.4 fold reported in Chapter 4 for sodium fluorescein at 2 hour post-injection. Unlike sodium fluorescein, however, there was no difference in brimonidine concentration at 4 hour between both eyes, suggesting other factors may also be important in the early distributive phase. In addition, due to the slower rate of initial distribution in the control group, cumulative tissue exposure was 1.3 fold higher than in the hyaluronidase-treated group (Table 6.18), coinciding with the slower clearance calculated.

6.3.4.3 IRIS-CILIARY BODY (ICB)

In contrast to the vitreous humour, brimonidine concentration in ICB increased over time as shown in Figure 6.11. C_{max} was 1.7 fold higher in the control than hyaluronidase-treated group but T_{max} was similar (8 hours) for both study groups. There was no difference in drug concentration at 1 hour between both eyes but rapid absorption was notable between 1 hour and 2 hour. The sustained accumulation of

brimonidine in the ICB led to a considerably higher degree of cumulative tissue exposure ($AUC_{0\text{-}8hours}$) compared to aqueous humour. Nevertheless, due to the prolonged absorption and retention period, a lack of elimination phase (Figure 6.11) has prevented the calculation of $AUC_{0\text{-}\infty}$, terminal half-life and clearance of brimonidine from and within the ICB.

6.3.4.4 CHOROID (CHO)

Consistent with the higher rate of initial distribution demonstrated in the vitreous humour of the hyaluronidase-treated eyes, total choroidal concentration was found to be 1.6 fold higher in the hyaluronidase-treated as compared to control eyes at 1 hour. Additionally, T_{max} was achieved at 1 hour in the hyaluronidase-treated group as compared to a range of 1 to 4 hours in the control group, further demonstrating more rapid initial distribution from the vitreous humour of the hyaluronidase-treated eyes, that subsequently led to a faster rate of drug transport across the choroid during the first hour post-injection.

C_{max} was higher in cho-macula (4.4 fold), cho-inferior (1.6 fold) and cho-nasal (5.3 fold) in control eyes, except in the cho-temporal region where the C_{max} was 6 fold higher in the hyaluronidase-treated group (Table 6.19). Similarly, cumulative tissue exposure ($AUC_{0\text{-}8hours}$) was overall 1.8 to 3.6 fold higher in control group apart from cho-temporal (Table 6.19). Nevertheless, at 8 hour post-injection, drug concentration was found to be higher in the control eyes, including cho-macula (1.8 fold), cho-superior (2.5 fold), cho-inferior (2.4 fold), cho-nasal (2.6 fold) and cho-temporal (1.4 fold). This suggested that the faster rate of initial distribution into the choroid led to an overall faster rate of drug clearance from the choroid of hyaluronidase-treated eyes (Table 6.18). Essentially, brimonidine remained detectable within the choroid at 8 hour after injection, with the lowest concentration found at cho-nasal and cho-temporal in both study groups (Figure 6.14). Due to a lack of elimination phase for cho-macula (control) and cho-inferior (control and hyaluronidase-treated), terminal half-life and clearance were not determined for these samples.

In addition, Figure 6.14 below shows that brimonidine was not distributed evenly within the choroid tissues of both study groups throughout the entire study duration. This suggested a lack of an equilibrium distribution phase in the choroid regardless of the vitreous state. However, the same figure clearly illustrated that eyes with a lower vitreous gel content (hyaluronidase-treated group) established a different drug distribution profile within the choroid from that of a normal vitreous (control group). Tissue concentration at cho-nasal was found to be always the lowest in the hyaluronidase-treated group, which was however, not the case in the control group.
In comparison to other part of the ocular tissues, tissue exposure was found highest in the choroid and such observation was the same for control and hyaluronidase-treated groups (Table 6.18).

6.3.4.5 RETINA (RET)

Brimonidine was rapidly absorbed into the retina of both groups, as shown by the early T_{max} of 1 hour following injection (Table 6.20). In contrast to choroid, concentration at 1 hour was found higher in the control eyes, including ret-macula (1.7 fold), ret-superior (1.9 fold), ret-inferior (1.9 fold), ret-nasal (1.5 fold) and ret-temporal (2.9 fold). The lower retinal concentration detected in the hyaluronidase treated eye at 1 hour may be due to the fact that most of the brimonidine that penetrated the retina has been cleared across to the choroid as was demonstrated by the higher choroidal concentration at 1 hour aforementioned. Therefore, the faster rate of initial distribution from the vitreous humour of the hyaluronidase-treated eyes may result in a faster rate of drug clearance from the retina.

In addition, C_{max} was higher in control than hyaluronidase-treated eyes, which included ret-macula (1.7 fold), ret-superior (1.9 fold), ret-inferior (1.9 fold), ret-nasal (1.5 fold) and ret-temporal (2.9 fold) as shown in Table 6.20. Terminal half-life was similar in both groups of around 1.3-2.7 hours with an exception of around 4 hours at ret-inferior. Clearance was found to be lower within the retina tissue of the control group and this was true regardless of whether different areas of the retina were compared individually or summed as a single section (Table 6.18). With lower drug

clearance, cumulative tissue exposure as determined from $AUC_{0\text{-}8hours}$ was higher in the control eyes at ret-macula (1.6 fold), ret-superior (2.5 fold), ret-inferior (1.4 fold), ret-nasal (2.0 fold) and ret-temporal (2.0 fold) (Table 6.21). When the concentrations of all regions within the retina tissues were summed as one single section, cumulative tissue exposure ($AUC_{0\text{-}\infty}$) was found to be 2.1 fold higher in control group with a two fold slower rate of clearance compared to the hyaluronidase-treated group (Table 6.18).

In addition, Figure 6.15 below shows that the absorption and distribution of brimonidine throughout the retina was not uniform in both study groups. At 1 hour following injection, higher concentration was detected at the ret-superior, ret-temporal and ret-macula, corresponding well with the levels detected at the choroid tissues (Figure 6.14) of both study groups. Brimonidine was found to be the lowest at ret-temporal 8 hours after injection and it was the same in both treated and untreated eyes. Moreover, Figure 6.15 also shows that there was a relatively high absorption of brimonidine at the ret-superior of control and hyaluronidase-treated eyes at 2 hour. This corresponds to the concentration detected at cho-superior, indicating brimonidine transport between both tissues.

In general, drug level remained detected in the retina at the end of the study, with higher concentrations found at ret-superior, ret-inferior and ret-temporal of the control eyes; the concentration was however, comparable between both study groups at ret-macula and was slightly lower in the control eyes at ret-nasal. When the concentrations of all regions within the retina tissues were summed as one single section, retinal concentration was overall 1.7 fold higher in control than hyaluronidase treated eyes at 8 hour. This further suggests that brimonidine was cleared faster from the retina of eyes with partial vitreous liquefaction as opposed to a normal eye with an intact vitreous.

When the retinal concentration was compared to other part of the ocular tissues, drug exposure ($AUC_{0\text{-}8hours}$) at the retina of both study groups was the second highest after choroid (Table 6.18).

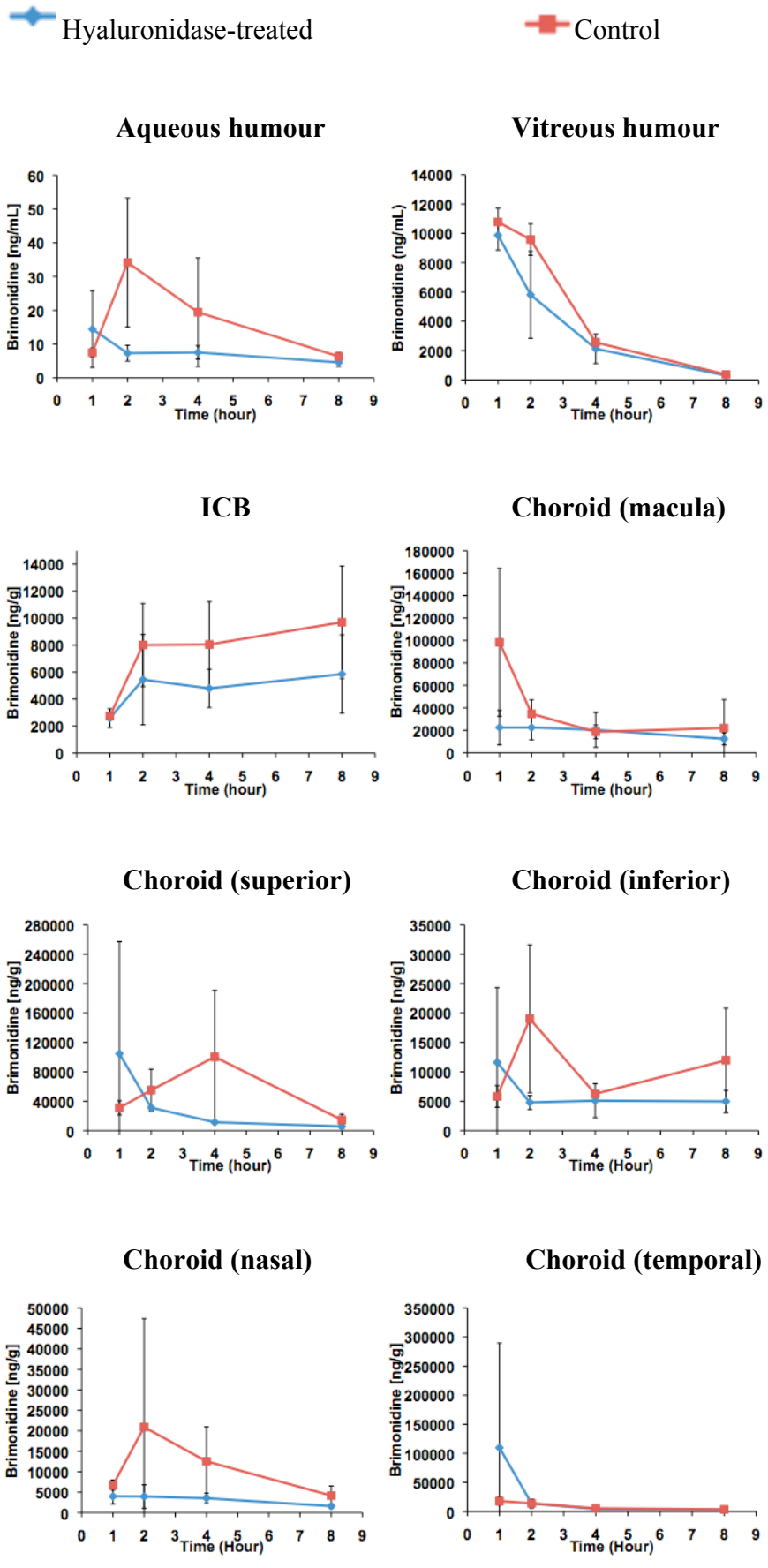
Hyaluronidase-treated
Control
Aqueous humour
Brimonidine [ng/mL]
Time (hour)
Vitreous humour
Brimonidine (ng/mL)
Time (hour)
ICB
Brimonidine [ng/g]
Time (hour)
Choroid (macula)
Brimonidine [ng/g]
Time (hour)
Choroid (superior)
Brimonidine [ng/g]
Time (hour)
Choroid (inferior)
Brimonidine [ng/g]
Time (Hour)
Choroid (nasal)
Brimonidine [ng/g]
Time (Hour)
Choroid (temporal)
Brimonidine [ng/g]
Time (Hour)

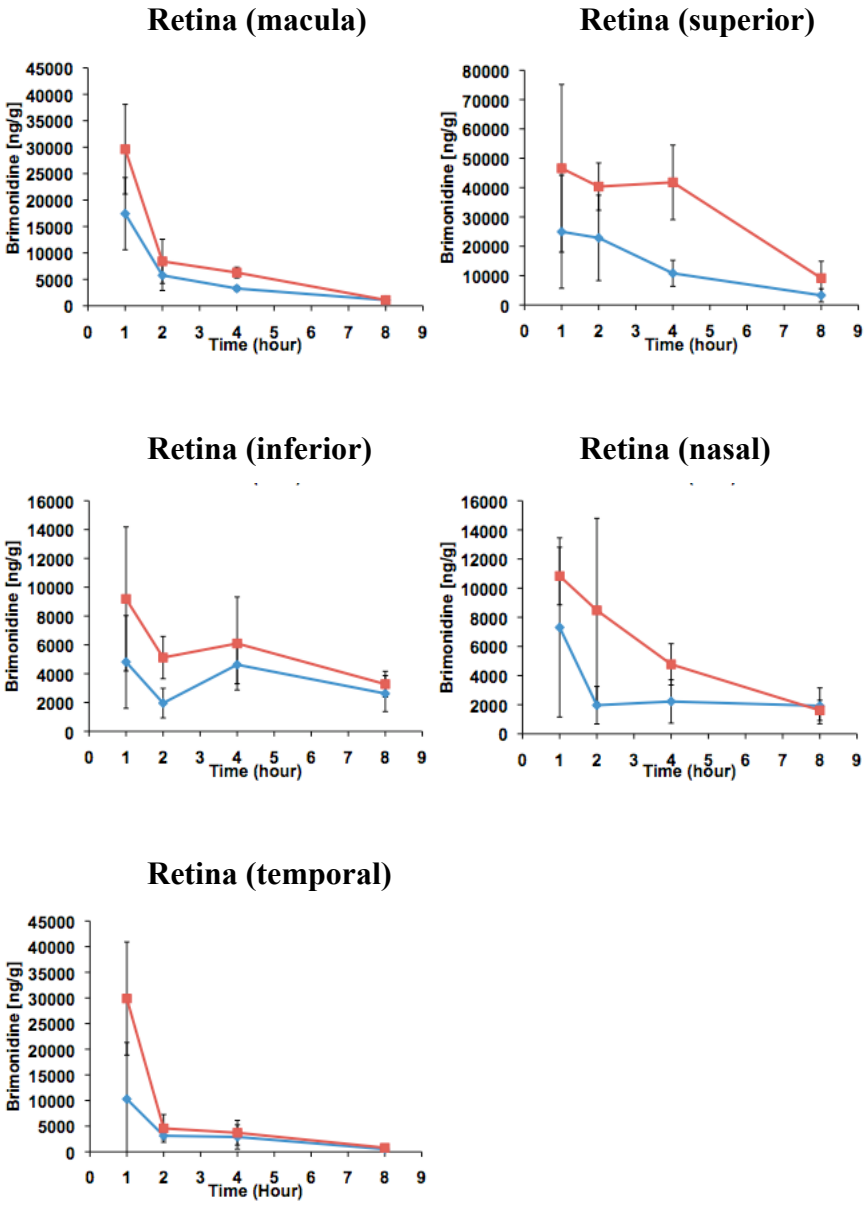

Figure 6.11 Tissue concentration (ng/mL or ng/g) of brimonidine in hyaluronidase-treated and control eyes following a single intravitreal injection of 30µg/20µL brimonidine tartrate in Dutch-belted rabbits (n=3 rabbits/time point). Y-axis error bar indicates the minimum and maximum values. Data was associated with large error, which reflects the variability within the study populations.

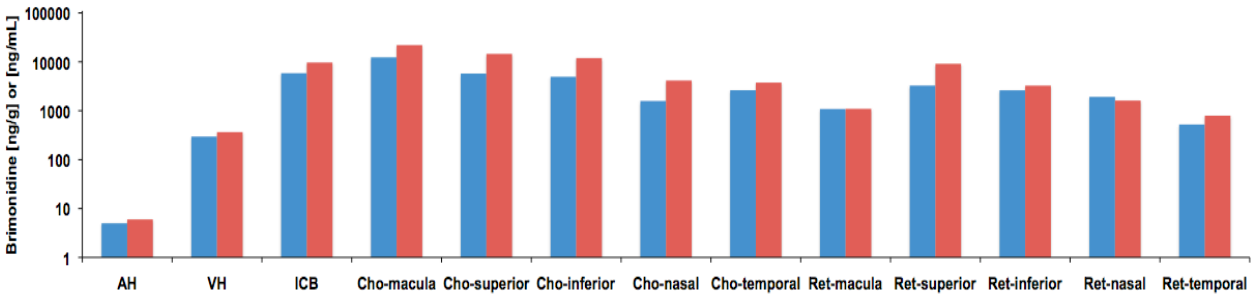

Figure 6.12 Brimonidine concentration (ng/g or ng/mL) in the aqueous humour, vitreous humour, ICB, choroid and retina of control and hyaluronidase-treated eyes at 8 hours after injection Blue: Hyaluronidase-treated; Red: Control.

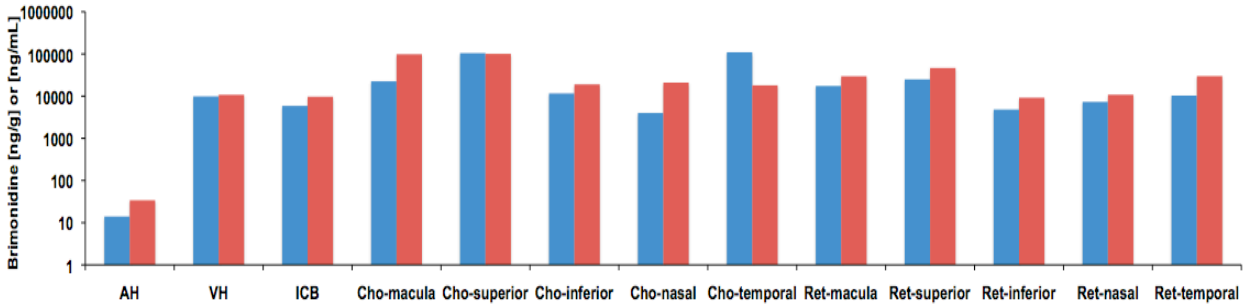

Figure 6.13 Maximum concentration (C_{max}) of brimonidine (ng/g or ng/mL) in aqueous humour, vitreous humour, ICB, choroid and retina of control and hyaluronidase-treated eyes following a single dose of 30µg/20µL intravitreal injection. Blue: Hyaluronidase-treated; Red: Control.

Parameters	Aqueous humour		Vitreous humour		ICB		Choroid		Retina	
	HT	Ctrl	HT	Ctrl	HT	Ctrl	HT	Ctrl	HT	Ctrl
C_{max} (µg/mL or µg/g)	0.01 ±0.01	0.03 ±0.02	9.9 ±1.0	10.8 ±0.9	5.9 ±2.9	9.7 ±4.2				
T_{max} (hour)	1	2	1	1	8	8				
$AUC_{0\text{-}8hrs}$ (µg.h/mL or µg.h/g)	0.06 ±0.02	0.13 ±0.08	25.6 ±8.7	33.6 ±3.1	36.8 ±15.8	58.3 ±22.7	111.1 ±99.4	183.7 ±200.0	41.7 ±34.2	89.3 ±94.4
$AUC_{0\text{-}\infty}$ (µg.h/mL or µg.h/g)	0.09 ±0.03	0.15 ±0.09	26.2 ±8.9	34.3 ±3.4			128.3 ±112.7	232.3 ±232.9	49.1 ±38.6	100.9 ±107.0
$t_{1/2}$ (hour)	4.23	2.47	1.39	1.37			2.18	2.98	2.69	2.53
Mean Clearance (mL/hr or g/hr)	353	197	1.15	0.88			0.23	0.13	0.61	0.30

Table 6.18 Pharmacokinetic parameters for aqueous humour, vitreous humour, ICB, choroid (total) and retina (total) following a single dose 30 µg/20µL intravitreal injection. HT: hyaluronidase-treated; Ctrl: control

Parameters	Cho-macula		Cho-superior		Cho-inferior		Cho-nasal		Cho-temporal	
	HT	Ctrl	HT	Ctrl	HT	Ctrl	HT	Ctrl	HT	Ctrl
C_{max} (µg/mL or µg/g)	22.5 ±11.0	98.4 ±65.9	104.7 ±152.4	100.3 ±90.5	11.6 ±12.7	19.0 ±12.6	4.0 ±1.9	20.9 ±26.5	109.8 ±179.9	18.0 ±7.1
T_{max} (hour)	2	1	1	4	1	2	1	2	1	1
$AUC_{0\text{-}8hrs}$ (µg.h/mL or µg.h/g)	141.8 ±894.7	250.3 ±153.1	197.0 ±159.5	443.7 ±339.6	44.0 ±27.0	77.0 ±38.4	23.6 ±10.8	84.0 ±71.0	149.0 ±198.3	63.3 ±28.2
$AUC_{0\text{-}\infty}$ (µg.h/mL or µg.h/g)	241.4 ±133.2		210.9 ±166.9	474.0 ±355.9			31.6 ±13.3	99.5 ±79.7	154.0 ±199.6	80.1 ±33.3
$t_{1/2}$ (hour)	5.58		1.67	1.44			3.47	2.58	1.30	3.10
Mean Clearance (mL/hr or g/hr)	0.12		0.14	0.06			0.95	0.30	0.20	0.38

Table 6.19 Pharmacokinetic parameters for choroid tissue following a single dose 30µg/20 µL intravitreal injection. HT: hyaluronidase-treated; Ctrl: control

Parameter	Ret-macula		Ret-superior		Ret-inferior		Ret-nasal		Ret-temporal	
	HT	Ctrl	HT	Ctrl	HT	Ctrl	HT	Ctrl	HT	Ctrl
C_{max} (µg/mL or µg/g)	17.4 ±6.8	29.6 ±8.5	25.0 ±19.3	46.6 ±28.6	4.8 ±3.2	9.2 ±5.0	7.3 ±6.2	10.8 ±2.0	10.3 ±11.0	29.9 ±110.3
T_{max} (hour)	1	1	1	1	1	1	1	1	1	1
$AUC_{0\text{-}8hrs}$ (µg.h/mL or µg.h/g)	38.1 ±13.6	63.3 ±18.2	98.2 ±58.9	250.7 ±90.3	26.9 ±11.2	41.7 ±18.7	20.8 ±15.0	41.1 ±17.1	24.7 ±19.7	49.5 ±23.2
$AUC_{0\text{-}\infty}$ (µg.h/mL or µg.h/g)	40.8 ±15.2	65.6 ±18.6	109.5 ±66.7	274.8 ±105.5	45.3 ±20.0	62.8 ±24.4		47.0 ±19.6	25.9 ±20.3	51.0 ±24.0
$t_{1/2}$ (hour)	1.75	1.47	2.39	1.82	4.88	4.46		2.53	1.63	1.34
Mean Clearance (mL/hr or g/hr)	0.74	0.46	0.27	0.11	0.66	0.48		0.64	1.16	0.59

Table 6.20 Pharmacokinetic parameters for retina tissue following a single dose 30µg/20 µL intravitreal injection. HT: hyaluronidase-treated; Ctrl: control

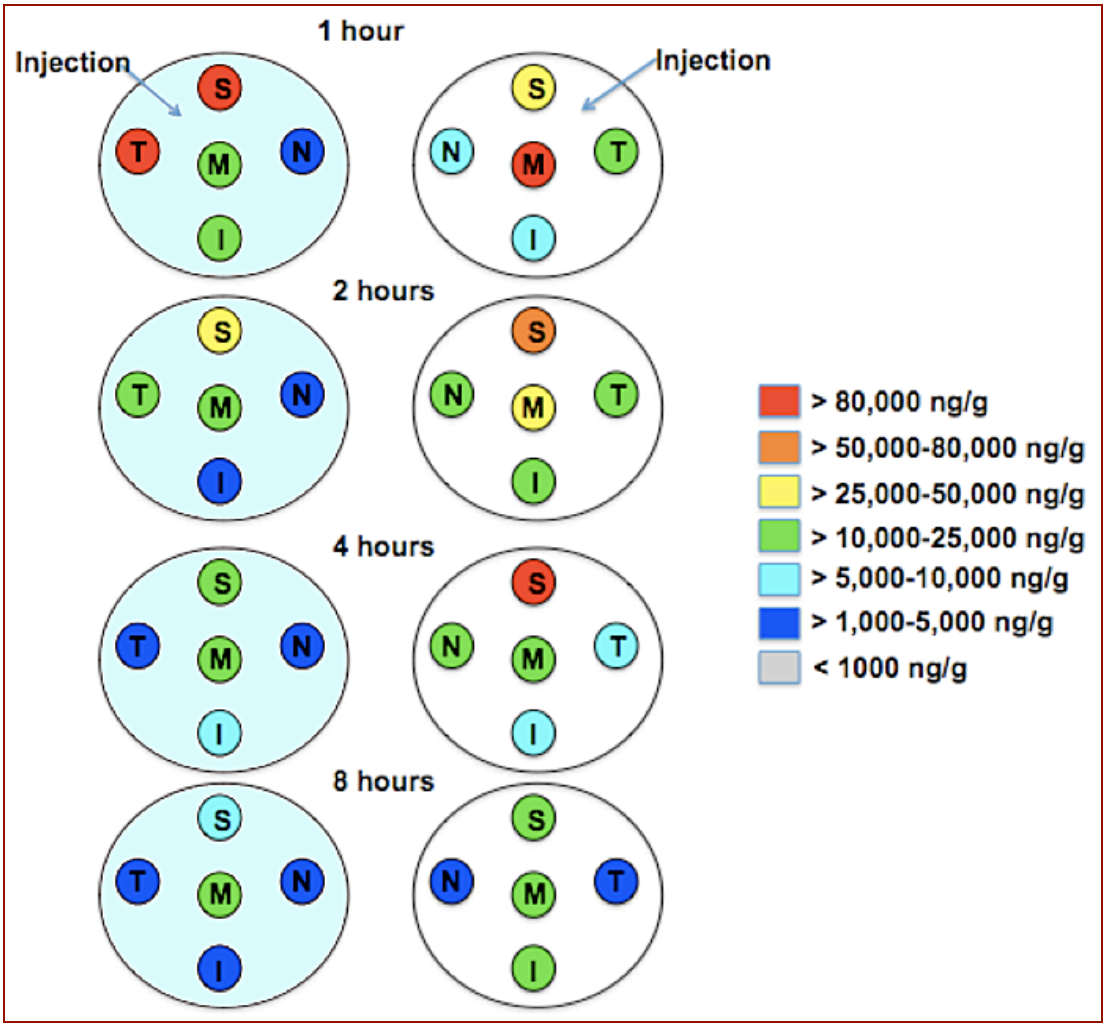

Figure 6.14 Comparison of brimonidine concentration at superior, inferior, macula, nasal and temporal areas of the choroid tissue following a single dose 30µg/20µL intravitreal injection. Left-panel: Hyaluronidase-treated eyes; Right panel: Control eyes.

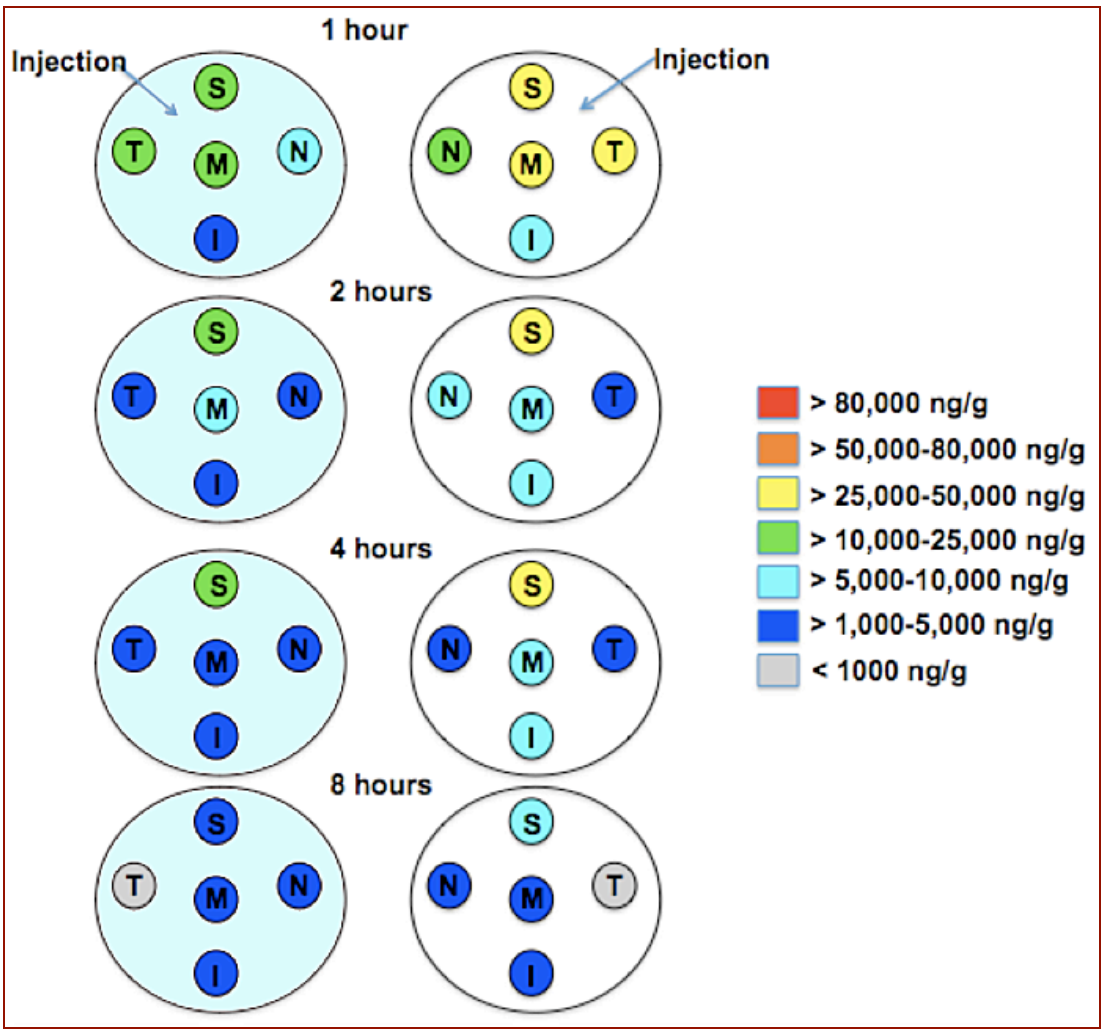

Figure 6.15 Comparison of brimonidine level at superior, inferior, macula, nasal and temporal areas of the retina tissue following a single dose 30µg/20 µL intravitreal injection. Left-panel: Hyaluronidase-treated eyes; Right panel: Control eyes.

6.3.5 TISSUE CONCENTRATIONS FOLLOWING INTRAVITREAL IMPLANTATION

Brimonidine concentration was determined in aqueous humour, vitreous humour, ICB, choroid and retina of the control and hyaluronidase-treated eyes following a single intravitreal implantation of 210 µg brimonidine tartrate PS DDS. Figure 6.16 below compares the ocular concentration-time profiles of brimonidine in aqueous humour, vitreous humour, ICB, choroid and retina of the control (untreated) eyes with that of the hyaluronidase-treated (treated) eyes and a summary table of the mean, standard deviation, minimum and maximum values of brimonidine concentration in analysed tissues are provided in Appendix (Table A6.19, A6.21, A6.23, A6.25 and A6.27). Figures 6.17 and 6.18 are semi-log column charts comparing tissue concentrations on day 28 and C_{max} of the ocular tissues respectively. Figures 6.19 and 6.20 below compare the absorption and distribution of brimonidine at different areas of the choroid and retina tissues respectively.

6.3.5.1 AQUEOUS HUMOUR (AH)

As shown in Figure 6.16, T_{max} was achieved on day 14 for both eyes with C_{max} 2.9 fold higher in control than hyaluronidase-treated eyes (Figure 6.18). In addition, tissue exposure ($AUC_{0\text{-}D28}$) was found to be 2.4 fold higher in the control group (Table 6.21). Brimonidine was undetectable in the aqueous humour of both eyes on day 28 (Figure 6.17). Therefore, terminal half-life, $AUC_{0\text{-}\infty}$ and clearance could not be determined in this case. In comparison to other ocular tissues, C_{max} and tissue exposure were the lowest in the aqueous humour (Figure 6.11 and Table 6.21).

6.3.5.2 VITREOUS HUMOUR (VH)

The degradation of polymer and dissolution of solid drug within the vitreous chamber controlled the rate of brimonidine released into the vitreous humour. Figure 6.16 shows that C_{max} achieved on day 14 in both eyes (1110 ng/mL for control and 915 ng/mL for hyaluronidase-treated eyes) corresponded to the burst release phase of

the DDS release profile on the same day (refer Section 6.3.7). In addition, the $AUC_{0-\infty}$, drug clearance and terminal half-life were also found to be comparable between both study groups (Table 6.21).

Vitreal concentration was generally lower than ICB, choroid and retina during the study period (Figure 6.16). However, a low level of brimonidine remained detected within the vitreous cavity of both hyaluronidase-treated and control eyes on day 28 but no difference was detected between them (Figure 6.17).

6.3.5.3 IRIS-CILIARY BODY (ICB)

The shape of the aqueous humour and ICB concentration-time curves conform closely to that of the vitreous humour suggesting a correlation between these tissues that is possibly due to the location of the DDS, that resided close to the ICB and anterior chamber. However, drug concentration was considerably higher in ICB as compared to AH and VH. On day 1, brimonidine was detected in the ICB of both eyes but concentration was 1.9 fold higher in the control group. However, no difference in brimonidine concentration was detected between both study groups on day 7, day 14 and day 28 (Figure 6.16).

In addition, C_{max} of the control (26447 ng/g) group was not significantly higher than that in the hyaluronidase-treated (21423 ng/g) group (Figure 6.16). However, in comparison to other ocular tissues, C_{max} of ICB was the highest among others (Figure 6.18). T_{max} was on day 14, and it was the same for both eyes (Table 6.21). $AUC_{0-\infty}$ and clearance were also not significantly different between both study groups. Terminal half-life as calculated from the elimination phase between day 14 and day 28 was around 4-5 days for both study groups.

6.3.5.4 CHOROID (CHO)

Brimonidine was detected within all areas of the choroid tissue on day 1 (Figure 6.16). The total drug concentration was similar for both study groups on day 1 and

day 14 but it was 3 fold and 4 fold higher in the control eyes on day 7 and day 28 respectively. Figure 6.18 shows that C_{max} was comparable between both eyes at cho-superior and cho-temporal. However, it was higher in the hyaluronidase-treated group by 1.5 fold at cho-macula but lower by 1.7 fold and 2.7 fold as compared to control at cho-inferior and cho-nasal respectively. When all regions of the tissues were summed as a single section, $AUC_{0-\infty}$, was calculated to be 1.7 fold higher in the control eyes alongside with 1.7 fold slower drug clearance as compared to the hyaluronidase-treated eyes.

Figure 6.19 illustrates that brimonidine concentration varies among superior, inferior, macula, temporal and nasal quadrants of the choroid tissues except on day 7 in hyaluronidase-treated eyes. Brimonidine remained detected on day 28 with a relatively higher average concentration present at cho-inferior and cho-temporal of both groups. In comparison to other ocular tissues, drug exposure of the choroid tissue was the second highest after ICB as shown in Table 6.21.

6.3.5.5 RETINA (RET)

Figure 6.16 shows that brimonidine was detected in the retina on day 1 following implantation. The total drug concentration calculated from all areas within the retina was approximately 2 fold higher in the control eyes as compared to the hyaluronidase-treated eyes on day 7 and day 28. However, no difference was observed on day 1 and day 14, which were days where the percentage of brimonidine released was higher.

T_{max} was achieved generally on day 14 except at ret-superior (hyaluronidase-treated), ret-inferior (control) and ret nasal (hyaluronidase-treated) at which T_{max} was on day 7 (Table 6.23). C_{max} was found to be 2.0 fold higher in the control group at ret-inferior and ret-superior but it was 1.4 fold lower than hyaluronidase-treated group at ret-macula (Table 6.23). No significant difference in C_{max} was detected between both groups at the rest of the retina areas (Table 6.23). Generally, terminal half-life was 2-4 days for the retina. When the concentrations of all regions within the retina tissues

were summed as one single section, the total $AUC_{0-\infty}$ and rate of clearance were not significantly different between both groups. However, when individual region was considered separately, $AUC_{0-\infty}$ was 1.3 and 1.7 fold higher in control eyes at ret-superior and ret-inferior but was comparable at ret-macula, ret-nasal and ret-temporal. Clearance was comparable between both groups at all areas except ret-inferior, where it was 1.8 fold higher in hyaluronidase-treated than control eyes.

Figure 6.20 illustrates that the absorption and distribution of brimonidine was not uniform throughout the retina except in hyaluronidase-treated eyes on day 14 and day 28. In comparison to choroid, tissue exposure of both study groups was lower in the retina as shown in Table 6.21.

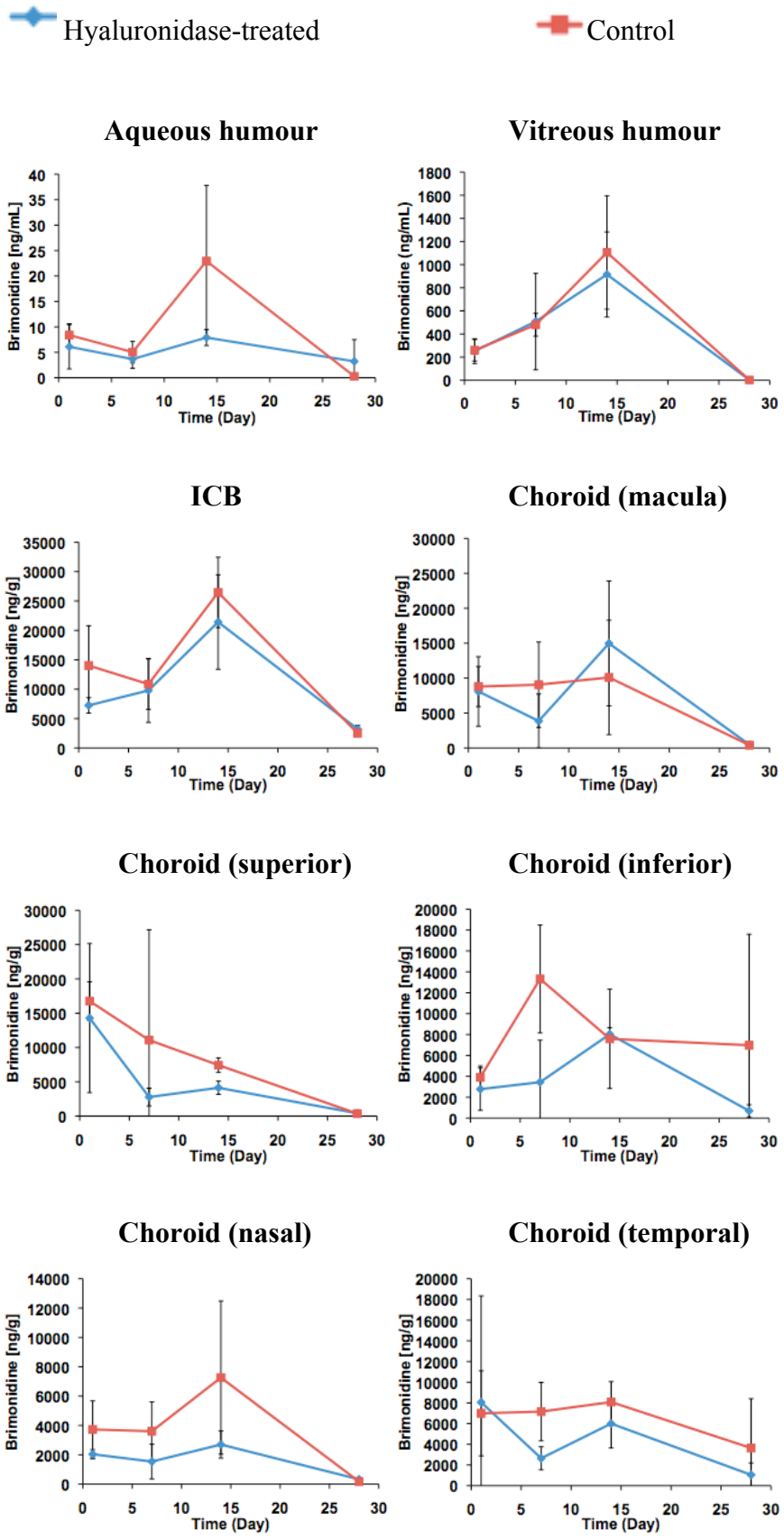
Hyaluronidase-treated
Control
Aqueous humour
Vitreous humour
ICB
Choroid (macula)
Choroid (superior)
Choroid (inferior)
Choroid (nasal)
Choroid (temporal)
Brimonidine [ng/mL]
Brimonidine [ng/g]
Time (Day)

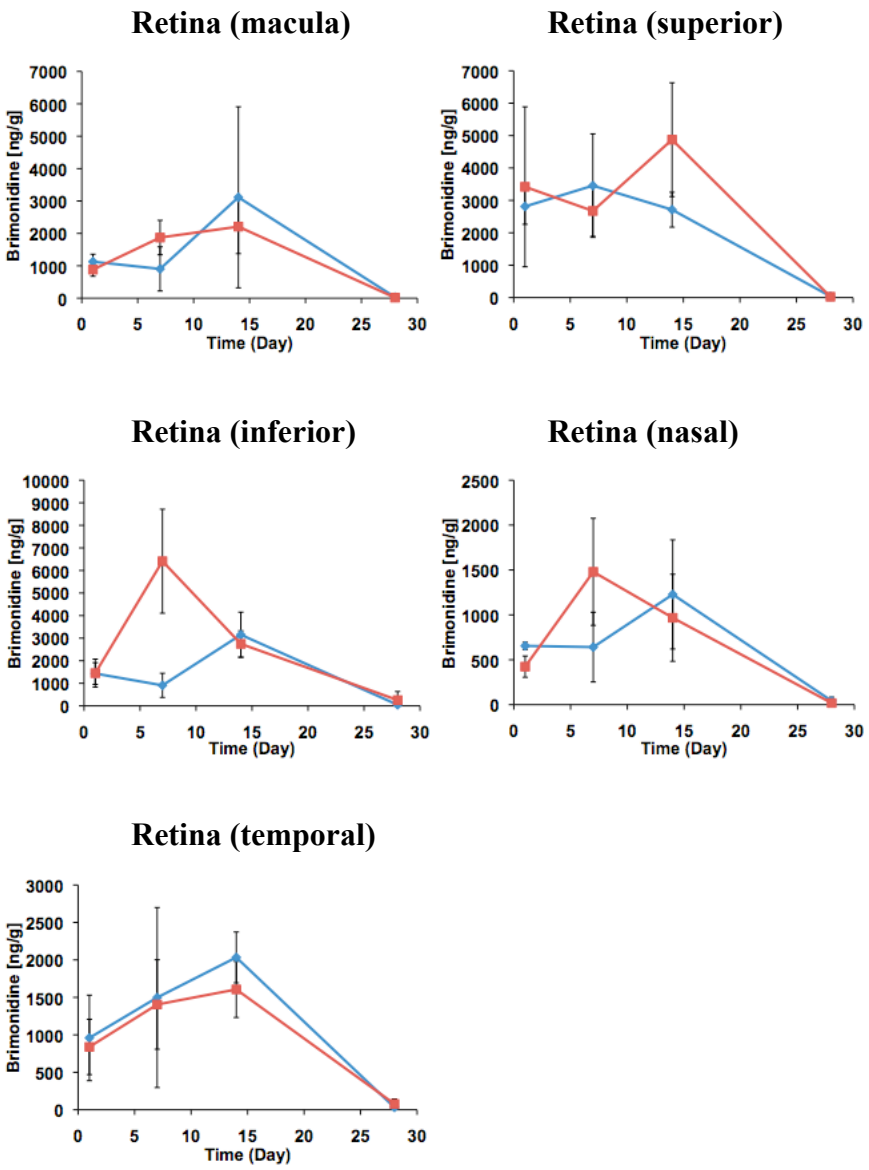

Figure 6.16 Tissue concentration of brimonidine in hyaluronidase-treated and control eyes following a single intravitreal implantation of 210 µg brimonidine tartrate in Dutch-belted rabbits (n=3 rabbits/time point). Data was associated with large error bars, which reflects the variability seen in the study populations. Y-axis error bar indicates the minimum and maximum values.

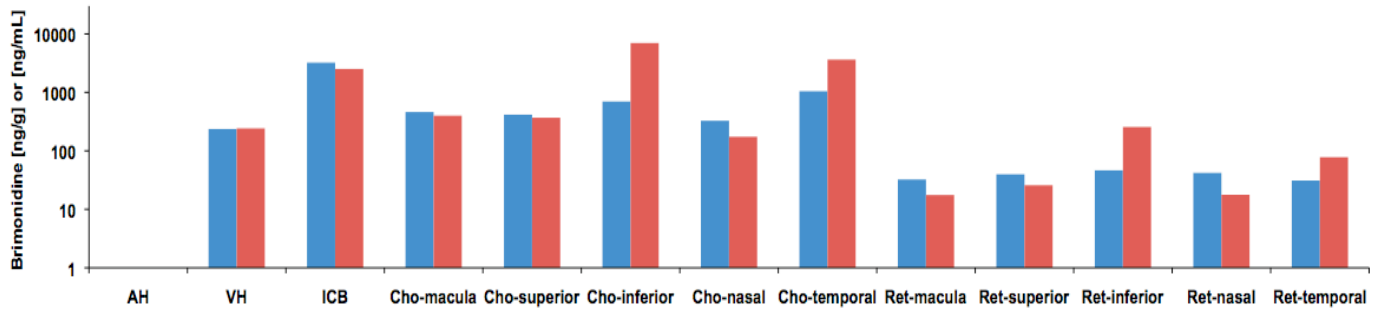

Figure 6.17 Mean brimonidine concentration (ng/g or ng/mL) in the aqueous humour, vitreous humour, ICB, choroid and retina of control and hyaluronidase-treated eyes on day 28 following implantation.
Blue: Hyaluronidase-treated; Red: Control; n=3.

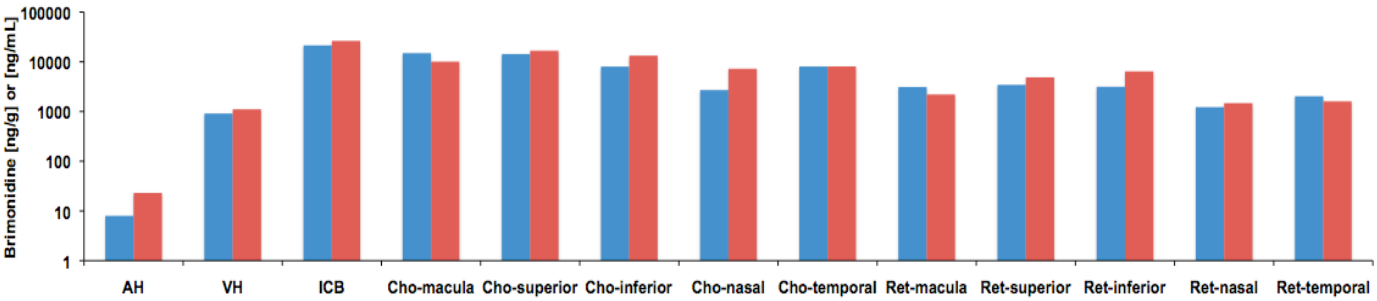

Figure 6.18 Maximum concentration (C_{max}) of brimonidine (ng/g or ng/mL) in aqueous humour, vitreous humour, ICB, choroid and retina of control and hyaluronidase-treated eyes following implantation. Blue: Hyaluronidase-treated; Red: Control; n=3.

Parameters	AH		VH		ICB		Choroid		Retina	
	HT	Ctrl	HT	Ctrl	HT	Ctrl	HT	Ctrl	HT	Ctrl
C_{max} (µg/mL or µg/g)	0.01 ±0.00	0.02 ±0.02	0.9 ±0.4	1.1 ±0.5	21.4 ±8.0	26.5 ±6.0				
T_{max} (day)	14	14	14	14	14	14				
$AUC_{0\text{-}8hrs}$ (µg.h/mL or µg.h/g)	0.13 ±0.07	0.30 ±0.18	13.8 ±7.0	15.7 ±6.1	336.4 ±128.7	415.0 ±115.9	122.6 ±75.5	186.8 ±75.9	40.5 ±19.0	49.8 ±34.6
$AUC_{0\text{-}\infty}$ (µg.day/mL or µg.day/g)			13.8 ±7.0	15.7 ±6.1	360.2 ±133.4	429.9 ±117.1	125.9 ±77.1	212.6 ±109.2	40.6 ±19.0	49.8 ±34.6
$t_{1/2}$ (day)			1.63	1.59	5.12	4.12	3.88	7.74	2.33	2.81
Mean Clearance (mL/day or g/day)			15.20	13.41	0.58	0.49	1.67	0.99	5.17	4.21

Table 6.21 Pharmacokinetic parameters for aqueous humour, vitreous humour, ICB, choroid (total) and retina (total) following single 210 µg intravitreal implantation. HT: hyaluronidase-treated; Ctrl: control

Parameters	Cho-macula		Cho-superior		Cho-inferior		Cho-nasal		Cho-temporal	
	HT	Ctrl	HT	Ctrl	HT	Ctrl	HT	Ctrl	HT	Ctrl
C_{max} (µg/mL or µg/g)	15.0 ±8.9	10.1 ±8.2	14.3 ±10.9	16.8 ±2.8	8.0 ±0.6	13.3 ±5.2	2.7 ±0.9	7.3 ±5.2	8.1 ±10.3	8.1 ±2.0
T_{max} (day)	14	14	1	1	14	7	14	14	1	14
$AUC_{0\text{-}8hrs}$ (µg.day/mL or µg.day/g)	213.8 ±138.7	198.5 ±137.9	114.3 ±59.0	211.3 ±128.6	121.2 ±44.0	228.8 ±161.6	47.8 ±19.2	113.9 ±75.0	115.7 ±76.0	181.4 ±86.8
$AUC_{0\text{-}\infty}$ (µg.day/mL or µg.day/g)	215.7 ±140.2	200.3 ±139.3	116.9 ±61.1	213.9 ±131.8	125.2 ±47.3		50.0 ±19.9	114.6 ±75.2	124.1 ±85.1	245.2 ±170.4
$t_{1/2}$ (day)	2.79	3.00	4.22	4.90	3.97		4.60	2.60	5.55	12.15
Mean Clearance (g/day)	0.98	1.05	1.80	0.98	1.68		4.21	1.83	1.69	0.86

Table 6.22 Pharmacokinetic parameters for choroid tissue following single 210µg intravitreal implantation. HT: hyaluronidase-treated; Ctrl: control

Parameters	Ret-macula		Ret-superior		Ret-inferior		Ret-nasal		Ret-temporal	
	HT	Ctrl	HT	Ctrl	HT	Ctrl	HT	Ctrl	HT	Ctrl
C_{max} (μg/mL or μg/g)	3.1 ±2.8	2.2 ±0.8	3.5 ±1.6	4.9 ±1.8	3.2 ±1.0	6.4 ±2.3	1.2 ±0.6	1.5 ±0.6	2.0 ±0.3	1.6 ±0.4
T_{max} (day)	14	14	7	14	14	7	14	7	14	14
$AUC_{0\text{-}8hrs}$ (μg.day/mL or μg.day/g)	42.8 ±34.8	38.6 ±13.0	61.1 ±18.1	80.7 ±32.2	44.3 ±16.0	77.4 ±25.9	19.7 ±9.3	21.4 ±9.5	34.7 ±13.5	29.5 ±9.6
$AUC_{0\text{-}\infty}$ (μg.day/mL or μg.day/g)	42.9 ±35.0	38.6 ±13.0	61.2 ±18.2	80.8 ±32.3	44.5 ±16.2	79.1 ±28.4	19.8 ±9.5	21.5 ±9.5	34.8 ±13.5	29.8 ±9.9
$t_{1/2}$ (day)	2.13	2.01	2.30	1.85	2.30	4.52	2.87	3.29	2.32	3.21
Mean Clearance (g/day)	4.90	5.44	3.43	2.60	4.72	2.66	10.60	9.78	6.04	7.04

Table 6.23 Pharmacokinetic parameters for retina tissue following single 210 μg intravitreal implantation. HT: hyaluronidase-treated; Ctrl: control

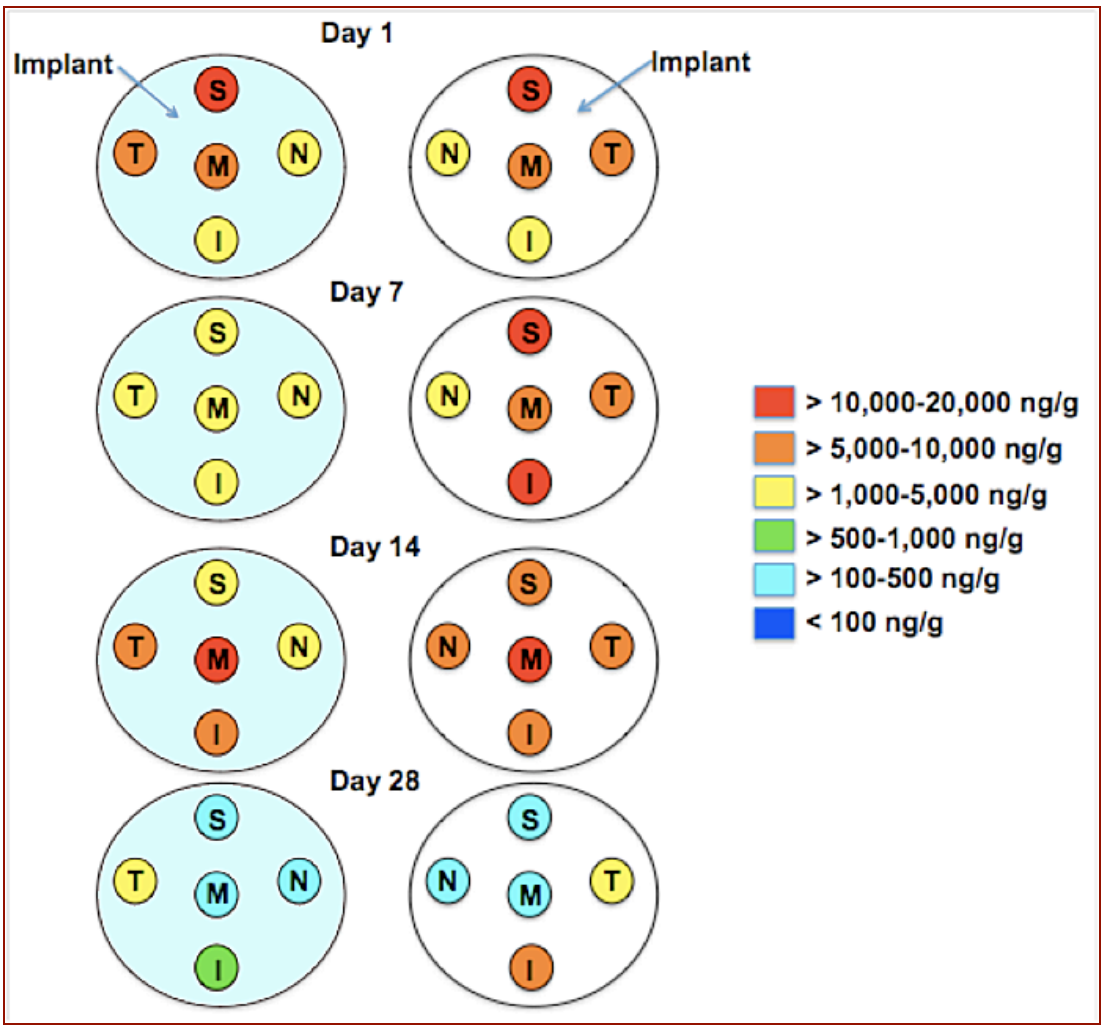

Figure 6.19 Comparison of brimonidine levels at superior, inferior, macula, nasal and temporal areas of the choroid tissue following single 210μg intravitreal implantation. Left-panel: Hyaluronidase-treated eyes; Right panel: Control eyes.

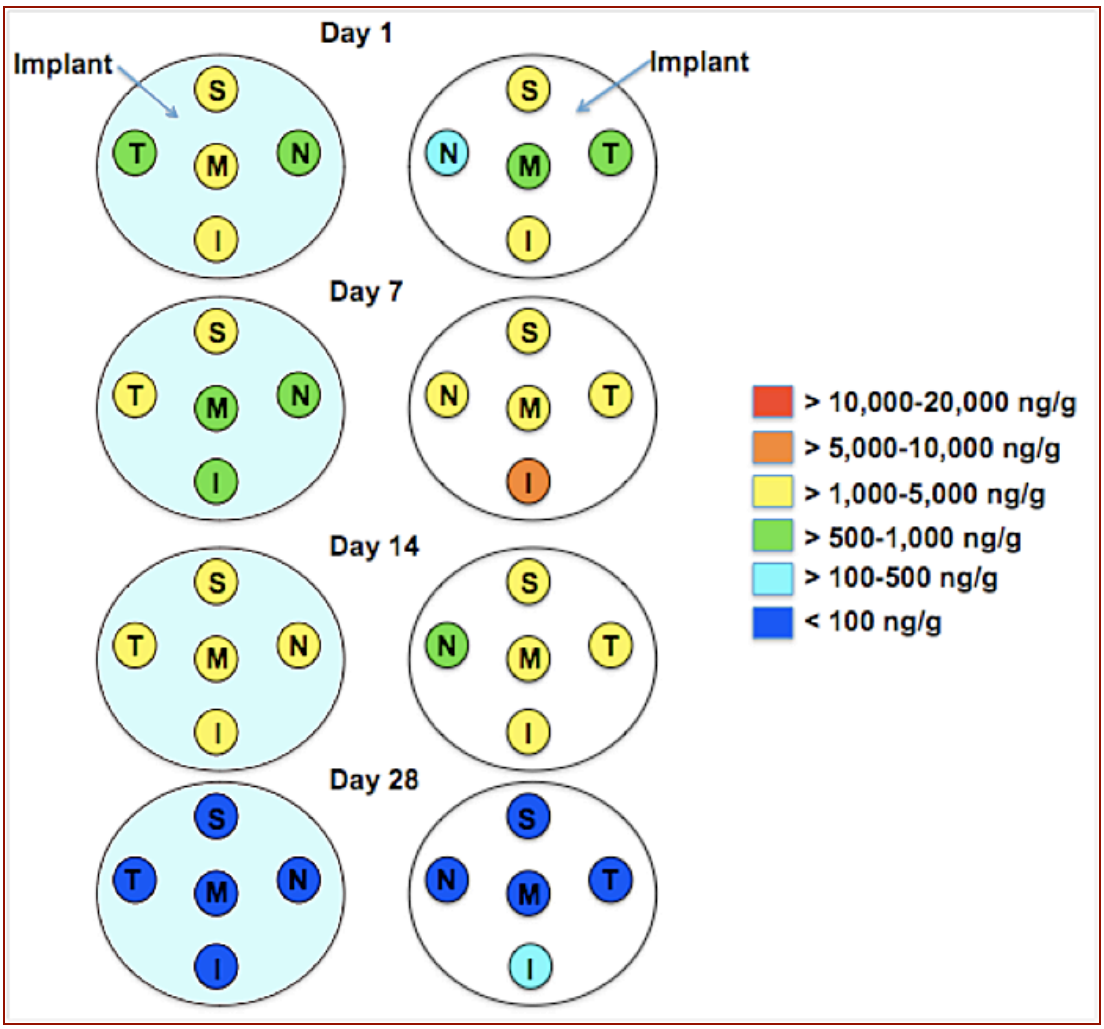

Figure 6.20 Comparison of brimonidine levels at superior, inferior, macula, nasal and temporal areas of the retina tissue following single 210μg intravitreal implantation. Left-panel: Hyaluronidase-treated eyes; Right panel: Control eyes.

6.3.6 COMPARISON BETWEEN INTRAVITREAL INJECTION AND INTRAVITREAL IMPLANTATION

Figure 6.21 shows that apart from ICB, C_{max} was lower in the aqueous humour, vitreous humour, choroid and retina with intravitreal implantation as compared to intravitreal injection. In addition, T_{max} of the ocular tissues following intravitreal implantation was at least 24 hours instead of a few hours for intravitreal injection. Due to the controlled release behaviour of the DDS, it should be appreciated that brimonidine concentration in the vitreous humour following intravitreal implantation was always lower than injection (Table 6.18, Table 6.21). Overall, tissue exposure to brimonidine following intravitreal injection could be ranked in the order of choroid > retina > ICB > vitreous humour > aqueous humour; while the ranking with implant was ICB > choroid > retina > vitreous humour > aqueous humour. Longer terminal half-life with slower clearance was also observed with implant as compared to injection (Table 6.18, Table 6.21).

Nevertheless, the effect of partial vitreous liquefaction on tissue exposure to brimonidine at retina, ICB and vitreous humour was more significant with injection than implantation. This suggests that the sustained-release behaviour of DDS could compensate for the higher rate of drug clearance from these tissues in the more liquefied vitreous.

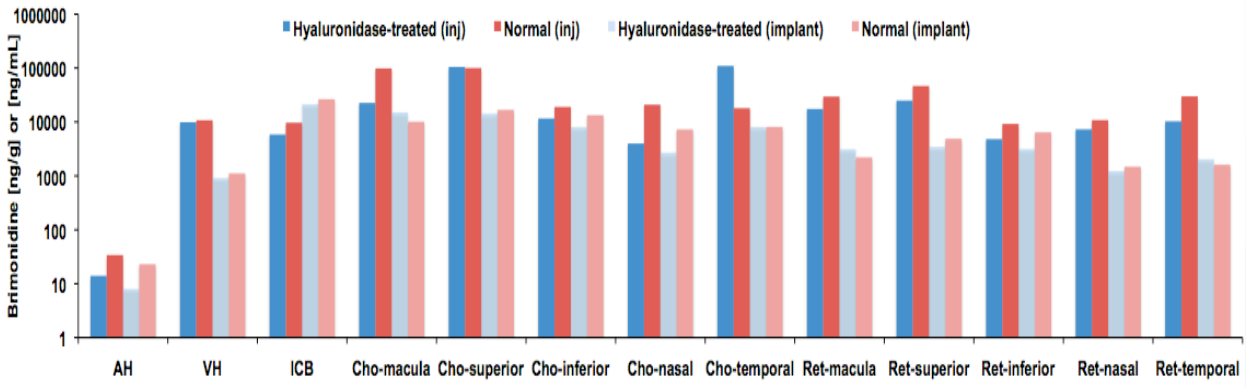

Figure 6.21 Maximum concentration (C_{max}) of brimonidine (ng/g or ng/mL) at the aqueous humour, vitreous humour, ICB, choroid and retina following intravitreal injection and implantation.

6.3.7 PERCENTAGE OF BRIMONIDINE RELEASED FROM DDS (PISTON-EXTRUDED)

The content of brimonidine in the DDS remnants collected at necropsy was determined using LCMS/MS. Figure 6.22 shows that the average *in vitro* release of brimonidine from the DDS was 14.86%, 28.83%, 54.14% and 98.62% on day 1, 7, 14 and 28 respectively. While the average *in vivo* release of brimonidine from DDS implanted into the hyaluronidase-treated eyes was 39.49%, 48.38%, 82.81% and 99.99% on day 1, 7, 14, and 28 post-implantation respectively; whereas it was 39.34%, 48.74%, 83.50%, 99.98% on day 1, 7, 14 and 28 post-implantation respectively in the control eyes. Higher initial burst and faster rate of drug release were observed when the DDS was implanted *in vivo*. However, there was no difference identified between the release profiles of hyaluronidase-treated and control eyes as shown in Figure 6.22.

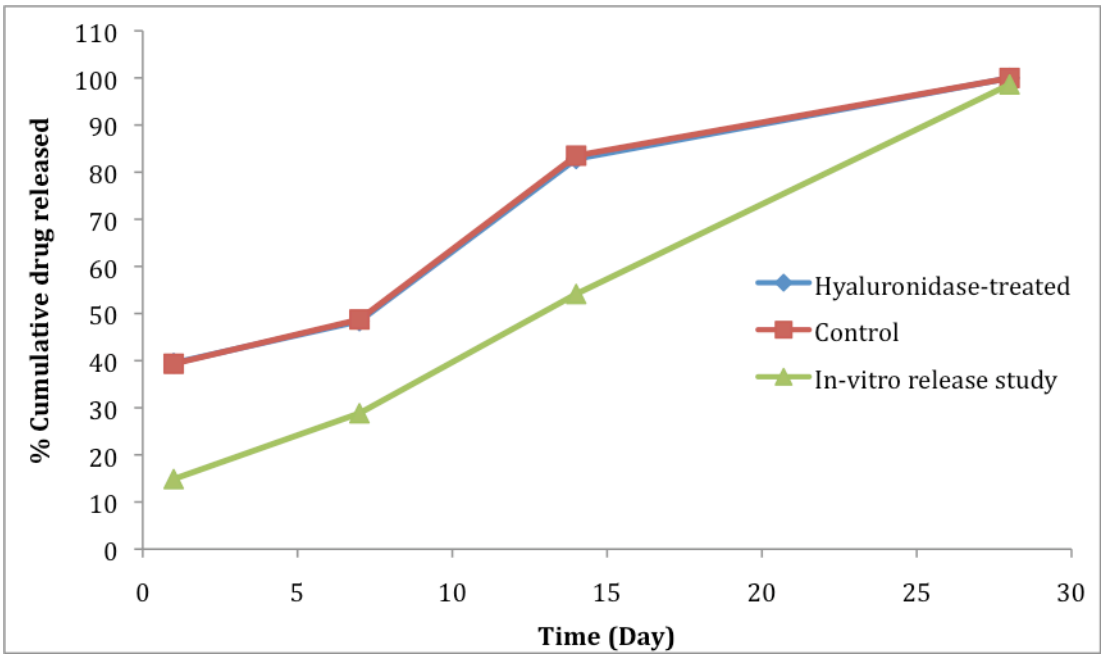

Figure 6.22 *In vitro and in vivo* (hyaluronidase-treated and control) cumulative drug release profiles of brimonidine on day 1, 7, 14 and 28 (n=2).

6.3.8 ASSESSMENT OF DDS DEGRADATION USING GPC AND SEM IMAGING

The DDSs implanted in hyaluronidase-treated and control eyes were collected at necropsy and imaged using SEM to compare the surface and cross-sectional morphologies. Due to the limited availability of the experimental sample, only one DDS at each time point representing each study group was imaged and analysed for molecular weight. Figure 6.23 below represents the original DDS before implantation, while Figures 6.24, 6.25, 6.26 and 6.27 are images of DDSs explanted from hyaluronidase-treated and control eyes on day 1, 7, 14 and 28 post-implantation respectively. The original DDS has a rough surface with a relatively smooth cross-sectional view. On day 1 post-implantation, the DDS surface became flakier as it was exposed to the vitreous humour environment but no significant pores developed within the DDS just yet for both study groups. The formation of pores became evident on day 7 and day 14 according to the cross-sectional images, which could be a result of drug released and polymer degradation and dissolution. The diameter of the DDS was also found to grow larger on day 7 and day 14 due to water uptake. A fibrous-like material covering the surface of DDS explanted from hyaluronidase-treated eye on day 7 was noted, and the material may be residuals originated from the vitreous components. Due to the extensive polymer degradation process that occurred over time, DDS was eventually fragmented into tiny remnants of polymers on day 28. There were no differences observed in the rate and the way the DDS was decayed between the hyaluronidase-treated and control eyes.

Molecular weight of each polymeric DDS was determined using GPC to compare the rate of degradation of DDS explanted from hyaluronidase-treated and control eyes. Figure 6.28 represents the GPC plots of DDS explanted on day 1, 7, 14 and 28. Polymers of the original DDS were eluted at 23.6 minutes and the molecular weight was calculated as 14028 Da based on the polystyrene standard curve. On day 1, the polymers of DDSs from both eyes were eluted at 23.8 minutes and the calculated molecular weight of 13010 Da was therefore the same for both study groups. However, the measurement was not significantly different from that of the original

DDS, suggesting no significant polymer degradation on day 1. On day 7, the retention time of the polymers shifted to later and instead of a clear peak, a shoulder that leaned onto the next peak at 28.8 minutes was observed. This indicated polymer degradation. A significant degree of polymer degradation was observed on day 14 and day 28 where the retention time of the polymer shifted and subsequently fused together with the peaks at 28.8 minutes. No clear peak of polymers could be identified on day 7, 14 and 28, rendering the calculation of the molecular weight unsuccessful for these samples. Nevertheless, our data showed that the polymer retention time was similar for control and hyaluronidase-treated eyes on day 1, 7, 14 and 28, suggesting similar rate and degree of degradation throughout the study period. Moreover, the unknown peak at 28.8 minutes that appeared at each time point for all DDSs did not change over-time and therefore would not be peaks from polymers or brimonidine. In this case, they may be regarded as unknown contaminants from extrusion process or animal tissues.

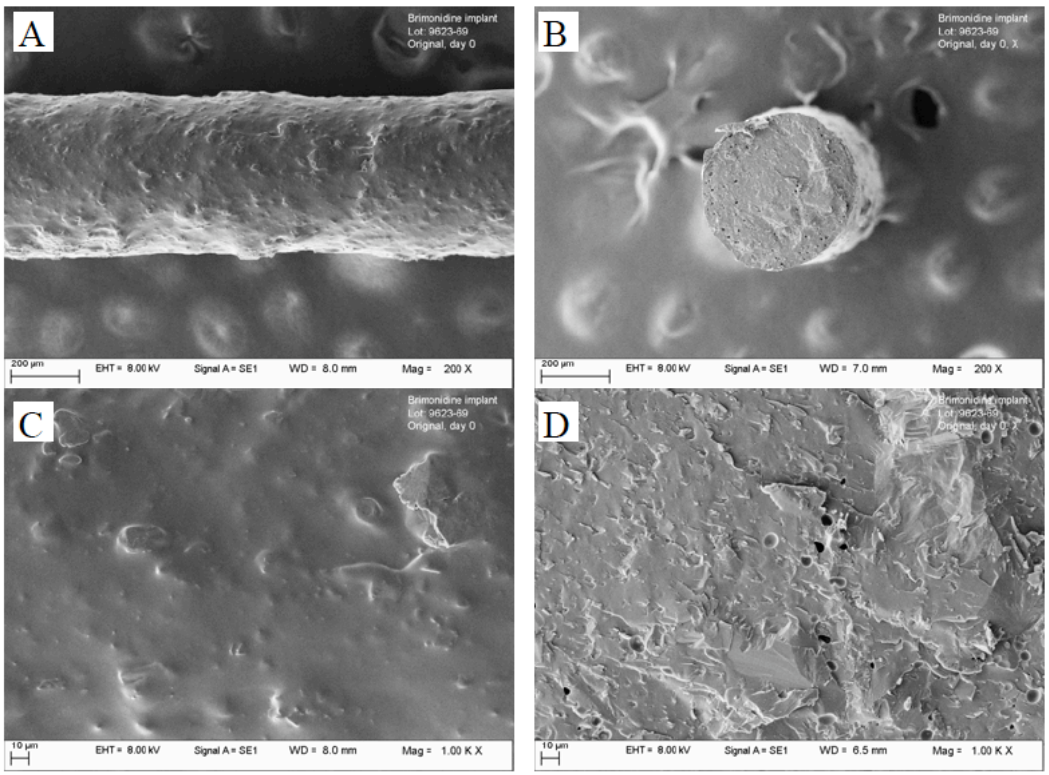

Figure 6.23 SEM images of the original brimonidine tartrate DDS before *in vivo* or *in vitro* study. Side views (A, C) and cross-sections (B,D).(Courtesy of Dr. Ruiwen Shi, Allergan Inc.)

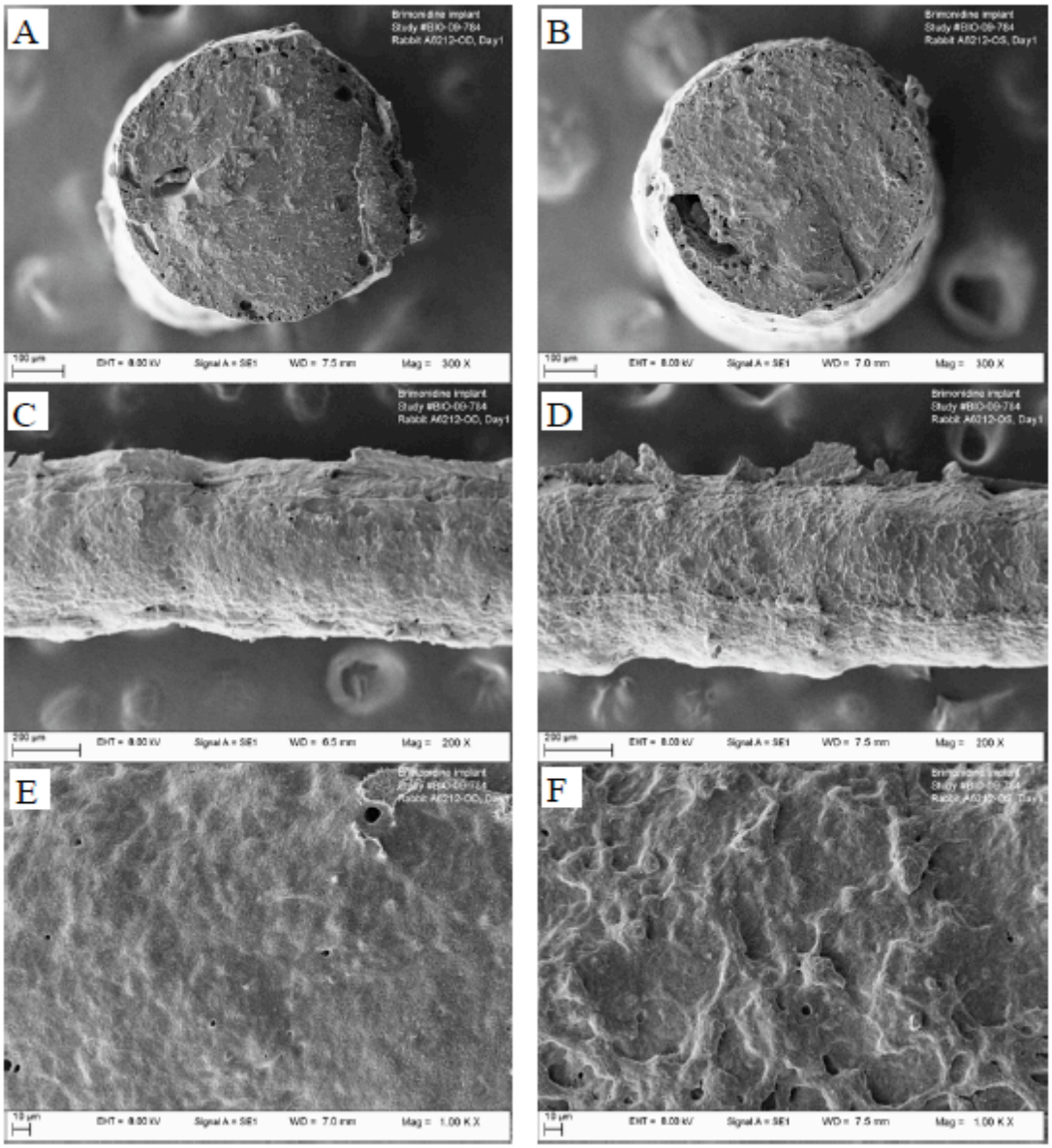

Figure 6.24 SEM images of the brimonidine tartrate DDSs explanted from hyaluronidase-treated (left panels) and control (right panels) eyes on day 1 after implantation. A, B are the cross-sectional images, while C, D, E and F are the side-view of the DDSs. **(**Courtesy of Dr. Ruiwen Shi, Allergan Inc.)

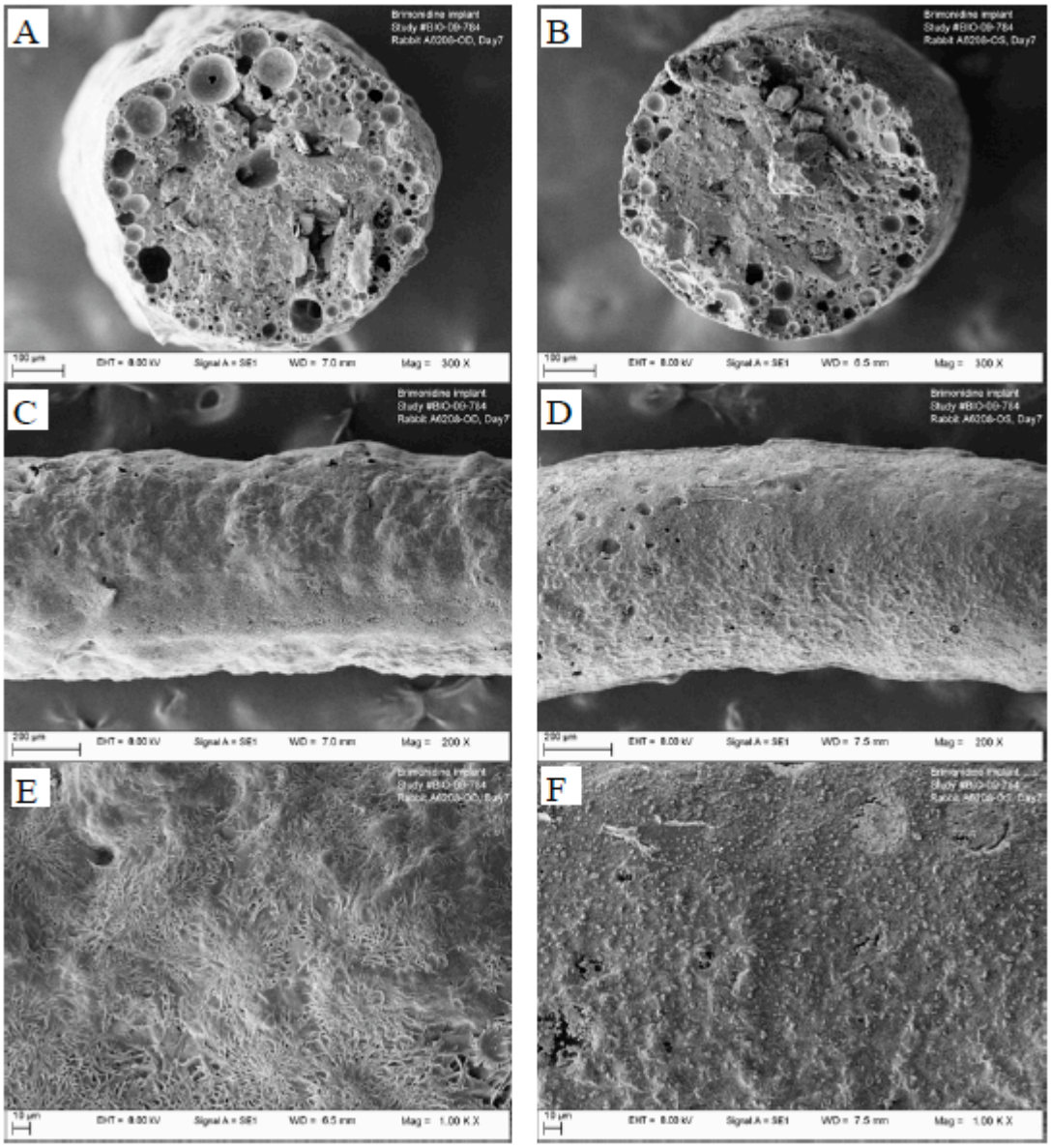

Figure 6.25 SEM images of the brimonidine tartrate DDSs explanted from hyaluronidase-treated (left panels) and control (right panels) eyes 7 days after implantation. A, B are the cross-sectional images, while C, D, E and F are the side-view of the DDSs. (Courtesy of Dr. Ruiwen Shi, Allergan Inc.)

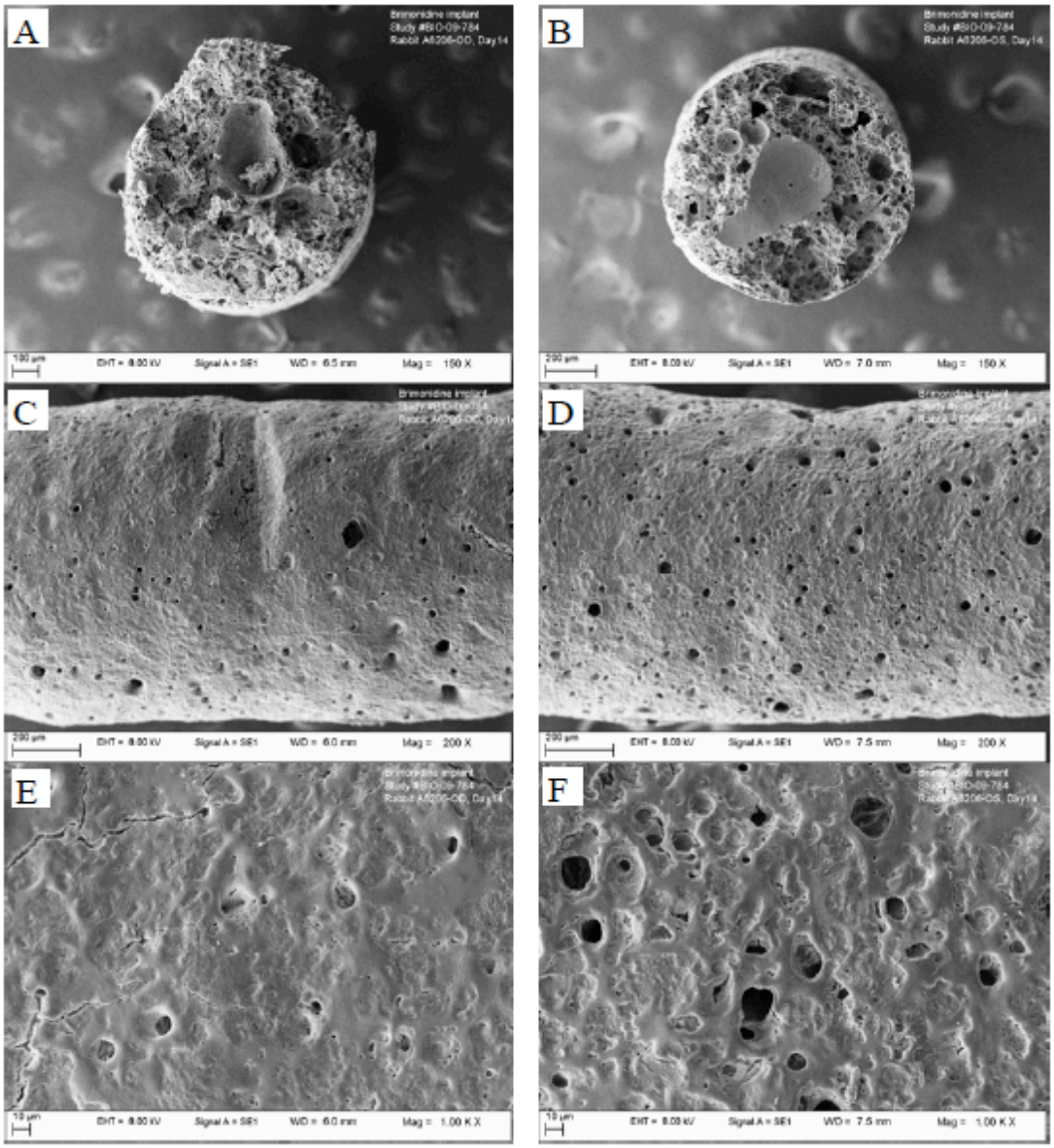

Figure 6.26 SEM images of the brimonidine tartrate DDSs explanted from hyaluronidase-treated (left panels) and control (right panels) eyes 14 days after implantation. A, B are the cross-sectional images, while C, D, E and F are the side-view of the DDSs. **(**Courtesy of Dr. Ruiwen Shi, Allergan Inc.)

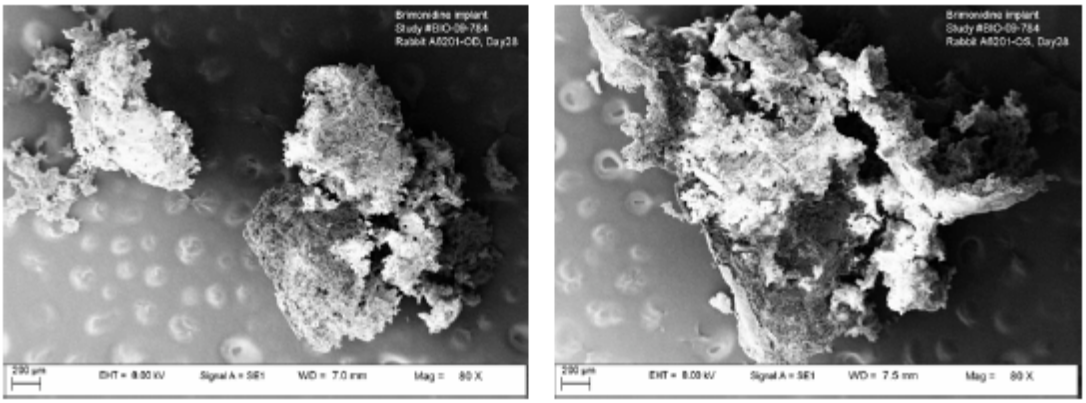

Figure 6.27 SEM images of the brimonidine tartrate DDSs explanted from hyaluronidase-treated (left panels) and control (right panels) eyes 28 days after implantation. DDSs were completely degraded into polymer remnants. (Courtesy of Dr. Ruiwen Shi, Allergan Inc.)

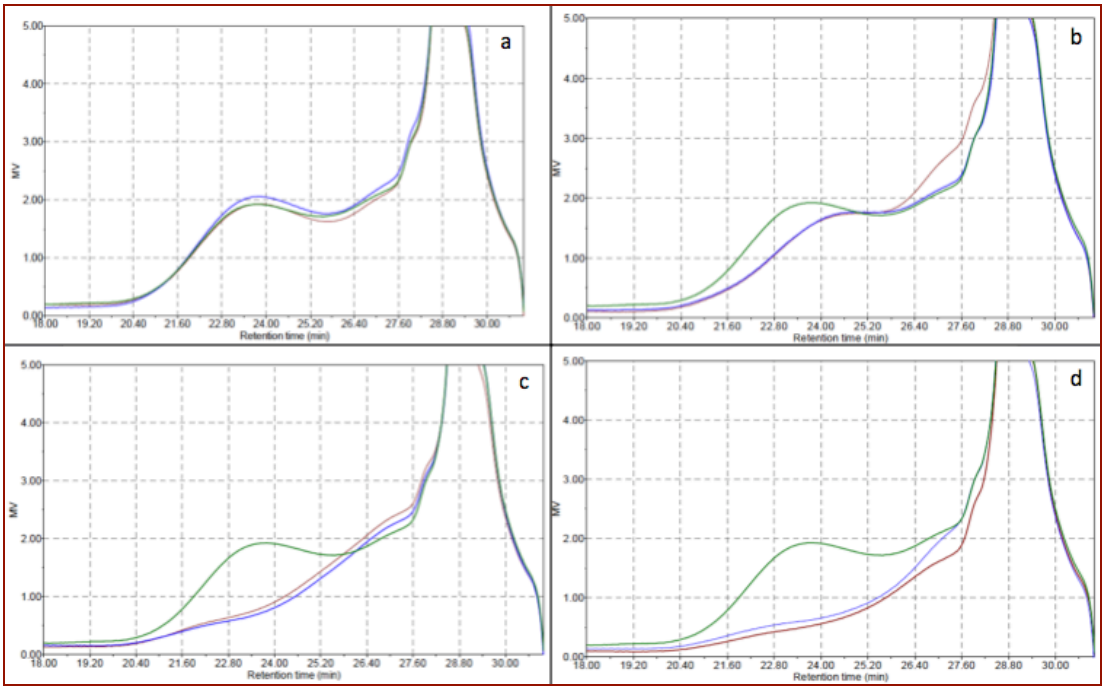

Figure 6.28 GPC chromatograms of the original brimonidine tartrate DDS (green) and the DDSs explanted on day 1(a), day 7(b), day 14 (c) and day 28 (d). Hyaluronidase-treated (blue); Control (brown). The scale of the graph has been set to display the polymer peaks at 23.6 minutes. (Courtesy of Dr. Ruiwen Shi, Allergan Inc.)

6.4 DISCUSSION

Since brimonidine is currently in clinical trials for the treatment of geographic atrophy associated with age-related macular degeneration and neuroprotective capabilities in glaucomatous patients, concentrations achieved at the choroid and retina will be relevant to the treatment of these ocular conditions.

6.4.1 INTRAVITREAL INJECTION

A faster rate of initial drug distribution was demonstrated in the hyaluronidase-treated eyes where the vitreal concentration was substantially lower at 2 hour, suggesting early clearance from the partially liquefied vitreous. This observation was further supported by the measured higher drug clearance from the vitreous of the hyaluronidase-treated eyes, based on the calculated cumulative tissue exposure and terminal elimination phase. Therefore, the capability of a partially liquefied vitreous to retain injected material was significantly reduced. This observation agreed with those reported in Chapter 4 for sodium fluorescein; however, the results obtained at 4 hours, were not in agreement with our previous study. The vitreal concentration of sodium fluorescein was 1.5 fold higher in the control than hyaluronidase-treated eyes at 5 hour, whereas brimonidine concentration in this study was similar in both study groups at 4 and 5 hours. This indicated that drug molecules with different physicochemical properties showed different distribution profiles and would be affected to a different degree by vitreous liquefaction. In the intact eye the half life of brimonidine in the vitreous was measured to be 1.4 hour compared to values reported in the literature in the rabbit of 3.5 hour for fluorescein (Kitano *et al.,* 1988). In contrast the observed permeability rate is lower for brimonidine, which is 1×10^{-6} (Zhang *et al.,* 2006) versus 4.7×10^{-6} for fluorescein (Moldow *et al*., 2001). The explanation for these observations is probably that sodium fluorescein does not associate with melanin, whereas brimonidine binds strongly to melanin. The impact of melanin binding on the kinetics of brimonidine has been reported (Acheampong *et al.,* 2002) and similar observations have also been documented for memantine (Koeberle *et al.,* 2006). Further support for this argument is evidenced by the

measured drug concentration at the ICB and superior region of the choroid, which were considerably higher in the control than hyaluronidase-treated group at 4 hour. Brimonidine binding to melanin may reduce the influence of partial vitreous liquefaction observed at 4 hours on the vitreous kinetics. The similar drug level detected in both study groups at 8 hour, indicates the completion of an initial diffusive phase. Despite this, brimonidine was cleared from the vitreous of both study groups relatively fast with a terminal half-life of around 1.4 hour. The result agreed with that reported in an internal study by Allergan (Allergan's report: PK-02-P033). The short terminal half-life of brimonidine would therefore justify the development of an intravitreal controlled-release brimonidine implant for long-term neuroprotection.

The concentration achieved at the choroid and retina tissues would be appropriate to the putative neuroprotective role of brimonidine. It was found that drug penetration into the choroid and retina occurred as early as 1 hour following direct injection. However, the mean clearance was higher but total cumulative drug exposure was lower at the choroid and retina of eyes with partial vitreous liquefaction. Moreover, C_{max} values at the macula region of the choroid and retina tissues were also lower in hyaluronidase-treated eyes. It is quite likely that early clearance events, happening before the first hour sample, were missed in our protocol. Nevertheless, Friedrich has suggested that cumulative drug exposure is a measure for therapeutic efficacy; and therefore the lower concentration achieved at the posterior segment of the eye alongside with a faster rate of drug clearance would increase the risk of subtherapeutic drug levels in individuals with partially liquefied vitreous, thereby leading to lower drug efficacy (Friedrich *et al.,* 1997b).

6.4.2 INTRAVITREAL IMPLANTATION

In contrast to intravitreal injection, tissue exposure to brimonidine at the retina was not significantly affected by vitreous liquefaction following implantation apart from the inferior region of the retina. Similarly, ICB and vitreous humour were also not significantly affected. Drug exposure to the choroid of the control eyes remained

higher and the calculated drug clearance was found to be slower as compared to hyaluronidase-treated group. Additionally, C_{max} and $AUC_{0-\infty}$ values of the aqueous humour were also found to be higher in the control than in hyaluronidase-treated eyes. Although tissue exposure to brimonidine at the retina, vitreous humour and ICB was not affected significantly, the reduced drug exposure at the two main elimination sites (choroid and aqueous humour) of the hyaluronidase-treated eyes still suggests a faster rate of drug clearance from eyes with a partial liquefied vitreous. The effected faster rate of drug clearance in the hyaluronidase-treated eyes, on overall therapeutic efficacy was not investigated in this study and will need to be examined further. On the other hand, a slightly higher C_{max} was observed at the macula zone of the choroid and retina in the hyaluronidase-treated eyes as compared to control. The explanation for this observation remains unclear and the question regarding whether or not this would increase the risk of ocular toxicity will need to be further investigated.

However, it was found that the more liquefied vitreous environment and the use of hyaluronidase did not affect the rate of drug release from the DDS, a finding supported by the data obtained from GPC and SEM analysis. Furthermore, images taken at necropsy showed varying degrees of DDS degradation between animals in the same treatment group, suggesting that the effect of partial vitreous liquefaction was not important. However, a variation in the DDS location between animals may have partly contributed to the spatial variation in choroidal and retinal concentrations as well as the large standard deviation observed in this study. Additionally, head movement may cause significant movement of the DDS within the eye, although settling onto the floor of the eye was not observed at necropsy.

The DDS had a 25% faster rate of drug release on day 1 when tested *in vivo* as compared to *in vitro*. This observation could be caused by ocular proteins or hyalocytes or perhaps due to the local accumulation of acidic degradation products from autocatalytic process (Oh *et al.,* 2006), which accelerated polymer degradation. In addition, Okabe has shown that *in vivo* drug release from implants was faster than *in vitro* following episcleral implantation (Okabe *et al.,* 2003), further suggesting a

lack of *in vitro* and *in vivo* correlation, which may be due to the fact that the sinking condition *in vivo* is not the same as that *in vitro.*

In addition, this study shows that drug disposition profiles following intravitreal implantation were different from that following intravitreal injection. The lower C_{max} achieved using controlled-release implant reduced the possibility of retinal toxicity and at the same time allowed for sustained drug delivery over a longer period of time. Similar advantages of intravitreal implant have also been demonstrated using mathematical modeling (Park *et al.,* 2005; Kathawate and Acharya, 2008). Additionally, tissue exposure to brimonidine following intravitreal injection differed from that following intravitreal implantation. This suggests that different delivery formulations results in a different degree of tissue exposure at the posterior segment of the eye.

Moreover, intravitreal implant reduced the effects of partial vitreous liquefaction on tissue exposure to brimonidine at the retina, vitreous humour and ICB. However, due to the position of the DDS in the vitreous cavity, which resides in close proximity to ICB and aqueous chamber, led to a higher drug exposure achieved in both tissues as compared to that following intravitreal injection.

6.4.3 SPATIAL VARIATION IN CHOROIDAL AND RETINAL DRUG CONCENTRATIONS

Spatial variation in the concentration of brimonidine within the choroid and retina may be related to the regional variation in the vitreous rheology (Chapter 2) that initially led to a non-uniform distribution within the vitreous chamber, and subsequently a varying degree of drug absorption within the choroid and retina. Since regional variation in the vitreous rheology became less apparent in a more liquefied vitreous, this explains the lower degree of spatial variation in choroidal and retinal drug concentration in the hyaluronidase-treated eyes as compared to control. In general, the significance of the finding could be revealed through the work by

Friedrich *et al.* (1997b), who proposed that a non-toxic dose injected at one position of the vitreous humour may be toxic if it was injected at different location.

In addition, Friedrich and coworkers have also modeled a variation in peak concentrations as a function to injection location based on a 15 μL injection volume (Friedrich *et al.,* 1997b). Peak concentration was higher in tissues situated next to the injection site. Similar observations were also obtained in our study where C_{max} achieved at the superior, macula and temporal regions of the retina were higher than that at the inferior and nasal quadrants of the eye following intravitreal injection. For intravitreal implantation, highest C_{max} was found at the ICB since DDS was placed in close proximity to this tissue. Additionally, the ICB also has similar concentration-time profile as the vitreous humour, suggesting that drug level achieved in this tissue was closely related to the vitreal drug concentration.

Moreover, it was found that the spatial variation in disposition was more apparent following intravitreal injection compared to implantation. This could be attributed to the failure to come to an equilibrium whereas the implant constantly replenished brimonidine into the tissues of posterior segment and therefore reduced the variation seen in the concentration between tissue samples.

6.4.4 MELANIN BINDING

As mentioned earlier, melanin binding may affect the ocular disposition of brimonidine, leading to a sustained accumulation of brimonidine in the ICB and choroid over time. Tissue exposure to brimonidine was higher in pigmented tissues (choroid and ICB) as compared to non-pigmented tissues such as the retina and aqueous humour. Similar observations had been previously reported in Dutch-belted rabbits (Acheampong *et al.,* 1995) and New Zealand pigmented rabbits (Acheampong *et al.,* 2002). Acheampong and coworkers suggested that the levels in the aqueous humour might be a measure of the unbound drug levels in the ICB. The drug level in the aqueous humour of both eyes declined gradually following intravitreal injection; however a plateau in drug concentration in the ICB suggested

that brimonidine had not been cleared from ICB over the period of the experiment. Drug release from ICB is a slow process (Araie *et al.,* 1982) and this phenomenon was the same for both treated and control eyes.

6.4.5 BRIMONIDINE OCULAR CLEARANCE

Generally, the elimination of brimonidine from the vitreous chamber occurs via three routes: 1) diffusion into the anterior chamber across the hyaloid membrane, 2) diffusion into the posterior lens capsule (the degree of uptake would be small) and 3) diffusion into the retina/choroid/sclera (Allergan report: PK-07-053). We detected lower brimonidine concentration in aqueous humour as compared to choroid and retina in both study groups, suggesting drug diffusion was leading towards the retina/choroid/sclera, although high aqueous humour turnover could also be a possible contributing factor. This pattern of drug disposition has been associated with posterior route of clearance (Acheampong *et al.,* 2002), although a small fraction of brimonidine was undeniably eliminated via the aqueous chamber. Furthermore, the work of Koeberle and colleagues (Koeberle *et al.,* 2006) supported the established view in which compounds that penetrated the retina were cleared via the posterior pathway. The study provided further evidence to support the posterior route of elimination for brimonidine since in this study, a relatively high concentration was detected in the retina. According to Zhang and coworkers, the clearance mechanism at the RPE could be a carrier-mediated transport process (Zhang *et al.,* 2006).

Since both control and hyaluronidase-treated groups showed similar pattern of ocular disposition with higher concentrations achieved at the choroid/RPE as compared to aqueous humour, suggesting that the route by which brimonidine was eliminated from the eye was not affected by the state of the vitreous humour. This finding is consistent with that reported for sodium fluorescein and FD 150 kDa in Chapter 4.

6.4.6 STUDY IMPLICATIONS AND LIMITATIONS

The validation results indicated that the analytical assays were sufficiently accurate and precise for the analysis of ocular tissues. A quantitative comparison of intraocular drug concentrations of normal and liquefied vitreous models was performed at different time points. This has provided a trend information, although our results showed considerable individual variation, which rendered the performance of statistical analysis unsuccessful based on n=3. Therefore, larger sample sizes should be attempted in the future studies. Additionally, the large tissue concentration variability observed could be partly related to the variability in tissue weight seen especially for small tissue samples such as retina and choroid. This issue could potentially be overcome in the future by drying the tissue samples prior to quantification and subsequently normalizing the drug content to tissue dry weight. This may optimize the accuracy and precision of the data. Furthermore, we assume that recirculation of brimonidine via systemic absorption was minimal and did not affect current data.

In this study, we observed a difference in drug distribution and clearance of brimonidine between normal and partially liquefied eyes following intravitreal injection and implantation, however, further pharmacological studies investigating the significance of this observation to therapeutic drug efficacy is deemed necessary. In addition, with the work done in this chapter, we confirm that partial vitreous liquefaction increases the rate of drug clearance, which could not be completely ascertained previously in Chapter 4. Moreover, in this chapter, we have also shown that partial vitreous liquefaction affected drug disposition to a different degree following intravitreal injection and intravitreal implantation, the latter of which was affected to a lesser degree. Even though our conclusion was written solely based on findings obtained from Dutch-belted rabbits; the significance observed in humans may be different and hence, is an area for further research.

6.5 CONCLUSION

In summary, this study has demonstrated that partial vitreous liquefaction affects the ocular disposition of brimonidine following intravitreal injection but to a lesser extent following intravitreal implantation. The penetration of brimonidine into the choroid and retina demonstrated in this study suggests the feasibility of using the intravitreal route of administration for neuroprotection. Due to the short terminal half-life of brimonidine, a sustained release implant will be a better option.

CHAPTER 7: SUMMARY AND FUTURE DIRECTIONS

The world population especially in developing countries is ageing and it has been projected that by year 2050, the proportion of people aged above 60 will increase from 19% to 34% of the overall population, while the proportion of children is set to decline from 18% to 16%. Since blindness and visual impairment are more prevalent among the elderly, visual disability is expected to rise markedly in the years to come. Age-related macular degeneration is one of the most common causes of blindness in the elderly population. It affects the macula region of the retina at the posterior segment of the eye, which is an area that is difficult to reach. Intravitreal drug delivery has been the treatment modality for this condition using the vitreous humour as a drug reservoir from which the injected dose is subsequently diffused and delivered to the macula area. A change in the vitreous state such as during vitreous liquefaction that occurs with age will alter the rate of drug distribution to the target site. To date, this issue has not been explored and young laboratory animals with a juvenile vitreous humour remain commonly used. The risk of this is that, the influence of convective forces will be underestimated in the firm, young vitreous gel, generating an inaccurate approximation of drug clearance and efficacy for the elderly. Therefore, a representative vitreous model will minimize this potential problem and drug disposition in an aged eye can be better assessed.

In the first part of this thesis, attention was focusing on characterization and imaging of the vitreous humour to better understanding the vitreous physical and mechanical properties. The limitations associated with conventional techniques were improved by introducing the first use of optical trapping and perfused Miyake-Apple eye preparation. The second part of the thesis involves the development of a partially liquefied vitreous model in Dutch-belted rabbits, and an assessment of the effects of vitreous liquefaction on the intravitreal distribution of sodium fluorescein, FD 150kDa and 1μm fluorescent particles. In addition, a comparison of the ocular disposition of brimonidine, released from a single bolus intravitreal injection and a single intravitreal implantation, was performed in a partially liquefied vitreous model.

The juvenile vitreous humour consists of 99% water and 1% solute, which contains mainly collagen and hyaluronan. Soluble proteins, acidic glycoproteins, proteoglycans and electrolytes forms the minority vitreous composition. These vitreous solutes exhibit topographical variation in distribution, generating a non-homogeneous matrix. In view of this, the mechanical properties cannot be represented by an average value and a regional characterization as performed in this thesis was necessary. The measurements based on conventional viscometry and oscillatory tests showed that the vitreous was a lightly-crosslinked viscoelastic solid gel that was more rubbery than viscous material. The anterior portion of the vitreous was more viscoelastic; however, the posterior-peripheral zone next to the retina had a stronger fibrillar network that resisted a greater degree of shear deformation. The central area of the vitreous by comparison was the least structured. This unique design of the vitreous protects the retina under condition of stress by hydraulic damping, and serves as a diffusional barrier in regulating material influx into and efflux from within the vitreous cavity. The regulation and barrier properties ensures optical transparency for vision and maintains osmotic and chemical equilibriums of the matrix.

The characterization of the vitreous rheological properties using conventional rheometry suggested regional measurements were appropriate. However, local measurements involve the isolation of portions of the vitreous gel. Since the sheep vitreous was a sufficiently strong gel, the isolation technique was performed without the collapse and mixing of the gel phase. However, this procedure may not be feasible for other animal species whose vitreous gel is less firm in structure, including the rabbit. In order to improve the accuracy and utility of the measurement, a more robust experimental approach was needed.

Optical trapping was first explored in this study to measure the viscosity of the vitreous liquid phase. The method allows measurements to be performed at a micron-length scale, and hence, local measurement of the viscoelastic properties is feasible. Using this technique, several microparticles can be trapped simultaneously in a

single piece of gel without regional dissection of the sample. This less destructive operating approach appears to be extremely useful. At this stage of development, the application of optical trapping was limited to the viscosity measurement of the liquid phase; however, measurement of the gel phase should be possible utilising recently improved trap characterization methods. We are currently monitoring the Brownian motion of the trapped particle using a fast camera and quadrant photodiode. The ultimate aim of this application will be to enable local measurements to be performed in an intact Miyake-Apple eye preparation, where microparticles can be trapped and monitored at different positions within the vitreous space.

Vitreous imaging within a Miyake-Apple eye preparation was based on the imaging technique established by Professors Miyake and Apple and applied to posterior photography of the intraocular lens. The imaging was accomplished by illuminating 10μm fluorescent microparticles through the cornea with a high intensity blue LED at a right angle to the inspection port. The *ex-vivo* eye preparation showed that particles funneled back along the needle path following intravitreal injection into the mid-vitreous. This observation may illustrate the route by which vitreous reflux occurs in the patient's eye. Since the geometry of the needle track may vary depending on the injection and vitreous properties, the magnitude of reflux is subject to inter-individual variation. In addition, the remnant needle track appears to be a wavy path leading to and beyond the injection pocket. This suggested that needle penetration and injection applied a hydrostatic force that stretched the elastic fibrillar network, which subsequently relaxed when the stress was partially relieved upon the withdrawal of the needle. This raises the suggestion that frequent intravitreal injection might permanently alter the vitreous structure over time, for instance, vitreous liquefaction may occur if the gel network is partially damaged. This aspect of research should be further investigated, as although the issue may be irrelevant to the elderly whose vitreous have already been significantly liquefied, the impact on a younger population may remain important., We have noted that in finite element modeling, the initial injection shape adopted is usually thought of as a sphere or cylinder; in reality, the shapes formed are more complex and may either be isolated or extend back to the point of entry. Simple geometrical descriptions may therefore

be over-simplistic. It would be interesting to explore the consequences of the injection geometry on retinal disposition..

The utility of the Miyake-Apple eye preparation was extended by incorporating the preparation into a perfusion system. In both 4mm and 8mm perfused Miyake-Apple eye preparations, a stable intraocular pressure was successfully maintained. Nevertheless, the Miyake-Apple surgical procedure caused a greater degree of tissue damage as reflected in the raised and unstable LDH levels. Future studies should include a histology cross-section of the neuroretina, RPE and Bruch's membrane to further confirm tissue viability. In spite of these limitations, it was clear that the pattern of particle movement differs between perfused and non-perfused Miyake-Apple eyes. This suggested that flow processes generated by a pressurized system will influence the kinetics of microparticles in the vitreous, and a diffusion mechanism alone is not sufficient to explain the results in this model. Although not an intact eye, we suspect that the perfused eye moves nearer to the *in vivo* situation and that convective forces are important.

An important query addressed in this thesis was the effects of vitreous liquefaction on ocular disposition of intravitreally injected substances. It has been noted that a representative model of an elderly vitreous was unavailable. A partially liquefied vitreous model was therefore developed in this study for the first time using treatment with the enzyme hyaluronidase although an alternative approach with collagenase was also examined and abandoned due to retinal inflammation. The approach using hyaluronidase enables partial vitreous liquefaction to be reproducibly generated in Dutch-belted rabbits within a short time period of 48 hours. Future models may examine the influence of collagen fibres that form upon aging, which may be important for drugs prone to protein binding. It would also be interesting to examine the formation of liquefied vitreous as bulk fluid or liquid pockets using optical methods such as a slit-lamp and relate this back to the experimental model.

To examine the impact of vitreous liquefaction on the intravitreal drug distribution, we employed three model systems of different molecular weights and sizes namely,

sodium fluorescein, FD 150kDa and 1μm fluorescent particles. HRA and ocular fluorophotometry analysis showed that the distribution and clearance of sodium fluorescein and FD 150kDa were significantly faster in the partially liquefied vitreous compared to normal vitreous. When 1μm fluorescent particles were injected into the liquefied vitreous, particles sedimented faster and the distribution was more dispersed and scattered. These observations suggested that vitreous diffusivity and convective current were enhanced in a more liquefied vitreous environment, leading to a faster rate of dispersion. However, the gradients of sodium fluorescein and FD 150kDa as measured by ocular fluorophotometry did not appear to be affected by the vitreous state. Overall, the combined use of HRA and ocular fluorophotometry serves as a powerful tool for understanding the intravitreal events *in vivo*.

Following this work, the disposition of brimonidine in the liquefied vitreous model after a single bolus intravitreal injection and a single intravitreal implantation was investigated. It was anticipated that analysis of brimonidine concentration in individual ocular tissues would provide a better understanding with regard to the effects of vitreous liquefaction on drug disposition. Brimonidine tartrate is a highly selective α_2-adrenergic agonist used for lowering the intraocular pressure in patients with open-angle glaucoma and ocular hypertension. It has been shown to play a role in neuroprotection against degeneration of the retinal ganglion cells and the optic nerve. Currently, a brimonidine tartrate posterior segment ocular drug delivery system is undergoing a Phase-II clinical trials to investigate visual improvement in patients with previous rhegmatogenous retinal detachment and in patients with diabetic macular ischemia or geographic atrophy due to age-related macular degeneration and retinitis pigmentosa. Generally, the cohorts of patients are elderly and therefore, the results obtained from this study will be relevant to compare with our models.

Using a validated LCMS/MS analytical method, the concentration of brimonidine in the aqueous humour, vitreous humour, iris-ciliary body, retina, choroid and residual implants of both study models (normal and liquefied vitreous) were determined. The tissue concentrations at different time points were analysed using a non-

compartmental model. The pharmacokinetic analysis showed that, partial vitreous liquefaction affects the ocular disposition of brimonidine to a lesser degree following intravitreal implantation as compared to intravitreal injection. For intravitreal injection, mean clearance and total cumulative drug exposure at the choroid and retina were lower in the liquefied vitreous model. The C_{max} achieved at the macula region of the choroid and retina was also found to be lower than normal eyes. From this, it was deduced that the faster rate of drug clearance from the liquefied vitreous increases the chances that subtherapeutic drug levels will be obtained in the macula area, leading to poorer drug efficacy.

The analysis of the brimonidine disposition data from the implant suggested negligible effects of vitreous liquefaction on drug exposure at the vitreous, retina and ICB. The lower drug concentrations measured at the two elimination routes, choroid and aqueous humour, suggested that a faster rate of drug clearance from eyes with partial vitreous liquefaction is likely. Additionally, the determination of the implant molecular weight at different time points suggested that the impact of partial vitreous liquefaction on the rate of implant degradation was not important. Supporting evidence was obtained when the residual implants were imaged using SEM. During the study, it was also noted that the rate of brimonidine release from the implant was accelerated *in vivo* as compared to the *in vitro* release study. The drug content of the implant was depleted by day 21 rather than the target delivery of 30 days. Future studies should include an *in-vitro* and *in-vivo* correlation study to optimize release in the eye.

Although the rate of distribution and clearance were different in liquefied and normal vitreous, the elimination pattern of brimonidine remained unaffected by enzymatic treatment as noted for sodium fluorescein and FD 150kDa. Both models showed a higher concentration of brimonidine in choroid/RPE than in the aqueous humour. This suggests that the route by which molecules were cleared from the eye is not affected by the vitreous state.

An important factor involving in the distribution and clearance kinetics of brimonidine is melanin-binding. An accumulation of brimonidine in melanotic tissues such as ICB and choroid was obvious in both study models. The binding was noted as early as the first time point. Unlike the case for sodium fluorescein, melanin-binding of brimonidine may reduce the effects of vitreous liquefaction, leading to a subtle difference seen in the vitreous kinetics between both models at the last two time points.

The approach used to analyse the concentration of brimonidine in the choroid and retina tissues was different from the established method reported in the literature. Prior to measurements, the choroid and retina tissues were separated into superior, inferior, macula, nasal and temporal segments. The primary advantage of this isolation technique was that it allowed drug concentration in the macula area to be quantified. The concentration-time profiles showed that brimonidine was not uniformly distributed within the tissues. Distribution and absorption processes were a function of injection position or implant location with higher concentrations detected in tissues next to these areas. Lower degrees of spatial variation were seen in the partially liquefied vitreous. This observation could be attributed to its more homogeneous vitreous rheology, which promoted a more uniform distribution behaviour. More importantly, the total concentration of the whole tissue does not equate to the concentration achieved at the macula area. Therefore, measurements made using the whole tissue may overestimate the actual drug concentration achieved in the macula. This suggested that regional quantitation of the concentration in the choroid and retina will be useful for cases where drug exposure at the macula area of the eye is important. Future studies will include regional sampling of the vitreous probably using freezing and cutting microtome sections to establish distribution contour in order to better relate vitreous kinetics to that of the choroid and retina.

In this study, quantitative comparisons and measurements of brimonidine concentrations in the ocular tissues of both study models were performed over a period of one month. A statistically significant difference could not be established

due to a small number of subjects but information regarding a trend was demonstrated. Future studies will use a larger sample size to confirm present findings. In addition, weighing of small tissue samples that were in contact with intracellular water and have a blood supply with variably emptied capillaries made the standardization of the weighing method extremely difficult. In addition, the weight of the intracellular water that bathed the tissue increases the measured weight of the tissue and compromises the accuracy of the data. Future studies should attempt to dry the tissue and relate drug content to dry weight.

In summary, a partially liquefied vitreous model was successfully developed. Small and large intravitreally injected molecules showed a faster rate of distribution and clearance in the partially liquefied vitreous. Pharmacokinetic analysis demonstrated lower drug exposure at the macula area as compared to normal eyes. While the effects of vitreous liquefaction were less pronounced following intravitreal implantation, drug exposure at the elimination sites was low. The implication of this study was revealed in the clinical study by Spielberg and Ley, who have shown that, older patients required more frequent injection of bevacizumab as compared to middle-aged population for a similar degree of clinical outcome (Spielberg and Ley, 2009). Clearly, the ocular disposition of the injected drug is different in an elderly compared to a younger aged individual. The study implied that data obtained from a young animal model would not be representative to that of the elderly. Hence, the use of a representative model in preclinical drug development is vital in estimating drug doses for the elderly. If the delivery systems are optimized, making additional injections can be avoided. This will significantly improve patient's clinical care and cut down the treatment cost.

REFERENCES

Abraham-Marin ML, Cortes-Luna CF, Alvarez-Rivera G, Hernandez-Rojas M, Quiroz-Mercado H, Morales-Canton V (2007) Intravitreal bevacizumab therapy for neovascular age-related macular degeneration: a pilot study. *Graefe's Arch Clin Exp Ophthalmol* **245**: 651-655.

Acheampong AA, Shackleton M, Tang-Liu D D-S (1995) Comparative ocular pharmacokinetics of brimonidine after a single dose application to the eyes of albino and pigmented rabbits. *Drug metabolism and disposition* **23(7)**: 708-712.

Acheampong AA, Shackleton M, John B, Burke J, Wheeler L, Tang-Liu D (2002) Distribution of brimonidine into anterior and posterior tissues of monkey, rabbit and rate eyes. *Drug metabolism and disposition* **30 (4)**: 421-429.

Adamson GM, Harman AW (1988) Comparison of the susceptibility of hepatocytes from postnatal and adult mice to hepatotoxins. *Biochemical pharmacology* **37 (21)**: 4183-4190.

Aguilar HE, Meredith TA, el-Massry A, Shaarawy A, Kincaid M, Dick J, Ritchie DJ, Reichley RM, Neisman MK (1995) Vancomycin levels after intravitreal injection. Effects of inflammation and surgery. *Retina* **15,** 428-432.

Akiba J, Ueno N, Chakrabarti B (1994) Mechanisms of photo-induced vitreous liquefaction. *Curr Eye Res* **13**: 505-512.

Akiba J, Kakehashi A, Ueno N, Tano Y, Chakrabarti B (1995) Serum-induced collagen gel contraction. *Graefe's Arch Clin Exp Ophthalmol* **233**: 430-434.

Algvere P, Bill A (1979) Drainage of microspheres and RBCs from the vitreous of aphakic and phakic eyes. *Arch Ophthalmol* **97**: 1333-1336.

Anand M, Rajagopal KR (2004) A shear-thinning viscoelastic fluid model for describing the flow of blood. *International Journal of Cardiovascular Medicine and Science* **4(2)**: 59-68.

Araie M, Takase M, Sakai Y, Ishii Y, Yokoyama Y, Kitagawa M (1982) Beta-adrenergic blockers: ocular penetration and binding to the uveal pigment. *Jpn J Ophthalmol* **26(3)**: 248-63.

Araie M, Maurice DM (1991) The loss of fluorescein, fluorescein glucuronide and fluorescein isothiocyanate dextran from the vitreous by the anterior and retinal pathways. *Exp Eye Res* **52 (1)**: 27-39.

Ashkin A (2000) History of optical trapping and manipulation of small-neutral particle, atoms and molecules. *IEEE Journal* **6 (6)**: 841-856.

Ashkin A (1997) Optical trapping and manipulation of neutral particles using lasers. *Proc Natl Acad Sci* **94**: 4853-4860.

Atluri H, Mitra AK (2003) Disposition of short-chain aliphatic alcohols in rabbit vitreous by ocular microdialysis. *Exp Eye Res* **76**: 315-320.

Bakri SJ, Snyder MR, Reid JM, Pulido JS, Singh RJ (2007) Pharmacokinetics of intravitreal bevacizumab (Avastin). *Ophthalmology* **114,** 855-859.

Balazs EA (1960) Physiology of the Vitreous body. In Vitreous body in retina surgery: special emphasis on reoperations. St Louis, C.V. Mosby, pp 29-48.

Balazs EA, Denlinger JL (1984) The Vitreous. In: H. Daveson, The Eye. Academic Press. **1a:** 533 - 589.

Balazs EA, Denlinger JL (1982) Aging changes in the vitreous. In: Sekular R, Kline D, Dosmukes N, ed. Aging and human visual function. Alan R. Liss, New York, pp. 45-57.

Barza M, Kane A, Baum J (1983) Pharmacokinetics of intravitreal carbenicillin, cefazolin, and gentamicin in rhesus monkeys. *Invest Ophthalmol Vis Sci* **24,** 1602-1606.

Baxter E, Fraser JRE, Harris GS (1971) Interaction between hyaluronic acid and serum dispersed in collagen gels. *Ann Rheum Dis* **30**: 419.

Bettelheim FA, Wang TJY (1976) Dynamic viscoelastic properties of bovine vitreous. *Exp Eye Res* **23**: 435-441.

Bishop P.N. (2000). Structural Macromolecules and Supramolecular Organisation of the Vitreous Gel. *Progress in Retinal and Eye Research* **19(3)**: 323-344.

Bishop PN, Mcleod D, Reardon A (1999) Effects of hyaluronan lyase, hyaluronidase and chondroitin ABC lyase on mammalian vitreous gel. *Invest Ophthalmol Vis Sci* **40**: 2173-2178.

Bito LZ, Baroody RA (1987) Ocular trace metal kinetics and toxicology. I. The distribution of intravitreally injected Cu^{++}within intraocular compartments and its loss from the globe. *Invest Ophthalmol Vis Sci* **28**: 101-105

Bettelheim FA, Zigler JM (2004) Regional mapping of molecular components of human liquid vitreous by dynamic light scattering. *Exp Eye Res* **79**: 713-718.

Bioanalytical method partial validation for the determination of brimonidine in rabbit retina using LC/MS/MS. Allergan Report Number: BMS-05-057.

Bodaghi B, Gendron G, Wechsler B, Terrada C, Cassoux N, Houng DLT, Lemaitre C, Fradeau C, LeHoang P and Piette JC (2007). Efficacy of interferon alpha in the treatment of refractory and sight threatening uveitis: a retrospective monocentric study of 45 patients. *Br J Ophthalmol* **91**: 335-339.

Boon CJF, Klevering BJ, Kuijk FJ, Hoyng CB (2008) Reflux after intravitreal injection of bevacizumab. *Ophthalmology* **115 (7)**: 1268-69.

Borzacchiello A, Ambrosio L, Netti P, Nicolais L (2004) Chapter 13: Rheology of biological fluids and their substitutes. In: Tissue engineering and novel delivery systems. Ed. Yaszemski MJ, Trantolo DJ, Lewandrowski K-U, Hasirci V, Altobelli DE, Wise DL. Marcel Dekker, USA.

Brau RR, Ferrer JM, Lee H, Castro CE, Tam BK, Tarsa PB, Matsudaira P, Boyce MC, Kamm RD, Lang MJ (2007) Passive and active microrheology with optical tweezers. *Journal of Optics A: Pure and Applied Optics* **9**: S103-S112.

Brazel CS, Peppas NA (1999) Recent studies and molecular analysis of drug release from swelling-controlled devices. *STP Pharma Sci* **9**: 473-485.

Brouzas D, Charakidas A, Moschos M, Koutsandrea C, Apostolopoulos M, Baltatzis S (2009) Bavacizumab (Avastin) for the management of anterior chamber neovascularization and neovascular glaucoma. *Clin Ophthalmol* **3**: 685-8.

Brown DJ, Bishop P, Hamdi H, Kenney MC (1996). Cleavage of structural components of mammalian vitreous by endogeneous matrix metalloproteinase-2. *Curr Eye Res* **15 (4)**: 439-45.

Busacca A (1967) Biomicroscopie et Histopathologie de I'Oeil, Vol III, pp 25-43. Zurich: Schweizer Druck-und Verlagshaus.

Candia OA, Gerometta R, Millar C, Podos SM (2010) Suppresion of corticosteroid-induced ocular hypertension in sheep by anecortave. *Arch Ophthalmol* **128 (3)**: 338-343.

Chan RW, Titze IR (1999) Viscoelastic shear properties of human vocal fold mucosa: measurement methodology and empirical results. *J Acoust Soc Am* **106 (4)** Pt. 1: 2008-2021.

Chastain JE (2003) Chapter 3: General considerations in ocular drug delivery. In Mitra AK, Ophthalmic drug delivery system, vol 130 of drugs and the pharmaceutical sciences Informa Health Care, USA, pp. 83-90.

Chew J, Werner L (2006) Miyake-Apple preparation of postmortem eyes: technique and applications. *Techniques in Ophthalmology* **4 (3)**: 102-107.

Chin HS, Park TS, Moon YS, Oh JH (2005) Difference in clearance of intravitreal triamcinolone acetonide between vitrectomized and nonvitrectomized eyes. *Retina* **25(5)**: 556-560.

Chopdar A, Chakravarthy U, Verma D (2003) Age-related macular degeneration. *BMJ* **326**: 485-488.

Civan MM, Macknight ADC (2004) The ins and outs of aqueous humour secretion. *Exp. Eye Res* **78**: 625-631.

Cobo LM, Forster RK (1981) The clearance of intravitreal gentamicin. *American journal of ophthalmology* **92**: 59-62.

Comper WD, Laurent TC (1978) Physiological function of connective tissue polysaccharides. *Physiological reviews* **58 (1):** 255-303.

Conway MD, Jermak CM, Peyman GA, Swanson HT, Blake DA (2008) Buffering capacity of bovine vitreous. *Retina* **28**: 150-153.

Cunha-Vaz J, Faria De Abreu JR, Campos AJ, Figo GM (1975). Early breakdown of the blood-retinal barrier in diabetes. *Br J Ophthalmol* **59**: 649-656.

Cunha-Vaz JG, Maurice DM (1967) The active transport of fluorescein by the retinal vessels and the retina. *J Physiol* **191**: 467-486.

Cui F, Cun D, Tao A, Yang M, Shi K, Zhao M, Guan Y (2005) Preparation and characterization of melittin-loaded poly (DL-lactic acid) or poly (DL-lactic-co-glycolic acid) microspheres made by the double emulsion method. *Journal of controlled release* **107**: 310-319.

Cunha-Vaz JG (1997) The blood-ocular barriers: past, present and future. *Documenta Ophthalmologica* **93**: 149-157.

de Coo FAM, Zonnenberg BA, Trap NH (1993) Prolonged normothermic perfusion of the isolated bovine eye. Initial Results. *Curr Eye Res* **12**: 293-301.

Desai KGH, Mallery SR, Schwendeman SP (2008) Formulation and characterization of injectable poly (DL-lactide-co-glycolide) implants loaded with N-acetylcystein, a MMP inhibitor. *Pharm Res* **25(3)**: 586-597.

Dias CS, Mitra AK (2000) Vitreal elimination kinetics of large molecular weight FITC-labeled dextrans in albino rabbits using a novel microsampling technique. *Pharm. Sci* **89**: 572-578.

Dithmar S, Holz FG (2008) Chapter 2: The technical fundamentals of fluorescence angiography. In: Fluorescein Angiography in Ophthalmology. Springer Medizin Verlag Heidelberg, pp 6-13.

Dong XG, Shi WY, Yuan GQ, Xie LX, Wang SG, Lin P (2006) Intravitreal implantation of the biodegradable cyclosporine A drug delivery system for experimental chronic uveitis. *Graefe's Arch clin Exp Ophthalmol* **244**: 492-497.

Durairaj C, Shah JC, Senapati S, Kompella UB (2009) Prediction of vitreal half-life based on drug physicochemical properties: quantitative structure-pharmacokinetic relationship (QSPKR). *Pharm Res* **26(5)**: 1236-60.

EID TM, Spaeth GL (1999) Chapter 1: Definition and classification of glaucomas. In: The glaucomas: Concepts and fundamental. Lippincott Williams and Wilkins USA.

Evans DW, Hosking SL, Gherghel D, Bartlett (2003) Contrast sensitivity improves after brimonidine therapy in primary open angle glaucoma: a case for neuroprotection. *Br J Ophthalmol* **87**: 1463-1465.

Evans JR, Fletcher AE, Wormald RPL, Ng ESW, Stirling S, Smeeth L, Breeze E, Bulpitt CJ, Nunes M, Jones D, Tulloch (2002) Prevalence of visual impairment in people aged 75 years and older in Britain: results from the MRC trial of assessment and management of older people in the community. *Br J Ophthalmol* **86**: 795-800.

Fahim MM, Haji S, Koonapareddy CV, Fan VC and Asbell PA (2006) Fluorophotometry as a diagnostic tool for the evaluation of dry eye disease. *BMC Ophthalmology* **6**: 20.

Falcone SJ, Palmeri DM, Berg RA (2006) Rheological and cohesive properties of hyaluronic acid. *J Biomad Mater Res* **76A**: 721-728.

Fatt I (1977) Hydraulic flow conductivity of the vitreous. *Invest Ophthalmol Vis Sci* **16**: 565-568.

Ferraz D, Bressanim G, Takahashi B., Pelayes D., and Takahashi W (2010) Three-monthly intravitreal bevacizumab injections for neovascular age-related macular degeneration: short-trem visual acuity results. *Eur J Ophthalmol* **20(4)**: 740-744.

Foged C, Brodin B, Frokjaer S, Sundblad A (2005) Particle size and surface charge affect particle uptake by human dendritic cells in an in vitro model. *Pharmaceutical nanotechnology* **298**: 315-322.

Fong DS, Custis P, Howes J, Hsu JW (2010) Intravitreal bevacizumab and ranibizumab for age-related macular degeneration A Multicenter, Retrospective Study. *Ophthalmology* **117(2)**: 298-302.

Foster A, Resnikoff S (2005) The impact of vision 2020 on global blindness. *Eye* **19**: 1133-1135.

Foulds WS, Allan D, Moseley H, Kyle PM (1985) Effect of intravitreal hyaluronidase on the clearance of tritiated water from the vitreous to the choroid. *Br J Ophthalmol* **69**, 529-532.

Fowlks WL (1963) Meridional flow from the corona ciliaris through the pararetinal zone of the rabbit vitreous. *Invest Ophthalmol Vis Sci* **2(1)**: 63-71.

Fraser JRE, Foo WK, Maritz JS (1972). Viscous interactions of hyaluronic acid with some proteins and neutral saccharides. *Ann Rheum Dis* **31**: 513-520.

Friedberg DN (1997) Cytomegalovirus retinitis: diagnosis and status of systemic therapy. *Journal of acquired immune deficiency syndromes and human retrovirology* **14**: S1-S6

Friedrich S, Saville B, Cheng Y (1997a) Drug distribution in the vitreous humour of the human eye: the effects of aphakia and changes in retinal permeability and vitreous diffusivity. *J Ocul Pharmacol Therapeut* **13(5)**: 445-459.

Friedrich S, Cheng Y-L, Saville B (1997b) Drug distribution in the vitreous humor of the human eye: the effects of intravitreal injection position
and volume. *Curr Eye Res* **16**: 663-669.

Fung AT, Reid SE, Jones MP, Healey PR, McCluskey PJ, Craig JC (2007) Meta-analysis of randomised controlled trials comparing latanoprost with brimonidine in the treatment of open-angle glaucoma, ocular hypertension or normal-tension glaucoma. *Br J Ophthalmol* **91**: 62-68.

Gad HA, El-Nabarawi MA, Abd El-Hady SS (2008) Formulation and evaluation of PLA and PLGA in situ implants containing Secnidazole and/or Doxycycline for treatment of periodontitis. *AAPS PharmSciTech* **9(3)**: 878-884

Gan IM, Ugahary LC, van Dissel JT, van Meurs JC (2005) Effect of intravitreal dexamethasone on vitreous vancomycin concentrations in patients with suspected postoperative bacterial endophthalmitis. *Graefes Arch Clin Exp Ophthalmol* **243,** 1186-1189.

Garner LF, Ooi CS, Smith G (1998) Refractive index of the crystalline lens in young and aged eyes. *Clin Exp Optom* **81 (4)**: 145-150.

Gaudreault J, Fei D, Rusit J, Suboc P, Shiu V (2005) Preclinical pharmacokinetics of Ranibizumab (rhuFabV2) after a single intravitreal administration. *Invest Ophthalmol Vis Sci* **46,** 726-733.

Gekka M, Miyata K, Nagai Y, Nemoto S, Sameshima T, Tanabe T, Maruoka S, Nakahara M, Kato S and Amano S (2004) Corneal epithelial barrier function in diabetic patients. **Cornea** *23 (1)*: 35-37.

Gerometta R, Podos SM, Danias J, Candia OA (2009) Steriod-induced ocular hypertension in normal sheep. *Invest Ophthalmol Vis Sci* **50**: 669-673.

Giordano GG, Refojo MF, Arroyo MH (1993) Sustained delivery of retinoic acid from microspheres of biodegradable polymer in PVR. *Invest Ophthalmol Vis Sci* **34**: 2743-2751.

Girkin CA. Principles of confocal scanning laser ophthalomology for the clinician. Heidelberg Engineering. Accessed August 2010. http://www.heidelbergengineering.com/wp-content/uploads/chapter-1_principles-of-confocal-scanning-laser-ophthalmoscopy-for-the-clinician.pdf

Gisladottir S, Loftsson T, Stefansson E (2009) Diffusion characteristics of vitreous humour and saline solution follow the Stokes Einstein equation. *Graefes Arch Clin Exp Ophthalmol* **247**: 1677-1684.

Göpferich A (1997) Polymer bulk erosion. *Macromolecules* **30**: 2598-2604.

González VH, Giuliari GP, Banda RM, Guel DA (2009) Intravitreal injection of pegaptanib sodium for proliferative diabetic retinopathy. *Br J Ophthalmol* **93(11)**: 1474-8.

Gorle AP, Gattani SG. (2009) Design and Evaluation of polymeric ocular drug delivery system. *Chem. Pharm Bull* **57(9)**: 914-919.

Gottlieb JL, Antoszyk AN, Hatchell DL, Saloupis P (1990) The safety of intravitreal hyaluronidase, a clinical and histologic study. *Invest Ophthalmol Vis Sci* **31**: 2345-2352.

Gupta DK, Henthorn TK (2009) Chapter 7: Pharmacologic principles. In: Barash PG, Cullen BF , Stoelting RK, Cahalan MK, Stock MC, ed, Clinical Anesthesia, 6th ed., Lippincott Williams & Wilkins, Philadelphia, USA, pp. 149.

Haller JA, Dugel P, Weinberg DV, Chou C, Whitcup SM (2009) Evaluation of the safety and performance of an applicator for a novel intravitreal dexamethasone drug delivery system for the treatment of macular edema. *Retina* **29**: 46-51.

Harooni M, McMillan T, Refojo M (1998) Efficacy and safety of enzymatic posterior vitreous detachment by intravitreal injection of hyaluronidase. *Retina* **18**: 16-22.

Hassenstein A, Meyer CH (2009) Clinical use and research applications of Heidelberg retinal angiography and spectral-domain optical coherence tomography-a review. *Clin Exp Ophthalmol* **37**: 130-143.

Hikichi T, Kado M, Yoshida A (2000) Intravitreal injection of hyaluronidase cannot induce posterior vitreous detachment in the rabbit. *Retina* **20(2)**: 195-198.

Holekamp NC, Shui YB, Beebe DC (2005) Vitrectomy surgery increases oxygen exposure to the lens: A possible mechanism for nuclear cataract formation. *Am J Ophthalmol* **139**: 302-310.

Hough LA, Ou-Yang HD (2006) Viscoelasticity of aqueous telechelic poly(ethylene oxide) solution: relaxation and structure. *Phy Rev E Stat Nonlin Soft Matter Phys* **73 (3 Pt 1)**: 031802.

Huang X, Brazel CS (2001) On the importance and mechanisms of burst release in matrix-controlled drug delivery system. *Journal of controlled release* **73**: 121-136.

Hughes PM, Olejnik O, Chang-Lin J-E, Wilson CG (2005) Topical and systemic drug delivery to the posterior segments. *Advanced drug delivery reviews* **57**: 2010-2032.

Hughes PM (2008) Topical delivery to the retina: reality or artifact. In: *Angiogenesis, exudation and degeneration meeting.*: Bascom Palmer Eye Institute, Florida.

Jaffe GJ, McCallum RM, Branchaud B, Skalak C, Butuner Z, Ashton P (2005) Long-term follow-up results of a pilot trial of a fluocinolone acetonide implant to treat posterior uveitis. *Ophthalmology* **112**: 1192-1198.

Jaffe NS (1969). The vitreous in clinical ophthalmology. St Louis, C.V. Mosby, USA.

Jorzik JJ, Bindewald A, Dithmar S, Holz FG (2005) Digital simultaneous fluorescein and indocyanine green angiography, autofluorescence and red-free imaging with a solid-state laser based confocal scanning laser ophthalmoscope. *Retina* **25**: 405-416.

Kaiser RJ, Maurice DM (1964) The diffusion of fluorescein in the lens. *Exp. Eye Res.* **3**: 156-165.

Kakeshi A, Ueno N, Chakrabarti B (1994) Molecular mechanisms of photochemically induced posterior vitreous detachment. *Ophthalmic Res* **26**: 51-59.

Kalapesi FB, Coroneo MT, Hill MA (2005) Human ganglion cells express the alpha-2 adrenergic receptor: relevance to neuroprotection. *Br J Ophalmol* **89**; 758-763.

Kanski JJ (1987) Uveitis: A colour manual of diagnosis and treatment. Butterworth-Heinemann Limited.

Kathawate J, Acharya S (2008) Computational modeling of intravitreal drug delivery in the vitreous chamber with different vitreous substitutes. *International Journal of Heat and Mass Transfer* **51**(23-24): 5598-5609.

Keen S, Leach J, Gibson G, Padgett MJ (2007) Comparison of a high-speed camera and a quadrant detector for measuring displacements in optical tweezers. *Journal of Optics A: Pure and Applied Optics* **9**: S264-DS266.

Kent AR, Nussdorf JD, David R, Tyson F, Small D, Fellows D (2001) Vitreous concentration of topically applied brimonidine tartrate 0.2%. *Ophthalmology* **108**; 784-787.

Keough EM, Wilcox LM, Connolly RJ, Hotte CE (1981) Comparative ocular blood flow. *Comp Biochem Physiol* **68A**: 269-271.

Kim C-j (2004) Chapter 6: Diffusion. In: Advanced pharmaceutics : physicochemical principles. CRC, London.

Kim H, Lizak MJ, Tansey G, Csaky KG, Robinson MR, Yuan P, Wang NS, Lutz RJ (2005) Study of ocular transport of drugs released from an intravitreal implant using magnetic resonance imaging. *Annals of biomedical engineering* **33 (2)**: 150-164.

Kitano S, Nagataki S (1986) Transport of fluorescein monoglucuronide out of the vitreous. *Invest Ophthalmol Vis Sci* **27**: 998-1001.

Knudsen LL (2002) Ocular fluorophotometry in human subjects and in swine-with particular reference to long-term pharmacokinetics. *Acta Ophthalmologica Scandinavica supplement* **235**: 6-24.

Kodama T, Reddy VN, Macri FJ (1983) The arterially perfused enucleated rabbit eye as a model for studying aqueous humour formation. *Ophthalmic Res* **15**: 225-233.

Koeberle MJ (2003) Investigation of factors involved in the disposition and pharmacokinetics of memantine in the isolated bovine eye. University of Strathclyde, Ph.D thesis.

Koeberle MJ, Hughes PM, Skellern GG & Wilson CG. (2006) Pharmacokinetics an disposition of memantine in the arterially perfused bovine eye. *Pharm Res* **23**: 2781-2798.

Kroese M, Burton H, Vardy S, Rimmer T, McCarter D (2002) Prevalence of primary open-angle glaucoma in general ophthalmic practice in the United Kingdom. *Br. J. Ophthalmol* **86**: 978-980

Kurkela R, Fraune E, Vihko P (1993) Pilot-scale production of murine monoclonal antibodies in agitated, ceramic-matrix or hollow-fiber cell cultre systems. *Biotechniques* **15 (4)**: 674-83.

Lafuente MP, Villegas-Perez MP, Sobrado-Calvo P, Garcia-Aviles A, Imperial JMD, Vidal-Sanz M (2001) Neuroprotection effects of alpha-2 selective adrenergic agonists against ischemia-induced retinal ganglion cell death. *Invest Ophthalmol Vis Sci* **42**; 2074-2084.

Lai G, Li Y, Li G (2008) Effect of concentration and temperature on the rheological behavior of collagen solution. *International journal of biological macromolecules* **42**: 285-291.

Laurent UB, Granath KA (1983) The molecular weight of hyaluronate in the aqueous humour and vitreous body of rabbit and cattle eyes. *Exp Eye Res* **36**: 481-492.

Lee B, Litt M, Buchsbaum G (1992) Rheology of the vitreous body. Part 1: Viscoelasticity of human vitreous. *Biorheology,* **29:** 521-533.

Lee B, Litt M, Buchsbaum G (1994a) Rheology of the vitreous body: Part 2. Viscoelasticity of bovine and porcine vitreous. *Biorheology* **31 (4)**: 327-338.

Lee B, Litt M, Buchsbaum G (1994b) Rheology of the vitreous body. Part 3: Concentration of electrolytes, collagen and hyaluronic acid. *Biorheology,* **31 (4)**, 339-351.

Lee SS, Harutyunyan I, D'Argenio DZ, Moats RA (2009) The effect of vitreous syneresis on drug transport. In proceedings: ARVO Summer Eye Research Conference, NIH, Bethesda. Abstract no. 8, pp.17.

Lee SS, Ghosn C, Yu Z, Zacharias LC, Kao H, Lanni C, Abdelfattah N, Kuppermann B, Csaky KG, D'Argenio DZ, Burke JA, Hughes PM, Robinson MR (2010) Vitreous VEGF clearance is increased following vitrectomy. *Invest Ophthalmol Vis Sci* **51**: 2135-2138.

Li S, Järvelä PK, Jäverlä PA (1997) A comparison between apparent viscosity and dynamic complex viscosity for polypropylene/maleated polypropylene blends. *Polymer engineering and science* **37 (1)**: 18-23.

Lin DM, Kalachandra S, Valiyaparambil J, Offenbacher S (2003) A polymeric device for delivery of anti-microbial and anti-fungal drugs in the oral environment: effect of temperature and medium on the rate of drug release. *Dental Materials* **19**: 589-596.

Liu W, Liu QF, Perkins R, Drusano G, Louie A, Madu A, Mian U, Mayers M, Miller MH (1998) Pharmacokinetics of sparfloxacin in serum and vitreous humour of rabbits: Physicochemical properties that regulate penetration of quinolone antimicrobials. *Antimicrobial agents and chemotherapy* **42 (6)**: 1417-1423.

Loo SCJC, Tan ZYS, Chow YJ and Lin SLI (2010) Drug release from irradiated PLGA and PLLA multi-layered films. *Journal of pharmaceutical sciences* **99 (7)**: 3060-71.

Lopez-Cortes LF, Pastor-Ramos MT, Ruiz-Valderas R, Cordero E,
Uceda-Montanes A, Claro-Cala CM, Lucero-Munoz MJ (2001) Intravitreal pharmacokinetics and retinal concentrations of ganciclovir and foscarnet after intravitreal administration in rabbits. *Invest Ophthalmol Vis Sci* **42,** 1024-1028.

Los LI (2008) The rabbit as an animal model for post-nasal vitreous matrix differentiation and degeneration. *Eye* **22**: 1223-1232.

Luan X, Bodmeier R (2006) Influence of the poly (lactide-co-glycolide) type on the leuprolide release from in situ forming microparticle systems. *Journal of controlled release* **110**: 266-272.

Lund-Andersen H, Sander B (2003) The vitreous. In: Kaufman PL, Alm A, ed. Adler's Physiology of the Eye, 10th ed. Mosby Inc, USA, pp. 293–316.

Malvern Instruments Ltd. Theology Training Module 6: Measurement Geometries (2010).

Malagnino N, Pesce G, Sasso A, Arimondo E (2002) Measurements of optical trapping efficiency and stiffness in optical tweezers. *Optics Communications* **214**: 15-24.

Mathews JP, Mathews D, Kelly SP (2003) Age-related macular degeneration: an overview. Continuing Professional Development. Accessed: August 2010. http://www.optometry.co.uk/articles/docs/163851ad24a0c8e4bc5d26e399a94c73_kelly20030221.pdf

Matsuura T, Hara Y, Maruoka S, Kawasaki S, Sasaki S, Annaka M (2004) Dynamic light scattering study on the calf vitreous body. *Macromolecules* **37**: 7784-7790.

Maurice DM, Mishima S (1984) Ocular pharmacokinetics. In: Sears ML, ed. Pharmacology of the eye. Springer-Verlag, New York, pp.19-116.

Maurice D (2001) Review: practical issues in intravitreal drug delivery. *J Ocul Pharmacol Ther* **17,** 393-401.

Mennel S, Schwendinger R, Hausmann N, Peter S (2007) Accessory optical device for the Heidelberg retina angiograph (HRA classic) to perform angiography of the vitreous cavity and the anterior eye segment. Brief Report. *Indian J Ophthalmol* **55**: 295-7.

Mensitieri M, Ambrosio L, Nicolais, Balzano L, Lepore D (1994) The rheological behaviour of animal vitreous and its comparison with vitreous substitutes. Journal of materials science: *Materials in medicine* **5**: 743-747.

Meredith TA (2006) Chapter 6: Intravitreal antimicrobials. In Jaffe GJ, Ashton P, Pearson PA, ed, Intraocular drug delivery, Taylor and Francis, London, UK, pp. 85-93.

Mezger TG (2006a) Chapter 8: Oscillatory tests. In: The rheology handbook. Page 114-162. 2nd Vincentz Network, Hannover, Germany.

Mezger TG (2006b) Chapter 3: Rotational tests. In: The rheology handbook. Page 29-40. 2nd Vincentz Network, Hannover, Germany.

Miller PE (2008) Chapter 1: Structure and function of the eye. In: Slatter's fundamentals of veterinary ophthalmology, 4th ed, Saunders, Elsevier, St Louis, Missouri, USA, pp. 17-19.

Missel (2002). Hydraulic flow and vascular clearance influences on intravitreal drug delivery. *Pharm Res* **19 (11)**: 1636-1647.

Miyajima M, Koshida A, Okada J, Kusai A, Ikeda M (1998) The effects of drug physico-chemical properties on release from copoly (lactic/glycolic acid matrix). *International journal of pharmaceutics* **169**: 255-263.

Moldow B, Sander B, Larsen M, Engler C, Li B, Rosenberg T, Lund-Andersen H (1998) The effect of acetazolamide on passive and active transport of fluorescein across the blood-retina barrier in retinitis pigmentosa complicated by macular oedema. *Graefes Arch Clin Exp Ophthalmol* **236:** 881-889.

Moldow B, Sander B, Larsen M, Lund-Andersen H (1999) Effects of acetazolamide on passive and active transport of fluorescein across the normal BRB. *Invest Ophthalmol Vis Sci* **40:** 1770-1775.

Moldow B, Larsen M, Sander B, Lund-Andersen H (2001) Passive permeability and outward active transport of fluorescein across the blood-retinal barrier in early ARM. *Br J Ophthalmol* **85:** 592-597.

Molloy JE, Padgett MJ (2002) Lights, action: optical tweezers. *Contemporary Physics* **43 (4)**: 241-258.

Montanes A, Claro-Cala CM, Lucero-Munoz MJ (2001) Intravitreal pharmacokinetics and retinal concentrations of ganciclovir and foscarnet after intravitreal administration in rabbits. *Invest Ophthalmol Vis Sci* **42,** 1024-1028.

Mruthyunjaya P, Khalatbari D, Yang P, Stinnett S, Tano R, Ashton P, Guo H, Nazzaro M, Jaffe GJ (2006) Efficacy of low-release-rate fluocinolone acetonide intravitreal implants to treat experimental uveitis. *Arch Ophthalmol* **124**: 1012-1018.

Muccioli C, Belfort R (2000) Treatment of cytomegalovirus retinitis with an intraocular sustained-release ganciclovir implant. *Brazillian journal of medical and biological reseach* **33**: 779-789.

Narayanan R, Kuppermann BD (2009) Hyaluronidase for pharmacologic vitreolysis. *Dev Ophthalmol* **44**: 20-25.

Nayak RC, Herman IM (1997) Measurement of glucose consumption by hybridoma cells growing in hollow fiber cartridge bioreactors: use of blood glucose self-monitoring devices. *Journal of immunological methods* **205**: 109-114.

Nickerson CS, Karageozian HL, Park J, Kornfield JA (2005) Internal tension: A novel hypothesis concerning the mechanical properties of the vitreous humour. *Macromol. Symp.* **227**: 183-189.

Nickerson CS, Park J, Kornfield JA, Karageozian H (2008) Rheological properties of the vitreous and the role hyaluronic acid. *Journal of biomechanics* **41**: 1840-1846.

Noulas AV, Skandalis SS, Feretis E, Theocharis DA, Karamanos NK (2004) Variations in content and structure of glycosaminoglycans of the vitreous gel from different mammalian species. *Biomed. Chromatogr.* **18**: 457-461.

Ocular Instruments Inc. Ocular Staurenghi 230 SLO Retina Lens. Accessed August 2010. http://www.ocular-instruments.com/downloads/pdfs/OSR230.pdf

Oguro, Y, Tsukahara Y, Saito I, Kondo T (1985) Estimation of the permeability of the blood-retinal barrier in normal individuals. *Invest Ophthalmol Vis Sci* **26,** 969-976.

Oh SH, Kang SK, Lee JH (2006) Degradation behavior of hydrophilized PLGA scaffolds prepared by melt-molding particulate-leaching method: Comparison with control hydrophobic one. Journal of materials science: *Materials in medicine* **17**: 131-137.

Okabe J, Kinura H, Kunou N, Okabe K, Kato A, Ogura Y (2003) Biodegradable intrascleral implant for sustained intraocular delivery of betamethasone phosphate. *Invest Ophthalmol Vis Sci* **44**: 740-744.

Osborne NN (2009) Recent clinical findings with memantine should not mean that the idea of neuroprotection in glaucoma is abandoned. Acta Opthalmol 87: 450-454.

Park J, Bungay PM, Lutz RJ, Augsburger JJ, Millard RW, Roy AS, Banerjee RK (2005) Evaluation of coupled convective-diffusive transport of drugs administered by intravitreal injection and controlled release implant. *Journal of Controlled Release* **105**: 279-295.

Patel (2004) Viscoelastic properties of polystyrene using dynamic rheometry. *Polymer Testing* **23**: 107-112.

Peeters L, Sanders NN, Braeckmans K, Boussery K, de Voorde JV, De Smedt SC, Demeester J (2005) Vitreous: A barrier to nonviral ocular gene therapy. *Invest Ophthalmol Vis Sci* 46: 3553-3561.

Pelis RM, Delamere NA (2009) Organic anion secretion across the ciliary body epithelium of the eye. *FASEB J.* **23** (Meeting Abstract Supplement) 797.9.

Pereira FAS, Werner L, Milverton EJ, Coroneo MT (2009) Miyake-Apple posterior video analysis/photographic technique. *J Cataract Refract Surg* **35**: 577-587.

Pharmacokinetic analysis of brimonidine (AGN 190342) in rabbit aqueous humour, vitreous humour, retina and plasma for Study PK-05-P067. Allergan Report Number: PK-07-053.

Pinon-Segundo E, Ganem-Quintanar A, Alonso-Perez V and Quintanar-Guerrero D (2004). Preparation and characterization of triclosan nanoparticles for periodontal treatment. *International journal of pharmaceutics* **294**: 217-232.

Pirie A (1949) The effect of hyaluronidase injection on the vitreous humor of the rabbit. *Br J Ophthalmol* **33**: 678-684.

Pitkänen L, Ruponen M, Nieminen J, Urtti A (2003) Vitreous is a barrier in nonviral gene transfer by cationic lipids and polymers. *Pharm Res* **20 (4)**: 576-583.

Pitkänen L, Ranta V, Moilanen H, Urtti A (2005) Permeability of retinal pigment epithelium: effects of permeant molecular weight and lipophilicity. *Invest Ophthalmol Vis Sci* **46**: 641-646.

Population Division, DESA, United Nations. III. Changing balance between age groups. World Population Ageing 1950-2050.

Prince JH, Diesem CD, Eglitis I, Ruskel GL (1960) Anatomy and histology of the eye and orbit in domestic animals. Thomas, C. C, Springfiled .

Quigley HA, Broman AT (2006) The number of people with glaucoma worldwide in 2010 and 2020. *Br J Ophthalmol* **90**: 262–267.

Raines MR (1988) Vitreous fluorophotometry: a review. *Journal of the Royal Society of Medicine* **81**: 403-406.

Reardon A, Heinegard D, McLeod D, Sheehan JK, Bishop PN (1998) The large chondroitine sulphate proteoglycan versican in mammalian vitreous. *Matrix Biology* **17**: 325-333.

Reddy VN, Thompson MR, Chakrapani B (1977) Amino acid transport across blood-aqueous barrier of mammalian species. *Exp Eye Res* **25**: 555-562.

Reece WO (2005) Chapter 5: The sensory organs. In: Troy DB ed., Functional anatomy and physiology of domestic animals, 3rd ed, Lippincott Wiliams and Wilkins, USA, pp. 132-134.

Repetto R (2006) An Analytical Model of the Dynamics of the Liquefied Vitreous Induced by Saccadic Eye Movements. *Meccanica* **41**: 101–117.

Riviere JE (1999) Comparative pharmacokinetics: Principles, techniques and applications. Blackwell Publishing, Iowa State Press.

Sakurai E, Ozeki H, Kunou N, Ogura Y (2001) Effect of particle size of polymeric nanospheres on intravitreal kinetics. *Ophthalmic Res* **33**: 31-36.

Sander B, Larsen M, Moldow B, Lund-Andersen H (2001) Diabetic macular edema: passive and active transport of fluorescein through the blood-retina barrier. *Invest Ophthalmol Vis Sci* **42:** 433-438.

Schachar RA, Chan RW, Fu M (2007) Viscoelastic shear properties of the fresh porcine lens. *Br J Ophthalmology* **91**: 366-368.

Schmidt C, Wenz R, Nies B, Moll F (1995) Antibiotic in vivo/in vitro release, histocompatibility and biodegradation of gentamicin implants based on lactic acid polymers and copolymers. *Journal of controlled release* **37**: 83-94.

Sebag J, Balazs EA (1984) Pathogenesis of cystoid macular edema: An anatomic consideration of vitreoretinal adhesions. *Surv Ophthalmol* **28 (suppl)**: 493-498.

Sebag J, Balazs EA (1985) Human vitreous fibres and vitreoretinal disease. *Trans Ophthalmol Soc UK* **104**: 123-128.

Sebag J (1987) Age-related changes in human vitreous structure. *Graefe's Arch Clin Exp Ophthalmol* **225**: 89-93.

Sebag J. (1989) The Vitreous. Springer-Verlag, New York.

Sebag J, Balazs EA (1989) Morphology and Ultrastructure of Human Vitreous Fibers. *Invest Ophthalmol Vis Sci* **30**: 1867-1871.

Sebag J (1998) Macromolecular structure of the corpus vitreous. *Prog. Polym. Sci*., **23**, 415-446.

Sebag J (2005) Molecular Biology of Pharmacologic Vitreolysis. *Trans Am Ophthalmol Soc* **103**: 473-494.

Sebag J, Ansari RR, Suh KI. (2007) Pharmacologic vitreolysis with microplasmin increases vitreous diffusion coefficients. *Graefes Arch Clin Exp Ophthalmol* **245**: 576-580.

Shen J (2002) Ocular pharmacokinetics of AGN 190342 following a single intravitreal injection into female albino rabbit eyes. Allergan report PK-02-P023

Shiels IA, Sanderson SD, Taylor SM (1999) Arterially perfused eye model of uveitis. *Australian Veterinary Journal* **77**: 100-104.

Short BG (2008) Safety evaluation of ocular drug delivery formulations: techniques and practical considerations. *Toxicol Pathol* **36**: 49-62.

Simoens P, Ghoshal NG (1981) Arterial supply to the optic nerve and the retina of the sheep. *J Anat* **133 (4)**: 481-497.

Sinko PJ, Singh Y (2006) Chapter 19: Rheology. In: Martin's physical pharmacy and pharmaceutical sciences. 6th ed, Wolters Kluwer Health, Philadelphia & Lippincott Williams & Wilkins, Baltimore, pp 469-491.

Smith JW, Serafini-Fracassini A (1967) The relationship of hyaluronate and collagen in the bovine vitreous body. *J Anat* **101 (1)**: 99-112.

Snowden JM, Swann DA (1980) Vitreous structure. V. The morphology and thermal stability of vitreous collagen fibers and comparison to articular cartilage (type II) collagen. *Invest Ophthalmol Vis Sci* **19 (6)**: 610-618.

Soman N, Banerjee R (2003) Artificial vitreous replacements. *Bio-medical Materials and Engineering* **13**: 59-74.

Spenlehauer G, Vert M, Benoit JP, Boddaert A (1989) In vitro and in vivo degradation of poly (D,L lactide/glycolide) type microspheres made by solvent avaporation method. *Biomaterials* **10**: 557-563.

Spielberg L, Leys A (2009) Intravitreal bevacizumab for hyopic choroidal neovascularization: short-term and 1-year results. *Bull. Soc. Belge Ophtalmol* **312**: 17-27.

Spraul CW, Grossniklaus E (1997) Vitreous haemorrhage, major review. *Surv Ophthalmol* **42**: 3- 39.

Stainer GA, Peyman GA, Meisels H and Fishman G (1977) Toxicity of selected antibiotics in vitreous replacement fluid. *Ann Ophthalmol* **9**: 615-618.

Staurenghi G, Viola F, Mainster MA, Graham RD, Harrington PG (2005) Scanning laser ophthalmoscope and angiography with a wide-field contact lens system. *Arch Ophthalmol* **123**: 244-252.

Stay MS, Xu J, Randolph TW, Barocas VH (2003) Computer simulation of convective and diffusive transport of controlled-release drugs in the vitreous humor. *Pharm Res* **20**: 96-102.

Stefánsson E (2009) Physiology of vitreous surgery. *Graefes Arch Clin Exp Ophthalmol* **247**: 147-163.

Stepanova LV, Marchenko IY, Sychev GM (2005) Direction of fluid transport in the lens. Translated from *Byulleten' Eksperimental'noi Biologii i Meditsiny* **139 (1)**: 57-58.

Sturesson C, Carlfors J, Edsman K, Andersson M (1993) Preparation of biodegradable poly (lactic-co-glycolic) acid microspheres and their in vitro release of timolol maleate. *International journal of pharmaceutics* **89**: 235-244.

Sugita S (2007). Intravitreal anti-inflammatory treatment for uveitis.
Br J Ophthalmol **91**: 135-136.

Suri S, Banerjee R (2006) In vitro evaluation of in situ gels as short term vitreous substitutes. *J Biomed Mater Res* **79A**: 650-664.

Svoboda K, Block SM (1994) Biological applications of optical forces. *Annu Rev Biophysics Biomol Struct* **23**: 247-285.

Swann DA, Constable IJ (1972) Vitreous structure I, Distribution of hyaluronate and protein. *Invest ophthalomol Vis Sci* **11 (3)**: 159-163.

Swindle KE, Hamilton PD, Shui YB, Beebe DC, Ravi N (2007) Characterization of Copolymeric Hydrogel Vitreous Substitutes that Gel In Situ. *Polymeric Materials: Science and Engineering*, **96**, 609-610.

Swindle KE, Ravi N (2007). Recent advances in polymeric vitreous substitutes. *Expert Rev. Ophthalmol* **2 (2)**: 255-265.

Swindle KE, Hamilton P, Ravi N (2008) In situ formation of hydrogels as vitreous substitutes: Viscoelastic comparison to porcine vitreous. *J Biomed. Mater Res* **87A**: 656-665.

Takahashi J, Hikichi T, Mori F, Kawahara A, Yoshida A, Peterson WM (2004) Effect of nucleotide P2Y2 receptor agonists on outward active transport of fluorescein across normal blood-retina barrier in rabbit. *Exp Eye Res* **78 (1)**: 103-108.

Takano S, Ishiwata S, Nakazawa M, Mizugaki M, Tamai M (1997) Determination of ascorbic acid in human vitreous humor by high-performance liquid chromatography with UV detection. *Curr Eye Res* **16 (6)**: 589-594.

Tanaka M, Qui H (2000) Pharmacological vitrectomy. *Seminars in Ophthalmology* **15**: 51-61.

The Eye Diseases Prevalence Research Group (2004) Causes and prevalence of visual impairment among adults in the United States. *Arch Ophthalmol* **122**: 477-485.

Thomas AV, Gilbert SJ, Duance VC (2000) Elevated levels of proteolytic enzymes in the aging human vitreous. *Invest Ophthalmol Vis Sci* **41 (11)**: 3299-3304.

Thompson JT, Glaser BM (1984) Effect of lensectomy on the movement of tracers from vitreous to aqueous. *Arch Ophthalmol* **102**: 1077-1078.

Tokita M, Fujiya Y, Hikichi K (1984) Dynamic viscoelasticity of bovine vitreous body. *Biorheology* **21**: 751-756.

Tripathi RC and Tripathi BJ (1984) Chapter 1: Anatomy of the human eye, orbit and adnexa. In Davson H.,The Eye, vol 1a: Vegetative physiology and biochemistry, 3rd Ed, Academic Press, London and New York.

Ueno N, Sebag J, Hirokawa H, Charkrabarti B (1987) Effects of visible-light irradiation on vitreous structure in the presence of a photosensitizer. *Exp. Eye Res.* **44**: 863-870.

Urtti A (2006) Challenges and obstacles of ocular pharmacokinetics and drug delivery. *Advanced drug delivery reviews* **58**: 1131-1135.

Van Best JA, Oosterhuis JA (1983) Computer fluorophotometry. *Documenta Opthalmologica* **56**: 89-97.

Velegola D, Lanni F (2001) Cell traction forces on soft biomaterials. I. microrheology of type I collagen gels. *Biophysical Journal **81***: 1786-1792.
Vermeulen KC, Wuite GJL, Stienen GLM, Schmidt CF (2006)Optical trap stiffenss in the presence and absence of spherical aberrations. *Applied Optics* **45**: 1812-1819.

Wakefield D, Chang JH (2005) Epidemiology of Uveitis in : Uveitis and related ocular inflammations: A global perspective from the international uveitis study group. *International Ophthalmology Clinics* **45 (2)**: 1-13.

Wang J, Wang BM, Schwendeman SP (2002) Characterization of the initial burst release of a model peptide from poly (D,L-lactide-co-glycolide) microspheres. *Journal of controlled release* **82**: 289-307.

Wang ZL, Zhang X, Xu X, Sun XD, Wang F (2005) PVD following plasmin but not hyaluronidase: implications for combination pharmacologic vitreolysis therapy *Retina* **25**: 38-43.

Wheeler LA, Gil DW, WoldeMussie E (2001) Role of alpha-2 adrenergic receptors in neuroprotection and glaucoma. *Survey of ophthalmology* **45 (3)**: S290-S294.

Williams MC (2004) Optical tweezers: Measuring piconewton forces. Northeastern University, department of physics and centre for interdisciplinary research on complex systems.

Williamson TH (2007) Chapter 4: Vitreous haemorrhage. In: Vitreoretinal surgery. Springer Berlin Heidelberg, pp: 49-52.

Williamson TH (2008). Chapter 12: Uveitis and allied disorders. In: Vitreoretinal surgery. Springer Berlin, Heidelbergh and New York, pp. 201.

Winkler BS, Cohn EM (1985) Hyaluronidase and retinal function. *Arch Ophthalmol* **103**: 1743-1746.

WoldeMussie E, Ruiz G, Wijono M, Wheeler LA (2001) Neuroprotection of retinal ganglion cells by brimonidine in rats with laser-induced chronic ocular hypertension. *Invest Ophthalmol Vis Sci* **42**: 2849-2855.

WoldeMussie E, Yoles E, Schwartz M, Ruiz G, Wheeler LA (2002) Neuroprotective effect of memantine in different retinal injury models in rats. *Journal of Glaucoma* **11**: 474-480.

Worst JGF, Los LI (1995) Chapter 3: Functional anatomy of the vitreous. In Cisternal anatomy of the vitreous. Amsterdam, Netherlands: Kugler Publications. pp. 33-48.

Wright AJ, Wood TA, Dickinson MR, Gleeson HF, Mullin T (2003) The transverse trapping force of an optical trap: factors effecting its measurement. *Journal of Modern Optics* **50**: 1521-1532.

Xu J, Heys JJ, Barocas VH, Randolph TW (2000) Permeability and diffusion in vitreous humor: implications for drug delivery. *Pharm Res* **17**: 664-669.

Yamamoto S, Manabe N, Fujioka K, Hoshino A, Yamamoto K (2007) Visualizing vitreous using quantum dots as imaging agents. *IEEE Transaction on Nanobioscience* **6 (1)**: 94-98.

Yazdani S, Hendi K, Pakravan M, Mahdavi M, Yaseri M (2009) Intravitreal bevacizumab for neovascular glaucoma: a randomized controlled trial. *J. Glaucoma* **18 (8)**: 632-7.

Yoles E, Wheeler LA, Schwartz M (1999) Alpha-2 adrenoceptor agonists are neuroprotective in a rat model of optic nerve degeneration. *Invest Ophthalmol Vis Sci* **40**; 65-73.

Yoo JY, Kim JM, Khang G, Kim MS, Cho SH, Lee HB, Kim YS (2004) Effect of lactide/glycolide monomers on release behaviors of gentamicin sulfate-loaded PLGA discs. *International Journal of Pharmaceutics* **276**: 1-9.

Young RW (1987) Pathophysiology of age-related macular degeneration. Survey of Ophthalmology 31 (5): 291-306.

Zhang N, Kanna R, Okamoto CT, Ryan SJ, Lee VHI, Hinton DR (2006). Characterization of brimonidine transport in retinal pigment epithelium. *Invest Ophthalmology Vis Sci* **47**: 287-294.

Zhang X, Wyss UP, Pichora D, Goosen MFA (1994) A mechanistic study of antibiotic release from biodegradable poly (d,l-lactide) cylinders. *Journal of controlled release* **31**: 129-144.

Zhu Q, Ziemssen F, Henke-Fahle S, Tatar O, Szurman P, Aisenbrey S, Schneiderhan-Marra N, Xu X, Grisanti S (2008) Vitreous levels of bevacizumab and vascular endothelial growth factor-A in patients with choroidal neovascularization. *Ophthalmology* **115**: 1750-1755, 1755 e1751.

Zhu YP, Wilson CG, Wilson WS (1996) An ex vivo model for the assessment of drug delivery to the eye: isolated bovine eye perfusion system. *European journal of pharmaceutics and biopharmaceutics* **42**: 405-410.

Zimmerman LR (1980) In vivo measurement of the viscoelasticity of the human vitreous humour. Brief communication. *Biophys. J* **29**: 539-544.

Zonas J (2007) Intravitreal triamcinolone actonide for diabetic retinopathy. *Dev.Ophthalmol* **39**: 96-110.

Appendixes

I Tables

Table A6.1 Preparation of brimonidine working solutions

Brimonidine working solution ID	Concentration of solution used (µg/mL)	Volume of solution added (mL)	Volume of diluent added (mL)	Final volume (mL)	Final concentration (µg/mL)
WS1	1000	0.75	0.75	1.50	500
WS2	1000	0.30	1.20	1.50	200
WS3	1000	0.15	1.35	1.50	100
WS4	500	0.15	1.35	1.50	50
WS5	200	0.15	1.35	1.50	20
WS6	50	0.45	1.05	1.50	15
WS7	50	0.30	1.20	1.50	10
WS8	50	0.15	1.35	1.50	5
WS9	20	0.15	1.35	1.50	2
WS10	10	0.15	1.35	1.50	1
WS11	5	0.15	1.35	1.50	0.5
WS12	5	0.12	1.38	1.50	0.4
WS13	2	0.15	1.35	1.50	0.2
WS14	1	0.15	1.35	1.50	0.1
WS15	0.5	0.12	1.38	1.50	0.04
WS16	0.2	0.15	1.35	1.50	0.02
WS17	0.1	0.15	1.35	1.50	0.01

Table A6.2 Preparation of brimonidine QC solutions

Brimonidine QC ID	Concentration of solution used (µg/mL)	Volume of solution added (mL)	Volume of diluent added (mL)	Final volume (mL)	Final concentration (µg/mL)
QC1	1000	0.75	0.75	1.50	500
QC2	1000	0.60	0.90	1.50	400
QC3	1000	0.15	1.35	1.50	100
QC4	500	0.15	1.35	1.50	50
QC5	500	0.12	1.38	1.50	40
QC6	50	0.75	0.75	1.50	25
QC7	50	0.30	1.20	1.50	10
QC8	50	0.15	1.35	1.50	5
QC9	10	0.15	1.35	1.50	1.0
QC10	5	0.12	1.38	1.50	0.4
QC11	0.5	0.60	0.90	1.50	0.2
QC12	0.5	0.12	1.38	1.50	0.04
QC13	0.04	0.75	0.75	1.50	0.02
QC14	0.02	0.75	0.75	1.50	0.01

Table A6.3 Preparation of brimonidine rabbit aqueous humour calibration standards

Aqueous humour standards	Concentration of BT working solution (µg/mL)	Volume of working solution added (µL)	Volume of blank AH added (µL)	Final volume in AH (µL)	Final concentration in AH (µg/mL)
AH5	50 (WS4)	2.5	47.5	50	2.5
AH6	20 (WS5)	2.5	47.5	50	1.0
AH7	5 (WS8)	2.5	47.5	50	0.25
AH8	1 (WS10)	2.5	47.5	50	0.05
AH9	0.5 (WS11)	2.5	47.5	50	0.025
AH10	0.2 (WS13)	2.5	47.5	50	0.01
AH11	0.1 (WS14)	2.5	47.5	50	0.005
AH12	0.04 (WS15)	2.5	47.5	50	0.002
AH13	0.02 (WS16)	2.5	47.5	50	0.001
AH blank	-	0	50	50	0
AH double blank	-	0	50	50	0

Table A6.4 Preparation of brimonidine rabbit aqueous humour quality control samples

Aqueous humour QC samples	Concentration of BT QC solution (µg/mL)	Volume of QC solution added (µL)	Volume of blank AH added (µL)	Final volume in AH (µL)	Final concentration in AH (µg/mL)
AH QC1	25 (QC6)	2.5	47.5	50	1.25
AH QC2	5 (QC8)	2.5	47.5	50	0.25
AH QC3	0.04 (QC12)	2.5	47.5	50	0.002
AH QC4	0.02 (QC13)	2.5	47.5	50	0.001

Table A6.5 Preparation of brimonidine rabbit vitreous humour calibration standards

Vitreous humour Standards ID	Concentration of BT working solution (µg/mL)	Volume of working solution added (µL)	Volume of blank VH added (µL)	Final volume in VH (µL)	Final concentration in VH (µg/mL)
VH3	50 (WS4)	5	95	100	2.5
VH4	10 (WS7)	5	95	100	0.5
VH5	5 (WS8)	5	95	100	0.25
VH6	1 (WS10)	5	95	100	0.05
VH7	0.5 (WS11)	5	95	100	0.025
VH8	0.2 (WS13)	5	95	100	0.01
VH9	0.1 (WS14)	5	95	100	0.005
VH10	0.04 (WS15)	5	95	100	0.002
VH11	0.02 (WS16)	5	95	100	0.001
VH blank	-	0	100	100	0
VH double blank	-	0	100	100	0

Table A6.6 Preparation of brimonidine rabbit vitreous humour quality control samples

Vitreous humour QC samples	Concentration of BT QC solutions (µg/mL)	Volume of QC solutions added (µL)	Volume of blank VH added (µL)	Final volume in VH (µL)	Final concentration in VH (µg/mL)
VH QC1	5 (QC8)	5	95	100	0.25
VH QC2	1 (QC9)	5	95	100	0.05
VH QC3	0.04 (QC12)	5	95	100	0.002
VH QC4	0.02 (QC13)	5	95	100	0.001

Table A6.7 Preparation of brimonidine rabbit ICB/Cho/Ret spiked calibration standards

ICB/Cho/Ret Standards ID	Concentration of BT working solution (µg/mL)	Volume of working solution added (µL)	Final amount of BT per piece of ICB/Cho/Ret (ng)
ICB/Cho/Ret 1	20 (WS5)	10	200
ICB/Cho/Ret 2	15 (WS6)	10	150
ICB/Cho/Ret 3	10 (WS7)	10	100
ICB/Cho/Ret 4	5 (WS8)	10	50
ICB/Cho/Ret 5	2 (WS9)	10	20
ICB/Cho/Ret 6	1 (WS10)	10	10
ICB/Cho/Ret 7	0.2 (WS13)	10	2
ICB/Cho/Ret 8	0.04 (WS15)	10	0.4
ICB/Cho/Ret 9	0.02 (WS16)	10	0.2
ICB/Cho/Ret 10	0.01 (WS17)	10	0.1
ICB/Cho/Ret blank	-	0	0
ICB/Cho/Ret double blank	-	0	0

Table A6.8 Preparation of brimonidine rabbit ICB/Cho/Ret spiked quality control samples

ICB/Cho/Ret QC samples	Concentration of BT QC solutions (µg/mL)	Volume of QC solutions added (µL)	Final amount of BT per piece of ICB/Cho/Ret (ng)
ICB/Cho/Ret QC1	10 (QC7)	10	100
ICB/Cho/Ret QC2	5 (QC8)	10	50
ICB/Cho/Ret QC3	0.02 (QC13)	10	0.2
ICB/Cho/Ret QC4	0.01 (QC14)	10	0.1

Table A6.9 Preparation of calibration standards for DDS analysis

DDS Standards ID	Concentration of BT working solution (µg/mL)	Volume of working solution added (µL)	Volume of 10% MeOH added (µL)	Volume of IS added (µL)	Final volume in implant (µL)	Final concentration in implant (ng/mL)
Neat 1	0.02 (WS16)	5	385	10	400	0.25
Neat 2	0.04 (WS15)	5	385	10	400	0.50
Neat 3	0.10 (WS14)	5	385	10	400	1.25
Neat 4	0.20 (WS13)	5	385	10	400	2.5
Neat 5	0.50 (WS11)	5	385	10	400	6.25
Neat 6	1.0 (WS10)	5	385	10	400	12.5
Neat 7	5.0 (WS8)	5	385	10	400	62.5
Neat 8	10.0 (WS7)	5	385	10	400	125
Neat 9	50.0 (WS4)	5	385	10	400	625
Blank	-	-	390	10	400	0
Double blank	-	-	400	-	400	0

Table A6.10 Preparation of quality control samples for DDS analysis

DDS QC samples	Concentration of BT QC (µg/mL)	Volume of BT QC added (µL)	Volume of mobile phase added (µL)	Volume of IS added (µL)	Final volume in implant (µL)	Final concentration in implant (ng/mL)
Neat QC1	0.02 (QC13)	5	385	10	400	0.25
Neat QC2	0.04 (QC12)	5	385	10	400	0.50
Neat QC3	10.0 (QC7)	5	385	10	400	125
Neat QC4	50 (QC4)	5	385	10	400	500

Table A6.11 Back-calculated concentrations for aqueous humour calibration curves

Acceptance criteria (µg/mL)								
- 20%	0.001	0.004	0.008	0.020	0.040	0.200	0.800	2.000
+20%	0.001	0.006	0.012	0.030	0.060	0.300	1.200	3.000
Nominal concentrations (µg/mL)								
	0.001 (LLOQ)	0.005	0.01	0.025	0.05	0.25	1.0	2.5
Run 1	0.001	0.005	0.010	0.024	0.049	0.250	0.947	2.500
N	1	1	1	1	1	1	1	1

Table A6.12 Back-calculated concentrations for vitreous humour calibration curves

Acceptance criteria (µg/mL)								
- 20%	0.001	0.004	0.008	0.020	0.040	0.200	0.400	2.000
+20%	0.001	0.006	0.012	0.030	0.060	0.300	0.600	3.000
Nominal concentrations (µg/mL)								
	0.001 (LLOQ)	0.005	0.01	0.025	0.05	0.25	0.5	2.5
Run 1	0.001	0.006	0.01	0.030	0.05	0.25	0.5	2.5
Run 2	0.001	0.005	0.01	0.030	0.05	0.25	0.5	2.5
Run 3	0.001	0.005	0.01	0.025	0.05	0.25	0.5	2.5
Run 4	0.001	0.005	0.01	0.026	0.05	0.25	0.5	2.7
Mean	0.001	0.005	0.01	0.025	0.05	0.25	0.5	2.5
SD	0.0001	0.0004	0.0003	0.0004	0.0012	0.0004	0.0194	0.1059
%RSD	9.48	8.24	3.08	1.67	2.43	0.16	3.92	4.20
% Accuracy	101.25	102.33	97.85	101.00	99.95	101	98.67	100.80
N	4	4	4	4	4	4	4	4

Table A6.13 Back-calculated concentrations for choroid calibration curves

Acceptance criteria (ng)										
- 20%	0.08	0.16	0.32	1.6	8	16	40	80	120	160
+20%	0.12	0.24	0.48	2.4	12	24	60	120	180	240
Nominal concentrations (ng)										
	0.1 LLOQ	0.2	0.4	2	10	20	50	100	150	200
Run 1	0.10	0.22	0.36	1.85	10.0	18.90	50.60	107	159	202
Run 2	0.10	0.19	0.36	1.92	9.73	18.60	49.80	102	158	203
Run 3	0.10	0.22	0.39	1.90	9.98	19.50	51.10	100	159	191
Run 4	0.10	0.18	0.42	1.95	9.83	19.40	51.70	101	155	199
Run 5	0.10	0.22	0.36	1.86	10.1	19.80	51.80	102	161	194
Mean	0.10	0.21	0.38	1.90	9.93	19.24	51.00	102	158	198
SD	0.003	0.019	0.029	0.042	0.147	0.483	0.828	2.702	2.191	5.167
%RSD	3.10	8.97	7.60	2.19	1.48	2.51	1.62	2.64	1.38	2.61
% Accuracy	99.30	103.50	94.25	94.80	99.28	96.20	102	102.40	105.60	98.90
N	5	5	5	5	5	5	5	5	5	5

Table A6.14 Back-calculated concentrations for ICB calibration curves

Acceptance criteria (ng)								
- 20%	0.08	0.16	0.32	1.6	8	40	80	160
+20%	0.12	0.24	0.48	2.4	12	60	120	240
Nominal concentrations (ng)								
	0.1(LLOQ)	0.2	0.4	2	10	50	100	200
Run 1	0.103	0.187	0.407	2.000	9.790	51.1	107	190
Run 2	No peak	0.200	0.401	2.020	9.600	50.7	107	188
Mean	-	0.287	0.404	3.01	9.695	50.9	107	189
N	2	2	2	2	2	2	2	2

Table A6.15 Back-calculated concentrations for retina calibration curves

Acceptance criteria (ng)										
- 20%	0.08	0.16	0.32	1.6	8	16	40	80	120	160
+20%	0.12	0.24	0.48	2.4	12	24	60	120	180	240
Nominal concentrations (ng)										
	0.1(LLOQ)	0.2	0.4	2	10	20	50	100	150	200
Run 1	0.0991	0.215	0.36	1.89	10.3	18.9	52.4	103	154	202
Run 2	0.106	0.179	0.388	2	10.1	18.9	52.7	103	153	204
Run 3	0.1	0.2	0.394	1.93	10.7	19.9	50.4	98.6	152	195
Mean	0.1017	0.198	0.38	1.94	10.37	19.23	51.83	101.53	153	200.33
SD	0.004	0.018	0.018	0.056	0.306	0.577	1.250	2.540	1	4.726
%RSD	3.69	9.13	4.77	2.87	2.95	3.00	2.41	2.50	0.65	2.36
%Accuracy	101.7	99	95.17	97	103.67	96.17	103.67	101.53	102	100.17
N	3	3	3	3	3	3	3	3	3	3

Table A6.16 Back-calculated concentrations for implant calibration curves

Acceptance criteria (ng/mL)									
- 20%	0.20	0.40	1.00	2.00	5.00	10.00	50.00	100	500
+20%	0.30	0.60	1.50	3.00	7.50	15.00	75.00	150	750
Nominal concentration (ng/mL)									
	0.25 (LLOQ)	0.50	1.25	2.50	6.25	12.50	62.50	125	625
Run 1	0.251	0.492	1.25	2.51	6.52	12.80	64.00	122	586
Run 2	0.249	0.493	1.30	2.50	6.56	12.60	63.70	121	582
Mean	0.250	0.493	1.28	2.51	6.54	12.70	63.85	122	584
N	2	2	2	2	2	2	2	2	2

Table 6.17 LLOQ of the brimondine tissue assays.

Tissue assays	Aqueous humour	Vitreous humour	Choroid	ICB	Retina	Implant
Nominal concentrations	0.001 µg/mL	0.001 µg/mL	0.1ng	0.1ng	0.1ng	0.25ng/mL
Assayed concentrations	0.0010	0.0010	0.1020	0.1030	0.1000	0.2490
	0.0009	0.0009	0.0752	0.0965	0.0920	0.2620
	0.0011	0.0009	0.1080	0.1210	0.1130	0.2700
		0.0009	0.0928	0.1350	0.0873	0.2510
		0.0010	0.1160		0.0917	0.2660
		0.0012	0.1300			
Mean	0.00101	0.0010	0.1040	0.1139	0.0968	0.2600
SD	0.00009	0.0001	0.0190	0.0175	0.0102	0.0100
% RSD	9.25	13.95	18.22	15.36	10.48	3.56
% Accuracy	101.13	97.90	104.00	113.88	96.80	103.84
n	3	6	6	4	5	5

Table A6.18 Concentration of Brimonidine (µg/mL) in aqueous humour following a single intravitreal injection of 30µg Brimonidine Tartrate (Group 1) in Dutch-belted rabbit eyes

	Brimonidine concentration (µg/mL)	
Time (hour)	Hyaluronidase-treated	Näive
1	0.014 ± 0.011 (0.002, 0.024)	0.007 ± 0.001 (0.006, 0.008)
2	0.007 ± 0.002 (0.006, 0.010)	0.034 ± 0.019 (0.016, 0.054)
4	0.008 ± 0.002 (0.006, 0.010)	0.019 ± 0.016 (0.010, 0.038)
8	0.005 ± 0.001 (0.003, 0.006)	0.006 ± 0.001 (0.005, 0.007)

Mean ± SD (min, max), n = 3 rabbits/time point

Hyaluronidase-treated = Right eye

Näive = Left eye

Table A6.19 Concentration of Brimonidine (µg/mL) in aqueous humour following a single intravitreal implantation of 210µg Brimonidine Tartrate (Group 2) in Dutch-belted rabbit eyes

	Brimonidine concentration (µg/mL)	
Time (Day)	Hyaluronidase-treated	Näive
1	0.006 ± 0.004 (0.003, 0.011)	0.008 ± 0.002 (0.006, 0.010)
7	0.004 ± 0.002 (0.002, 0.006)	0.005 ± 0.002 (0.003, 0.007)
14	0.008 ± 0.002 (0.006, 0.009)	0.023 ± 0.015 (0.011, 0.040)
28	NC (BLQ, BLQ)	NC (BLQ, BLQ)

Mean ± SD (min, max), n = 3 rabbits/time point

Hyaluronidase-treated = Right eye

Näive = Left eye

BLQ < 0.001µg/mL

NC = not calculable due to two or more samples were BLQ

Table A6.20 Concentration of Brimonidine (µg/mL) in vitreous humour following a single intravitreal injection of 30µg Brimonidine Tartrate (Group 1) in Dutch-belted rabbit eyes

	Brimonidine concentration (µg/mL)	
Time (hour)	Hyaluronidase-treated	Näive
1	9.87 ± 1.02 (8.71, 10.60)	10.78 ± 0.935 (9.83, 11.70)
2	5.81 ± 2.97 (2.97, 8.90)	9.58 ± 1.08 (8.34, 10.3)
4	2.12 ± 1.00 (1.36, 3.26)	2.56 ± 0.09 (2.47, 2.65)
8	0.297 ± 0.111 (0.229, 0.426)	0.366 ± 0.133 (0.213, 0.456)

Mean ± SD (min, max), n = 3 rabbits/time point

Hyaluronidase-treated = Right eye

Näive = Left eye

Table A6.21 Concentration of Brimonidine (µg/mL) in vitreous humour following a single intravitreal implantation of 210µg Brimonidine Tartrate DDS (Group 2) in Dutch-belted rabbit eyes

	Brimonidine concentration (µg/mL)	
Time (Day)	Hyaluronidase-treated	Näive
1	0.252 ± 0.107 (0.129, 0.322)	0.260 ± 0.093 (0.152, 0.315)
7	0.508 ± 0.418 (0.193, 0.982)	0.480 ± 0.098 (0.377, 0.573)
14	0.915 ± 0.368 (0.495, 1.18)	1.11 ± 0.490 (0.546, 1.46)
28	0.002 ± 0.001 (0.001, 0.004)	0.002 ± 0.001 (0.001, 0.004)

Mean ± SD (min, max), n = 3 rabbits/time point

Hyaluronidase-treated = Right eye

Näive = Left eye

Table A6.22 Concentration of Brimonidine (ng/g) in iris-ciliary body (ICB) following a single intravitreal injection of 30µg Brimonidine Tartrate (Group 1) in Dutch-belted rabbit eyes

	Brimonidine concentration (ng/g)	
Time (hour)	Hyaluronidase-treated	Näive
1	2588 ± 699 (2095, 3388)	2733 ± 239 (2458, 2894)
2	5443 ± 3346 (2116, 8808)	8011 ± 3082 (5189, 11299)
4	4793 ± 1421 (3835, 6425)	8050 ± 3170 (4928, 11265)
8	5857 ± 2906 (2730, 8473)	9700 ± 4162 (5159, 13333)

Mean ± SD (min, max), n = 3 rabbits/time point

Hyaluronidase-treated = Right eye

Näive = Left eye

Table A6.23 Concentration of Brimonidine (ng/g) in iris-ciliary body (ICB) following a single intravitreal implantation of 210µg Brimonidine Tartrate DDS (Group 2) in Dutch-belted rabbit eyes

	Brimonidine concentration (ng/g)	
Time (Day)	Hyaluronidase-treated	Näive
1	7239 ± 1317 (6459, 8759)	14023 ± 6766 (8920, 21698)
7	9787 ± 5430 (4752, 15541)	10860 ± 4295 (5936, 13832)
14	21423 ± 8033 (12450, 27948)	26447 ± 5994 (21662, 33170)
28	3221 ± 633 (2543, 3796)	2512 ± 201 (2337, 2732)

Mean ± SD (min, max), n = 3 rabbits/time point

Hyaluronidase-treated = Right eye

Näive = Left eye

Table A6.24 Concentration of Brimonidine (ng/g) in choroid at macula (a), superior (b), inferior (c), nasal (d) and temporal (e) zones of the eye following a single intravitreal injection of 30µg Brimonidine Tartrate (Group 1) in Dutch-belted rabbit eyes

Table A6.24a

	Brimonidine concentration (ng/g) at macula zone	
Time (hour)	Hyaluronidase-treated	Näive
1	22436 ± 15456 (5667, 36111)	98428 ± 65896 (46316, 172500)
2	22471 ± 10969 (9862, 29804)	34707 ± 12479 (22083, 47037)
4	20321 ± 15563 (8525, 37960)	18578 ± 5977 (14638, 25455)
8	12364 ± 5437 (6776, 17636)	22034 ± 25302 (3815, 50923)

Table A6.24b

	Brimonidine concentration (ng/g) at superior zone	
Time (hour)	Hyaluronidase-treated	Näive
1	104669 ± 152428 (14915, 280667)	30964 ± 9627 (21351, 40606)
2	31168 (13652, 48684)*	55101 ± 28503 (27333, 84286)
4	11374 ± 306 (11025, 11596)	100307 ± 90472 (23421, 200000)
8	5751 ± 3077 (2699, 8852)	14587 ± 7875 (8242, 23400)

Table A6.24c

	Brimonidine concentration (ng/g) at inferior zone	
Time (hour)	Hyaluronidase-treated	Näive
1	11609 ± 12721 (3747, 26286)	5818 ± 1845 (4163, 7807)
2	4786 ± 1183 (3568, 5930)	19016 ± 12581 (4821, 28790)
4	5094 ± 2879 (1871, 7412)	6246 (3859, 8632) *
8	4962 ± 1906 (2788, 6346)	11956 ± 8845 (4189, 21583)

Table A6.24d

	Brimonidine concentration (ng/g) at nasal zone	
Time (hour)	Hyaluronidase-treated	Näive
1	3979 ± 1880 (2500, 6095)	6733 ± 1228 (5936, 8147)
2	3940 ± 2870 (1167, 6898)	20905 ± 26495 (2805, 51316)
4	3519 ± 1220 (2500, 4871)	12527 ± 8434 (4961, 21621)
8	1584 ± 497 (1012, 1907)	4160 ± 2345 (2337, 6805)

Table A6.24e

	Brimonidine concentration (ng/g) at temporal zone	
Time (hour)	Hyaluronidase-treated	Näive
1	109836 ± 179854 (4007, 317500)	18036 ± 7141 (13744, 26279)
2	13802 ± 7753 (6893, 22188)	14189 ± 6138 (7128, 18240)
4	4410 ± 1841 (2515, 6192)	5484 ± 3179 (3286, 9129)
8	2630 ± 664 (1864, 3044)	3762 ± 1147 (2560, 4843)

Mean ± SD (min, max), each time point has n = 3 rabbits; unless otherwise stated

* n=2 eyes as one of the samples was unavailable for analysis.

Hyaluronidase-treated = Right eye

Näive = Left eye

Table A6.25 Concentration of Brimonidine (ng/g) in choroid at macula (a), superior (b), inferior (c), nasal (d) and temporal (e) zones of the eye following a single intravitreal implantation of 210µg Brimonidine Tartrate DDS (Group 2) in Dutch-belted rabbit eyes

Table A6.25a

	Brimonidine concentration (ng/g) at macula zone	
Time (day)	Hyaluronidase-treated	Näive
1	8093 ± 4973 (2711, 12517)	8798 ± 2867 (5882, 11613)
7	3861 ± 3860 (581, 8114)	9057 ± 6121 (3110, 15338)
14	14971 ± 8931 (5395, 23075)	10102 ± 8183 (4887, 19533)
28	461 ± 352 (80, 774)	399 ± 314 (145, 750)

Table A6.25b

	Brimonidine concentration (ng/g) at superior zone	
Time (day)	Hyaluronidase-treated	Näive
1	14290 ± 10869 (6581, 26722)	16766 ± 2809 (13935, 19552)
7	2775 ± 1290 (1490, 4070)	11079 ± 16080 (1277, 29636)
14	4130 ± 959 (3046, 4867)	7433 ± 1057 (6522, 8591)
28	415 ± 352 (53, 757)	368 ± 451 (91, 888)

Table A6.25c

	Brimonidine concentration (ng/g) at inferior zone	
Time (day)	Hyaluronidase-treated	Näive
1	2772 ± 2027 (1297, 5084)	3904 ± 1088 (2695, 4806)
7	3442 ± 4019 (918, 8076)	13321 ± 5166 (8295, 18616)
14	8027 ± 632 (7658, 8757)	7588 ± 4750 (2282, 11444)
28	697 ± 586 (315, 1371)	6977 ± 10621 (638, 19238)

Table A6.25d

	Brimonidine concentration (ng/g) at nasal zone	
Time (day)	Hyaluronidase-treated	Näive
1	2037 ± 313 (1695, 2308)	3728 ± 1948 (2462, 5972)
7	1539 ± 1183 (491, 2822)	3604 ± 2000 (2346, 5911)
14	2700 ± 923 (2020, 3750)	7261 ± 5222 (1419, 11474)
28	327 ± 104 (222, 429)	174 ± 49 (137, 229)

Table A6.25e

	Brimonidine concentration (ng/g) at temporal zone	
Time (day)	Hyaluronidase-treated	Näive
1	8059 ± 10276 (2071, 19924)	6992 ± 4111 (2705, 10902)
7	2645 ± 1114 (1881, 3924)	7160 ± 2822 (4574, 10170)
14	6000 ± 2355 (4173, 8659)	8084 ± 1974 (6130, 10077)
28	1044 ± 1144 (38, 2289)	3639 ± 4765 (256, 9088)

Mean ± SD (min, max), each time point has n = 3 rabbits; unless otherwise stated

Hyaluronidase-treated = Right eye

Näive = Left eye

Table A6.26 Concentration of Brimonidine (ng/g) in retina at macula (a), superior (b), inferior (c), nasal (d) and temporal (e) zones of the eye following a single intravitreal injection of 30µg Brimonidine Tartrate (Group 1) in Dutch-belted rabbit eyes

Table A6.26a

	Brimonidine concentration (ng/g) at macula zone	
Time (hour)	Hyaluronidase-treated	Näive
1	17425 ± 6826 (12251, 25161)	29617 ± 8482 (19889, 35469)
2	5757 ± 2855 (2664, 8293)	8412 ± 4173 (4723, 12941)
4	3274 ± 417 (2837, 3667)	6288 ± 1019 (5111, 6892)
8	1087 ± 630 (502, 1755)	1098 ± 204 (877, 1277)

Table A6.26b

	Brimonidine concentration (ng/g) at superior zone	
Time (hour)	Hyaluronidase-treated	Näive
1	24954 ± 19278 (12748, 47180)	46587 ± 28575 (13597, 63611)
2	22857 ± 14551 (6897, 35385)	40346 ± 14551 (31261, 46666)
4	10789 ± 4436 (6964, 15652)	41785 ± 12713 (27547, 52000)
8	3281 ± 2256 (1094, 5600)	9141 ± 5760 (3891, 15302)

Table A6.26c

	Brimonidine concentration (ng/g) at inferior zone	
Time (hour)	Hyaluronidase-treated	Näive
1	4814 ± 3216 (2513, 8489)	9189 ± 4996 (4766, 14607)
2	1958 ± 1028 (1038, 3068)	5118 ± 1466 (3678, 6609)
4	4624 ± 1325 (3576, 6113)	6097 ± 3228 (4048, 9818)
8	2621 ± 1250 (1204, 3565)	3274 ± 891 (2252, 3889)

Table A6.26d

	Brimonidine concentration (ng/g) at nasal zone	
Time (hour)	Hyaluronidase-treated	Näive
1	7305 ± 6152 (2117, 14101)	10833 ± 1976 (8955, 12894)
2	1964 ± 1287 (568, 3103)	8479 ± 6315 (3263, 15500)
4	2221 ± 1490 (1063, 3902)	4771 ± 1419 (3717, 6385)
8	1922 ± 1232 (589, 3020)	1614 ± 693 (871, 2244)

Table A6.26e

	Brimonidine concentration (ng/g) at temporal zone	
Time (hour)	Hyaluronidase-treated	Näive
1	10288 ± 11022 (3081, 22976)	29887 ± 11031 (19375, 41373)
2	3130 ± 744 (2508, 3953)	4567 ± 2707 (2209, 7523)
4	2892 ± 2363 (602, 5321)	3716 ± 2402 (2102, 6476)
8	523 ± 237 (262, 725)	792 ± 442 (453, 1291)

Mean ± SD (min, max), each time point has n = 3 rabbits; unless otherwise stated

Hyaluronidase-treated = Right eye

Näive = Left eye

Table A6.27 Concentration of Brimonidine (ng/g) in retina at macula (a), superior (b), inferior (c), nasal (d) and temporal (e) zones of the eye following a single intravitreal implantation of 210µg Brimonidine Tartrate DDS (Group 2) in Dutch-belted rabbit eyes

Table A6.27a

	Brimonidine concentration (ng/g) at macula zone	
Time (day)	Hyaluronidase-treated	Näive
1	1128 ± 230 (922, 1376)	882 ± 206 (655, 1057)
7	904 ± 681 (490, 1690)	1872 ± 532 (1269, 2272)
14	3115 ± 2794 (1415, 6340)	2210 ± 833 (1248, 2692)
28	33 ± 38 (10, 76)	18 ± 4 (13, 21)

Table A6.27b

	Brimonidine concentration (ng/g) at superior zone	
Time (day)	Hyaluronidase-treated	Näive
1	2811 ± 549 (2181, 3188)	3420 ± 2469 (1874, 6267)
7	3455 ± 1598 (2024, 5179)	2674 ± 784 (1992, 3531)
14	2713 ± 539 (2221, 3289)	4874 ± 1757 (3000, 6483)
28	40 ± 19 (18, 56)	26 ± 8 (18, 34)

Table A6.27c

	Brimonidine concentration (ng/g) at inferior zone	
Time (day)	Hyaluronidase-treated	Näive
1	1433 ± 482 (970, 1931)	1450 ± 620 (802, 2039)
7	910 ± 536 (294, 1269)	6411 ± 2305 (3787, 8107)
14	3151 ± 1002 (2324, 4265)	2747 ± 583 (2186, 3351)
28	46 ± 46 (17, 99)	256 ± 381 (14, 695)

Table A6.27d

	Brimonidine concentration (ng/g) at nasal zone	
Time (day)	Hyaluronidase-treated	Näive
1	655 ± 40 (612, 689)	424 ± 119 (345, 560)
7	641 ± 389 (209, 960)	1480 ± 596 (794, 1881)
14	1228 ± 608 (818, 1927)	968 ± 485 (439, 1392)
28	42* (BLQ, 76)	18** (BLQ, 18)

Table A6.27e

	Brimonidine concentration (ng/g) at temporal zone	
Time (day)	Hyaluronidase-treated	Näive
1	959 ± 571 (404, 1544)	839 ± 369 (568, 1260)
7	1498 ± 1201 (407, 2786)	1405 ± 597 (728, 1855)
14	2034 ± 339 (1647, 2280)	1606 ± 375 (1369, 2039)
28	31 ± 14 (19, 47)	78 ± 66 (21, 151)

Mean ± SD (min, max), each time point has n = 3 rabbits; unless otherwise stated

* n=3 eyes but one of the samples was BLQ

** n=3 eyes but two of the samples were BLQ

Hyaluronidase-treated = Right eye

Näive = Left eye

II Figures

Figure A6.1 Linear regression curve of brimonidine in rabbit aqueous humour, n=1

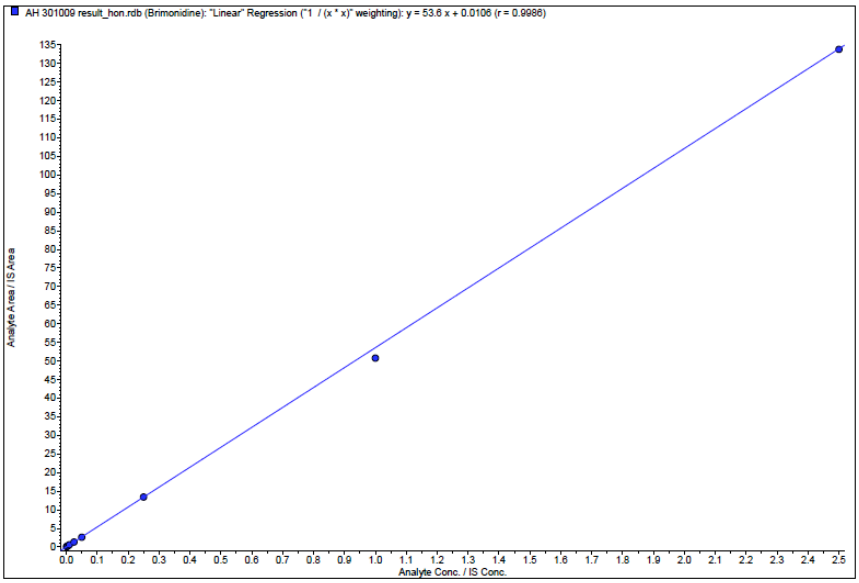

Figure A6.2 Linear regression curve of brimonidine in rabbit vitreous humour, n=2

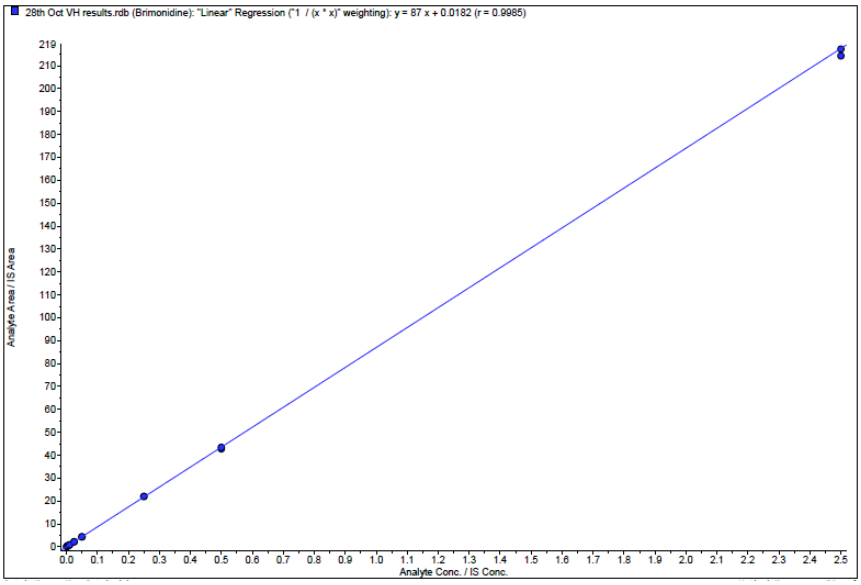

Figure A6.3 Linear regression curve of brimonidine in rabbit choroid, n=1.

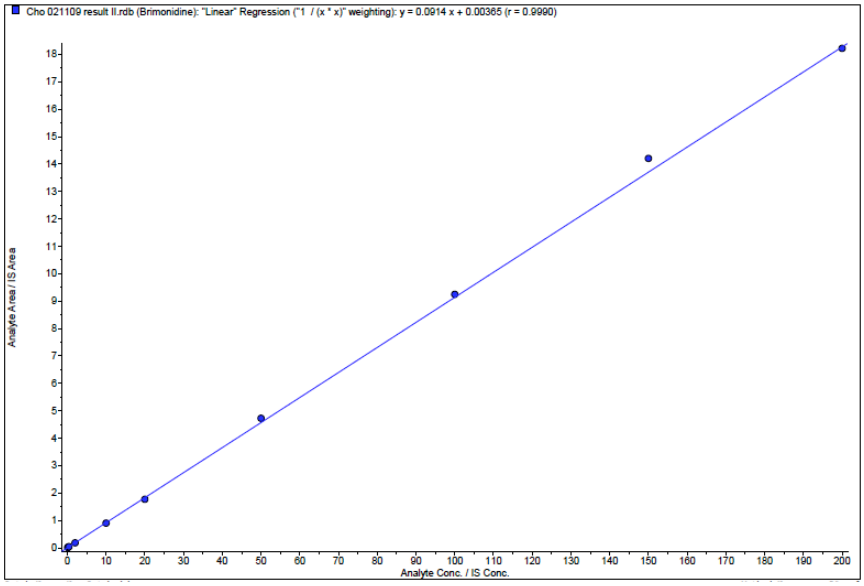

Figure A6.4 Linear regression curve of brimonidine in rabbit ICB, n=1.

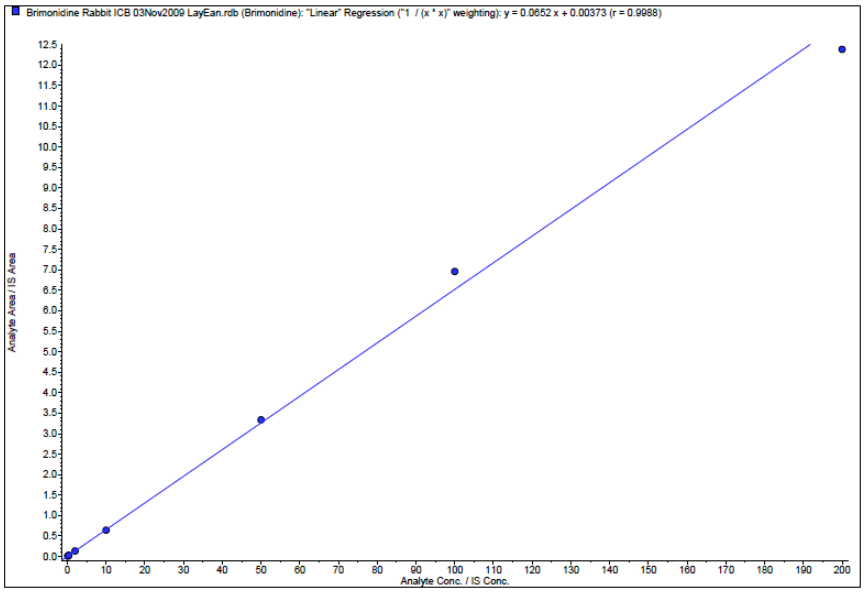

Figure A6.5 Linear regression curve of brimonidine in rabbit retina, n=1.

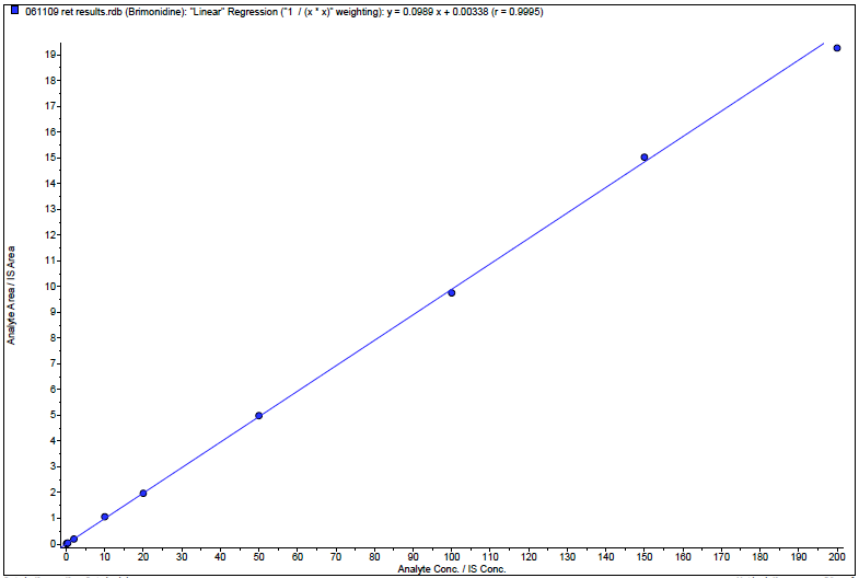

Figure A6.6 Linear regression curve of brimonidine in mobile phase, n=1.

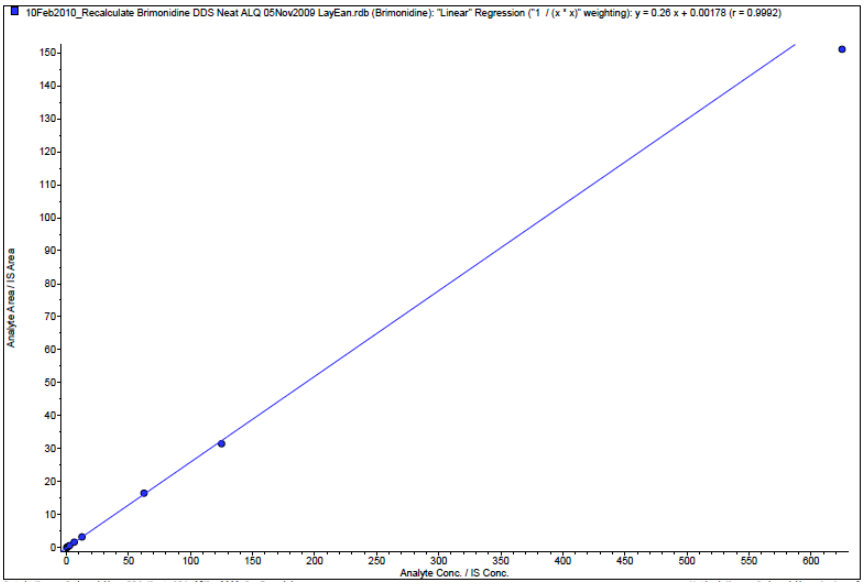

PUBLICATIONS

Tan L.E., Orilla W.C., Hughes P.M., Tsai S., Burke J., Wilson C.G. Effects of vitreous liquefaction on intravitreal distribution of sodium fluorescein, fluorescence dextran and fluorescent microparticles. [Invest Ophthalmol Vis Sci. 2010 Sep 29. doi: 10.1167/iovs.10-5813, Epub ahead of print]

Laude A. **Tan L.E**., Wilson C.G., Lascaratos G., Elashry M., Aslam T., Patton N, Dhillon B. (2010) Intravitreal therapy for neovascular age-related macular degeneration and inter-individual variations in vitreous pharmacokinetics. Prog Retin Eye Res. [Article in press; Available online 7th May 2010]

Wilson C.G., **Tan L.E.**, Mains J. Principles of retinal drug delivery from within the vitreous. In: Drug Product Development for the Back of the Eye. Ed. Edelhauser H, Kompella U [Submitted to Springer]

Tan L.E., Orilla W.C., Tsai S., Hughes P.M., Wilson C.G., Burke J. Effects of vitreous liquefaction on the intravitreal distribution of sodium fluorescein, fluorescein dextran and fluorescent microparticles [Selected Oral Presentation with travel grant award]. In: ARVO Summer Eye Research Conference; 2009 July 31-Aug 1, NIH Bethesda, p 19. Abstract nr 11

Wilson C.G., **Tan L.E.** , Girkin J.M. Barriers to intravitreal drug delivery to the retina. Presented in ARVO Summer Eye Research Conference; 2009 July 31-Aug 1, NIH Bethesda, p 14. Abstract nr 3.

Tan L.E., Watts F.E., Wright A.J., Girkin J.M. and Wilson C.G. The use of optical tweezers to measure the viscosity of the vitreous humour. [Poster presentation]. In: 2nd Pharmsci Fair 2009, Nice, France.

Tan L.E., Watts F.E., Wright A.J., Girkin J.M. and Wilson C.G. Preliminary results: Use of optical tweezers in the viscosity measurement of the vitreous humour. [Poster presentation] In: The Eye Symposium " Science to Surgery", 2007, Edinburgh, United Kingdom.